

**EFFECT OF RICE HUSK ASH AND PALM OIL FUEL
ASH ON MICROSTRUCTURE AND CHLORIDE
PENETRATION OF BLENDED CEMENT PASTES**

Wunchock Kroehong

**A Thesis Submitted in Partial Fulfillment of the Requirements for the
Degree of Doctor of Philosophy of Engineering in Civil Engineering**

Suranaree University of Technology

Academic Year 2012

ผลของถ้าเกลบและถ้าปาดม้ำมันต่อโครงสร้างจุลภาคและการแทรกซึม
คลอไรด์ของซีเมนต์เพสต์ผสม

นายวันโชค เครือหงษ์

วิทยานิพนธ์นี้เป็นส่วนหนึ่งของการศึกษาตามหลักสูตรปริญญาวิศวกรรมศาสตรดุษฎีบัณฑิต
สาขาวิชาวิศวกรรมโยธา
มหาวิทยาลัยเทคโนโลยีสุรนารี
ปีการศึกษา 2555

**EFFECT OF RICE HUSK ASH AND PALM OIL FUEL ASH ON
MICROSTRUCTURE AND CHLORIDE PENETRATION
OF BLENDED CEMENT PASTES**

Suranaree University of Technology has approved this thesis submitted in partial fulfillment of the requirements for the Degree of Doctor of Philosophy

Thesis Examining Committee

(Prof. Dr. Suksun Horpibulsuk)

Chairperson

(Asst. Prof. Dr. Theerawat Sinsiri)

Member (Thesis Advisor)

(Prof. Dr. Chai Jaturapitakkul)

Member

(Assoc. Prof. Dr. Sittichai Seangatith)

Member

(Dr. Nattapong Damrongwiriyanupap)

Member

(Prof. Dr. Sukit Limpijumngong)
Vice Rector for Academic Affairs

(Assoc. Prof. Ft. Lt. Dr. Kontom Chamniprasat)
Dean of Institute of Engineering

วันโชค เครือหงษ์ : ผลของเถ้าแกลบและเถ้าปาล์มน้ำมันต่อโครงสร้างจุลภาคและการแทรกซึมคลอไรด์ของซีเมนต์เพสต์ผสม (EFFECT OF RICE HUSK ASH AND PALM OIL FUEL ASH ON MICROSTRUCTURE AND CHLORIDE PENETRATION OF BLENDED CEMENT PASTES) อาจารย์ที่ปรึกษา : ผู้ช่วยศาสตราจารย์ ดร.ธีรวัฒน์ ลินศิริ, 244 หน้า.

วัตถุประสงค์ของวิทยานิพนธ์ฉบับนี้ เพื่อศึกษาผลของเถ้าแกลบและเถ้าปาล์มน้ำมันต่อโครงสร้างจุลภาคและการแทรกซึมคลอไรด์ของซีเมนต์เพสต์ โดยนำเถ้าแกลบ เถ้าปาล์มน้ำมัน และทรายแม่น้ำมาบดให้มีความละเอียด 2 ขนาด คือขนาดอนุภาคใกล้เคียงกับปูนซีเมนต์และขนาดอนุภาคเล็กกว่าปูนซีเมนต์ การศึกษาแบ่งออกเป็น 2 ส่วน ส่วนที่ 1 นำปูนซีเมนต์ปอร์ตแลนด์ประเภทที่ 1 มาแทนที่ด้วยเถ้าแกลบหรือเถ้าปาล์มน้ำมันหรือทรายแม่น้ำ ในอัตราส่วนร้อยละ 10 20 30 และ 40 โดยน้ำหนักของวัสดุประสาน ควบคุมอัตราส่วนน้ำต่อวัสดุประสานเท่ากับ 0.35 ทุกอัตราส่วนผสม ทดสอบกำลังอัด การสูญเสียน้ำหนักเมื่อได้รับความร้อนและการกระจายขนาดของโพรงของซีเมนต์เพสต์ผสม ส่วนที่ 2 ใช้เถ้าปาล์มน้ำมันแทนที่ปูนซีเมนต์ปอร์ตแลนด์ประเภทที่ 1 ในอัตราส่วนร้อยละ 10 20 30 และ 40 โดยน้ำหนักของวัสดุประสาน โดยมีอัตราส่วนน้ำต่อวัสดุประสานคงที่เท่ากับ 0.35 นำซีเมนต์เพสต์ผสมไปแช่ในสารละลายโซเดียมคลอไรด์เข้มข้น 3% เป็นเวลา 90 วัน จากนั้นนำไปทดสอบหาปริมาณคลอไรด์ทั้งหมด คลอไรด์อิสระ โครงสร้างจุลภาคของเพสต์ภายใต้การแทรกซึมของคลอไรด์ และวิเคราะห์การแทรกซึมคลอไรด์ของเพสต์โดยโปรแกรมไฟไนท์เอลิเมนต์ของตัวอย่างแช่ในสารละลายโซเดียมคลอไรด์เข้มข้น 3% เป็นเวลา 90 วัน

ผลการทดสอบในส่วนที่ 1 กำลังอัดของเพสต์เนื่องจากปฏิกิริยาไฮเดรชันมีค่าลดลงตามการลดลงของปูนซีเมนต์ กำลังอัดของเพสต์เนื่องจากการอัดตัวของอนุภาคมีค่าเพิ่มขึ้นตามการแทนที่เพิ่มขึ้นของทราย กำลังอัดของเพสต์เนื่องจากปฏิกิริยาปอซโซลานมีลักษณะไม่เชิงเส้นและมีค่าเพิ่มขึ้นตามความละเอียดของเถ้าแกลบและเถ้าปาล์มน้ำมันตามการแทนที่ที่มากขึ้นและตามอายุการบ่มของเพสต์ นอกจากนี้ การแทนที่ปูนซีเมนต์ที่เหมาะสมของเถ้าแกลบและเถ้าปาล์มน้ำมันในเพสต์คือร้อยละ 30 โดยน้ำหนักของวัสดุประสาน การสูญเสียน้ำหนักเมื่อได้รับความร้อน (ที่อุณหภูมิ 30-450 องศาเซลเซียส) ของเพสต์ เนื่องจากการอัดตัวและเนื่องจากปฏิกิริยาปอซโซลาน มีค่าเพิ่มขึ้นตามอายุการบ่ม ความละเอียดของอนุภาคและตามการแทนที่ที่มากขึ้น นอกจากนี้ขนาดโพรงวิกฤติและขนาดโพรงเฉลี่ยของเพสต์แทนที่ด้วยเถ้าแกลบและเถ้าปาล์มน้ำมันมีขนาดเล็กกว่าซีเมนต์เพสต์ควบคุม

ผลการทดสอบในส่วนที่ 2 พบว่า ซีเมนต์เพสต์ผสมเถ้าปาล์มน้ำมันมีค่าสัมประสิทธิ์การแพร่กระจายของคลอไรด์และระดับความเข้มข้นของคลอไรด์อิสระต่ำกว่าซีเมนต์เพสต์ที่ใช้ปูนซีเมนต์ปอร์ตแลนด์ประเภทที่ 1 นอกจากนี้ ความสัมพันธ์ระหว่างค่าสัมประสิทธิ์การแพร่กระจายของคลอไรด์และขนาดโพรงวิกฤตมีลักษณะความสัมพันธ์เชิงเส้นและเพิ่มขึ้นตามขนาดโพรงวิกฤต ความละเอียดและการแทนที่ที่เพิ่มขึ้นของเถ้าปาล์มน้ำมันส่งผลให้คลอไรด์อิสระและค่าสัมประสิทธิ์การแพร่กระจายของคลอไรด์ลดลง การใช้เถ้าปาล์มน้ำมันแทนที่ปูนซีเมนต์ปอร์ตแลนด์ประเภทที่ 1 พบว่ามียอด (Peak) ของ Friedel's salt ในเพสต์ต่ำกว่าซีเมนต์เพสต์ที่ใช้ปูนซีเมนต์ปอร์ตแลนด์ประเภทที่ 1 นอกจากนี้การใช้เถ้าปาล์มน้ำมันที่มีความละเอียดและแทนที่ปูนซีเมนต์ในปริมาณที่มากขึ้นทำให้ยอด (Peak) ของ Friedel's salt ลดลง อย่างไรก็ตามการเพิ่มการแทนที่ปูนซีเมนต์ด้วยเถ้าปาล์มน้ำมันทำให้การเก็บกักคลอไรด์ทางด้านกายภาพเพิ่มขึ้น



WUNCHOCK KROEHONG : EFFECT OF RICE HUSK ASH AND
PALM OIL FUEL ASH ON MICROSTRUCTURE AND CHLORIDE
PENETRATION OF BLENDED CEMENT PASTES. THESIS ADVISOR :
ASST. PROF. THEERAWAT SINSIRI, Ph.D., 244 PP.

RICE HUSK ASH/PALM OIL FUEL ASH/MICROSTRUCTURE/CHLORIDE
PENETRATION/FINITE ELEMENT ANALYSIS

This thesis aims to study the effect of rice husk ash and palm oil fuel ash on the microstructure and chloride penetration of blended cement pastes. Rice husk ash (RHA), palm oil fuel ash (POFA) and river sand (RS) were ground to obtain two finenesses: one was the same size as the cement and the other was smaller than the cement. The study is divided into two parts. In part 1, Type I Portland cement (OPC) was replaced by RHA or POFA or RS at 0%, 10%, 20%, 30% and 40% by weight of binder. A water to binder ratio (W/B) of 0.35 was used for all paste mixes. The compressive strength, thermogravimetric analysis and pore size distribution of the blended cement pastes were investigated. In part 2, POFA was used to replace ordinary Portland cement at 0%, 10%, 20%, 30% and 40% by weight of binder. A constant water to binder ratio (W/B) of 0.35 was used. The pastes were immersed in 3 % solution for 90 days. After that the total chloride content, free chloride content, microstructure chloride penetration and the chloride penetration of pastes using the finite element program were examined at 90 days immersion in 3% NaCl solution.

The results in part 1 showed that compressive strengths of the pastes due to the hydration reaction decreased with decreasing cement content. The compressive

strengths of the pastes due to the filler effect increased with increasing RS replacement. The compressive strengths of the pastes due to the pozzolanic reaction were nonlinear and increased with increasing fineness of RHA and POFA, cement replacement rate and age of the paste. In addition, the optimum replacement level of RHA and POFA in pastes was 30% by weight of binder. The mass loss (at 30°C-450°C) of the pastes due to the filler effect and the pozzolanic reaction increased with increasing curing time, particle fineness and cement replacement rate as resulted in an increase compressive strength. Moreover, the critical pore size and average pore diameter of the pastes containing RHA and POFA were lower than those of the OPC paste.

The results in part 2 indicated that POFA pastes had a lower chloride diffusion coefficient and concentration profile of free chloride than that of the OPC paste. In addition, relationship between the chloride diffusion coefficient and critical pore diameters is linearly correlated and increases with increasing critical pore diameters. The increasing fineness and replacement of POFA resulted in the decrease of free chloride and of the chloride diffusion coefficient. POFA pastes had a lower peak intensity of Friedel's salt than that of the OPC paste. In addition, the increase in POFA replacement and POFA fineness decreased the peak intensity of Friedel's salt in paste. However, increasing the replacement of cement by palm oil fuel ash resulted in an increasing physically bound chloride.

School of Civil Engineering

Academic Year 2012

Student's Signature _____

Advisor's Signature _____

ACKNOWLEDGEMENTS

I would like to take this opportunity to thank my advisor, Asst. Prof. Dr. Theerawat Sinsiri, and co-advisor, Prof. Dr. Chai Jaturapitakkul, for their guidance, valuable and kind advice, and helpful suggestions. I am also grateful to my committee members, Prof. Dr. Suksun Horpibulsuk, Assoc. Prof. Dr. Sittichai Seangatith and Dr. Nattapong Damrongwiriyanupap, for their constructive evaluation of this thesis. I am thankful to Prof. Dr. Yunping Xi, from the University of Colorado at Boulder, USA, for his valuable suggestions and comments when I was conducting research at the University of Colorado.

I would like to acknowledge the financial support from the Commission on Higher Education of Thailand for a grant under the Strategic Scholarships for Frontier Research Network for the Joint Ph.D. Program, Thai Doctoral degree. Thank also to the Thailand Research Fund (TRF) for financial support under the TRF Senior Research Scholar, Grant No. RTA5380002 and the TRF New Researcher Scholar, Grant No. MRG5280178.

I would also like to thank the Department of Civil Engineering, Rajamangala University of Technology Tawan-ok, and Suranaree University of Technology, Nakorn Ratchasima, Thailand, for providing facilities and equipment for my research.

Finally, I am grateful to my parents and the Kroehong family for their support and encouragement throughout the study period.

Wunchock Kroehong

TABLE OF CONTENTS

	Page
ABSTRACT (THAI).....	I
ABSTRACT (ENGLISH).....	III
ACKNOWLEDGEMENTS	V
TABLE OF CONTENTS.....	VI
LIST OF TABLES.....	XVII
LIST OF FIGURES.....	XVIII
SYMBOLS AND ABBREVEVIATIONS.....	XXVI
CHAPTER	
I INTRODUCTION.....	1
1.1 Statement of problem.....	1
1.2 Objectives.....	5
1.3 Scope of study.....	6
1.4 Outline of the thesis.....	7
1.5 References.....	8
II THEORETICAL BACKGROUND	
AND LITERATURE REVIEW.....	12
2.1 Pozzolanic materials.....	12

TABLE OF CONTENTS (Continued)

	Page
2.2 Study of biomass ash in concrete.....	14
2.2.1 Rice husk ash.....	14
2.2.2 Palm oil fuel ash.....	16
2.3 Effect of mineral admixture on compressive strengths.....	19
2.3.1 Hydration reaction.....	19
2.3.2 Filler effect.....	20
2.3.3 Pozzolanic reaction.....	21
2.4 Pore structure of hardened cement pastes.....	23
2.4.1 Classification of pores in hardened cement pastes.....	23
2.4.2 Factors influencing the pore structure of pastes.....	24
2.4.2.1 Water-to-cement ratio.....	24
2.4.2.2 Curing time.....	26
2.4.2.3 Compressive strength.....	27
2.4.2.4 Temperature.....	28
2.4.2.5 Supplementary cementitious materials.....	29

TABLE OF CONTENTS (Continued)

	Page
2.5 Marine environment.....	31
2.5.1 Submerged zone.....	32
2.5.2 Tidal zone.....	32
2.5.3 Splash zone.....	32
2.5.4 Atmospheric zone.....	32
2.6 Corrosion of steel in concrete.....	33
2.7 Chloride ion penetration of concrete.....	35
2.7.1 Chloride in concrete.....	36
2.7.1.1 Bound chloride.....	37
2.7.1.2 Free chloride.....	38
2.7.1.3 Relationship between bound chloride and free chloride.....	38
2.7.2 Factors affecting chloride resistance.....	39
2.7.2.1 Cement composition.....	39
2.7.2.2 Type of chloride.....	42
2.7.2.3 Water-to-cement ratio.....	42
2.7.2.4 Pore structure.....	43
2.7.2.5 Curing time.....	45

TABLE OF CONTENTS (Continued)

	Page
2.7.2.6 Temperature.....	46
2.7.2.7 Exposure condition.....	46
2.7.2.8 Supplementary cementitious materials.....	47
2.8 Modeling of chloride ingress into cement paste.....	49
2.8.1 Governing equation.....	50
2.8.2 Finite element analysis.....	52
2.9 Summary of the literature review.....	54
2.9.1 Study of biomass ash in concrete.....	54
2.9.2 Effect of mineral admixture on compressive strength.....	55
2.9.3 Pore structure of hardened cement paste.....	55
2.9.4 Chloride ion penetration of concrete.....	56
2.9.5 Modeling of chloride ingress into cement paste.....	56
2.10 Research Framework.....	57
III EXPERIMENTAL PROGRAM.....	68
3.1 Materials.....	69
3.1.1 Cement.....	69
3.1.2 Biomass ash.....	69
3.1.3 Inert material.....	69

TABLE OF CONTENTS (Continued)

	Page
3.2 Method of study.....	69
3.2.1 Mixture proportions of pastes.....	73
3.2.2 List of abbreviations.....	74
3.3 Test program.....	75
3.3.1 Determination of properties of materials.....	75
3.3.2 Determination of compressive strength.....	75
3.3.2.1 Evaluation of the percentage Compressive strength of paste due to the hydration reaction.....	75
3.3.2.2 Evaluation of the percentage compressive strength of paste due to the filler effect.....	76
3.3.2.3 Evaluation of the percentage compressive strength of paste due to the pozzolanic reaction.....	77
3.3.3 Microstructure of the blended cement paste.....	78
3.3.3.1 Thermal analysis.....	78
3.3.3.2 Determination of the porosity of the pastes.....	78

TABLE OF CONTENTS (Continued)

	Page
3.3.4 Chloride penetration into blended cement paste.....	79
3.3.4.1 Total chloride content.....	80
3.3.4.2 Free chloride content.....	81
3.3.5 Microstructure of the blended cement paste	
chloride penetration.....	81
3.3.6 Numerical simulation of the blended cement paste	
chloride penetration.....	82
3.3.6.1 Geometric model.....	83
3.3.6.2 Material parameter.....	83
3.4 References.....	86
IV RESULTS AND DISCUSSIONS.....	88
4.1 Physical properties of materials.....	88
4.2 Chemical and mineralogical analysis.....	92
Part I.....	95
4.3 Compressive strength.....	95
4.4 Assessing the effect of biomass ashes with different	
finenesses on the compressive strength of blended	
cement paste	99

TABLE OF CONTENTS (Continued)

	Page
4.4.1 Influence of cement content on the percentage compressive strength of paste.....	99
4.4.2 Influence of the filler effect on the percentage compressive strength of paste.....	102
4.4.3 Influence of the pozzolanic reaction on the percentage compressive strength of pastes.....	104
4.4.4 Generating an empirical equation for the prediction of the percentage compressive strength of the blended cement paste.....	108
4.4.4.1 Role of the blended cement paste containing biomass ash on the percentage of compressive strength.....	108
4.4.4.2 Verification.....	113
4.5 Effect of biomass ashes fineness on the hydrated Phase of blended cement paste.....	114
4.5.1 Hydrated phase of cement pastes containing rice husk ash and palm oil fuel ash.....	114
4.5.2 Ca(OH) ₂ content.....	119

TABLE OF CONTENTS (Continued)

	Page
4.6 Effect of biomass ashes fineness on the pore size distribution of blended cement paste.....	121
4.6.1 Total porosity of the cement paste.....	121
4.6.2 Effect of rice husk ash and palm oil Fuel ash fineness on the pore size distribution of the pastes.....	123
4.6.3 Effect of rice husk ash and palm oil fuel ash fineness on the average pore diameter of the cement paste.....	129
4.6.4 Relationships between the compressive Strength and total porosity of the pastes.....	130
4.7 Role of filler effect and pozzolanic reaction of biomass ashes on hydrated phase of blended cement paste.....	133
4.7.1 Influence of ground river sand on hydrated phase.....	133
4.7.2 Influence of pozzolanic reaction on hydrated phase.....	135
4.7.3 Relationships between mass losses of C-S-H +C ₂ ASH ₈ +C ₄ AH ₁₃ and compressive strength	140

TABLE OF CONTENTS (Continued)

	Page
4.8 The role of filler effect and pozzolanic reaction of biomass ashes on pore size distribution of blended cement paste.....	141
4.8.1 Influence of filler effect on total porosity.....	141
4.8.2 Influence of pozzolanic reaction on total porosity.....	143
4.8.3 The effect of the pozzolanic reaction on the pore size distribution.....	146
Part II.....	147
4.9 Chloride penetration profile.....	147
4.9.1 Effect of cement type on the chloride penetration profile	147
4.9.2 Effect of palm oil fuel ash on the chloride penetration profile.....	148
4.10 Chloride diffusion coefficient (D_c)	150
4.10.1 Effect of cement type on the chloride diffusion coefficient.....	150
4.10.2 Effect of palm oil fuel ash on the chloride diffusion coefficient.....	151

TABLE OF CONTENTS (Continued)

	Page
4.11 Microstructure of blended cement paste	
chloride penetration.....	155
4.11.1 X-ray diffraction analysis	155
4.11.2 Relationship between chloride diffusion	
coefficient and the critical pore	
diameters of blended cement pastes.....	157
4.12 Concentration of free chloride.....	158
4.12.1 Experimental results.....	158
4.12.2 Numerical results.....	161
4.12.3 Experimental and numerical results.....	165
4.13 References.....	168
V CONCLUSIONS AND RECOMMENDATIONS.....	175
5.1 Conclusions.....	175
5.1.1 PART I Effect of biomass ashes fineness	
on compressive strength and microstructure	
of blended cement paste.....	175
5.1.2 PART II Chloride penetration into blended	
cement paste.....	177
5.2 Recommendations for future work	178

TABLE OF CONTENTS (Continued)

	Page
APPENDICES	
APPENDIX A. Compressive strength of OPC, RS, RHA and POFA pastes.....	179
APPENDIX B. Total chloride of OPC, SRPC and POFA pastes.....	193
APPENDIX C. Free chloride of OPC, SRPC and POFA pastes.....	196
APPENDIX D. Chloride binding of OPC, SRPC and POFA pastes.....	199
APPENDIX E. Modeling of chloride ingress into cement paste.....	202
APPENDIX F. List of publications.....	221
BIOGRAPHY	244

TABLE OF TABLES

Table	Page
2.1 Chemical requirement for pozzolan by ASTM C618.....	13
2.2 Physical requirement for pozzolan by ASTM C618.....	13
2.3 Classification of pores in hydrated cement pastes.....	24
2.4 Empirical models relating the porosity and compressive strength of cement based materials.....	28
3.1 Mixture proportions of pastes in part 1.....	73
3.2 Mixture proportions of pastes in part 2.....	74
4.1 Physical properties of the materials.....	91
4.2 Chemical compositions of the materials.....	93
4.3 Compressive strengths of the pastes.....	97
4.4 Best fit of the pozzolanic constants for the isotherms.....	107
4.5 Total porosity of OPC paste and pastes containing RHA and POFA.....	122
4.6 Ca(OH)_2 content of pastes.....	136
4.7 Material parameter and input data for blended cement paste.....	162

TABLE OF FIGURES

Figure	Page
2.1 Schematic representation of the effects of mineral admixture on compressive strength of mortar.....	19
2.2 DTA-TG thermogram of blended cement paste containing metakaolin; a = CSH, b = C ₂ ASH ₈ , C = C ₂ AH ₁₃ , d = C ₃ AH ₆	22
2.3 Effect of W/C on threshold pore width of cement pastes.....	25
2.4 Relationship between median pore size and compressive strength of the hardened cement pastes.....	26
2.5 Relationship between pore median size and curing time of the hardened cement pastes.....	27
2.6 Effect of curing temperature on pore size distribution of cement paste at 7 days.....	29
2.7 Average pore diameters of blended cement pastes containing metakaolin.....	30
2.8 Exposure classifications in a marine environment.....	31
2.9 Corrosion reactions on steel.....	35

TABLE OF FIGURES (Continued)

Figure	Page
2.10 Diagram type of chloride in concrete.....	36
2.11 Photomicrograph of Friedel's salt.....	37
2.12 Predicted binding data together with the fitted Langmuir adsorption isotherm for a 0.45 w/c ratio.....	41
2.13 Relationship between the diffusion coefficients of chloride ions and the critical pore radius of the paste.....	44
2.14 Relationship between chloride ion diffusion coefficients and critical pore diameter.....	45
2.15 Proposed model results.....	49
3.1 Illustration of material with different particles size in OPC paste.....	71
3.2 Experimental program.....	72
3.3 Immersion of paste specimen in 3% NaCl solution.....	80
3.4 Paste specimens coring and cutting for chloride test.....	81
3.5 Paste sample used for the numerical model.....	83
4.1 Scanning electron micrographs of the materials.....	89
4.2 Particle size distributions of the materials.....	91
4.3 X-ray diffraction patterns of the materials.....	94
4.4 Relationship between the percentage compressive strength of ground river sand paste and age.....	100

TABLE OF FIGURES (Continued)

Figure	Page
4.5 Relationship between the percentage compressive strength of paste due to the hydration reaction and the percentage replacement of CRS.....	100
4.6 Relationships between the percentage compressive strength of paste due to the filler effect and the replacement of river sand (CRS and FRS).....	103
4.7 Relationships between the percentage compressive strength due to the pozzolanic reaction of RHA pastes and age.....	105
4.8 Relationships between the percentage compressive strength due to the pozzolanic reaction of POFA paste and age.....	105
4.9 Relationships between the percentage compressive strengths of blended cement pastes containing CRHA and CPOFA with the same particle size as that of OPC.....	106
4.10 Relationships between the percentage compressive strengths of the blended cement paste containing FRHA and FPOFA with particle sizes smaller than that of OPC.....	112
4.11 Comparison between the predicted and experimental percentage compressive strength of blended cement pastes containing biomass ashes.....	113

TABLE OF FIGURES (Continued)

Figure	Page
4.12 TGA curve results of OPC paste and 20RHA pastes.....	114
4.13 TGA curve results of OPC paste and 40RHA pastes.....	115
4.14 TGA curve results of OPC paste and 20POFA pastes.....	115
4.15 TGA curve results of OPC paste and 40POFA pastes.....	116
4.16 DTG curve results of OPC paste and 20RHA pastes.....	116
4.17 DTG curve results of OPC paste and 40RHA pastes.....	117
4.18 DTG curve results of OPC paste and 20POFA pastes.....	117
4.19 DTG curve results of OPC paste and 40POFA pastes.....	118
4.20 Ca(OH) ₂ content of RHA paste.....	120
4.21 Ca(OH) ₂ content of POFA paste.....	121
4.22 Relationships between the cumulative pore volume and diameter of 20RHA paste.....	124
4.23 Relationships between the cumulative pore volume and pore diameter of 20POFA paste.....	124
4.24 Relationships between the cumulative pore volume and pore diameter of 40RHA paste.....	125

TABLE OF FIGURES (Continued)

Figure	Page
4.25 Relationships between the cumulative pore volume and pore diameter of 40POFA paste.....	125
4.26 Relationships between the differential pore volume and pore diameter of 20RHA paste.....	126
4.27 Relationships between the differential pore volume and pore diameter of 20POFA paste.....	126
4.28 Relationships between the differential pore volume and pore diameter of 40RHA paste.....	127
4.29 Relationships between the differential pore volume and pore diameter of 40POFA paste.....	127
4.30 Relationship between average pore diameter and age.....	130
4.31 Relationships between compressive strength and total porosity of RHA paste.....	132
4.32 Relationships between compressive strength and total porosity of POFA paste.....	132
4.33 TGA curve results of OPC paste and RS pastes.....	134
4.34 Ca(OH) ₂ content of OPC paste and RS pastes.....	134
4.35 Reduction of Ca(OH) ₂ content of CRHA and CPOFA pastes.....	137
4.36 Reduction of Ca(OH) ₂ content of FRHA and FPOFA pastes.....	137

TABLE OF FIGURES (Continued)

Figure	Page
4.37 TGA curve results of CRS, CRHA and CPOFA pastes.....	138
4.38 TGA curve results for OPC, FRHA and FPOFA pastes.....	138
4.39 Mass losses of $C-S-H+C_2ASH_8+C_4AH_{13}$ and compressive strength of paste at 90 days.....	141
4.40 Total porosity of OPC and RS pastes.....	142
4.41 Total porosity of OPC, CRS and CRHA pastes.....	144
4.42 Total porosity of the OPC, CRS and CPOFA pastes.....	144
4.43 Total porosity of the OPC, FRS and FRHA pastes.....	145
4.44 Total porosity of the OPC, FRS and FRHA pastes.....	145
4.45 Average pore diameters with curing.....	147
4.46 Chloride penetration profile of Portland cement type I (OPC) and V (SRPC) cement paste at 90 days immersion in 3% NaCl solution.....	148
4.47 Chloride penetration profile of OPC paste and POFA pastes at 90 days immersion in 3% NaCl solution.....	149

TABLE OF FIGURES (Continued)

Figure	Page
4.48 Chloride diffusion coefficient of Portland cement type I (OPC) and V (SRPC) cement paste at 90 days immersion in 3% NaCl solution.....	151
4.49 Chloride diffusion coefficients of OPC paste and POFA pastes at 90 days immersion in 3% NaCl solution.....	153
4.50 Effect of palm oil fuel ash fineness on chloride diffusion coefficients of blended cement paste at 90 days immersion in 3% NaCl solution.....	154
4.51 X-ray diffraction patterns of pastes at 90 days immersion in 3% NaCl solution F = Friedel's salt.....	155
4.52 Relationships between the diffusion coefficients of chloride ion and the critical pore diameters of blended cement paste.....	158
4.53 Free chloride of Portland cement type I and V cement paste at 90 days immersion in 3% NaCl solution.....	159
4.54 Free chloride of of OPC paste and POFA pastes at 90 days immersion in 3% NaCl solution	160
4.55 Finite element models for chloride penetration of paste specimen	162
4.56 Numerical results of OPC and SRPC paste at 90 days immersion in 3% NaCl solution.....	163

TABLE OF FIGURES (Continued)

Figure	Page
4.57 Numerical results of CPOFA pastes at 90 days immersion in 3% NaCl solution.....	163
4.58 Numerical results of FPOFA pastes at 90 days immersion in 3% NaCl solution.....	164
4.59 Comparision numerical results of OPC and SRPC paste at 90 days immersion in 3% NaCl solution.....	165
4.60 Comparision numerical results of CPOFA pastes at 90 days immersion in 3% NaCl solution.....	166
4.61 Comparision numerical results of FPOFA paste at 90 days immersion in 3% NaCl solution.....	167



SYMBOLS AND ABBREVIATIONS

$AgNO_3$	=	Silver nitrate
$AASHTO$	=	American association of state highway and transportation officials
$ASTM$	=	American society for testing materials
Al_2O_3	=	Aluminum trioxide
$BRHA$	=	Black rice husk ash
C	=	Coarse
$CaCl_2$	=	Calcium chloride
CaO	=	Calcium oxide
$CaCO_3$	=	Calcium carbonate
$Ca(OH)_2$	=	Calcium hydroxide
C_b	=	Bound chloride
C_f	=	Free chloride
c_f	=	Nodal free chloride concentration
CH	=	Calcium hydroxide
C_{ic}	=	Compressive strength of the paste containing inert material with the same particle size of cement
Cl	=	Chloride ions

SYMBOLS AND ABBREVIATIONS (continued)

C_o	=	Chloride concentration at paste surface
C_{opc}	=	Compressive strength of OPC paste
$CPOFA$	=	Coarse palm oil fuel ash
$CRHA$	=	Coarse ground rice husk ash
CRS	=	Coarse ground river sand
Cr	=	Critical pore radius of the paste
C_s	=	Specific heat
C_T	=	Total chloride
$C(x, t)$	=	Total chloride concentration (% by weight of binder) at depth x and exposure time t
C_3A	=	Tricalcium aluminate
C_4AF	=	Tetracalcium aluminoferrite
C_2S	=	Dicalcium silicate
C_3S	=	Tricalcium silicate
$C-S-H$	=	Calcium silicate hydrate
$C-A-S-H$	=	Calcium aluminum silicate hydrate
C_2ASH_8	=	Calcium aluminum silicate hydrate
C_4AH_{13}	=	Calcium aluminate hydrate
$C-A-H$	=	Calcium aluminate hydrate

SYMBOLS AND ABBREVIATIONS (continued)

C°	=	Degree celsius
[C]	=	Capacitance matrix
D_c	=	Chloride diffusion coefficient
d_c	=	Critical pore diameter of the paste
DTG	=	Derivative thermogravimetric analysis
DTA	=	Differential thermal analysis
d_{50}	=	Median particle size
[D]	=	Chloride diffusion coefficient matrix
F	=	Fine
$FeCl_2$	=	Ferric chloride
FEM	=	Finite element method
Fe^{2+}	=	Ferrous ions
Fe_2O_3	=	Iron oxide
$Fe(OH)_2$	=	Ferrous hydroxide
FPOFA	=	Fine ground palm oil fuel ash
FRHA	=	Fine ground rice husk ash
FRS	=	Fine ground river sand
GGBS	=	Ground granulated blast furnace slag

SYMBOLS AND ABBREVIATIONS (continued)

HCl	=	Hydrogen chloride
H_2O	=	Water
J_c	=	Chloride flux
K	=	Potassium
k_x	=	Thermal conductivity in global x direction
[K]	=	Conduction matrix
K_2O	=	Potassium oxide
LOI	=	Loss on ignition
M	=	Molar
$MgCl_2$	=	Magnesium chloride
MgO	=	Magnesium oxide
MIP	=	Mercury intrusion porosimetry
$NaCl$	=	Sodium chloride
Na	=	Sodium
Na_2O	=	Sodium oxide
N_c	=	Shape function
[N]	=	Element shape functions
nm	=	Nanometer
OH^-	=	Hydroxyl ions
O_2	=	Oxygen
OPC	=	Ordinary Portland cement

SYMBOLS AND ABBREVIATIONS (continued)

p	=	Porosity
$P_{b,(p,s,t)}$	=	Percentage compressive strength of the paste containing RHA or POFA compared with OPC paste
P_F	=	Percentage compressive strength of the paste due to the filler effect
PEA	=	Pulverized fuel ash
P_H	=	Percentage compressive strength of the paste due to the hydration reaction
$P_{i,(p,s,t)}$	=	Percentage compressive strength of the paste containing inert material compared with OPC paste
$P_{if(p,t)}$	=	Percentage compressive strength of the paste containing inert material with high fineness compared with OPC paste
$P_{ic,(p,t)}$	=	Percentage compressive strength of the paste containing inert material with the same particle size as the cement compared with OPC paste
$POFA$	=	Ground palm oil fuel ash
$P_{PZ,t}$	=	Percentage compressive strength of the paste due to the pozzolanic reaction
Q	=	Heat generation
R	=	Percentage replacement of RS or RHA or POFA
RTA	=	Roads and traffic authority

SYMBOLS AND ABBREVIATIONS (continued)

<i>RCPT</i>	=	Rapid chloride penetration testing
<i>RMT</i>	=	Rapid migration testing
<i>RHA</i>	=	Ground rice husk ash
<i>RS</i>	=	Ground river sand
<i>SCM</i>	=	Supplementary cement materials
<i>SEM</i>	=	Scanning electron microscope
<i>SF</i>	=	Silica fume
<i>SiO₂</i>	=	Silicon dioxide
<i>SO₃</i>	=	Sulfur trioxide
<i>SRPC</i>	=	Sulfate resistance Portland cement
<i>T</i>	=	Temperature
<i>TGA</i>	=	Thermogravimetric analysis
<i>t</i>	=	Curing time
<i>x</i>	=	Depth of paste measured from the surface
<i>W/B</i>	=	Water to binder ratio
<i>W/C</i>	=	Water to cement ratio
<i>XRD</i>	=	X-ray diffraction
<i>XRF</i>	=	X-ray fluorescence
<i>4Fe(OH)₃</i>	=	Ferric hydroxide
σ	=	Compressive strength at porosity <i>p</i>
σ_0	=	Compressive strength at zero porosity

SYMBOLS AND ABBREVIATIONS (continued)

α, β	=	Pozzolanic constants
μm	=	Micrometre
$\frac{\partial C_f}{\partial C_T}$	=	Chloride binding capacity
ΔF_p	=	Filler effect
ΔP_p	=	Pozzolanic reaction



CHAPTER I

INTRODUCTION

1.1 Statement of problem

Long-term durability of reinforced concrete structures in marine environments and from de-icing salts are problems mainly because of sulfate attack and the corrosion of the steel under chloride attack. The chloride-induced corrosion of embedded reinforcement is one of the most severe durability problems for concrete structures in a marine environment. Initially, steel embedded in concrete has a thin passive film on its surface that prevents the steel from further corroding. Chloride-induced corrosion begins when the concentration of chloride at the steel bars reaches a threshold value that destroys the protective film layer. This degradation mechanism leads to a series of structural problems, such as a reduction in the cross-sectional area of the reinforcement, cracking, delamination of the concrete cover, and weakening of the steel concrete bond, thereby reducing the load carrying capacity of the reinforced concrete structure (Bastidas-Arteaga et al., 2011; Marsavina et al., 2009; Martin-Perez et al., 2000). To solve this problem, many supplementary cement materials (SCMs) have been suggested; for example, fly ash, ground granulated blast furnace slag, silica fume, and metakaolin have been found to be beneficial in resisting the ingress of chloride ions into concrete. This resistance is caused by the microstructure densification imparted by the pozzolanic reaction or secondary reaction from these

materials. In addition, concrete containing pozzolan has a lower average pore size and critical pore size than that of control concrete (Li and Ding, 2003).

Numerous studies have utilized by-product materials such as fly ash, rice husk ash, palm oil fuel ash, and bagasse ash as pozzolans to reduce the cement content in mixtures. Rice husk ash (RHA) is a waste material from electricity generation power plants. In Thailand, the annual production of RHA has been approximated at 1.6 million tons (Wansom et al., 2010). Several researchers have shown that the main chemical composition of rice husk is silicon dioxide (SiO_2) and has the highest amorphous silica content when the rice husk ash is burnt between 500-700°C (de Sensale et al., 2008; Nair et al., 2008). Thus, RHA is a pozzolanic material and can be used as a SCM, replacing Portland cement Type I by up to 30% by weight of binder (Chatveera and Lertwattanakul, 2009; Ganesan et al., 2008). Rukzon et al. (2009) have found that rice husk ash with high fineness improves the compressive strength and reduces the porosity of concrete. Studies have also shown that the use of RHA as a partial replacement for Type I Portland cement improves the water permeability (Givi et al., 2010) and chloride penetration (Chindaprasirt et al., 2008b) of concrete.

POFA is a by-product from biomass thermal power plants where palm oil residues are burned to generate electricity. More than 100,000 tons of POFA are produced every year in Thailand (Chindaprasirt et al., 2007). POFA is rarely utilized, and disposing of this waste may lead to future environmental problems. Many researchers have studied the use of POFA as a partial replacement of cement in concrete. The main chemical constituent of POFA is silicon dioxide (Chindaprasirt et al., 2008a; Tangchirapat et al., 2007). Tangchirapat et al. (2007) found that ground

POFA is a good pozzolanic material and can be used to replace Portland cement by up to 30% by binder weight of binder. Sata et al. (2004) showed that POFA with a high fineness exhibits an excellent pozzolanic reaction and can be used as a supplementary material to produce high-strength concrete. In addition, the use of POFA can improve concrete strength and water permeability (Chindaprasirt et al., 2007). Furthermore, the partial replacement of OPC with POFA assists in the sulfate (Tangchirapat et al., 2009) and chloride (Chindaprasirt et al., 2008a) penetration resistance of concrete.

Cyr et al. (2006) reported that the effect of mineral admixtures on compressive strength is comprised of three factors. First, the strength is proportional to the amount of cement in the mixture, an effect known as the dilution effect. Second, the fineness and amount of the powder also affect the strength by contributing to the nucleation and packing effects. The nucleation effect accelerates the hydration process and makes the paste more homogeneous. The packing effect is a suitable arrangement of small particles that fill the voids of the paste and increases the compressive strength. Finally, a pozzolanic reaction occurs between Ca(OH)_2 and the SiO_2 and Al_2O_3 from pozzolanic materials, producing calcium silicate hydrate C-S-H (Goldman and Bentur, 1993; Gopalan, 1993; Isaia et al., 2003; Kiattikomol et al., 2000). Many researchers have studied this pozzolanic reaction using ASTM C618, strength activity index ASTM C311, X-ray diffraction (XRD), thermogravimetric analysis (TGA), and chemical titration. Tangpagasit et al. (2005) have examined the use of river sand (as an inert material) as a replacement for Portland cement type I to evaluate the packing effect and pozzolanic reaction of fly ash in mortar. They found that river sand is an inert material and the packing effect is not dependent on the age of the mortar but

rather on the particle size, while the pozzolanic reaction depends on the fineness and age of the mortar.

Previous studies have already reported the influence of RHA and POFA finenesses on compressive strength and observed that the ash with median particle larger than OPC (~15 μm) can be used to replace OPC at 10% while smaller size than OPC can be replaced at 20% to 30% by weight of binder (Ganesan et al., 2008; Tangchirapat and Jaturapitakkul, 2010). However, separation influences of hydration reaction, filler effect and pozzolanic reaction on compressive strength and microstructure of blended cement pastes have not been well defined. In addition, a few researches presented chloride penetration of the blended cement pastes. If a by-product material from biomass plants can be used as a cement replacement in concrete, it will help to reduce energy due to reducing the production of cement clinker and reduce the volume of waste disposed in landfills.

1.2 Objectives

The objectives of this study are:

- 1.2.1 To investigate the effect of biomass ashes with different finenesses on the compressive strength, hydrate phase, and pore size distribution of blended cement paste
- 1.2.2 To establish an empirical model to predict the percentage compressive strength of paste due to the hydration reaction, filler effect, and pozzolanic reaction of blended cement paste
- 1.2.3 To investigate the chloride penetration profile and microstructure of blended cement paste containing POFA with different finenesses under chloride penetration
- 1.2.4 To investigate free chloride penetration by comparing the experimental chloride concentration with the numerical concentration obtained using finite element analysis

1.3 Scope of study

The materials used in this study consisted of Type I and V Portland cements (OPC), rice husk ash (RHA), palm oil fuel (POFA), and inert material (RS). The RHA, POFA and RS were ground to two different sizes. For the first fineness, RHA, POFA, and RS were ground using a grinding machine to have the same particle size as that of OPC. For the second fineness, RHA, POFA, and RS were ground to have a finer particle size than that of cement. Ground RHA, POFA, and RS were used to partially replace Type I Portland cement by 0%, 10%, 20%, 30% and 40% by weight of binder. A water-to-binder (W/B) ratio of 0.35 was used for all mixtures.

The specimens were tested for compressive strength after 7, 28, 60 and 90 days to establish an empirical model to predict the compressive strength of the paste as a result of the hydration reaction, filler effect, and the pozzolanic reaction of the RHA and POFA. In addition, the blended cement pastes containing 20% and 40% of RHA, POFA, and RS were tested by thermogravimetric analysis, and their pore size distributions were measured. Furthermore, pastes containing 10%, 20%, 30% and 40% of POFA were used to obtain chloride penetration profiles. Finally, a numerical model was established and used to estimate the free chloride penetration, and the experimental chloride concentration was compared with the numerical chloride concentration obtained using the FEM program ABAQUS.

1.4 Outline of the thesis

This thesis composed of five chapters. The first chapter presented the introduction of the study, the statement of problem, the objective, and the scope of the study. The theoretical background and literature review is shown in Chapter 2. Chapter 3 introduces the experimental program and all parameter that used in this study. In Chapter 4, results of the study are determined and discussed. Finally, the conclusions and suggestions from this study are presented in Chapter 5.



1.5 References

- Bastidas-Arteaga, E., Chateauneuf, A., Synchez-Silva, M., Bressolette, P., and Schoefs, F. (2011). A comprehensive probabilistic model of chloride ingress in unsaturated concrete. **Engineering Structures**. 33(3): 720-730.
- Chatveera, B., and Lertwattanaruk, P. (2009). Evaluation of sulfate resistance of cement mortars containing black rice husk ash. **Journal of Environmental Management**. 90(3): 1435-1441.
- Chindaprasirt, P., Homwuttiwong, S., and Jaturapitakkul, C. (2007). Strength and water permeability of concrete containing palm oil fuel ash and rice husk-bark ash. **Construction and Building Materials**. 21(7): 1492-1499.
- Chindaprasirt, P., Rukzon, S., and Sirivivatnanon, V. (2008a). Effect of carbon dioxide on chloride penetration and chloride ion diffusion coefficient of blended Portland cement mortar. **Construction and Building Materials**. 22(8): 1701-1707.
- Chindaprasirt, P., Rukzon, S., and Sirivivatnanon, V. (2008b). Resistance to chloride penetration of blended Portland cement mortar containing palm oil fuel ash, rice husk ash and fly ash. **Construction and Building Materials**. 22(5): 932-938.
- Cyr, M., Lawrence, P., and Ringot, E. (2006). Efficiency of mineral admixtures in mortars: Quantification of the physical and chemical effects of fine admixtures in relation with compressive strength. **Cement and Concrete Research**. 36(2): 264-277.

- De Sensale, G. R., Ribeiro, A. B., and Gonçalves, A. (2008). Effects of RHA on autogenous shrinkage of Portland cement pastes. **Cement and Concrete Composites**. 30(10): 892-897.
- Ganesan, K., Rajagopal, K., and Thangavel, K. (2008). Rice husk ash blended cement: Assessment of optimal level of replacement for strength and permeability properties of concrete. **Construction and Building Materials**. 22(8): 1675-1683.
- Givi, A. N., Rashid, S. A., Aziz, F. N. A., and Salleh, M. A. M. (2010). Assessment of the effects of rice husk ash particle size on strength, water permeability and workability of binary blended concrete. **Construction and Building Materials**. 24(11): 2145-2150.
- Goldman, A., and Bentur, A. (1993). The influence of microfillers on enhancement of concrete strength. **Cement and Concrete Research**. 23(4): 962-972.
- Gopalan, M. K. (1993). Nucleation and pozzolanic factors in strength development of class F fly ash concrete. **ACI Materials Journal**. 90(2): 117-121.
- Isaia, G. C., Gastaldini, A. L. G., and Moraes, R. (2003). Physical and pozzolanic action of mineral additions on the mechanical strength of high-performance concrete. **Cement and Concrete Composites**. 25(1): 69-76.
- Kiattikomol, K., Jaturapitakkul, C., and Tangpagasit, J. (2000). Effect of insoluble residue on properties of Portland cement. **Cement and Concrete Research**. 30(8): 1209-1214.
- Li, Z., and Ding, Z. (2003). Property improvement of Portland cement by incorporating with metakaolin and slag. **Cement and Concrete Research**. 33(4): 579-584.

- Marsavina, L., Audenaert, K., De Schutter, G., Faur, N., and Marsavina, D. (2009). Experimental and numerical determination of the chloride penetration in cracked concrete. **Construction and Building Materials**. 23(1): 264-274.
- Martin-Perez, B., Zibara, H., Hooton, R. D., and Thomas, M. D. A. (2000). A study of the effect of chloride binding on service life predictions. **Cement and Concrete Research**. 30(8): 1215-1223.
- Nair, D. G., Fraaij, A., Klaassen, A. A. K., and Kentgens, A. P. M. (2008). A structural investigation relating to the pozzolanic activity of rice husk ashes. **Cement and Concrete Research**. 38(6): 861-869.
- Rukzon, S., Chindaprasirt, P., and Mahachai, R. (2009). Effect of grinding on chemical and physical properties of rice husk ash. **International Journal of Minerals, Metallurgy and Materials**. 16(2): 242-247.
- Sata, V., Jaturapitakkul, C., and Kiattikomol, K. (2004). Utilization of palm oil fuel ash in high-strength concrete. **Journal of Materials in Civil Engineering**. 16(6): 623-628.
- Tangchirapat, W., and Jaturapitakkul, C. (2010). Strength, drying shrinkage, and water permeability of concrete incorporating ground palm oil fuel ash. **Cement and Concrete Composites**. 32(10): 767-774.
- Tangchirapat, W., Jaturapitakkul, C., and Kiattikomol, K. (2009). Compressive strength and expansion of blended cement mortar containing palm oil fuel ash. **Journal of Materials in Civil Engineering**. 21(8): 426-431.

- Tangchirapat, W., Saeting, T., Jaturapitakkul, C., Kiattikomol, K., and Siripanichgorn, A. (2007). "Use of waste ash from palm oil industry in concrete. **Waste Management**. 27(1): 81-88.
- Tangpagasit, J., Cheerarot, R., Jaturapitakkul, C., and Kiattikomol, K. (2005). Packing effect and pozzolanic reaction of fly ash in mortar. **Cement and Concrete Research**. 35(6): 1145-1151.
- Wansom, S., Janjaturaphan, S., and Sinthupinyo, S. (2010). Characterizing pozzolanic activity of rice husk ash by impedance spectroscopy. **Cement and Concrete Research**. 40(12): 1714-1722.



CHAPTER II

THEORETICAL BACKGROUND AND LITERATURE REVIEW

This chapter provides the theoretical background and literature review of pozzolanic materials, the effect of mineral admixtures on compressive strength, the pore structure of hardened cement paste, the corrosion of steel in concrete, chloride ion penetration of concrete, the modeling of chloride ingress into cement paste, and use of biomass ash as a supplementary cementitious material.

2.1 Pozzolanic materials

A pozzolan is defined by ASTM C125 as a siliceous and aluminous material that, in itself, possesses little or no cementitious value but, in finely divided form and in the presence of moisture, will chemically react with calcium hydroxide at ordinary temperatures to form compounds possessing cementitious properties.

As seen in Tables 2.1 and 2.2, depending on their chemical compositions and physical properties, pozzolanic materials can be classified into three classes, according to ASTM C 618 (2001): Class N, Class F and Class C. Pozzolanic materials have been widely used as cement replacements in concrete because they have the advantages of cost reduction, heat reduction in concrete, increased durability, a decrease in concrete drying shrinkage, and a reduction in the amount of cement used.

Table 2.1 Chemical requirement for pozzolan by ASTM C 618

Chemical requirement	Class		
	N	F	C
SiO ₂ + Al ₂ O ₃ + Fe ₂ O ₃	>70.0	>70.0	50
Sulfur trioxide (SO ₃), max %	4.0	5.0	5.0
Moisture content, max %	3.0	3.0	3.0
Loss on ignition (LOI), max %	10.0	6.0	6.0

Table 2.2 Physical requirement for pozzolan by ASTM C 618

Chemical requirement	Class		
	N	F	C
Fineness:			
Amount retained when wet sieved on 45 µm (No 325), max, %	34	34	34
Strength activity index			
- At 7 days, min, percent of control	75	75	75
- At 28 days, min, percent of control	75	75	75
Water requirement, max, percent of control	115	105	105
Soundness:			
- Autoclave expansion or contraction, max, %	0.8	0.8	0.8
Strength activity index			
- Density, max variation from average, %	5	5	5
- Percentage retained on 45 µm (No 325), max variation percentage point from average	5	5	5

2.2 Study of biomass ash in concrete

Biomass ash is a by-product obtained from biomass power plants. Many researchers have studied the use of biomass ashes such as rice husk ash, bagasse ash, and palm oil ash as constituents in concrete (Chusilp et al., 2009; Rukzon and Chindaprasirt, 2008; Sata et al., 2004). The result indicated that biomass ashes with high fineness are excellent pozzolanic material and can be used as a cement replacement in concrete.

2.2.1 Rice husk ash

Rice husk ash (RHA) is a by-product of electricity generation in biomass power plants. It can be estimated that 1,000 kg of rice grain produces approximately 200 kg of rice husk, of which 20%, or 40 kg, becomes RHA (Mehta, 1977). Mehta (1977) reported that RHA is a highly reactive pozzolan and consists of a high amount of amorphous SiO_2 that could contribute to a higher compressive strength than a Portland cement control. In Thailand, the annual production of RHA has been approximated at 1.6 million (Wansom et al., 2010). Several researchers have shown that the main chemical composition of rice husk is SiO_2 , which has the highest amount of amorphous silica burnt between 500-700°C (de Sensale et al., 2008; Nair et al., 2008).

Zhang and Malhotra (1996) found that due to the highly pozzolanic nature of RHA, it could be used as a supplementary cementing material to produce high-performance concrete. These results agree with Ismail and Waliuddin (1996) who reported that the compressive strength increased by more than 80 MPa as compared to high strength concrete when replacing 10% of the Portland cement with RHA.

Ganesan et al. (2008) studied the optimal level of replacement for strength and permeability properties of concrete. The results indicated that the compressive strength and splitting tensile strength of concrete with 30% RHA were higher than that of the control concrete. In addition, concretes containing up to 35% RHA had a lower coefficient of water absorption than that of the control concrete. This result is due to the pozzolanic reaction and pore refinement resulting from the finer particles of RHA in the concrete. Chindapasirt et al. (2008) studied the resistance to chloride penetration of blended Portland cement mortar containing rice husk ash. The 100 mm diameter x 50 mm height epoxy-coated specimens was conditioned, and at the age of 28 days, rapid chloride penetration testing (RCPT) was conducted in accordance with the method described in ASTM C1202. Further, the specimens were immersed in a 3% NaCl solution and kept immersed for 30 days. Chloride penetration depths were tested using a 0.1 M AgNO₃ solution in accordance with RTA T263. They found that RHA can be used as a pozzolan material to replace part of the Portland cement to produce a mortar with high strength and good resistance to chloride penetration.

Chatveera and Lertwattanaruk (2011) studied the durability of concrete containing rice husk ash. They concluded that black rice husk ash can be classified as a pozzolanic material of type N. The autogenous shrinkage of the concrete with BRHA is lower than that of OPC concrete and decreases with an increasing percentage of replacement (from 20% to 40%) of BRHA. In addition, the BRHA provides a positive effect on weight loss for concrete exposed to hydrochloric and sulfuric acid attack.

2.2.2 Palm oil fuel ash

Palm oil fuel ash has been found to have a low pozzolanic reaction rate, and 10% POFA can be used as a cement replacement in concrete (Awal and Hussin, 1997; Tay, 1990). The large particle and porous structure results in a very low rate of the pozzolanic reaction. Later, Sata et al. (2004) investigated the utilization of POFA in high-strength concrete. They found that high-strength concrete can be produced by using ground POFA to replace Type I Portland cement by up to 30% by weight of binder. At 28 days, the compressive strength of concretes containing 10%, 20% and 30% POFA were 81.3, 85.9 and 79.8 MPa, respectively. Concrete containing 20% POFA had the highest strength. This is slightly higher than that of concrete containing 5% condensed silica fume and was 92-94% of the strength of 10% condensed silica fume concrete. In addition, Sata et al. (2007) found that the use of POFA to partially replace Type I Portland cement has no significant effect on the splitting tensile strength and modulus of elasticity as compared with the properties of the control concrete or silica fume concrete. This result suggests that POFA can be used to substitute Portland cement to produce high-strength concrete without altering the mechanical properties of concrete.

Tangchirapat et al. (2007) studied the use of waste ash from the palm oil industry in concrete. Type I Portland cement was replaced by POFA at 10%, 20%, 30% and 40% by weight of binder. They found that the compressive strength of the concrete containing the original size POFA with median particle size, d_{50} , of 183.0 μm was lower than that of the control concrete. This result can be explained by POFA having large particles with high porosity, which reduces the compressive strength. The replacement of Type I Portland cement by 10% POFA with d_{50} of 15.9 μm and

20% POFA with d_{50} of 7.4 μm at 90 days resulted in a higher compressive strength than that of the control concrete. The high fineness of the POFA, which led to a larger pozzolanic reaction and resulted in small particles that could fill in the voids of the concrete mixture, led to an increase in the compressive strength of the concrete. The results are similar to the findings of other researchers (Chindaprasirt et al., 2005; Chindaprasirt et al., 2007b; Isaia et al., 2003). In addition, when concrete is immersed in a 5% magnesium sulfate solution for 364 days, the concrete mixed with 30% POFA of high fineness (d_{50} of 7.4 μm) had the same expansion level as that of the control Type V concrete. This result suggests that the optimum replacement level of Type I Portland cement by high fineness POFA is 30%.

Chindaprasirt et al. (2007a) investigated the permeability of concrete containing POFA. They found that the compressive strength of concrete containing 20% ground POFA was higher than that of the control concrete and decreases with an increase in the replacement percentage. In addition, the 20% and 40% POFA concretes had lower permeability than the control concrete, and the permeability was dependent on the cement replacement ratio and the age of concretes. Later, Tangchirapat and Jaturapitakkul (2010) studied the effect of POFA fineness on permeability and the drying shrinkage of concrete. It was found that the use of 10-30% of high fineness POFA (with a median particle size smaller than OPC) as a cement replacement in concrete reduces the water permeability and drying shrinkage of concrete. This result is due to the pozzolanic reaction and packing effect of small particles, which produced concrete with a denser matrix (Mehta, 1985). where the pore structure was transformed from coarser to finer pores (Li and Ding, 2003).

Chindaprasirt et al. (2008) studied the resistance to chloride penetration of blended cement mortar containing POFA. Rapid chloride penetration testing (RCPT), rapid migration testing (RMT), and chloride penetration depth testing was conducted after 30 days of immersion in a 3% NaCl solution of mortar. The results indicated that POFA can be used to improve the resistance to chloride penetration and that it is more effective than fly ash. Afterwards, Chindaprasirt et al. (2011) found that a 30% replacement level of POFA produces high-strength and high-workability concrete with good resistance to both chloride penetration and corrosion.

Sata et al. (2010) studied the compressive strength and heat evolution of concrete containing POFA. The temperature rise of fresh concrete decreased as the ground POFA content increased. This result can be explained by a reduction in the amount of cement in concrete, causing a reduction of heat due to hydration. Moreover, concrete containing 30% of ground POFA had the smallest temperature rise. This result agreed with the findings of (Chusilp et al., 2009), who found that the maximum temperature rise for concrete containing ground bagasse ash was lower than for the control concrete.

Currently, the amount of RHA and POFA produced from biomass power plants increases annually, while its reuse remains negligible. It is expected that the use of these ashes in concrete will improve the strength and durability of concrete while reducing the amount of RHA and POFA being disposed as waste in landfills and leading to environmental problems.

2.3 Effect of mineral admixture on compressive strengths

When pozzolan materials such as fly ash silica fume or agro-waste ash are used to partially replace cement, the compressive strength of the cement paste or mortar is attributed to three factors: the hydration reaction, the filler effect, and the pozzolanic reaction as shown in Figure 2.1.

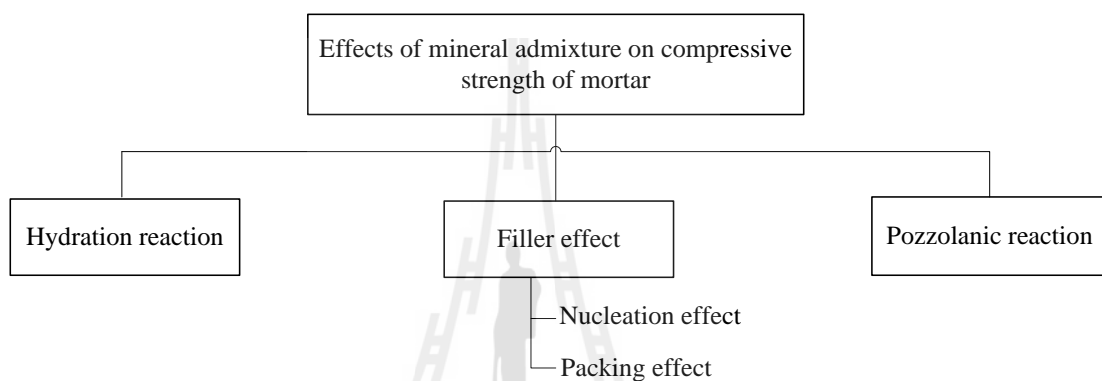
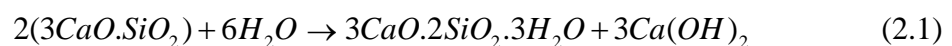


Figure 2.1 Schematic representation of the effects of mineral admixture on compressive strength of mortar (Cyr et al., 2006)

2.3.1 Hydration reaction

The hydration reaction is the reaction between Portland cement and water. The chemical reactions of pure cement compounds have been described by (Mindress and Young 1981) as follows:



The hydration of tricalcium silicate ($3\text{CaO}\cdot\text{SiO}_2$) and dicalcium silicate ($2\text{CaO}\cdot\text{SiO}_2$) produces calcium silicate hydrates (C-S-H) and calcium hydroxide $\text{Ca}(\text{OH})_2$. C-S-H is the main product of Portland cement hydration; its presence increases with increasing curing time and results in an increase in the compressive strength.

2.3.2 Filler effect

The filler effect is the proper arrangement of small particles to fill voids and contributes to an increase in compressive strength without any chemical reaction (Chindaprasirt et al., 2011; Jaturapitakkul et al., 2011; Tangpagasit et al., 2005). These results are due to nucleation and the packing effect. When Portland cement was partially replaced by the small particle sized ash, there was a dispersion of cement particles. Thus, they are able to accelerate the hydration production and make the paste more homogeneous. The packing effect is exhibited as small particles that fill the voids of the paste, allowing for denser packing within the material particles and the matrix phase (Cyr et al., 2006; Isaia et al., 2003; Sata et al., 2010).

Jaturapitakkul et al. (2011) studied the filler effect of different particles on the compressive strength of mortar. Type I Portland cement was partially replaced by ground river sand, which is a non-reactive material (Kiattikomol et al., 2000). The results showed that the compressive strengths of the mortars containing inert material are almost constant and independent of the age of the mortar. In addition, the compressive strength of mortars containing inert material with smaller particle OPC is 2.7-5.8% of the control mortar.

2.3.3 Pozzolanic reaction

A pozzolanic reaction is the reaction of Ca(OH)_2 with the SiO_2 and Al_2O_3 from pozzolanic materials, which produces an increase in calcium silicate hydrate C-S-H (Goldman and Bentur, 1993; Gopalan,1993; Isaia et al., 2003; Kiattikomol et al., 2000)

Billong et al. (2011) studied the pozzolanic reaction of paste containing metakaolin. They found that amorphous silica reacted with Ca(OH)_2 to form calcium silicate hydrates. The reaction can be illustrated by Equations (2.3) and (2.4). According to the chemistry of cement conventions, $\text{C}=\text{CaO}$, $\text{S}=\text{SiO}_2$, $\text{A}=\text{Al}_2\text{O}_3$ and $\text{H}=\text{H}_2\text{O}$. In addition, the DTA/TG thermogram of blended cement paste containing metakaolin is shown in Figure 2.2. The DTA curve of C-S-H and C_2ASH_8 was recorded at 120°C and at $170\text{-}200^\circ\text{C}$, respectively. Similar results have also been reported by others (Barbhuiya et al., 2009; Nochaiya et al., 2009). These researchers reported that the DTG curve of C-S-H, C_2ASH_8 , and Ca(OH)_2 was detected at $105\text{-}110^\circ\text{C}$, $155\text{-}183^\circ\text{C}$ and $448\text{-}475^\circ\text{C}$, respectively.



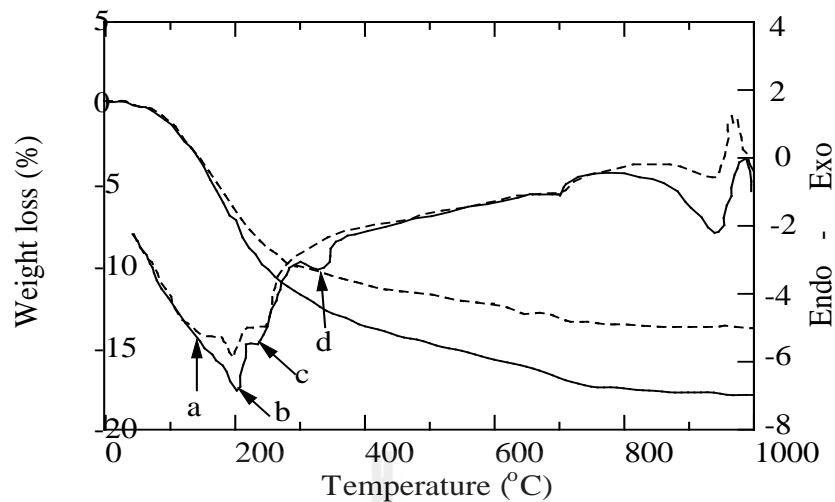


Figure 2.2 DTA-TG thermogram of blended cement paste containing metakaolin;

a=CSH, b=C₂ASH₈, C=C₂AH₁₃, and d=C₃AH₆ (Billong et al., 2011)

Poon et al. (2001) studied the rate of the pozzolanic reaction of metakaolin in cement paste. They found that the Ca(OH)₂ content in OPC paste indicates the degree of hydration of the cement, while the Ca(OH)₂ consumption in blended cement paste is related to the degree of the pozzolanic reaction. In addition, metakaolin had higher reactivity than fly ash due to the high surface area of metakaolin. The results are similar to the study by (Chindaprasirt et al., 2007b), who found that the blended cement paste containing classified fly ash showed a lower Ca(OH)₂ than that with the original fly ash. This is due to the high fineness, which had more surface area to provide the silica and alumina compound with higher pozzolanic activity than the original fly ash. Thus, blended cement paste becomes more homogenous and results in denser paste. These results confirm that finer pozzolans created a greater pozzolanic reaction and allowed the small particles to fill in voids in the mortar mixture, thereby increasing the compressive strength (Isaia et

al., 2003). The factors contributing to good pozzolanic reaction of pozzolan materials are a low unburnt carbon content and a high amorphous SiO_2 content.

From the literature review, many researchers have reported that pozzolan materials are used to partially replace cement and that the compressive strength of cement paste or mortar is attributed to three factors: the hydration reaction, the filler effect, and the pozzolanic reaction. However, the influence of each of these three factors on the compressive strength of blended cement pastes has not yet been well defined.

2.4 Pore structure of hardened cement pastes

The pore structure (e.g. total porosity, pore size distribution, average pore and critical pore of the pore system) is the most important characteristic used in determining the performance of hardened cement pastes and affects strength, permeability, diffusivity, shrinkage and creep (Halamickova et al., 1995; Ye et al., 2006). A classification of pores in cement paste is given in Table 2.3.

2.4.1 Classification of pores in hardened cement pastes

Hardened cement paste is a porous material. The porosity and pore structure are very important in determining permeability and durability. The pore system in cement-based materials consists of two types of pores (Chindaprasirt et al., 2007b; Mindress and Young, 1981): (a) gel pores with a diameter of less than 10 nm that affect shrinkage and fatigue and (b) capillary pores that are divided into large capillary pores with diameters between 50-10,000 nm, which affect the compressive strength and permeability, and medium capillary pores with diameters between 10-50 nm, which influence the compressive strength, permeability, and shrinkage.

Table 2.3 Classification of pores in hydrated cement pastes (Chindaprasirt et al., 2007b; Mindress and Young, 1981)

Pore category	Diameter	Description	Affected
Capillary pore	50 nm to 10,000 nm	Large capillary	Strength, Permeability
	10 nm to 50 nm	Medium capillary	Strength, Permeability Shrinkage
Gel pore	2.5 to 10 nm	Small capillaries	Shrinkage to 50% RH
	0.5 to 2.5 nm	Micropore	Shrinkage, creep
	≤ 0.50 nm	Micropores (internal layer)	Shrinkage, creep

2.4.2 Factors influencing the pore structure of pastes

2.4.2.1 Water-to-cement ratio

The dependence of the engineering properties of concrete and other cement composites on the water-to-cement ratio (W/C) is very well known. Previous research found that compressive strength, durability and the quality of other engineering properties are increased when W/C is decreased (Sear et al., 1996). Cook and Hover (1999) investigated the effect of W/C on the porosity of cement paste. Samples with W/C values of 0.35, 0.40, 0.50 and 0.60 were prepared and then tested by mercury intrusion porosimetry (MIP). The total porosity of paste was measured to range from 16 to 56%, increasing with W/C. The threshold pore width of the cement pastes also increased with W/C, as observed in Figure 2.3, where the threshold pore width ranged from 2 μm to 20 nm.

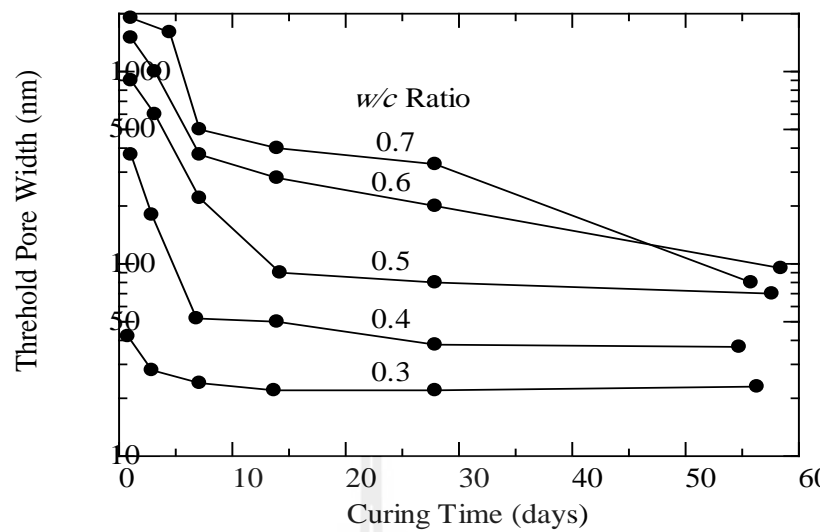


Figure 2.3 Effect of W/C on the threshold pore width of cement pastes (Cook and Hover, 1999)

Zivica (2009) studied the effects of very low W/C values and reported that at a W/C value of 0.4, there was a parabolic dependence of compressive strength on the median pore size, as illustrated in Figure 2.4. However, at lower W/C values, a linear relationship was observed. This phenomenon is most likely a consequence of two factors that led to the decrease in W/C values: less hydration product is necessary to fill the pore space in the hardened cement pastes, and principal changes in the pore structure and matrix occur with a decrease in W/C.

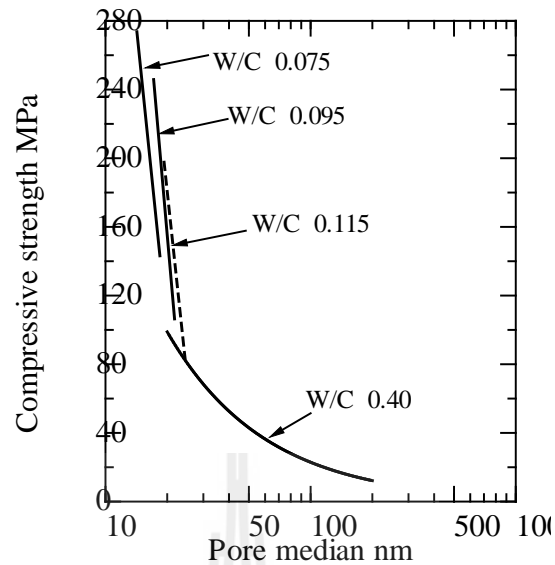


Figure 2.4 Relationship between median pore size and compressive strength of the hardened cement pastes (Zivica, 2009)

2.4.2.2 Curing time

It is well known that curing concrete increases compressive strength and that increasing compressive strength produces lower total porosity. Cui and Cahyadi (2001) studied the permeability and pore structure of OPC pastes. OPC pastes were tested at W/C values of 0.30 and 0.40. They were cured under moist conditions for 7, 35 and 210 days, and the total porosity and critical pore diameters of the pastes were found to decrease with increasing curing time. This decrease is a result of calcium silicate hydrate growing into the pore space of the hardened cement paste. Two peaks are present in the log differential intrusion volume as a function of pore diameter plot shown in Figure 2.5. The first peak represents the capillary pore with a diameter larger than $0.1\mu\text{m}$, and the second peak represents the gel pores with a diameter less than $0.01\mu\text{m}$.

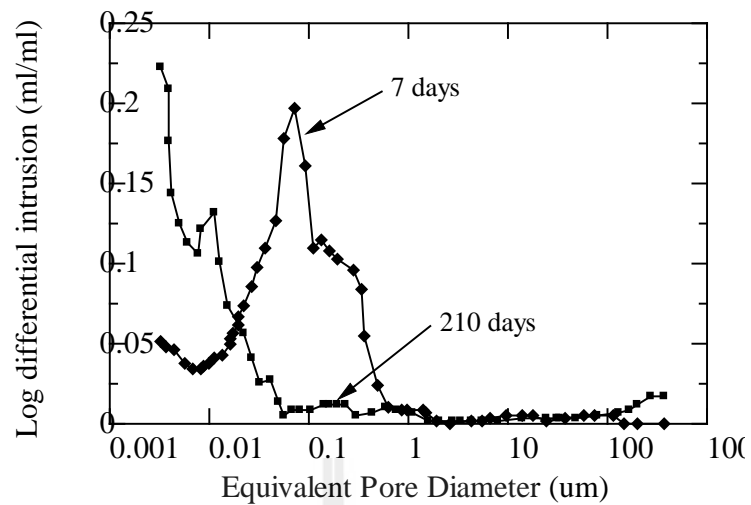


Figure 2.5 Relationship between pore median size and curing time of the hardened cement pastes (Cui and Cahyadi, 2001)

2.4.2.3 Compressive strength

The strength of concrete is influenced by the volume of all of the voids in the concrete: entrapped air, capillary pores, and gel pores. Many researchers have reported on the relationship between compressive strength and porosity, as shown in Table 2.4. Where σ is compressive strength at porosity p , σ_0 is compressive strength at zero porosity and p, x is porosity.

Table 2.4 Empirical models relating the porosity and compressive strength of cement based materials

Equation	Equation fitted	Mathematic law	Derivation by
Hasselmann	$\sigma = 77 - 206p$	Linear	(Hasselman, 1964)
Ryshkewitch	$\sigma = 144 \exp(8.6p)$	Exponential	(Ryshkevitch, 1953)
Schiller	$\sigma = 102 \ln\left(\frac{0.385}{p}\right)$	Logarithmic	(Schiller, 1971)
Balshin	$\sigma = \sigma_0 (1 - p)^n$	Power	(Balshin, 1949)
Poon	$\sigma = -505.6x + 192.47$	Linear	(Poon et al., 1997)
Poon	$\sigma = 303.34(1 - x)^{6.5468}$	Power	(Poon et al., 1997)

2.4.2.4 Temperature

Fall and Samb (2006) studied the influence of curing temperature on the porosity of hardened cement paste. The curing temperatures studied were 0°C, 20°C, 25°C, 35°C and 50°C. They found that cement paste curing temperature of 50°C produced the lowest total porosity. This result can be attributed to the fact that the higher curing temperature accelerates the cement hydration process. Thus, cement paste cured at higher temperatures will have more cement hydration products and a finer porosity than cement paste cured at lower temperatures. The effect of curing temperature on the pore size distribution of cement paste at 7 days is illustrated in Figure 2.6.

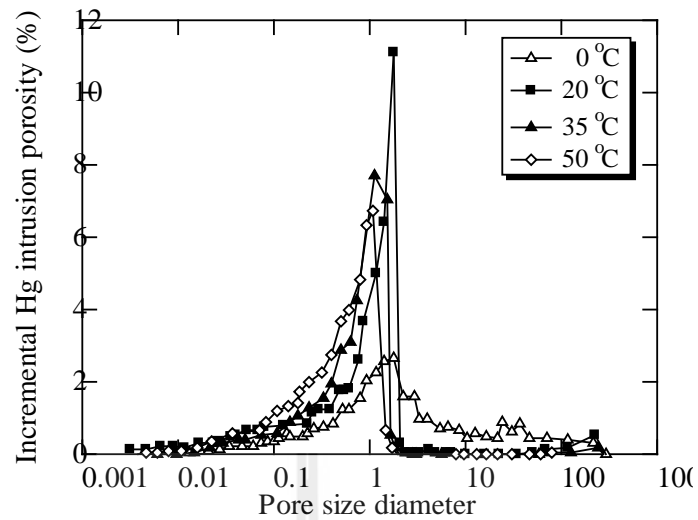


Figure 2.6 Effect of curing temperature on the pore size distribution of cement paste at 7 days (Fall and Samb 2006)

2.4.2.5 Supplementary cementitious materials

Frías and Cabrera (2000) studied the influence of metakaolin on pore size distribution. OPC was partially replaced with 0%, 10%, 15%, 20% and 25% metakaolin by weight of binder. The water-to-binder (W/B) ratio was constant at 0.55 for all mixtures. The cement pastes containing metakaolin were observed to have a lower average pore diameter than that of the OPC paste. In addition, the average pore diameters of the blended cement pastes containing metakaolin decreased from 40 to 14.5 nm for curing times between 1 and 56 days, as observed in Figure 2.7. For longer curing times, the average pore diameter was almost constant. This decrease in pore diameter is due to the reaction of metakaolin with Ca(OH)_2 , which consequently leads to pore size refinement.

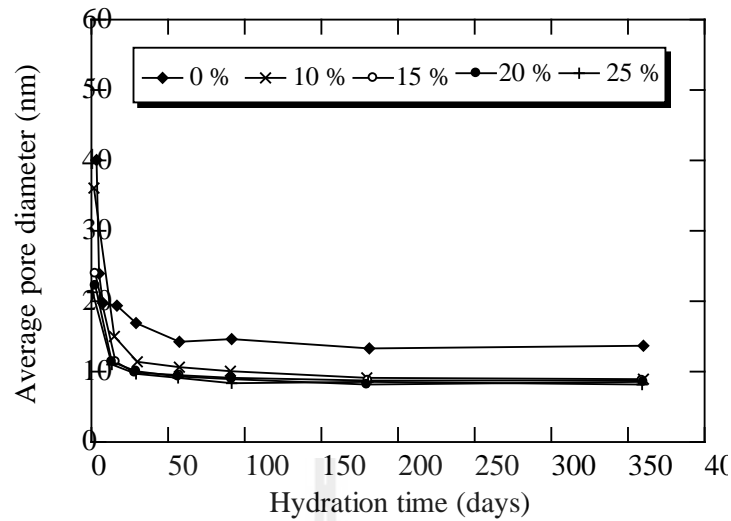


Figure 2.7 Average pore diameters of blended cement pastes containing metakaolin (Frías and Cabrera, 2000)

Chindaprasirt et al. (2005) studied the effect of fineness on the compressive strength and pore size of blended cement paste. They found that the pore size distribution and the average pore diameter of blended cement paste containing fly ash decreased with an increase in fly ash content and fineness. In addition, the gel porosity of blended cement pastes containing classified fly ash was higher than those of the original fly ash and OPC pastes. Later, Chindaprasirt et al. (2007b) found that a higher fineness of fly ash plays an important role in the compressive strength and pore size of the blended cement paste. This effect results from small particles filling the voids of the paste and thus allowing for denser packing between the particles of the material and the matrix phase.

Rukzon et al. (2009) found that rice husk ash with high fineness had lower porosity than of the OPC mortar because the better filler effect dispersion caused an increase in the pozzolanic reaction. In addition, previous research has shown that the pore structure of blended cement paste containing pozzolan materials transformed from coarser to finer pores (Li and Ding, 2003).

2.5 Marine environment

The damage sustained by reinforced concrete in marine environments depends on exposure conditions. The four different exposure zones in marine environment are shown in Figure 2.8. Chalee et al. (2007) performed an analysis of a seawater site in Chonburi, Thailand and found that the ambient temperature ranges from 25°C to 35°C, the pH of the seawater ranges from 7.9 to 8.2, and the chloride and sulfate composition in the seawater ranges from 16,000 to 18,000 ppm and from 2200 to 2600 ppm, respectively.

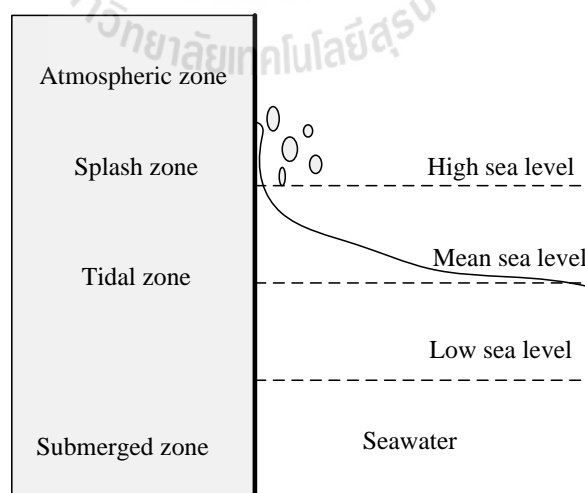


Figure 2.8 Exposure classifications in a marine environment (Bertolini et al., 2004)

2.5.1 Submerged zone

The submerged zone represents the portion of the structure that is submersed continuously under sea water. The rate of corrosion due to chloride is lower in this zone than in the tidal zone and is dependent on the availability of oxygen. The damage to reinforced concrete submerged in this zone is mainly caused by sulfate.

2.5.2 Tidal zone

Reinforced concrete in the tidal zone is subjected to a wetting and drying cycle and undergoes a combination of abrasion and erosion due to the temperature, moisture, salt and oxygen.

2.5.3 Splash zone

The splash zone is part of the structure that is subject to cyclic wetting and drying by seawater. The transport of chloride ions into reinforcement concrete in this zone is facilitated by a combination of moisture, salt and oxygen. The damage to the concrete is mainly caused by the chloride.

2.5.4 Atmospheric zone

The atmospheric zone is the part of the structure that is above the splash zone and far from the sea water. The damage to concrete in this zone is mainly caused by chloride and is similar to the damage caused in the splash zone.

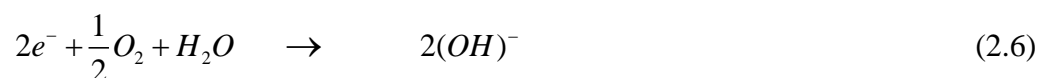
2.6 Corrosion of steel in concrete

The chloride-induced corrosion of embedded reinforcement is one of the major deterioration problems for reinforced concrete worldwide. It is well known that the reinforcing steel in concrete is protected from corrosion by a passive film. This effect, however, can be inhibited by the destruction of the passive film by aggressive ions. When chloride ions enter the concrete, the protective passive layer of the steel surface can be destroyed. The passive layer breaks down, resulting in the appearance of an area of rust on the steel surface. An increased volume of rust affects the internal tensile stress in the concrete covering when this stress exceeds the tensile strength of the concrete. The concrete covering is damaged by cracking, delamination, and spalling. This problem may cause structural damage because of the reduction of the bond between the steel and concrete and the decrease in cross-sectional area (Broomfield, 1996). The reactions are depicted in Figure 2.9.

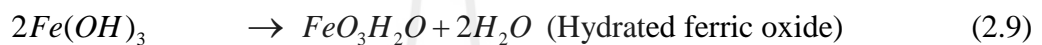
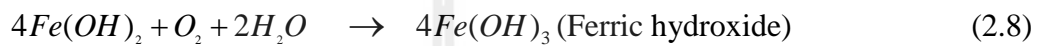
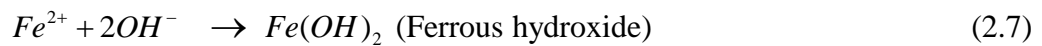
The corrosion will start at the ferrous iron anode:



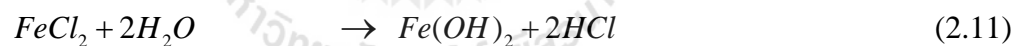
The two electrons ($2e^{-}$) created in the anodic reaction must be consumed elsewhere on the steel surface to preserve electrical neutrality. Therefore, a cathodic reaction involving water and oxygen will take place to consume the electrons and result in the hydroxyl ions shown in Equation. (2.6).



The ferrous ions (Fe^{2+}) will combine with the hydroxyl ions (OH^-) to form ferrous hydroxide, as in Equation. (2.7), which then becomes ferric hydroxide ($Fe(OH)_3$) by consuming water and oxygen, which decomposes into hydrated ferric oxide (rust) and water.



Fe^{2+} reacts with chloride ions to become ferric chloride ($FeCl_2$) and then consumes water to become rust as shown in Equations (2.10) and (2.11)



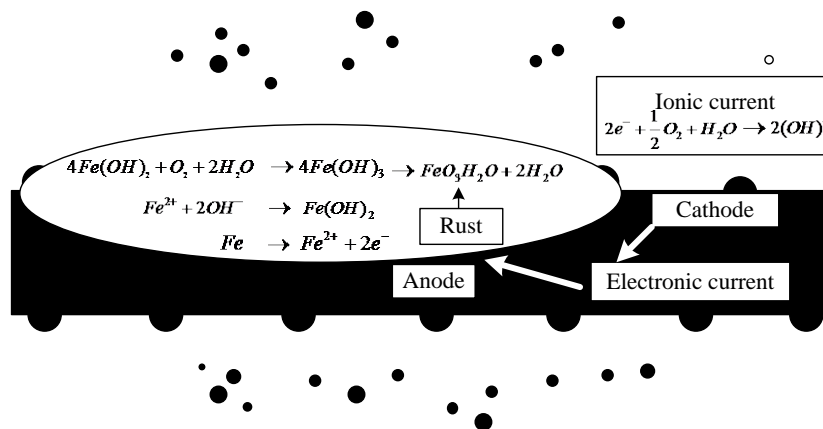


Figure 2.9 Corrosion reactions on steel (Broomfield, 1996)

2.7 Chloride ion penetration of concrete

Chloride in concrete can originate from two main sources: as internal chloride in the chlorides added to the mixed concrete (such as from the contamination of aggregates or the use of sea water or other saline contaminated water) or as external chloride by entering into the concrete post hardening (where the chloride is found in the marine environment or deicing salts).

2.7.1 Chloride in concrete

Chloride in concrete structures in two forms: as bound chloride and as free chloride, as depicted in Figure 2.10. Many researchers have found that the total chloride concentration is the sum of this bound and free chloride, as shown in Equation (2.12).

$$C_T = C_b + C_f \quad (2.12)$$

where C_T is the total chloride, C_b is the bound chloride and C_f is the free chloride

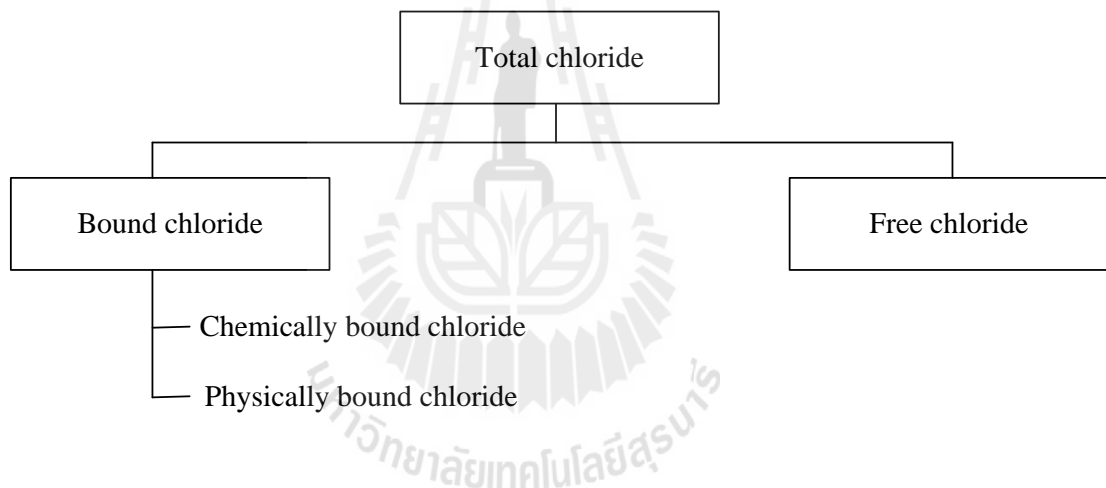


Figure 2.10 Diagram type of chloride in concrete

2.7.1.1 Bound chloride

The transport rate of chloride originating from the bound chloride in hydrated cement paste into concrete is very significant and is dependent on the chemical and physical reaction mechanisms.

(1) Chemically bound chloride is chloride that reacts with tricalcium aluminate (C_3A) to form calcium chloroaluminate (Friedel's salt), and the mechanism by which this occurs is shown in Equation (2.13). The photomicrograph of Friedel's salt in Figure 2.11 illustrates its morphology as being a hexagonal slice of approximately 2-3 μm in size (Luo et al., 2003).

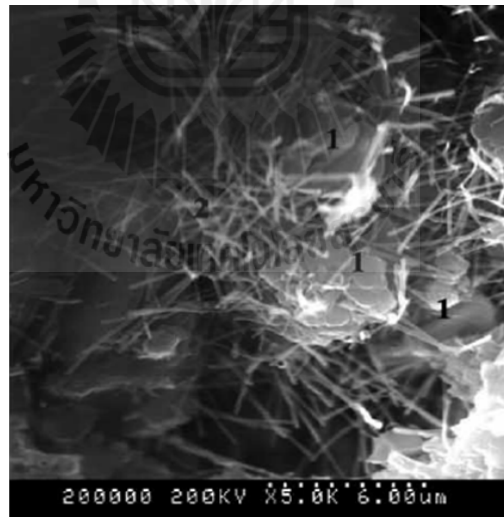


Figure 2.11 Photomicrograph of Friedel's salt, 1= Friedel's salt (Luo et al., 2003)

(2) Physically bound chloride forms from the adsorption of chloride onto the surface of C-S-H, C-A-H, ettringite, and monosulfate.

2.7.1.2 Free chloride

Free chloride is dissolved in the concrete solution and can move according to the concentration gradient. It is this form of chloride that is responsible for initiating the process of corrosion.

2.7.1.3 Relationship between bound chloride and free chloride

Chloride reacts chemically with tricalcium aluminate (C_3A) or its hydration to form calcium chloro-aluminate, $3CaO \cdot Al_2O_3 \cdot CaCl_2 \cdot 10H_2O$, commonly known as Friedel's salt. The chloride can be physically adsorbed on the surface of hydration or during a pozzolanic reaction. However, many researchers have represented the relationship between bound chloride and free chloride as follows.

Linear isotherm:

$$C_b = \gamma C_f \quad (2.14)$$

Freundlich isotherm:

$$C_b = \alpha C_f^\beta \quad (2.15)$$

Langmuir isotherm:

$$C_b = \frac{\alpha C_f}{1 + \beta C_f} \quad (2.16)$$

where C_b is the bound chloride, C_f is the free chloride and γ, α, β are the constants determined by experiments.

2.7.2 Factors affecting chloride resistance

Chloride transport in concrete is largely dependent on the characteristics of the cement paste including the cement composition, the type of chloride, the curing condition, the temperature, the exposure condition, and the supplementary cementitious materials used.

2.7.2.1 Cement composition

Arya et al. (1990) studied the effect of OPC and sulfate-resistant Portland cement (SRPC) using a 20 g/L NaCl solution. They found that the SRPC had lower chloride binding than of the OPC. There was also a lower amount of C_3A in the SRPC. Zibara (2001) found that C_3A plays the most significant role in the chloride binding capacity of cement. The chloride binding of C_3A was good in the high concentration range (1.0-3.0 M), while it was not as good at the low concentration range of 0.1 M. In addition, the chloride binding capacity of C_4AF is one third of that of C_3A . It was also previously reported that OPC performs better than SRPC in terms of chloride binding, chloride diffusivity, and reinforcement corrosion (Page et al., 1981; Rasheeduzzafar et al., 1990).

Glass and Buenfeld (2000) studied the effect of C_3A on chloride binding. OPC containing 2%, 8% and 14% C_3A and having a W/C ratio of 0.45 was used, as shown in Figure 2.12. The results indicated that the predicted maximum bound chloride contents for the 2%, 8% and 14% C_3A cements are 0.97%, 1.32% and 1.67% chloride ion by weight of cement. Chloride binding increases significantly as the C_3A content increases as a result of the reaction between the chloride ions and C_3A that forms Friedel's salt.

Ramachandran (1971) studied the effect of C_3S and C_2S on chloride binding and found that higher contents of C_3S and C_2S affect the physical binding of chloride, which results from the adsorption of the chloride ions to the C-S-H.

The SO_3 content of cement also affects the chloride binding. SO_3 has a negative influence on the chloride binding capacity, especially at low chloride concentrations (0.1 M), because the sulfates react with C_3A and C_4AF to form ettringite or monosulphate (Zibara, 2001).

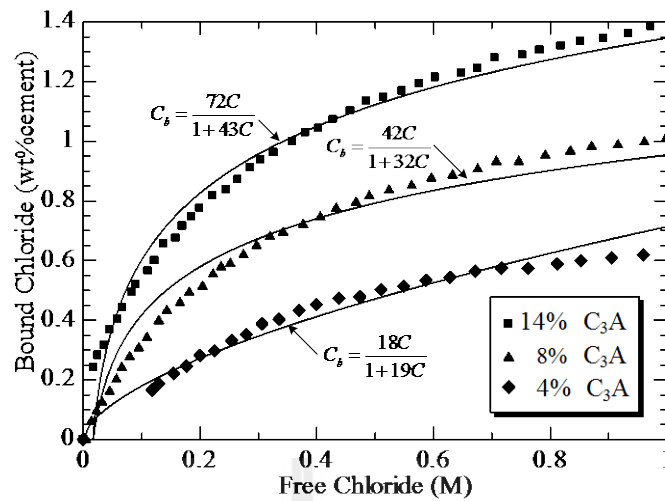


Figure 2.12 Predicted binding data together with the fitted Langmuir adsorption isotherm for a 0.45 W/C ratio (Glass and Buenfeld, 2000)

Oh and Jang (2007) investigated the effect of cement type on chloride. It was found that the diffusion coefficient of type I cement mixtures is lower than that of type V cement mixtures because of the different chloride binding effects of various types of cement. The C_3A content affects the binding capacity, and the C_3A content of type I cement is higher than that of type V cement. In addition, Sumranwanich and Tangtermsirikul (2004) found that type III cement paste had a higher fixed chloride content than Type I cement paste because type III cement had a higher fineness, and, thus, more hydration products were produced.

2.7.2.2 Type of chloride

Tritthart (1989) studied the effect of sodium chloride (NaCl), calcium chloride (CaCl₂), magnesium chloride (MgCl₂) and hydrogen chloride (HCl) on chloride binding in cement paste (W/C =0.6) after 3 months of curing when the total chloride addition was 1% Cl of the cement weight. The results indicated that the use of CaCl₂ led to more bound chloride than NaCl, MgCl₂ and HCl. Similarly, Delagrave et al. (1997) showed that the chloride binding was much higher when calcium was the cation rather than sodium. Neville (1995) also pointed out in his review that calcium chloride leads to more chloride binding than sodium chloride in cement paste.

2.7.2.3 Water-to-cement ratio

Liu and Winslow (1995) studied the effect of W/C on chloride permeability. W/C values of 0.32, 0.40, 0.50 and 0.60 were used, and the chloride permeability was determined in accordance with AASHTO Test T277-83. The results indicated that chloride permeability depends on W/C and curing time. A similar conclusion was also reported by (Sumranwanich and Tangtermsirikul, 2004) who found that W/C increases with total chloride content, while the fixed chloride content is decreased because chloride can be more easily enter into concrete. Pastes with low W/C were also found to be denser. In addition, Moon et al. (2006) investigated the W/B ratio on chloride diffusivity in concrete. The experimental results showed that the average pore diameter increases with the W/B ratio and relates proportionally to the chloride diffusivity of the concrete.

Chalee et al. (2007) studied the effect of the W/C ratio on covering the depth of fly ash concrete in marine environment. The W/C ratio of fly ash concrete was varied at 0.45, 0.55 and 0.65. They found that the cement concrete had a higher rate of chloride penetration than that of fly ash concrete. A decrease in the W/C ratio could reduce the covering depth required for the initial corrosion of the steel bar. Later, Chalee and Jaturapitakkul (2009) found that a decrease in the W/C ratio resulted in a decrease in the chloride diffusion coefficient (D_c) because the W/C ratio influences the water permeability of cement concrete.

2.7.2.4 Pore structure

The pore structure of cement affects important transport properties. Cement-based materials contain air voids, capillary pores and gel pores. Many researchers have studied the effect of the average pore diameter and critical pore diameter on chloride diffusivity. Halamickova et al. (1995) found that the coefficient of chloride ion diffusion varied linearly with critical pore radius and depended on the W/C ratio as shown in Figure 2.13. The diffusion coefficient of paste is expressed as the following:

$$D_c = (-4.3 \times 10^{-12}) + (6.5 \times 10^{-13}) Cr \quad (2.17)$$

where D_c is the diffusion coefficient (m^2/s) and Cr is critical pore radius of the paste

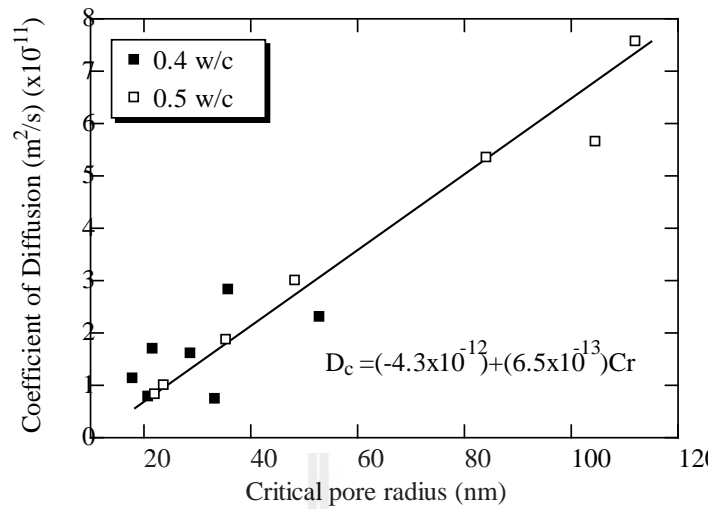


Figure 2.13 Relationship between the diffusion coefficients of chloride ions and the critical pore radius of the paste (Halamicckova et al., 1995).

Yang et al. (2006) performed a linear regression analysis and found that the diffusion coefficient obtained from a ponding test increases with an increase in continuous pore or critical pore radius. Capillary porosity and critical pore diameter or continuous pore diameter are the most important characteristics of the pore structure in relation to the diffusion coefficient of chloride ions in concrete. This relationship is shown in Figure 2.14.

$$D_c = (0.0496d_c - 2.8534) \times 10^{-12} \quad (2.18)$$

where D_c is the diffusion coefficient (m²/s) and d_c is critical pore diameter of the paste

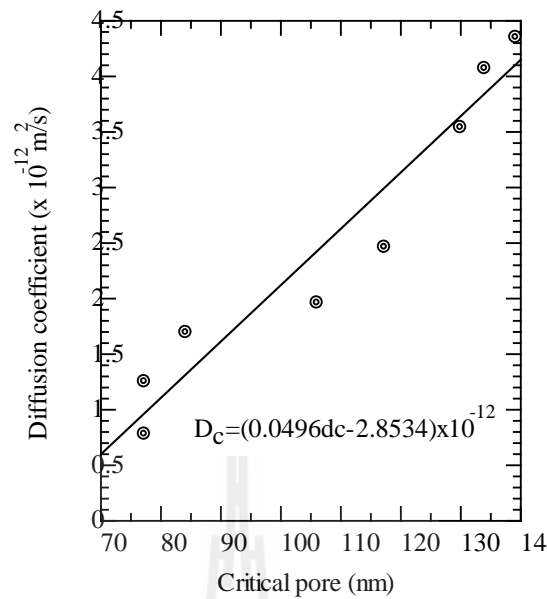


Figure 2.14 Relationship between chloride ion diffusion coefficients and critical pore diameter (Yang et al., 2006)

2.7.2.5 Curing time

Curing methods and duration are important for controlling concrete quality, including, in particular, the strength and durability of the concrete. Sumranwanich and Tangtermsirikul (2004) investigated chloride binding in OPC. Specimens were cast into 50 mm diameter and 10 mm thick. The cement pastes were cured for 1, 7 and 28 days. At the end of water curing, they were exposed to salt water containing 3.0% chloride ions for 28, 56 and 91 days. The results indicated that cement pastes with the same exposure to a shorter curing time had higher total chloride and free chloride levels than those exposed to longer curing times. This result is because the pastes cured for less time had bigger pore diameters that subsequently affected the chloride penetration into the paste. Pastes immersed for longer times in saltwater contained a higher total chloride and fixed chloride content.

2.7.2.6 Temperature

Al-Khaja (1997) investigated the effect of exposure temperature on chloride ingress into concrete. Concrete samples were cured in water at $22\pm 2^\circ\text{C}$ for 28 days. At the age of 29 days, specimens were immersed in 3% NaCl, and the temperature was maintained at 20 and 45°C . The results showed that the exposure temperature increased the chloride content, which is the main factor affecting the chloride ingress into concrete. Nguyen et al. (2009) studied the effect of environmental temperature on the chloride diffusion of mortars. Cylinder samples 100 mm in diameter and 200 mm in height were prepared. After curing in water at $20\pm 1^\circ\text{C}$ and 90% relative humidity, the chloride diffusion coefficient and penetration depths of chloride of the specimens were measured from the NT build 443 at temperatures of 5°C , 21°C and 35°C . It was found that the chloride diffusion coefficient increased with temperature. In addition, the impact of temperature on chloride transport led to an increase in the chloride penetration depths.

2.7.2.7 Exposure condition

Liam et al. (1992) studied the diffusion coefficient (D_c) and surface chloride (C_s) content of a 24 year-old reinforced concrete jetty structure in a marine environment. They found that the amount of chloride content in the splash zone near sea-level is more than that in the tidal zone, which may be due to the wet/dry cycle. Water absorption may lead to very rapid penetration of chloride. However, Ann et al. (2009) showed that the amount of chloride in the tidal zone is greater than that in the splash zone. In addition, Song et al. (2008) investigated the chloride transport of concrete from different sea areas in the UK, Japan and Venezuela. The research indicated that concrete structures exposed to a tropical

environment were more sensitive to chloride attack because the tropical climate affected the chloride ion transport into concrete. This result is due to the high relative humidity, temperature and chloride concentration, all of which facilitate the transport of chloride ions into concrete. Furthermore, studies on the effect of the distance from sea on chloride content revealed which found that structures located on the coast close to the sea are important to chloride (Mustafa and Yusof, 1994).

2.7.2.8 Supplementary cementitious materials

Kayyali and Qasrawi (1992) investigated the chloride binding capacity of blended cement paste containing fly ash. 30% of the Type I Portland cement was replaced by Type F fly ash, and NaCl was dissolved in the mixed water prior to the start of mixing. The experimental results showed that the dehydration of calcium chloroaluminate hydrate (Friedel's salt) was observed at temperatures ranging from 335°C to 350°C. In addition, the DTA peak indicated that the area of formation of Friedel's salt is larger in the fly ash cement paste than in the paste without fly ash.

Arya and Xu (1995) studied the chloride binding of cementitious materials. Type I Portland cement was partially replaced by 35% pulverized fuel ash (PFA), 35% ground granulated furnace slag (GGBS), and 10% silica fume (SF). NaCl was dissolved in water at 1% by weight of cement. Specimens were cured at 3, 7, 14, 28 and 90 days. The amount of chloride binding occurred in the following order: GGBS > PFA > OPC > SF.

Sumranwanich and Tangtermsirikul (2004) studied the effect of the type of fly ash on chloride content. They found that cement paste using Type C fly ash (with high CaO content) had a lower total chloride penetration profile than that using Type F fly ash (with low CaO content) because high CaO fly ash has denser and smaller pores than low CaO fly ash.

Chalee et al. (2010) studied the use of fly ash concrete in a marine environment for long-term design life analysis and found that increasing the amount of concrete containing fly ash reduced the chloride penetration, chloride penetration coefficient and steel corrosion in the concrete. In addition, after 7 years exposure to sea water, no corrosion of the embedded steel bar at a 50 mm concrete cover depth was observed for concrete containing 25-50% of fly ash and having a W/B ratio of 0.65. Later, Cheewaket et al. (2010) observed that increasing the fly ash replacement of cement in concrete resulted in an increase in its chloride binding capacity. These results confirm that the use of fly ash in concrete enhances its resistance to chloride penetration. This resistance results from the chloride binding of concrete depending on the two main mechanisms of physical adsorption and chemical reaction (Luo et al., 2003). In addition, the pozzolanic reaction occurs because of the SiO_2 and Al_2O_3 contained in the fly ash, which react with $\text{Ca}(\text{OH})_2$ and thus increase the compressive strength while refining the pore structure in the blended cement paste; these results are in agreement with (Li and Ding, 2003).

2.8 Modeling of chloride ingress into cement paste

Numerical studies have focused on developing an algorithm to estimate chloride penetration depth. Truc et al. (2000) presented a numerical model based on the finite difference method and the Nernst-Planck equation for the simulation of the transport of Cl^- , K^+ , Na^+ and OH^- through saturated concrete during a migration test. Martin-Perez et al. (2001) studied an algorithm based on Fick's second law for the numerical modeling transport of chloride through concrete. Many researchers have implemented finite element programs, such as ABAQUS, ANSYS and COSMOS thermal software (Chen and Mahadevan, 2008; Lin et al., 2010; Marsavina et al., 2009). Guzman et al., (2011) determined that the free chloride numerical results are in close agreement with experimental results. This proposed model results is shown in Figure 2.15.

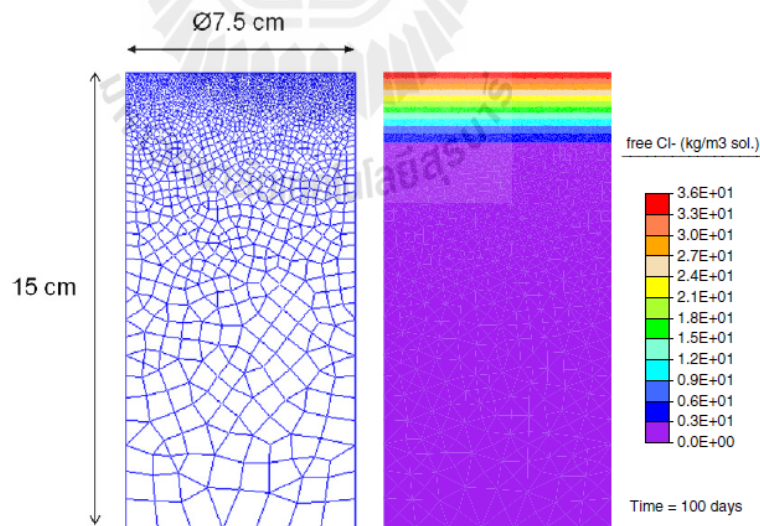


Figure 2.15 Proposed model results (Guzman et al., 2011)

2.8.1 Governing equation

The ionic flux through a saturated porous medium is described by Fick's first law. Chloride ions from an exposed surface moves into the cement matrix due to the concentration gradient. The movement is expressed as follows:

$$J_c = -D_c \nabla C_f \quad (2.19)$$

where J_c is the chloride flux, D_c is the diffusion coefficient (m^2/s), and C_f is the free chloride concentration (g/g). The mass balance equation for chloride ions can be expressed using Fick's second law as follows:

$$\frac{\partial C_T}{\partial t} = -\nabla J_c \quad (2.20)$$

Substituting Equation (2.19) into Equation (2.20), the following equation is obtained:

$$\frac{\partial C_T}{\partial t} = \nabla (D_c \nabla C_f) \quad (2.21)$$

$$\frac{\partial C_T}{\partial t} = \frac{\partial}{\partial x} \left(D_c \frac{\partial C_f}{\partial x} \right) \quad (2.22)$$

The total chloride amount is shown in Equation (2.23). The chloride binding capacity of the paste is slope of a binding isotherm. The binding isotherm relates the free and bound chloride concentrations at equilibrium and is characteristic of each cementitious system as in the following:

$$C_T = C_b + C_f \quad (2.23)$$

Isotherm, chloride binding capacity can be expressed as:

$$\frac{\partial C_f}{\partial C_T} = \alpha \quad (2.24)$$

$$\frac{\partial C_T}{\partial t} = D_c \frac{\partial^2 C_f}{\partial x^2} \quad (2.25)$$

Substituting $\partial C_T = \frac{1}{\alpha} \partial C_f$, we have

$$\frac{1}{\alpha} \frac{\partial C_f}{\partial t} = D_c \frac{\partial^2 C_f}{\partial x^2} \quad (2.26)$$

where C_T is the concentration of total chloride (g/g), C_f is the concentration of free chloride (g/g), D_c is the chloride diffusion coefficient (m^2/s), t is exposure time, and x is the depth of paste measured from the surface (m).

2.8.2 Finite element analysis

Numerical simulations were performed using the governing equation, Equation (2.26). The free chloride concentration (C_f) is expressed by the shape function $[N_c]$ and nodal free chloride concentration $\{c_f\}$. The shape function connects the properties in an element with the properties in a node.

$$C_f(x, y, z, t) = [N_c(x, y, z)] \{c_f(t)\} \quad (2.27)$$

where $[N_c]$ is element shape functions for C_f . The element shape function derivative matrix can be expressed as Equations (2.28) and (2.29), respectively.

$$[N_c] = [N_1 \quad N_2 \quad \dots \quad N_n] \quad (2.28)$$

$$[B] = \left[\frac{\partial N_1}{\partial x} \quad \frac{\partial N_2}{\partial x} \quad \dots \quad \frac{\partial N_n}{\partial x} \right] \quad (2.29)$$

The value of $\{c_f\}$ is obtained as follows:

$$\{c_f\} = [c_{f1} \quad c_{f2} \quad \dots \quad c_{fn}]^T \quad (2.30)$$

Substituting Equation (2.27) into Equation (2.26) and applying the Galerkin method, the following equation is obtained:

$$\int_V [N_c(x, y, z)]^T \left\{ \frac{\partial([N(x, y, z)]\{c_f(t)\})}{\partial t} + D_c \frac{\partial^2([N(x, y, z)]\{c_f(t)\})}{\partial x^2} \right\} dV = 0 \quad (2.31)$$

The finite element of transient mass diffusion can be obtained as follows:

$$[C] \frac{\partial \{c_f(t)\}}{\partial t} + [K] \{c_f(t)\} = \{Q\} \quad (2.32)$$

$[C]$, $[K]$, $[D]$ and $\{Q\}$ of Equation (2.32) are expressed by the following equations, respectively:

$$[K] = \int_V [B]^T [D] [B] dV \quad (2.33)$$

$$[C] = \int_V [N]^T [N] dV \quad (2.34)$$

$$[D_c] = \begin{bmatrix} D_i & 0 \\ & . & 0 \\ 0 & 0 & D_n \end{bmatrix} \quad (2.35)$$

$$\{Q\} = \int f [N]^T c_f dS \quad (2.36)$$

where f is the boundary flux, and c_f is the free chloride concentration of exposure surface condition. Numerical simulation based on a finite element method is a good alternative for modeling the chloride penetration into concrete using a diffusion coefficient and transient analysis.

2.9 Summary of the literature review

A brief summary of the literature review is presented. This summary comprises five topics.

2.9.1 Study of biomass ash in concrete

In general, there is a consensus that biomass ash is an excellent pozzolanic material suitable for use in concrete when it is of high fineness. In particular, blended mortar or paste containing pozzolan materials with high fineness has a lower average pore diameter and critical pore size than OPC paste. These properties result from the reaction of biomass ash with Ca(OH)_2 , which increases compressive strength and pore refinement. This effect is an important factor for permeability and chloride ion diffusion.

2.9.2 Effect of mineral admixture on compressive strength

Pozzolan materials are used as a partial replacement for Portland cement in concrete. From the literature, it is well known that the compressive strength of mortar or concrete is attributed to three factors: the hydration level, the act of small particles filling the voids of pastes and thereby dispersing cement particles, and the reaction between the siliceous and aluminous material from pozzolanic materials and calcium hydroxide.

2.9.3 Pore structure of hardened cement paste

Pores that are present in cement paste or in concrete can be divided into gel pores and capillary pores, which increase and decrease according to the hydration reaction. The structure of cement paste relies significantly on the water-to-cement ratio, curing time, compressive strength, temperature, and supplementary cementitious materials. The pore structure (e.g., the total porosity, the average pore diameter, and the critical pore size of the paste) is one factor that influences the properties of cement materials, such as their strength, permeability and durability. However, most research has reported that the total porosity, average pore diameter and critical pore diameter of blended cement paste containing pozzolan materials were lower than the values for OPC paste.

2.9.4 Chloride ion penetration of concrete

Chloride attack is one of the major threats to the durability of reinforced concrete structures in a marine environment, where it is subjected to de-icing salts. The penetration of chloride depassivates steel and initiates the corrosion of the reinforcement bar. The penetration rate of chloride depends on the diffusion coefficient and high-performance concrete should have a low permeability. Chloride binding affects the transport rate of chloride into concrete. Previous research has suggested that the use of fly ash in concrete resulted in higher chloride binding than for control concrete.

2.9.5 Modeling of chloride ingress into cement paste

The finite element method is a tool to solve problems in engineering, such as stress analysis, bulking, heat transfer, and fluid flow. The simulation of chloride penetration through concrete is based on Fick's second law. Many researchers implement finite element programs such as ABAQUS, ANSYS and COSMOS thermal software. The results found that the free chloride numerical results are in close agreement with experimental results.

The literature review shows that by-products from biomass power plants such as RHA and POFA can be used as cement replacements. Thus, this research aims to study the effect of RHA and POFA of different finenesses on the compressive strength and microstructure of the blended cement paste. To test for durability, a study of the chloride penetration of the blended cement paste will also be conducted. The benefits of this research are that it may help to lead to a reduction of both cement usage and the volume of by-product waste disposed in landfills.

2.10 Research framework

From the literature review, many researchers have reported that pozzolan materials are used to partially replace cement and that the compressive strength of cement paste or mortar is attributed to three factors: the hydration reaction, the filler effect, and the pozzolanic reaction. In addition, previous research has shown that the pore structure of blended cement paste containing pozzolan materials transformed from coarser to finer pores. Thus, the use of pozzolan materials can improve concrete strength, and chloride penetration resistance of concrete. Type I Portland cement (OPC) was replaced by RHA or POFA or RS at 0%, 10%, 20%, 30% and 40% by weight of binder. The compressive strength, thermogravimetric analysis and pore size distribution of the blended cement pastes were investigated. POFA was used to replace ordinary Portland cement at 0%, 10%, 20%, 30% and 40% by weight of binder. The pastes were immersed in 3 % solution for 90 days. After that the total chloride content, free chloride content and microstructure chloride penetration were examined at 90 days immersion in 3% NaCl solution.

2.11 References

- Al-Khaja, W. A. (1997). Influence of temperature, cement type and level of concrete consolidation on chloride ingress in conventional and high-strength concretes. **Construction and Building Materials**. 11(1): 9-13.
- Ann, K. Y., Ahn, J. H., and Ryou, J. S. (2009). The importance of chloride content at the concrete surface in assessing the time to corrosion of steel in concrete structures. **Construction and Building Materials**. 23(1): 239-245.

- Arya, C., Buenfeld, N. R., and Newman, J. B. (1990). Factors influencing chloride-binding in concrete. **Cement and Concrete Research**. 20(2): 291-300.
- Arya, C., and Xu, Y. (1995). Effect of cement type on chloride binding and corrosion of steel in concrete. **Cement and Concrete Research**. 25(4): 893-902.
- Awal, A. S. M. A., and Hussin, M. W. (1997). The effectiveness of palm oil fuel ash in preventing expansion due to alkali-silica reaction. **Cement and Concrete Composites**. 19(4): 367-372.
- Balshin, M. Y. (1949). Relation of mechanical properties of powder metals and their porosity and the ultimate properties of porous metal-ceramic materials. **Dokl Akad SSSR**. 67 (5): 831-834.
- Barbhuiya, S. A., Gbagbo, J. K., Russell, M. I., and Basheer, P. A. M. (2009). Properties of fly ash concrete modified with hydrated lime and silica fume. **Construction and Building Materials**. 23(10): 3233-3239.
- Bertolini, L., Elsener, B., Pedferri, P., 1938- , and Polder, R. (2004). **Corrosion of steel in concrete**. Cambridge: 392.
- Billong, N., Melo, U. C., Kamseu, E., Kinuthia, J. M., and Njopwouo, D. (2011). Improving hydraulic properties of lime-rice husk ash (RHA) binders with metakaolin (MK). **Construction and Building Materials**. 25(4): 2157-2161.
- Broomfield, J. P. (1996). **Corrosion of steel in concrete**. England. Taylor & Francis: 1-10.
- ASTM C618. (2001). Standard specification for coal fly ash and raw or calcined natural pozzolan for use as a mineral admixture in concrete. **Annual Book of ASTM Standards**. vol. 04.02.

- Chalee, W., Ausapanit, P., and Jaturapitakkul, C. (2010). Utilization of fly ash concrete in marine environment for long term design life analysis. **Materials and Design**. 31(3): 1242-1249.
- Chalee, W., and Jaturapitakkul, C. (2009). Effects of W/B ratios and fly ash finenesses on chloride diffusion coefficient of concrete in marine environment. **Materials and Structures**. 42(4): 505-514.
- Chalee, W., Teekavanit, M., Kiattikomol, K., Siripanichgorn, A., and Jaturapitakkul, C. (2007). Effect of W/C ratio on covering depth of fly ash concrete in marine environment. **Construction and Building Materials**. 21(5): 965-971.
- Chatveera, B., and Lertwattanaruk, P. Durability of conventional concretes containing black rice husk ash. **Journal of Environmental Management**. 92(1): 59-66.
- Chatveera, B., and Lertwattanaruk, P. (2011). Durability of conventional concretes containing black rice husk ash. **Journal of Environmental Management**. 92(1): 59-66.
- Cheewaket, T., Jaturapitakkul, C., and Chalee, W. (2010). Long term performance of chloride binding capacity in fly ash concrete in a marine environment. **Construction and Building Materials**. 24(8): 1352-1357.
- Chen, D., and Mahadevan, S. (2008). Chloride-induced reinforcement corrosion and concrete cracking simulation. **Cement and Concrete Composites**. 30(3): 227-238.
- Chindapasirt, P., Chotetanorm, C., and Rukzon, S. (2011). Use of palm oil fuel ash to improve chloride and corrosion resistance of high-strength and high-workability concrete. **Journal of Materials in Civil Engineering**. 23(4): 499-503.

- Chindapasirt, P., Homwuttiwong, S., and Jaturapitakkul, C. (2007a). Strength and water permeability of concrete containing palm oil fuel ash and rice husk-bark ash. **Construction and Building Materials**. 21(7): 1492-1499.
- Chindapasirt, P., Jaturapitakkul, C., and Sinsiri, T. (2005). Effect of fly ash fineness on compressive strength and pore size of blended cement paste. **Cement and Concrete Composites**. 27(4): 425-428.
- Chindapasirt, P., Jaturapitakkul, C., and Sinsiri, T. (2007b). Effect of fly ash fineness on microstructure of blended cement paste. **Construction and Building Materials**. 21(7): 1534-1541.
- Chindapasirt, P., Rukzon, S., and Sirivivatnanon, V. (2008). Resistance to chloride penetration of blended Portland cement mortar containing palm oil fuel ash, rice husk ash and fly ash. **Construction and Building Materials**. 22(5): 932-938.
- Chusilp, N., Jaturapitakkul, C., and Kiattikomol, K. (2009). Utilization of bagasse ash as a pozzolanic material in concrete. **Construction and Building Materials**. 23(11): 3352-3358.
- Cook, R. A., and Hover, K. C. (1999). Mercury porosimetry of hardened cement pastes. **Cement and Concrete Research**. 29(6): 933-943.
- Cui, L., and Cahyadi, J. H. (2001). Permeability and pore structure of OPC paste. **Cement and Concrete Research**. 31(2): 277-282.
- Cyr, M., Lawrence, P., and Ringot, E. (2006). Efficiency of mineral admixtures in mortars: Quantification of the physical and chemical effects of fine admixtures in relation with compressive strength. **Cement and Concrete Research**. 36(2): 264-277.

- de Sensale, G. R., Ribeiro, A. B., and Gonçalves, A. (2008). Effects of RHA on autogenous shrinkage of Portland cement pastes. **Cement and Concrete Composites**. 30(10): 892-897.
- Delagrave, A., Marchand, J., Ollivier, J.-P., Julien, S., and Hazrati, K. (1997). Chloride binding capacity of various hydrated cement paste systems. **Advanced Cement Based Materials**. 6(1): 28-35.
- Fall, M., and Samb, S. S. (2006). Influence of curing temperature on strength, deformation behaviour and pore structure of cemented paste backfill at early ages. **Construction and Building Materials**. In Press:Corrected Proof.
- Frías, M., and Cabrera, J. (2000). Pore size distribution and degree of hydration of metakaolin-cement pastes. **Cement and Concrete Research**. 30(4): 561-569.
- Ganesan, K., Rajagopal, K., and Thangavel, K. (2008). Rice husk ash blended cement: Assessment of optimal level of replacement for strength and permeability properties of concrete. **Construction and Building Materials**. 22(8): 1675-1683.
- Glass, G. K., and Buenfeld, N. R. (2000). The influence of chloride binding on the chloride induced corrosion risk in reinforced concrete. **Corrosion Science**. 42(2): 329-344.
- Goldman, A., and Bentur, A. (1993). The influence of microfillers on enhancement of concrete strength. **Cement and Concrete Research**. 23(4): 962-972.
- Gopalan, M. K. (1993). Nucleation and pozzolanic factors in strength development of class F fly ash concrete. **ACI Materials Journal**. 90(2): 117-121.

- Guzman, S., Galvez, J. C., and Sancho, J. M. (2011). Cover cracking of reinforced concrete due to rebar corrosion induced by chloride penetration. **Cement and Concrete Research**. 41(8): 893-902.
- Halamickova, P., Detwiler, R. J., Bentz, D. P., and Garboczi, E. J. (1995). Water permeability and chloride ion diffusion in portland cement mortars: Relationship to sand content and critical pore diameter. **Cement and Concrete Research**. 25(4): 790-802.
- Hasselman. (1964). Effect of small fraction of spherical porosity on elastic moduli of glass. **J Am Ceram Soc**. 47:52–53.
- Isaia, G. C., Gastaldini, A. L. G., and Moraes, R. (2003). Physical and pozzolanic action of mineral additions on the mechanical strength of high-performance concrete. **Cement and Concrete Composites**. 25(1): 69-76.
- Jaturapitakkul, C., Tangpagasit, J., Songmue, S., and Kiattikomol, K. (2011). Filler effect and pozzolanic reaction of ground palm oil fuel ash." **Construction and Building Materials**. 25(11): 4287–4293.
- Kayyali, O. A., and Qasrawi, M. S. (1992). Chloride Binding Capacity in Cement-Fly-Ash Pastes. **Journal of Materials in Civil Engineering**. 4(1): 16-26.
- Kiattikomol, K., Jaturapitakkul, C., and Tangpagasit, J. (2000). Effect of insoluble residue on properties of Portland cement. **Cement and Concrete Research**. 30(8): 1209-1214.
- Li, Z., and Ding, Z. (2003). Property improvement of Portland cement by incorporating with metakaolin and slag. **Cement and Concrete Research**. 33(4): 579-584.

- Liam, K. C., Roy, S. K., and wood, D. O. N. (1992). Chloride ingress measurements and corrosion potential mapping study of a 24-year-old reinforced concrete jetty structure in a tropical marine environment. **Magazine of Concrete Research**. 44: 205 –215.
- Lin, G., Liu, Y., and Xiang, Z. (2010). Numerical modeling for predicting service life of reinforced concrete structures exposed to chloride environments. **Cement and Concrete Composites**. 32(8): 571-579.
- Liu, Z., and Winslow, D. (1995). "Sub-distributions of pore size: A new approach to correlate pore structure with permeability. **Cement and Concrete Research**. 25(4): 769-778.
- Luo, R., Cai, Y., Wang, C., and Huang, X. (2003). Study of chloride binding and diffusion in GGBS concrete. **Cement and Concrete Research**. 33(1): 1-7.
- Marsavina, L., Audenaert, K., De Schutter, G., Faur, N., and Marsavina, D. (2009). Experimental and numerical determination of the chloride penetration in cracked concrete. **Construction and Building Materials**. 23(1): 264-274.
- Martin-Perez, B., Pantazopoulou, S. J., and Thomas, M. D. A. (2001). Numerical solution of mass transport equations in concrete structures. **Computers & Structures**. 79(13): 1251-1264.
- Mehta, P. K. (1985). Influence of fly ash characteristics on the strength of portland-fly ash mixtures. **Cement and Concrete Research**. 15(4): 669-674.
- Mindress, and Young , J., F. (1981). **Concrete**. Prentice-Hall:Engle Cliffs.
- Moon, H. Y., Kim, H. S., and Choi, D. S. (2006). Relationship between average pore diameter and chloride diffusivity in various concretes. **Construction and Building Materials**. 20(9): 725-732.

- Mustafa, M. A., and Yusof, K. M. (1994). Atmospheric chloride penetration into concrete in semitropical marine environment. **Cement and Concrete Research**. 24(4): 661-670.
- Nair, D. G., Fraaij, A., Klaassen, A. A. K., and Kentgens, A. P. M. (2008). A structural investigation relating to the pozzolanic activity of rice husk ashes. **Cement and Concrete Research**. 38(6): 861-869.
- Neville, A. (1995). Chloride attack of reinforced concrete: an overview. **Materials and Structures**. 28(2): 63-70.
- Nguyen, T. S., Lorente, S., and Carcasses, M. (2009). Effect of the environment temperature on the chloride diffusion through CEM-I and CEM-V mortars: An experimental study. **Construction and Building Materials**. 23(2): 795-803.
- Nochaiya, T., Wongkeo, W., Pimraksa, K., and Chaipanich, A. (2009). Microstructural, physical, and thermal analyses of Portland cement–fly ash–calcium hydroxide blended pastes. **Journal of Thermal Analysis and Calorimetry**. 100 (1):101-108
- Oh, B. H., and Jang, S. Y. (2007). Effects of material and environmental parameters on chloride penetration profiles in concrete structures. **Cement and Concrete Research**. 37(1): 47-53.
- Page, C. L., Short, N. R., and El Tarras, A. (1981). Diffusion of chloride ions in hardened cement pastes. **Cement and Concrete Research**. 11(3): 395-406.
- Poon, C. S., Lam, L., Kou, S. C., Wong, Y. L., and Wong, R. (2001). Rate of pozzolanic reaction of metakaolin in high-performance cement pastes. **Cement and Concrete Research**. 31(9): 1301-1306.

- Poon, C. S., Wong, Y. L., and Lam, L. (1997). The influence of different curing conditions on the pore structure and related properties of fly-ash cement pastes and mortars. **Construction and Building Materials**. 11(7-8): 383-393.
- Ramachandran, V. (1971). Possible states of chloride in the hydration of tricalcium silicate in presence of calcium chloride. **Materials and Structures**. 4(1): 3-12.
- Rasheeduzzafar, Al-Saadoun, S. S., Al-Gahtani, A. S., and Dakhil, F. H. (1990). Effect of tricalcium aluminate content of cement on corrosion of reinforcing steel in concrete. **Cement and Concrete Research**. 20(5): 723-738.
- Rukzon, S., and Chindaprasirt, P. (2008). Mathematical model of strength and porosity of ternary blend Portland rice husk ash and fly ash cement mortar. **Computers and Concrete**. 5(1): 75-88.
- Rukzon, S., Chindaprasirt, P., and Mahachai, R. (2009). Effect of grinding on chemical and physical properties of rice husk ash. **International Journal of Minerals, Metallurgy and Materials**. 16(2): 242-247.
- Ryshkevitch, R. (1953). Compression strength of porous sintered alumina and zirconia. **J Am Ceram Soc**. 36(2):65-68.
- Sata, V., Jaturapitakkul, C., and Kiattikomol, K. (2004). Utilization of palm oil fuel ash in high-strength concrete. **Journal of Materials in Civil Engineering**. 16(6): 623-628.
- Sata, V., Jaturapitakkul, C., and Kiattikomol, K. (2007). Influence of pozzolan from various by-product materials on mechanical properties of high-strength concrete. **Construction and Building Materials**. 21(7): 1589-1598.

- Sata, V., Jaturapitakkul, C., and Rattanashotinunt, C. (2010). Compressive Strength and Heat Evolution of Concretes Containing Palm Oil Fuel Ash. **Journal of Materials in Civil Engineering**. 22 (10):1033-1038.
- Schiller, K. K. (1971). Strength of porous materials. **Cement and Concrete Composites**. 1: 419-422.
- Sear, L. K. A., Dews, J., Kite, B., Harris, F. C., and Troy, J. F. (1996). Abrams law, air and high water-to-cement ratios. **Construction and Building Materials**. 10(3): 221-226.
- Song, H. W., Lee, C. H., and Ann, K. Y. (2008). Factors influencing chloride transport in concrete structures exposed to marine environments. **Cement and Concrete Composites**. 30(2): 113-121.
- Sumranwanich, T., and Tangtermsirikul, S. (2004). A model for predicting time-dependent chloride binding capacity of cement-fly ash cementitious system. **Materials and Structures**. 37(6): 387-396.
- Tangchirapat, W., and Jaturapitakkul, C. (2010). Strength, drying shrinkage, and water permeability of concrete incorporating ground palm oil fuel ash. **Cement and Concrete Composites**. 32(10): 767-774.
- Tangchirapat, W., Saeting, T., Jaturapitakkul, C., Kiattikomol, K., and Siripanichgorn, A. (2007). Use of waste ash from palm oil industry in concrete. **Waste Management**. 27(1): 81-88.
- Tangpagasit, J., Cheerarot, R., Jaturapitakkul, C., and Kiattikomol, K. (2005). Packing effect and pozzolanic reaction of fly ash in mortar. **Cement and Concrete Research**. 35(6): 1145-1151.

- Tay, J.-H. (1990). Ash from oil-palm waste as concrete material. **Journal of Materials in Civil Engineering**. 2(2): 94-105.
- Tritthart, J. (1989). Chloride binding in cement II. The influence of the hydroxide concentration in the pore solution of hardened cement paste on chloride binding. **Cement and Concrete Research**. 19(5): 683-691.
- Truc, O., Ollivier, J.-P., and Nilsson, L.-O. (2000). Numerical simulation of multi-species transport through saturated concrete during a migration test -- MsDiff code. **Cement and Concrete Research**. 30(10): 1581-1592.
- Wansom, S., Janjaturaphan, S., and Sinthupinyo, S. (2010). Characterizing pozzolanic activity of rice husk ash by impedance spectroscopy. **Cement and Concrete Research**. 40(12): 1714-1722.
- Yang, C. C. (2006). On the relationship between pore structure and chloride diffusivity from accelerated chloride migration test in cement-based materials. **Cement and Concrete Research**. 36(7): 1304-1311.
- Yang, C. C., Cho, S. W., and Wang, L. C. (2006). The relationship between pore structure and chloride diffusivity from ponding test in cement-based materials. **Materials Chemistry and Physics**. 100(2-3): 203-210.
- Ye, G., Lura, P., and van Breugel, K. (2006). Modelling of water permeability in cementitious materials. **Materials and Structures**. 39(9): 877-885.
- Zivica, V. (2009). Effects of the very low water/cement ratio. **Construction and Building Materials**. 23(12): 3579-3582.

CHAPTER III

EXPERIMENTAL PROGRAM

This chapter explains the details of the experimental program. The study is divided into two parts. The first part showed mixed proportions of paste and a method for determining the component of the compressive strength of paste that results from the hydration reaction, the filler effect, and the pozzolanic reaction. The microstructure of the blended cement paste was studied using thermal gravimetry analysis (TGA) and mercury intrusion porosimeter (MIP). Part 2 examined the chloride penetration into blended cement paste and consists of tests to determine the total chloride content, the free chloride content. In addition, the microstructure of pastes, and numerical finite element methods was also performed.

3.1 Materials

3.1.1 Cement

Ordinary Portland cement type I (OPC) and sulfate resistance Portland cement Type V (SRPC) were used in this study.

3.1.2 Biomass ash

Two types of biomass ash were used in this study: rice husk ash (RHA) and palm oil fuel ash (POFA).

RHA is a by-product material from electricity generation biomass power plants. In this study, RHA was collected from power plants in the Roiet Province of Thailand.

POFA is a by-product from biomass thermal power plants where oil palm residues are burned to generate electricity. In this study, POFA from a power plant in the Chumphon Province of Thailand was used.

3.1.3 Inert material

The inert material used was ground river sand (RS)

3.2 Method of study

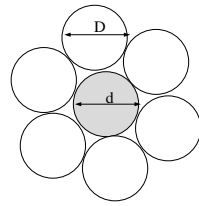
Original RHA, original POFA and RS are ground to two different sizes as shown in Figure 3.1. The median particle size of the materials are proposed to be of the same size as that of cement and as the filler between the particle sizes of cement, which was calculated using Equations (3.1) and (3.2), respectively. An overview of the experimental procedure is shown in Figure 3.2.

As shown in Figure 3.1(a), if the median particle size of the material is the same as that of OPC ($\sim 15 \mu\text{m}$), the material does not act as a filler.

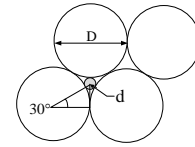
$$d = D = 15 \mu\text{m} \quad (3.1)$$

If the median particle size of the material is smaller than cement and acts as a filler between the particles of cement as shown in Figure 3.1(b), then the median size of the filler material can be calculated as shown in Equation 3. 2, (Lu and Likos, 2004).

$$d = c \cos 30^\circ \frac{D/2}{D/2 + d/2} = 0.15D = 0.15(15) = 2.25 \mu\text{m} \quad (3.2)$$



(a) Median particle size equal to
that of OPC



(b) Minimum median particle size
for filler

Figure 3.1 Illustration of material with different particles size in OPC paste



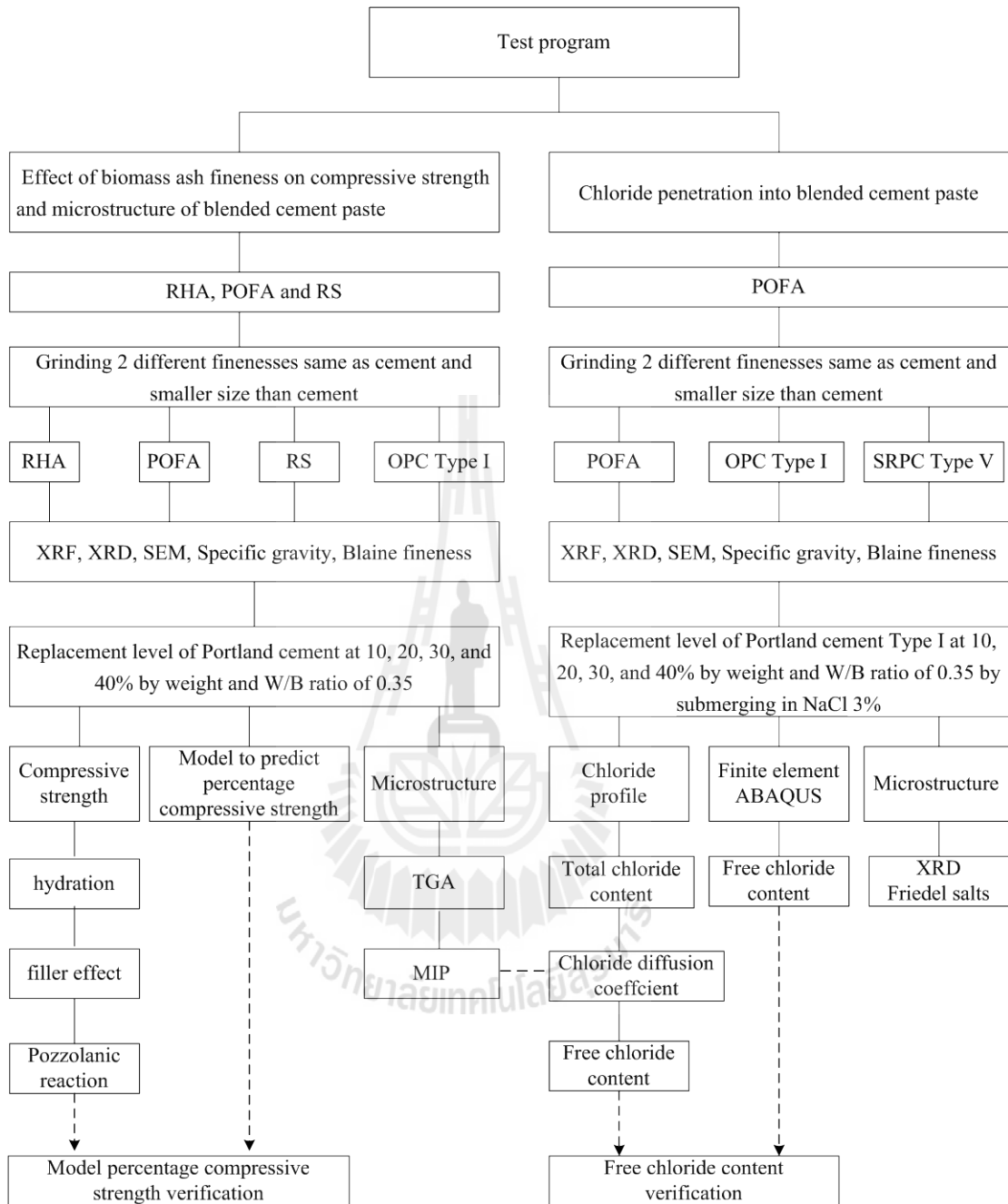


Figure 3.2 Experimental program

3.2.1 Mixture proportions of pastes

In Part 1, ground RHA, POFA, and RS were used to partially replace Type I Portland cement at 0%, 10%, 20%, 30% and 40% by binder weight as shown in Table 3.1. The normal consistency of paste OPC was 25.5% while those of RHA and POFA were higher than that paste OPC and increased with increasing particle fineness and cement replacement rate. This is due to the particles of ashes having high porosity, and thus absorbing more water, resulting in higher water consumption.

Table 3.1 Mixture proportions of pastes in part 1

Symbol	Mixture proportions (%)							W/B	Normal Consistency (%)
	OPC	CRS	CRHA	CPOFA	FRS	FRHA	FPOFA		
OPC	100	-	-	-	-	-	-	0.35	25.5
10CRS	90	10	-	-	-	-	-	0.35	25.7
20CRS	80	20	-	-	-	-	-	0.35	25.8
30CRS	70	30	-	-	-	-	-	0.35	25.9
40CRS	60	40	-	-	-	-	-	0.35	26.1
10CRHA	90	-	10	-	-	-	-	0.35	27.5
20CRHA	80	-	20	-	-	-	-	0.35	28.1
30CRHA	70	-	30	-	-	-	-	0.35	29.7
40CRHA	60	-	40	-	-	-	-	0.35	31.5
10CPOFA	90	-	-	10	-	-	-	0.35	26.7
20CPOFA	80	-	-	20	-	-	-	0.35	27.6
30CPOFA	70	-	-	30	-	-	-	0.35	28.3
40CPOFA	60	-	-	40	-	-	-	0.35	29.5
10FRS	90	-	-	-	10	-	-	0.35	26.1
20FRS	80	-	-	-	20	-	-	0.35	26.4
30FRS	70	-	-	-	30	-	-	0.35	26.8
40FRS	60	-	-	-	40	-	-	0.35	27.2
10FRHA	90	-	-	-	-	10	-	0.35	32.8
20FRHA	80	-	-	-	-	20	-	0.35	33.5
30FRHA	70	-	-	-	-	30	-	0.35	35.6
40FRHA	60	-	-	-	-	40	-	0.35	37.8
10FPOFA	90	-	-	-	-	-	10	0.35	31.8
20FPOFA	80	-	-	-	-	-	20	0.35	33.5
30FPOFA	70	-	-	-	-	-	30	0.35	35.1
40FPOFA	60	-	-	-	-	-	40	0.35	36.5

In Part 2, Type I Portland cement was partially replaced by POFA at 0%, 10%, 20%, 30% and 40% by binder weight as shown in Table 3.2. Two sets of pastes with a water-to-binder (W/B) ratio of 0.35 were prepared.

Table 3.2 Mixture proportions of pastes in part 2

Symbol	Mixture proportions (%)				W/B
	OPC	SRPC	CPOFA	FPOFA	
OPC	100	-	-	-	0.35
SRPC	-	100	-	-	0.35
10CPOFA	90		10	-	0.35
20CPOFA	80		20	-	0.35
30CPOFA	70		30	-	0.35
40CPOFA	60	-	40	-	0.35
10FPOFA	90	-	-	10	0.35
20FPOFA	80	-	-	20	0.35
30FPOFA	70	-	-	30	0.35
40FPOFA	60	-	-	40	0.35

3.2.2 List of abbreviations

Paste symbol {10, 20, 30, 40} {C, F} {OPC, SRPC, POFA, RHA, RS}

where:

OPC	=	Ordinary Portland cement type I
SRPC	=	Sulfate resistance Portland cement type V
POFA	=	Ground palm oil fuel ash
RHA	=	Ground rice husk ash
RS	=	River sand
C	=	Coarse
F	=	Fine

3.3 Test program

3.3.1 Determination of properties of materials

(1) The specific gravity of the RHA, POFA, RS, OPC and SRPC was measured according to ASTM C188.

(2) The fineness of the RHA, POFA, RS, OPC and SRPC was measured according to ASTM C204 2001.

(3) The chemical composition of the RHA, POFA, RS, OPC and SRPC was measured using X-ray fluorescence.

(4) The amorphous structure of the RHA, POFA, and RS was determined using quantitative XRD analysis with Bruker's TOPAS software. The XRD scans were performed for 2θ between 10° and 65° using with an increment of $0.02^\circ/\text{step}$ and a scan speed of 0.5 sec/step.

(5) Particle size analysis of the RHA, POFA, RS, OPC and SRPC was conducted using laser particle size analysis.

3.3.2 Determination of compressive strength

Cube specimens of size 50 x 50 x 50 mm were prepared in accordance with ASTM C109 except that no sand was used in the mixture and were tested to determine the compressive strength at the ages of 7, 28, 60 and 90 days. An average of five samples was taken for each compressive strength value reported.

3.3.2.1 Evaluation of the percentage compressive strength of paste due to the hydration reaction

The percentage compressive strength of a paste due to the hydration reaction (P_H) is the ratio between the compressive strength of the paste containing

inert material with the same particle size of cement and the compressive strength of the OPC paste. The percentage compressive strength of a paste due to the hydration reaction is calculated by the following equation:

$$P_H = \left(\frac{C_{ic}}{C_{opc}} \right) \times 100 \quad (3.3)$$

where P_H is the percentage compressive strength of the paste due to the hydration reaction (%), C_{ic} is the compressive strength of the paste containing inert material with the same particle size of cement (MPa) and C_{opc} is the compressive strength of OPC paste (MPa).

3.3.2.2 Evaluation of the percentage compressive strength of paste due to the filler effect

The percentage compressive strength of paste due to the filler effect (P_F) is the difference in the percentage compressive strength between the paste with inert material with high fineness and the paste with inert material with the same particle size as the cement. The percentage compressive strength of paste due to the filler effect is calculated by the following equation:

$$P_F = (P_{if(p,t)} - P_{ic(p,t)}) \quad (3.4)$$

where (P_F) is the percentage compressive strength of the paste due to the filler effect (%), $P_{if(p,t)}$ is the percentage compressive strength of the paste containing inert material with high fineness compared with OPC paste (%) and $P_{ic,(p,t)}$ is the percentage compressive strength of the paste containing inert material with the same particle size as the cement compared with OPC paste (%). $P_{if(p,t)}$ and $P_{ic,(p,t)}$ have the same replacement (p) and the same age (t).

3.3.2.3 Evaluation of the percentage compressive strength of paste due to the pozzolanic reaction

The percentage compressive strength of paste due to the pozzolanic reaction ($P_{PZ,t}$) is the difference in the percentage compressive strength between the RHA or POFA paste and the inert material paste. The percentage compressive strengths of paste due to the pozzolanic reaction were calculated by the following equation:

$$P_{PZ,t} = (P_{b,(p,s,t)} - P_{i,(p,s,t)}) \quad (3.5)$$

where $P_{PZ,t}$ is the percentage compressive strength of the paste due to the pozzolanic reaction (%), $P_{b,(p,s,t)}$ is the percentage compressive strength of the paste containing RHA or POFA compared with OPC paste (%) and $P_{i,(p,s,t)}$ is the percentage compressive strength of the paste containing inert material compared with OPC paste (%), $P_{b,(p,s,t)}$ and $P_{i,(p,s,t)}$ have the same replacement (p), fineness (s) and age (t).

3.3.3 Microstructure of the blended cement paste

3.3.3.1 Thermal analysis

Thermal analysis is a widely used method for determining the presence of hydration products such as ettringite, calcium silicate hydrate (C-S-H), calcium aluminum silicate hydrate (C_2ASH_8), calcium aluminate hydrate (C_4AH_{13}), calcium hydroxide ($Ca(OH)_2$) and calcium carbonate ($CaCO_3$) (Bai et al., 2003). Thermogravimetric analysis was carried out using Netzsch STA 409 C/CD equipment. The sample was heated from room temperature to $1000^\circ C$ at a heating rate of $10^\circ C/min$ under a nitrogen atmosphere. The thermogravimetric (TG) signal was used to calculate the weight loss during heating and to estimate the content of $Ca(OH)_2$ and carbonated phases. The $Ca(OH)_2$ content was calculated from the weight loss between 450 and $580^\circ C$ (El-Jazairi and Illston, 1977). Furthermore, the derivative thermogravimetric (DTG) data of the weight loss can be used to further determine each phase (Chaipanich and Nochaiya, 2010)

3.3.3.2 Determination of the porosity of the pastes

The measurement of the distribution of pore diameters in the hardened cement pastes, determined by mercury intrusion porosimetry (MIP), was conducted at a pressure capacity of 228 MPa. After curing, all cube specimens were split from the middle portion of the hardened blended cement paste and 3-6 mm pieces weighing between 1 and 1.5 g were used. To stop the hydration reaction, the samples were submerged directly into liquid nitrogen for 5 min and were then evacuated at a pressure of 0.5 Pa at $-40^\circ C$ for 48 h. This method has been used previously to stop the hydration reaction of cement paste (Galle, 2001; Konecny and

Naqvi, 1993). The pressure was determined by the Washburn equation (Washburn, 1921), and the pore diameters were calculated by the Washburn equation as follows:

$$d = \frac{-4\gamma \cos \theta}{P} \quad (3.6)$$

where d is the pore diameter (μm), γ is the surface tension of the mercury (dynes/cm), θ is the contact angle (degree) and P is the applied pressure (MPa).

3.3.4 Chloride penetration into blended cement paste

Specimens (100 mm diameter and 200 mm in height) were prepared in accordance with ASTM C39 except that no sand was used in the mixture. The cast specimens were removed from the mold. Afterwards, they were cured in saturated lime water at $23 \pm 2^\circ\text{C}$. After curing to the age of 27 days, they were cut into 60 mm pieces. The lateral and bottom surfaces of the cylinders were coated with epoxy. The samples were immersed in 3% NaCl solution for 90 days as shown in Figure 3.3, after that the chloride penetration into blended cement paste was measured.



(a) Specimen pastes coated with epoxy



(b) Specimen pastes immersed in 3% NaCl solution for 90 days

Figure 3.3 Immersion of paste specimen in 3% NaCl solution

3.3.4.1 Total chloride content

After 90 days of the chloride exposure period, the specimen was dry-cut from the top surface, which was 10 mm thick as shown in Figure 3.4. The paste was ground into a powder sample that could pass through a No. 20 sieve. Nitric acid was mixed into the 10 g powder sample in a beaker, and the mixture was heated on a hot plate for 3 minutes. After removal of the beaker from the hot plate and filtering the solution, the filtrate was used to analyze the total chloride content using auto-titration equipment according to ASTM C1152.



Figure 3.4 Paste specimens coring and cutting for chloride test

3.3.4.2 Free chloride content

The method to determine the free chloride content is similar to that used for the total chloride content. 10 g of powder samples and distilled water were mixed in a beaker. The mixture was heated on the hot plate for 5 minutes, and then the sample was left to stand for 24 h before filtering the solution. The filtrate was used to analyze the free chloride content using auto titration equipment according to ASTM C1218.

3.3.5 Microstructure of the blended cement paste chloride penetration

After 90 days of the chloride exposure period, the specimen was dry-cut from the top surface, which was 10 mm thick. The paste was ground to a powder sample that could pass through a No. 200 sieve. The amount of Friedel's salt was determined using semi-quantitative XRD. The XRD scans were performed for 2θ between 10° and 25° using an increment of $0.02^\circ/\text{step}$ and a scan speed of 0.5 sec/step .

3.3.6 Numerical simulation of the blended cement paste under chloride penetration

Finite element analysis was used to numerically solve the chloride diffusion equation using Fick's second law Equation (3.7). The numerical simulation by the FEM program, ABAQUS thermal software, was used to study the chloride penetration in the blended cement paste. The governing equation used in ABAQUS was Equation (3.8).

$$\frac{\partial C_T}{\partial t} = \frac{\partial}{\partial x} \left(D_c \frac{\partial C_f}{\partial x} \right) \quad (3.7)$$

$$\rho C_s \frac{\partial T}{\partial t} = \frac{\partial}{\partial x} \left(k_x \frac{\partial T}{\partial x} \right) + Q \quad (3.8)$$

where T is the temperature, t is time, ρ is the density, C_s is the specific heat, k_x is the thermal conductivities in global x direction, respectively, and Q represents the heat generation rate. Equation (3.7) is similar to Equation (3.8) if $\rho=1$ and Q is 0. Thus, for the simulation of chloride penetration, the temperature T is replaced by the total chloride concentration C_T while the thermal conductivity k_x is replaced by the diffusion coefficient D_c and the specific heat is replaced by the chloride binding capacity $\frac{\partial C_f}{\partial C_T}$.

3.3.6.1 Geometric model

The geometric model used in the present study is shown in Figure 3.5. It is a paste of 100 mm width and 60 mm height. The cement paste is exposed to 3% NaCl and 100% relative humidity (RH) on the top surface and inside specimen. The other boundaries are assumed to be insulated. The element is an isoparametric element for the finite element model

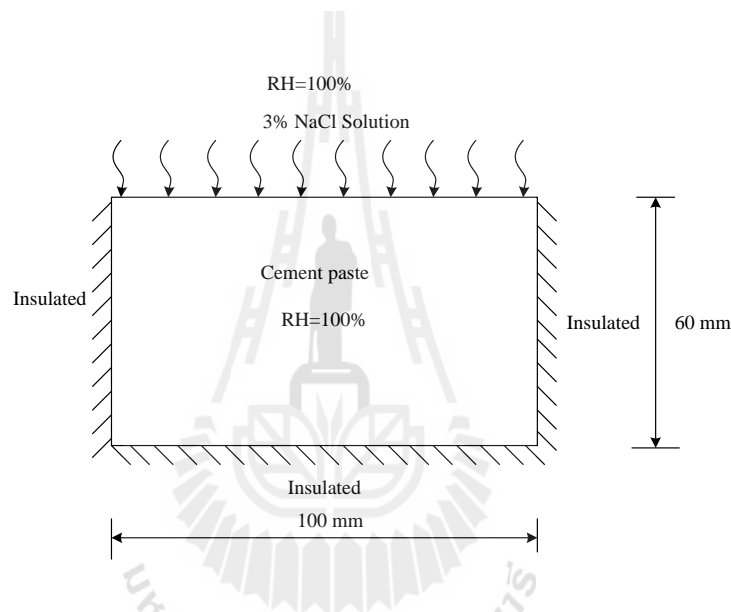


Figure 3.5 Paste sample used for the numerical model

3.3.6.2 Material parameter

(1) Chloride diffusion coefficient

The chloride ion transport in the paste can be modeled by Fick's second law in the following form for one-dimension (Crank, 1975):

$$\frac{\partial C}{\partial t} = D_c \frac{\partial^2 c}{\partial x^2} \quad (3.9)$$

Considering the constant diffusion coefficient, an analytical solution of Equation (3.9) is given by:

$$C(x,t) = C_0 \left[1 - \operatorname{erf} \left(\frac{x}{2\sqrt{D_c t}} \right) \right] \quad (3.10)$$

where $C(x,t)$ is the total chloride concentration (% by weight of binder) at depth x and exposure time t

t is time (second)

x is distance from paste surface

D_c is diffusion coefficient (m^2/s) at exposure time t

erf is error function

The apparent chloride diffusion coefficient D_c is calculated from the concentration profile of the specimen tested by curve-fitting of Equation (3.10).

(2) Chloride binding capacity

The total chloride is the sum of the free and bound chloride as shown in Equation (3.11). The chloride binding capacity describes the ratio between the change of free chloride content and the total chloride content. The chloride binding relation is best defined by isotherm described by Equation (3.12). Thus, the derivative of Equation (3.12) can be rewritten as Equation (3.13), where α is the slope of the line.

$$C_T = C_f + C_b \quad (3.11)$$

$$\frac{\partial C_f}{\partial C_T} = \alpha \quad (3.12)$$

where C_T is the total chloride, C_b is the bound chloride and C_f is the free chloride and α is the constants determined by experiments

Chloride penetration into blended cement paste containing POFA was determined by the experimental value while numerical simulation is used to solve the diffusion depth using Fick's second law and the finite element method program. The numerical simulation studies the calculation of the amount of free chloride, in order to verify the experimental results.

3.4 References

- Bai, J., Chaipanich, A., Kinuthia, J. M., O'Farrell, M., Sabir, B. B., Wild, S., and Lewis, M. H. (2003). Compressive strength and hydration of wastepaper sludge ash-ground granulated blastfurnace slag blended pastes. **Cement and Concrete Research**. 33(8): 1189-1202.
- ASTM C39. (2001). Standard test method for compressive strength of cylindrical concrete specimens. **Annual book of ASTM standards**: vol. 04.02.
- ASTM C109. (2001). Standard test method for compressive strength of hydraulic cement mortars (using 2-in. or [50 mm] cube specimens). **Annual book of ASTM standards**: vol. 04.01.
- ASTM C188. (2001). Standard test method for density of hydraulic cement. **Annual book of ASTM standards**: vol. 04.01.
- ASTM C204. (2001). Standard test method for fineness of hydraulic cement by air permeability apparatus. **Annual book of ASTM standards**: vol. 04.01.
- ASTM C1152. (2001). Standard test method for acid-soluble chloride in mortar and concrete. **Annual book of ASTM standards**: vol. 04.02.
- ASTM C1218. (2001). Standard test method for water-soluble chloride in mortar and concrete. **Annual book of ASTM standards**: vol. 04.02.
- Chaipanich, A., and Nochaiya, T. (2010). Thermal analysis and microstructure of Portland cement-fly ash-silica fume pastes. **Journal of Thermal Analysis and Calorimetry**. 99(2): 487-493.
- Crank. (1975). **The mathematics of diffusion**. Oxford press: London.

- El-Jazairi, B., and Illston, J. M. (1977). A simultaneous semi-isothermal method of thermogravimetry and derivative thermogravimetry, and its application to cement pastes. **Cement and Concrete Research**. 7(3); 247-257.
- Galle, C. (2001). Effect of drying on cement-based materials pore structure as identified by mercury intrusion porosimetry: A comparative study between oven-, vacuum-, and freeze-drying. **Cement and Concrete Research**. 31(10): 1467-1477.
- Konecny, L., and Naqvi, S. J. (1993). The effect of different drying techniques on the pore size distribution of blended cement mortars. **Cement and Concrete Research**. 23(5): 1223-1228.
- Lu, N., and Likos, W. J. (2004). **Unsaturated soil mechanics**. New Jersey: John Wiley & Sons Inc.
- Washburn, E. W. (1921). **Note on method of determining the distribution of pore size in porous materials**. Proc. Natl. Acad. Sci. USA (7): 115–116.

CHAPTER IV

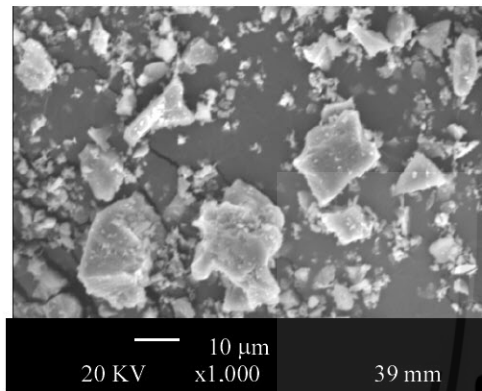
RESULTS AND DISCUSSIONS

In this chapter, the results are presented and discussed of two 2 parts of experimental. In part I, influence of the hydration reaction, filler effect and pozzolanic reaction on compressive strength, hydrate phase and pore size distribution are discussed. In part II, chloride penetration and microstructure of cement paste containing POFA with different finenesses under chloride penetration are reported.

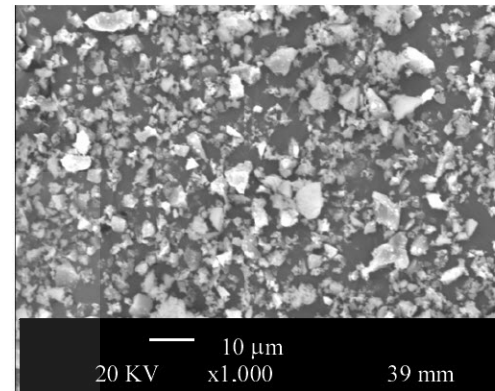
4.1 Physical properties of materials

The SEM photographs of the materials are shown in Figure 4.1. It was found that the ground RHA and POFA consisted of irregular and crushed particles. A similar conclusion was also reported by the other researcher (Chindaprasirt et al., 2008). The physical properties of the materials are presented in Table 4.1. The first group of materials (CRHA, CPOFA and CRS) had particle sizes equal to that of cement. The specific gravities of CRHA, CPOFA and CRS were 2.29, 2.36 and 2.59, respectively. The Blaine fineness values of CRHA, CPOFA and CRS were 7,600, 6,700 and 3,900 cm^2/g , respectively. For the small particle group (FRHA, FPOFA and FRS), the specific gravities and Blaine finenesses of FRHA, FPOFA and FRS were 2.31, 2.48, 2.61 and 18,000, 14,900 and 6,300 cm^2/g , respectively. The particle size distributions

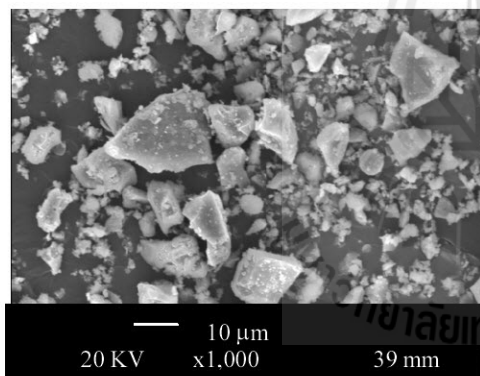
of the materials are shown in Figure 4.2. The median particle sizes of CRHA, CFOFA and CRS were close to the particle size of the cement, while those of FRHA, FPOFA and FRS were smaller than that of the cement.



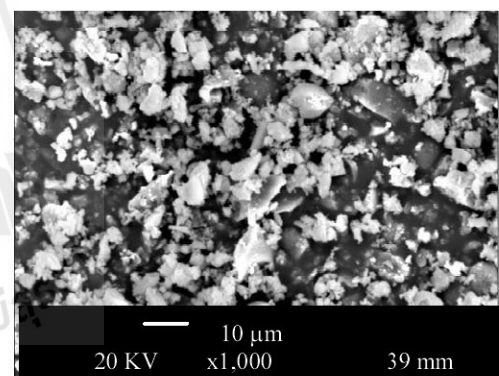
(a) Ground coarse rice husk ash (CRHA)



(b) Ground fine rice husk ash (FRHA)

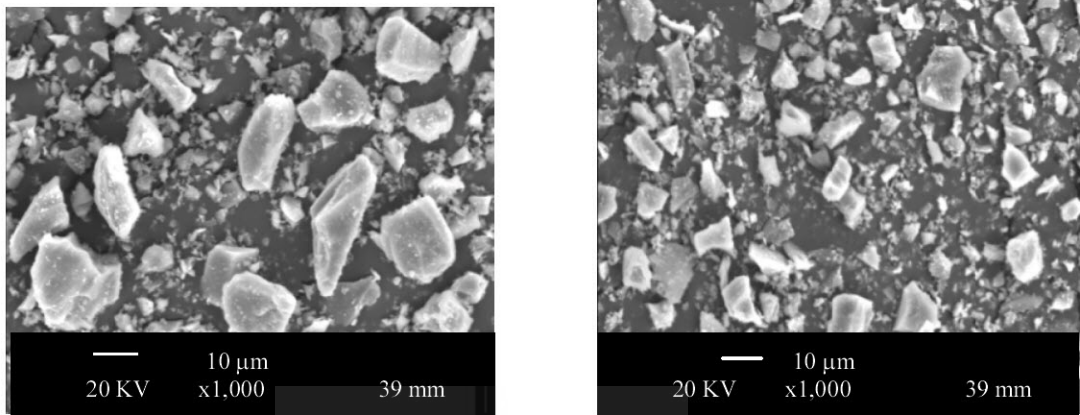


(c) Ground coarse palm oil fuel ash (CPOFA)



(d) Ground fine palm oil fuel ash
(FPOFA)

Figure 4.1 Scanning electron micrographs of the materials



(e) Ground coarse river sand (CRS)

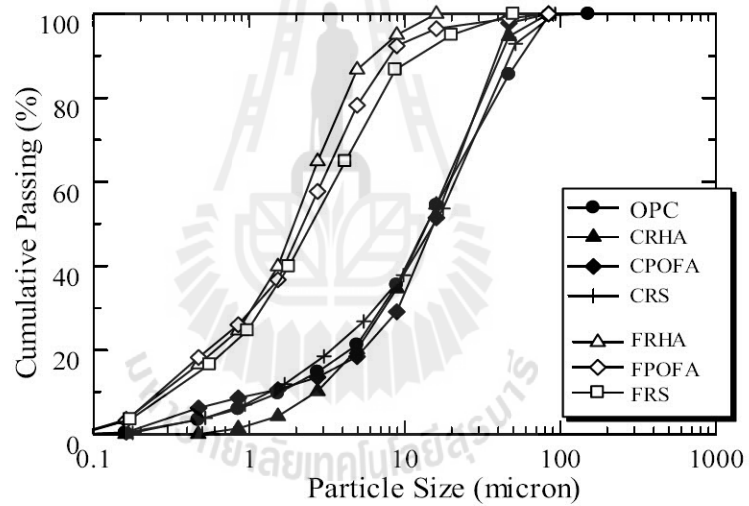
(f) Ground fine river sand (FRS)

Figure 4.1 Scanning electron micrographs of the materials (continued)



Table 4.1 Physical properties of the materials

Sample	Specific gravity	Median particle size, d_{50} (μm)	Blaine fineness (cm^2/g)
OPC	3.14	14.6	3,600
CRHA	2.29	14.8	7,600
CPOFA	2.36	15.6	6,700
CRS	2.59	15.9	3,900
FRHA	2.31	1.9	18,100
FPOFA	2.48	2.1	14,900
FRS	2.61	2.2	6,300

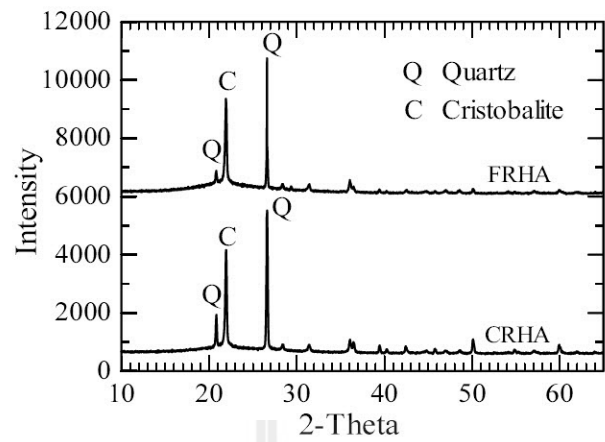
**Figure 4.2** Particle size distributions of the materials

4.2 Chemical and mineralogical analysis

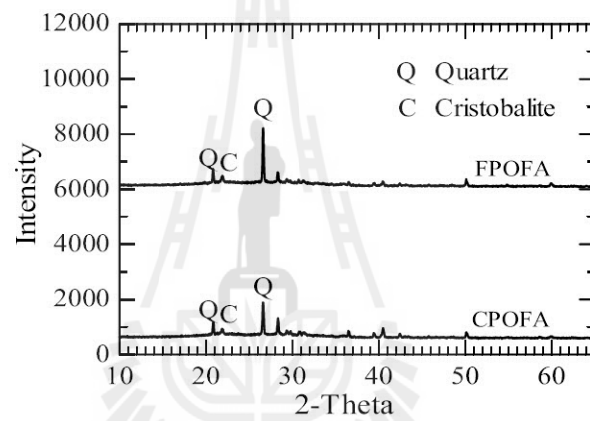
The chemical compositions of the materials are shown in Table 4.2. SiO₂ is the major chemical component of CRHA, FRHA, CPOFA and FPOFA and is 88.8%, 87.8%, 54.0% and 55.7%, respectively. LOI and SO₃ are within the limits of 10.0% and 4%, respectively. The total amounts of SiO₂, Al₂O₃ and Fe₂O₃ in CRHA and FRHA were 91.1% and 89.2%, respectively, which are higher than the 70% for Class N pozzolan specified by ASTM C618. However, the total amounts of SiO₂, Al₂O₃ and Fe₂O₃ of CPOFA and FPOFA were 56.9% and 58.6%, respectively, both of which are less than 70%. A similar finding was also reported by other researchers (Awal and Hussin, 1997). They found that POFA had a total SiO₂, Al₂O₃ and Fe₂O₃ content less than 70%. In the case of insoluble material river sand (RS), the main chemical component of CRS and FRS was also SiO₂ and was 92.0% and 91.2%, respectively. In addition, the X-ray diffraction patterns of the materials are shown in Figure 4.3. The percentage of amorphous material was determined by the quantitative XRD analysis based on the Rietveld method, which was calculated using Bruker's TOPAS. The amorphous contents of CRHA, FRHA, CPOFA and FPOFA were 70.1%, 69.6%, 70.2% and 67.2% (by mass), respectively. The percentages of crystalline CRS and FRS were 100% (by mass). The results confirm that river sand is an inert material, which is similar to the results of previous research (Tangpagasit et al., 2005).

Table 4.2 Chemical compositions of the materials

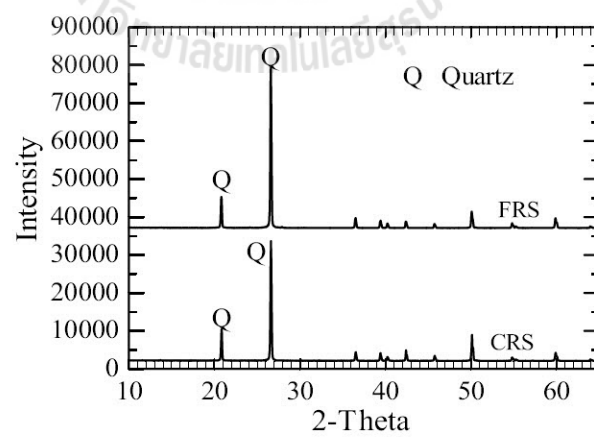
Chemical compositions by weight (%)	OPC	SRPC	CRHA	FRHA	CPOFA	FPOFA	CRS	FRS
Silicon dioxide (SiO ₂)	20.8	21.5	88.8	87.8	54.0	55.7	92.0	91.2
Aluminum oxide (Al ₂ O ₃)	4.7	3.5	0.6	0.5	0.9	0.9	1.6	1.8
Iron oxide (Fe ₂ O ₃)	3.4	4.5	1.7	0.9	2.0	2.0	0.6	0.2
Calcium oxide (CaO)	65.3	66.2	1.1	1.2	12.9	12.5	0.9	0.7
Magnesium oxide (MgO)	-	1.2	0.6	0.6	4.9	5.1	0.1	0.1
Sodium oxide (Na ₂ O)	0.1	0.1	0.2	0.2	1.0	1.0	0.1	0.1
Potassium oxide (K ₂ O)	0.4	0.3	2.0	2.2	13.5	11.9	2.2	2.3
Sulfur trioxide (SO ₃)	2.7	2.3	0.1	0.1	4.0	2.9	-	-
Loss on ignition (LOI)	0.9	1.2	3.6	5.2	3.7	4.7	2.1	1.8
SiO ₂ + Al ₂ O ₃ + Fe ₂ O ₃	-	-	91.1	89.2	56.9	58.6	94.2	93.2
Quantitative XRD Rietveld method								
Amorphous (%)	-	-	70.1	69.6	70.2	67.2	-	-
Crystalline (%)	-	-	29.9	30.4	29.8	32.8	100.0	100.0
Quartz	-	-	59.3	56.2	65.0	73.0	100.0	100.0
Cristobalite	-	-	40.7	43.8	35.0	27.0	-	-



(a) RHA



(b) POFA



(c) RS

Figure 4.3 X-ray diffraction patterns of the materials

Part I

4.3 Compressive strength

Table 4.3 shows the compressive strengths at 7, 28, 60 and 90 days for the OPC paste, which were 53.0, 75.0, 84.6 and 99.1 MPa, respectively. At 7 days, the compressive strengths of pastes containing 10%-40% of CRHA with the same particle size as cement were lower than that of the OPC paste because of the low cement content, which resulted in a significant reduction in the normalized strength (Megat Johari et al., 2011; Tangchirapat and Jaturapitakkul, 2010). Additionally, the compressive strengths of the 10CRHA and 20CRHA pastes at 28 days were 76.5 and 74.2 MPa or about 102% and 98.9% of that of the OPC paste, respectively, while those of the 30CRHA and 40CRHA pastes at 28 and 90 days were 70.5, 64.7 and 100.0, 92.1 MPa or about 94%, 86.3% and 100.9%, 92.9% of that of the OPC paste, respectively. In the case of pastes containing FRHA (small particle size of RHA), the compressive strengths of the 10FRHA, 20FRHA and 30FRHA pastes were 55.9, 52.9 and 50.3 MPa or 105.5%, 99.8% and 94.9% of that of the OPC paste at 7 days and increased to 81.7, 78.7 and 74.9 MPa or 108.9%, 104.9% and 99.9% of that of the OPC paste at 28 days, respectively.

For the group mixed with ground palm oil fuel ash, the pastes containing 10-40% CPOFA had compressive strengths that were lower than that of OPC paste at 7 days. The 28 days compressive strengths were 74.8, 72.0, 66.7 and 61.5 MPa with a normalized strength of 99.7%, 96.0%, 88.9% and 82.0% for the 10CPOFA, 20CPOFA, 30CPOFA and 40CPOFA pastes, respectively. At 90 days, they increased to 104.5, 102.0, 97.1 and 88.1 MPa with a normalized strength of 105.4%, 102.9%, 98.0% and 88.9% of the OPC paste, respectively. For the pastes with a small particle

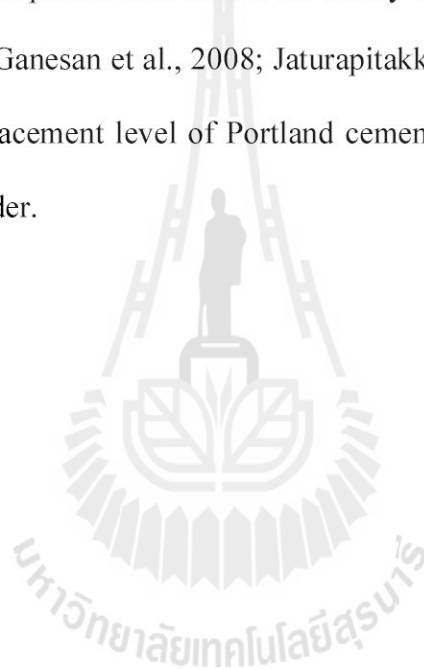
size, the compressive strengths of the 10FPOFA and 20FPOFA pastes at 28 and 90 days were 79.3, 77.3 and 111.3, 109.6 MPa or about 105.7%, 103.1% and 112.3%, 110.6% of the strength of the OPC paste, respectively. Moreover, at 30% and 40% FPOFA, the compressive strengths at 90 days were 104.0 and 94.1 MPa or about 104.9% and 95.0% of that of the OPC paste, respectively.

The compressive strength of blended cement paste at 7-28 days increased with age but decreased with an increase in the replacement of ash. The increased compressive strength of blended cement paste can be explained by three factors: the hydration reaction, the filler effect and the pozzolanic reaction. The hydration reaction is the strength proportionate to the amount of cement in the mix. The filler effect has two causes, the nucleation effect and packing effect, which depend significantly on the fineness of material. The nucleation effect arises when the small particles are dispersed in the blended cement paste and enhance the cement hydrate while the packing effect occurs when small particles fill the voids of the paste (Cyr et al., 2006; Gopalan, 1993; Montgomery et al., 1981; Rukzon and Chindaprasirt, 2012). Therefore, the blended cement paste containing biomass ash with high fineness was more homogeneous and denser, which increased the compressive strength of the paste. Finally, the pozzolanic reaction occurs because of the SiO_2 and Al_2O_3 contained in the biomass ash, which react with Ca(OH)_2 and produce an additional calcium silicate hydrate (C-S-H).

Table 4.3 Compressive strengths of the pastes

Symbol	Compressive strength (MPa)				Normalized compressive strength (%)			
	7 days	28 days	60 days	90 days	7 days	28 days	60 days	90 days
OPC	53.0	75.0	84.6	99.1	100.0	100.0	100.0	100.0
10CRHA	52.4	76.5	88.5	107.6	98.9	102.0	104.6	108.6
20CRHA	49.8	74.2	88.3	106.0	94.0	98.9	104.4	107.0
30CRHA	46.5	70.5	83.7	100.0	87.7	94.0	98.9	100.9
40CRHA	42.4	64.7	77.4	92.1	80.0	86.3	91.5	92.9
10FRHA	55.9	81.7	94.7	116.2	105.5	108.9	111.9	117.3
20FRHA	52.9	78.7	93.1	113.2	99.8	104.9	110.0	114.2
30FRHA	50.3	74.9	89.6	107.9	94.9	99.9	105.9	108.9
40FRHA	44.5	66.9	79.5	96.1	84.0	89.2	94.0	97.0
10CPOFA	51.3	74.8	86.3	104.5	96.8	99.7	101.6	105.4
20CPOFA	48.3	72.0	84.6	102.0	91.1	96.0	99.6	102.9
30CPOFA	44.5	66.7	78.6	97.1	84.0	88.9	92.9	98.0
40CPOFA	41.0	61.5	72.8	88.1	77.4	82.0	85.7	88.9
10FPOFA	53.7	79.3	93.3	111.3	101.3	105.7	109.9	112.3
20FPOFA	51.9	77.3	92.2	109.6	97.9	103.1	108.6	110.6
30FPOFA	48.3	72.8	86.3	104.0	91.1	96.9	101.6	104.9
40FPOFA	44.0	66.5	78.6	94.1	83.0	88.7	92.6	95.0
10CRS	48.3	68.2	77.2	90.1	91.1	90.9	91.3	90.9
20CRS	42.9	60.8	67.9	78.6	80.9	81.1	80.3	79.3
30CRS	36.9	53.1	60.8	70.2	69.6	70.8	71.9	70.8
40CRS	31.5	45.6	51.5	59.6	59.4	60.8	60.9	60.1
10FRS	49.9	69.9	79.1	92.8	94.2	93.2	93.5	93.6
20FRS	45.0	63.4	70.8	82.1	84.9	84.5	83.7	82.8
30FRS	39.1	56.5	64.1	74.5	73.8	75.3	75.8	75.2
40FRS	34.2	49.2	55.4	63.9	64.5	65.6	65.5	64.5

Comparing the RHA and POFA blended cement pastes in terms of the same replacement and same fineness, the normalized strengths of RHA pastes were slightly higher than those of POFA pastes because RHA contains more SiO_2 than POFA. The results indicated that RHA was more reactive than POFA, and the results agree with Tangpagasit et al., (2005). In addition, the results suggest that the replacement of cement type I by RHA and POFA up to 30% by weight of binder does not impair the compressive strength of pastes. The results are nearly identical to the results obtained by other researchers (Ganesan et al., 2008; Jaturapitakkul et al., 2011a), who reported that the optimum replacement level of Portland cement Type I by RHA or POFA is 30% by weight of binder.



4.4 Assessing the effect of biomass ashes with different finenesses on the compressive strength of blended cement paste

4.4.1 Influence of cement content on the percentage compressive strength of paste

The percentage compressive strength of ground river sand paste with age (P_H) is shown in Figure 4.4. For pastes containing CRS with the same particle size as that of cement, the percentage compressive strengths of CRS pastes at any age were almost constant. The same trend was also reported by Jaturapitakkul et al., (2011a); Tangpagasit et al., (2005). In contrast, the relationship between the percentage compressive strengths of pastes due to the hydration reaction and the percentage replacement of CRS paste is shown in Figure 4.5. The percentage compressive strength decreased linearly with replacement of CRS. The results suggest that the percentage compressive strength of pastes containing inert material with the same particle size as cement does not depend on age but rather depends on the cement content.

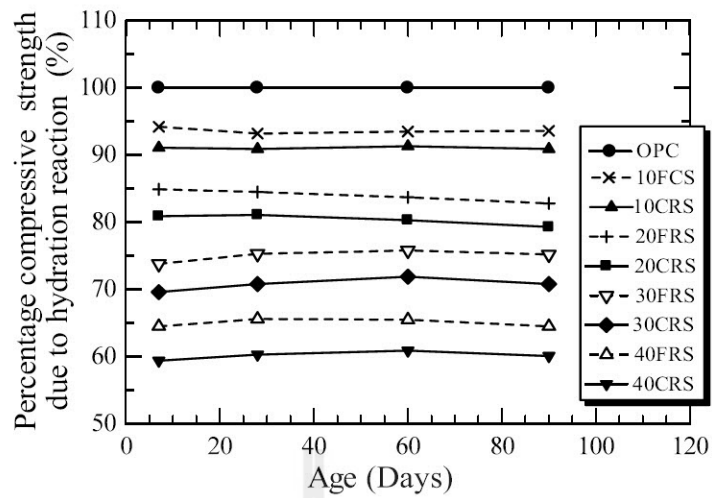


Figure 4.4 Relationship between the percentage compressive strength of ground river sand paste and age

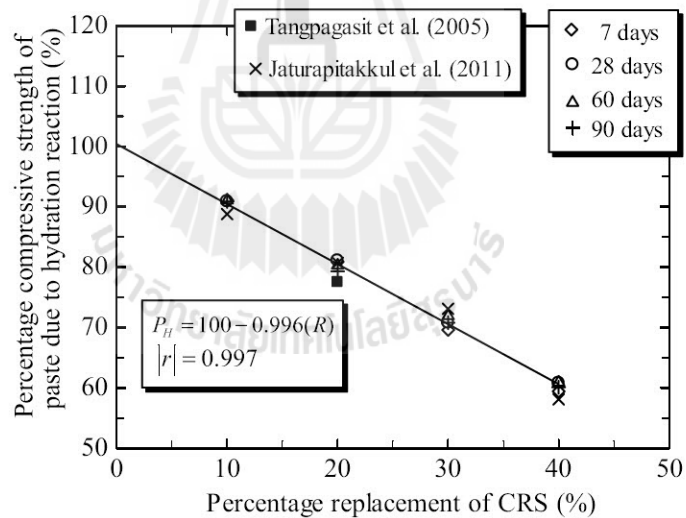


Figure 4.5 Relationship between the percentage compressive strength of paste due to the hydration reaction and the percentage replacement of CRS

The empirical equations can be expressed for the percentage compressive strength of paste due to the hydration reaction in terms of (R) as follows:

$$P_H = 100.4 - 0.996(R) \quad (4.1)$$

where P_H is percentage compressive strength due to the hydration reaction of paste (%) and R is the replacement of Portland cement by 10%-40% an inert material. The correlation value of 0.997 indicates a strong linear relationship between the percentage compressive strength and the percentage replacement of CRS.

When the data of Tangpagasit et al. (2005) and Jaturapitakkul et al. (2011) are plotted in Figure 4.5 and compared with percentage compressive strength due to the hydration reaction of paste. The data of Tangpagasit et al. (2005) and Jaturapitakkul et al. (2011) are very close to the trend line of percentage replacement of CRS paste, and it can be used to predict the value percentage compressive strength due to the hydration reaction of paste.

4.4.2 Influence of the filler effect on the percentage compressive strength of paste

The relationship between the percentage compressive strength of ground river sand with different finenesses of paste and age are shown in Figure 4.4. The pastes with particles smaller than OPC had a higher percentage compressive strength than the pastes with large particle size and had an almost constant value (Jaturapitakkul et al., 2011a; Tangpagasit et al., 2005). Figure 4.6 shows the percentage compressive strengths of ground river sand with different finenesses of paste and replacements with river sand. The percentage compressive strength of paste due to the filler effect tended to increase with the amount of cement replacement and was approximately 2.2-5.1% of the strength of the OPC paste. This is due to the small particles dispersed into the blended cement paste and accelerated the hydration reaction. In addition, the packing effect occurred as the small particles filled the voids of the paste (Cyr et al., 2006; Gopalan, 1993; Lee et al., 2012; Montgomery et al., 1981). Therefore, the paste was more homogeneous and denser, which resulted in the increased compressive strength of the paste. These results suggest that a particle size smaller than OPC has very important role in increasing the compressive strength by the filler effect (Chindaprasirt et al., 2005). The results of the filler effect for pastes agrees closely with the result obtained by Jaturapitakkul et al., (2011b), who reported that the difference in the percentage compressive strengths between mortar containing the same particle sizes of inert material and small sizes of inert material was up to 5.8% of the strength of the mortar.

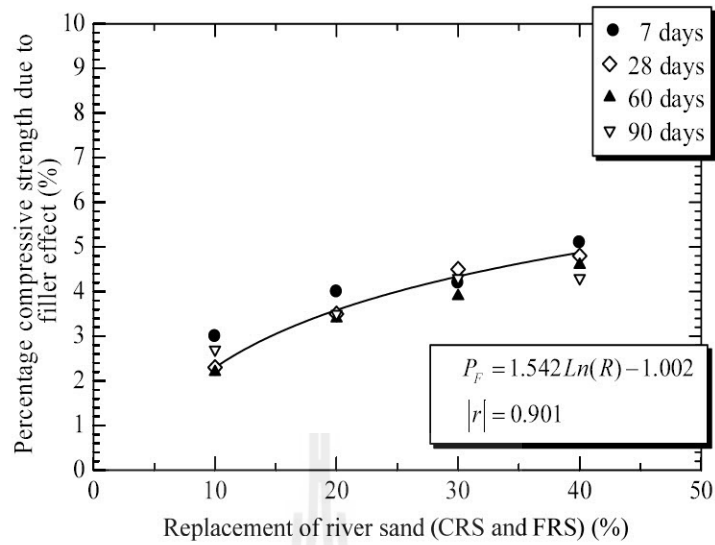


Figure 4.6 Relationships between the percentage compressive strength of paste due effect and the replacement of river sand (CRS and FRS)

The empirical equation to predict the percentage of the compressive strength of the paste due to the filler effect in terms of replacement (R) is proposed as follows:

$$P_F = 1.542 \ln(R) - 1.002 \quad (4.2)$$

where P_F is the percentage compressive strength of the paste due to the filler effect (%) and R is the replacement of Portland cement by inert material (%). It was found that P_F is represented by a logarithmic equation and has good correlation. The empirical equation also suggest that the percentage compressive strength of the paste due to the filler effect of the blended cement paste increased with an increase in the replacement of inert material.

4.4.3 Influence of the pozzolanic reaction on the percentage compressive strength of pastes

Figures 4.7 and 4.8 show the percentage compressive strength of paste due to the pozzolanic reaction of RHA and POFA, respectively. The pozzolanic reaction increased with age and with the replacement of RHA or POFA. In addition, the high fineness of RHA or POFA was more efficient for the pozzolanic reaction than the coarse fineness because the high fineness of the ash provided a large surface area to contribute silica and alumina compounds for the pozzolanic reaction (Cordeiro et al., 2011; Cordeiro et al., 2008). These compounds reacted with Ca(OH)_2 from the hydrated cement and produced an increase in calcium silicate hydrate. In addition, the percentage compressive strength due to the pozzolanic reaction of higher replacement paste increased more than that of the lower replacement paste. The blended cement paste containing a high replacement of the ash showed a decrease of Ca(OH)_2 content compared with the low replacement paste (Kroehong et al., 2011). In addition, the reduction of Ca(OH)_2 affected the increase of the calcium silicate hydrate from the pozzolanic reaction (Aly et al., 2012).

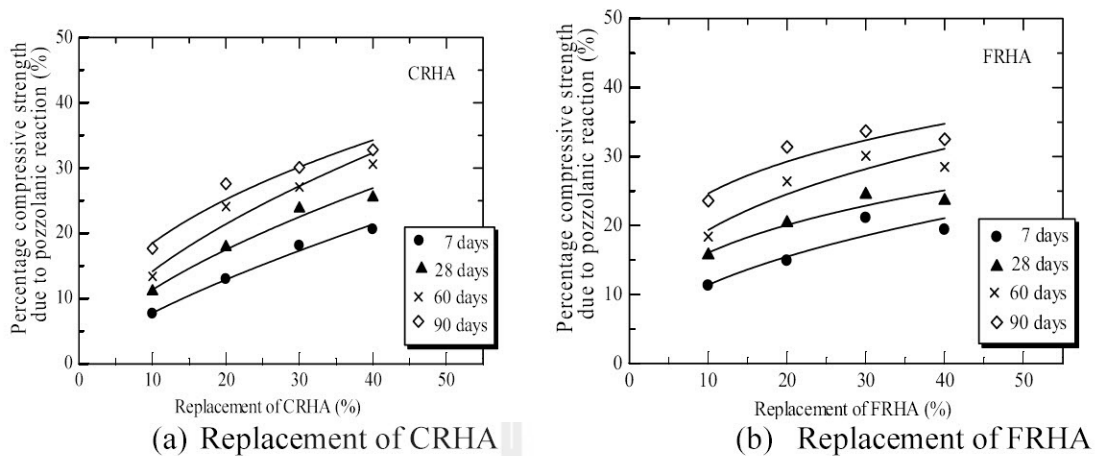


Figure 4.7 Relationships between the percentage compressive strength due to the pozzolanic reaction of RHA pastes and age

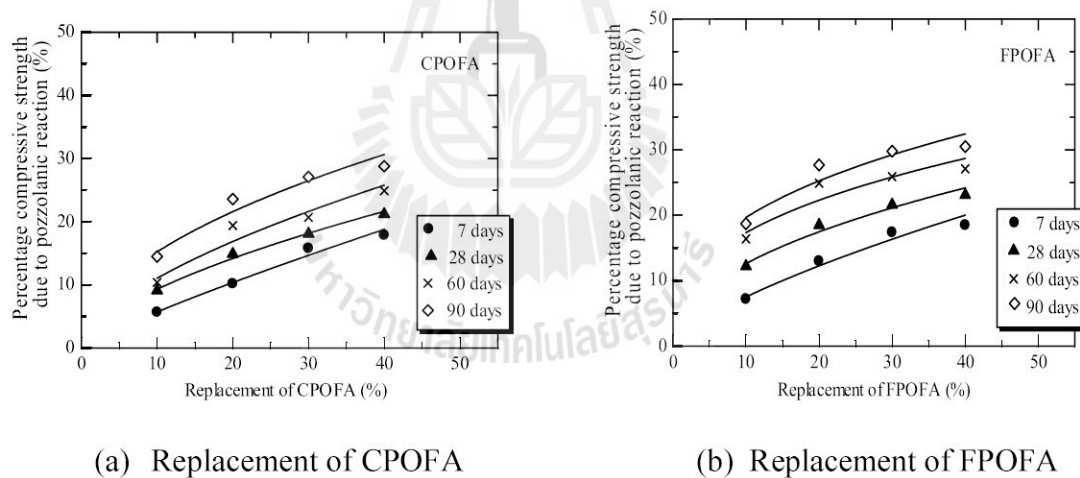


Figure 4.8 Relationships between the percentage compressive strength due to the pozzolanic reaction of POFA paste and age

Comparing the percentage compressive strength of paste due to the pozzolanic reaction in Figures 4.7 and 4.8, the RHA pastes had a higher percentage compressive strength of paste due to the pozzolanic reaction than the POFA pastes. The maximum percentage compressive strength due to the pozzolanic reaction of RHA and POFA pastes were 33.7% and 30.5% that of the OPC paste, respectively, because RHA has a higher SiO₂ content than POFA. The results confirmed that the percentage compressive strength of paste due to the pozzolanic reaction increased with age, fineness, and the replacement rate of the ash.

Figures 4.7 and 4.8 show that the percentage compressive strength due to the pozzolanic reaction is explicitly nonlinear and is best fit with nonlinear isotherms, which are shown in the same figure. Thus, the equation to predict the percentage compressive strength of paste due to the pozzolanic reaction is:

$$P_{PZ,t} = \alpha R^\beta \quad (4.3)$$

where $P_{PZ,t}$ is the percentage compressive strength of the paste due to the pozzolanic reaction at a specified age ($t = 7, 28, 60$ and 90 days), R is the rice husk ash or palm oil fuel ash replacement (%) and α and β are the pozzolanic constants. The pozzolanic constants for the isotherm fitted from experimental results of the pastes are presented in Table 4.4.

Table 4.4 Best fit of the pozzolanic constants for the isotherms

Binder Type	Days	Pozzolanic constants		Correlation
		α	β	
CRHA	7	1.479	0.723	0.993
	28	2.728	0.617	0.988
	60	3.593	0.595	0.948
	90	6.633	0.445	0.943
FRHA	7	4.098	0.444	0.895
	28	7.667	0.321	0.923
	60	8.817	0.341	0.865
	90	13.940	0.247	0.837
CPOFA	7	0.792	0.856	0.993
	28	2.273	0.611	0.991
	60	2.703	0.611	0.939
	90	4.798	0.502	0.949
FPOFA	7	1.462	0.709	0.972
	28	4.590	0.449	0.974
	60	7.513	0.363	0.884
	90	8.551	0.361	0.899

4.4.4 Generating an empirical equation for the prediction of the percentage compressive strength of the blended cement paste

4.4.4.1 Role of the blended cement paste containing biomass ash on the percentage of compressive strength

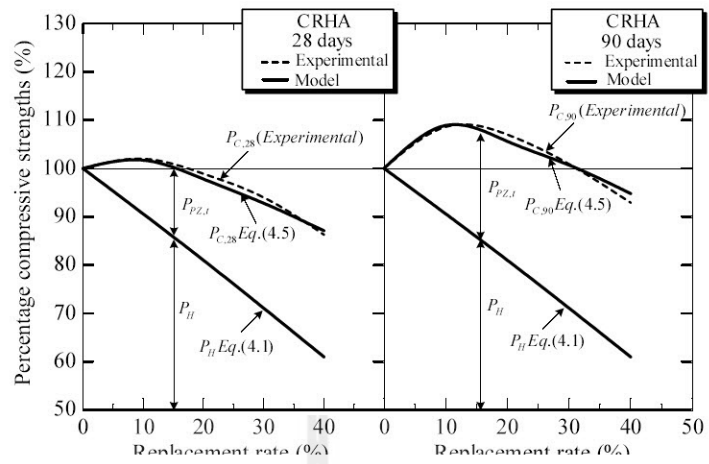
The percentage compressive strength of the blended cement paste containing biomass ash with the same particle size as cement is related to the hydration reaction and pozzolanic reaction as follows:

$$P_{C,t} = P_H + P_{PZ,t} \quad (4.4)$$

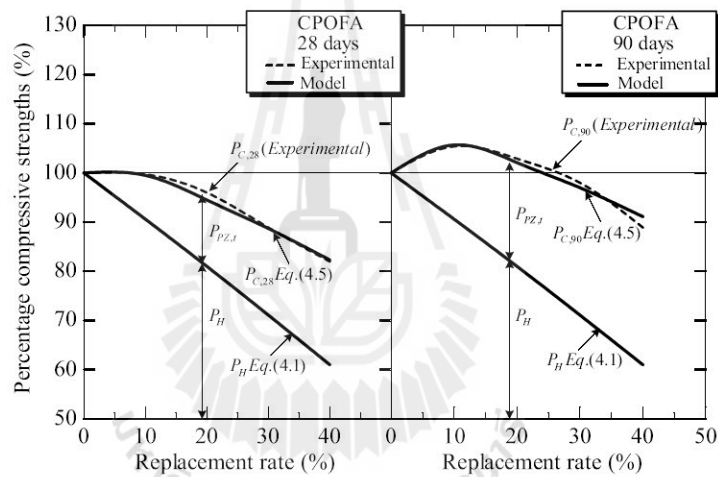
Equation (4.5) can be rewritten as follows:

$$P_{C,t} = 100.4 - 0.996(R) + \alpha R^\beta \quad (4.5)$$

where $P_{C,t}$ is the total percentage compressive strength of the paste at a specified age ($t=7, 28, 60$ and 90 days), P_H is the percentage compressive strength of the paste due to the hydration reaction, $P_{PZ,t}$ is the percentage compressive strength of the paste due to the pozzolanic reaction at various curing times ($t=7, 28, 60$ and 90 days), R is the percentage replacement of RHA or POFA and α and β are the pozzolanic constants. The prediction using Equation (4.5) and experimental results are shown in Figure 4.9. This equation is useful to predict the percentage compressive strength of blended cement pastes containing RHA and POFA.



(a) Coarse rice husk ash (CRHA)



(b) Coarse palm oil fuel ash (CPOFA)

Figure 4.9 Relationships between the percentage compressive strengths of blended cement pastes containing CRHA and CPOFA with the same particle size as that of OPC

For the mixture of biomass ash with a particle size smaller than that of OPC, the percentage compressive strength of paste is due to the hydration reaction, filler effect and pozzolanic reaction as follows:

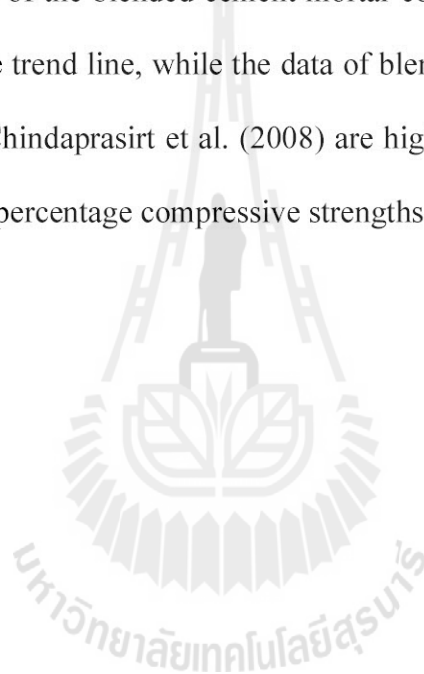
$$P_{C,t} = P_H + P_F + P_{PZ,t} \quad (4.6)$$

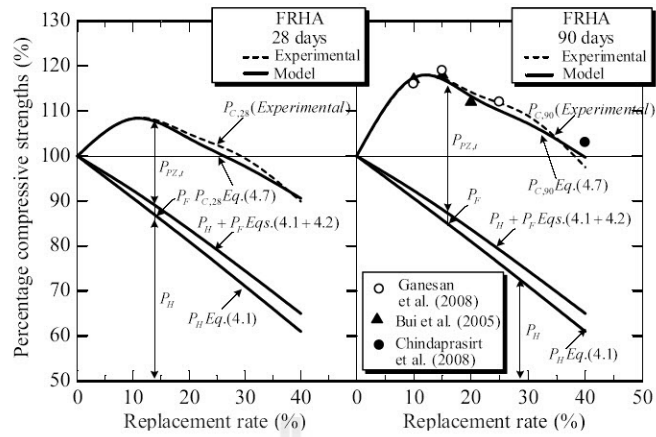
Equation (4.6) can be rewritten as follows:

$$P_{C,t} = 99.398 - 0.996(R) + 1.542Ln(R) + \alpha R^\beta \quad (4.7)$$

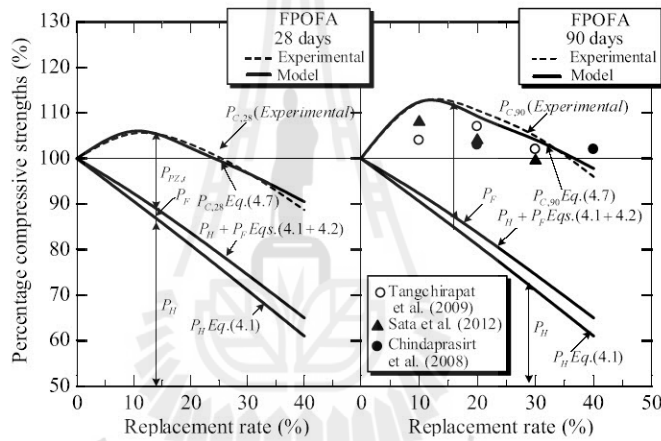
where $P_{C,t}$ is the total percentage compressive strength of the paste at a specified age ($t=7, 28, 60$ and 90 days), P_H is the percentage compressive strength of the paste due to the hydration reaction, P_F is the percentage compressive strength of the paste due to the filler effect, $P_{PZ,t}$ is the percentage compressive strength of the paste due to the pozzolanic reaction at a specified age ($t=7, 28, 60$ and 90 days), R is the percentage replacement of RHA or POFA, and α and β are the pozzolanic constants. The percentage compressive strength of the pastes according to this equation was compared with the actual test specimens, as shown in Figure 4.10. The equation suggests that the percentage compressive strength of the paste due to the pozzolanic reaction is higher than that due to the filler effect. Moreover, it is also useful to predict the percentage compressive strength of pastes with the curing time and amounts of replacement of RHA and POFA.

The percentage compressive strengths of the blended cement mortar containing RHA at 90 days from Bui et al. (2005), Ganesan et al. (2008) and Chindaprasirt (2008) are plotted in Figure 4.10 (a) and compared with the trend line of the blended cement paste, the value of the percentage compressive strength of blended cement mortar are near the trend line of blended cement paste. The data of Tangchirawat et al. (2009) and Sata et al. are plotted in Figure 4.10 (b), it is found that the percentage compressive strengths of the blended cement mortar containing POFA at 90 days are slightly lower than the trend line, while the data of blended cement mortar containing 40% of POFA from Chindaprasirt et al. (2008) are higher the trend line. Thus, it can be used to predict the percentage compressive strengths of the blended cement paste.





(a) Fine rice husk ash FRHA



(b) Fine palm oil fuel ash FPOFA

Figure 4.10 Relationships between the percentage compressive strengths of the blended cement paste containing FRHA and FPOFA with particle sizes smaller than that of OPC

4.4.4.2 Verification

The measured percentage compressive strengths of the pastes for $W/B = 0.35$, $R = 10\%-40\%$, and $d = 7, 28, 60$ and 90 days were compared with the predicted results according to Equations (4.5) and (4.7), which are shown in Figure 4.11. The measured and predicted values are reasonably close. The error from prediction is satisfied with the mean absolute percent error, which is less than 2.4%.

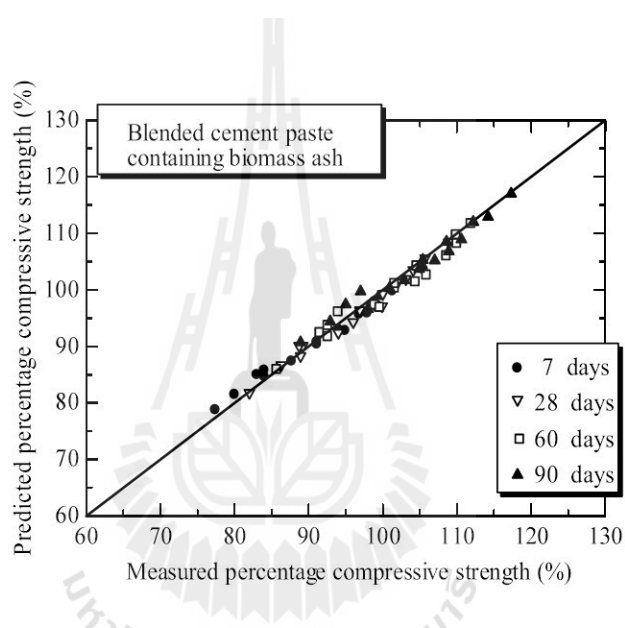


Figure 4.11 Comparison between the predicted and experimental percentage compressive strength of blended cement pastes containing biomass ashes

4.5 Effect of biomass ash fineness on the hydrated phase of blended cement paste

4.5.1 Hydrated phase of cement pastes containing rice husk ash and palm oil fuel ash

Thermogravimetric analysis (TGA) results of the OPC paste and pastes containing RHA and POFA are given in Figures 4.12, 4.13, 4.14 and 4.15. Three step mass loss transitions were found. The first step shows the mass loss of dehydration such as ettringite, C-S-H and C_2ASH_8 , which occurred at 105-450°C (Bai et al., 2003). The second step mass loss of $Ca(OH)_2$ was detected between 450-580°C (El-Jazairi and Illston, 1977), and the third step at 580-1000°C showed the mass loss of calcium carbonate ($CaCO_3$) (El-Jazairi and Illston, 1977).

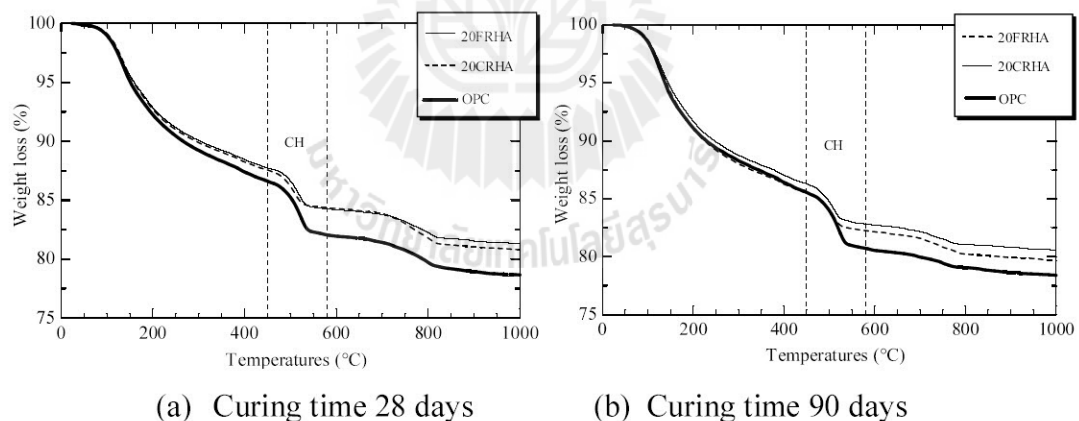


Figure 4.12 TGA curve results of OPC paste and 20RHA pastes

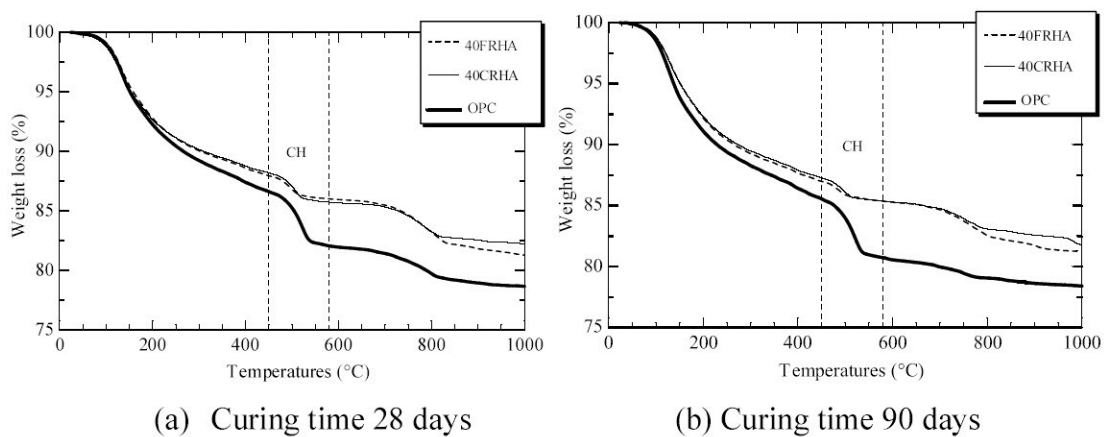


Figure 4.13 TGA curve results of OPC paste and 40RHA pastes

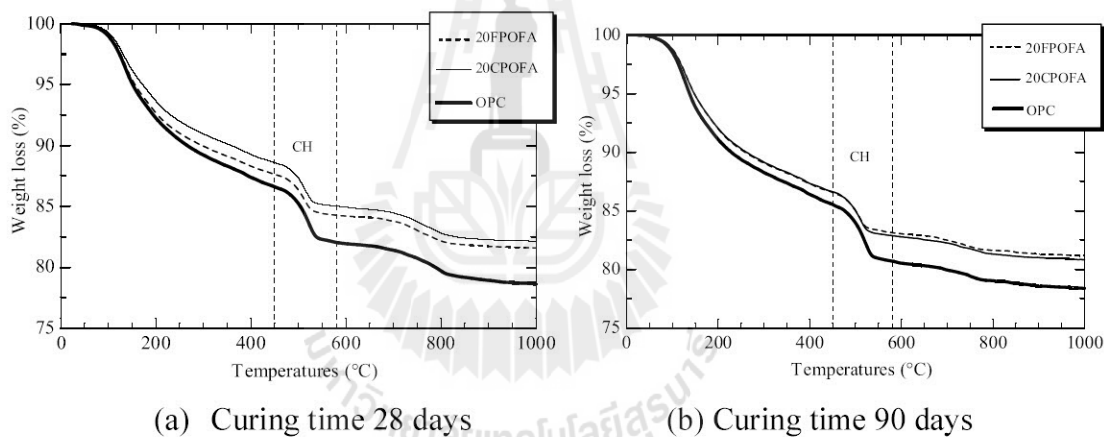


Figure 4.14 TGA curve results of OPC paste and 20POFA pastes

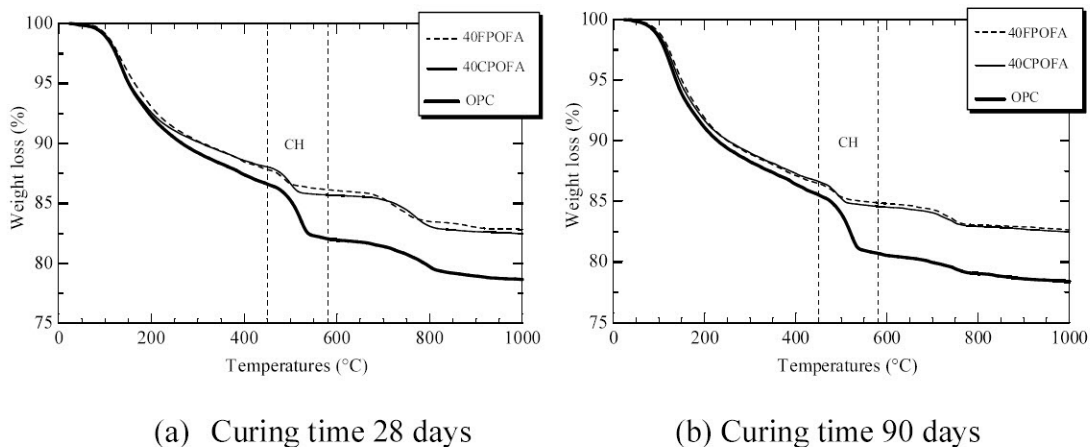


Figure 4.15 TGA curve results of OPC paste and 40POFA pastes

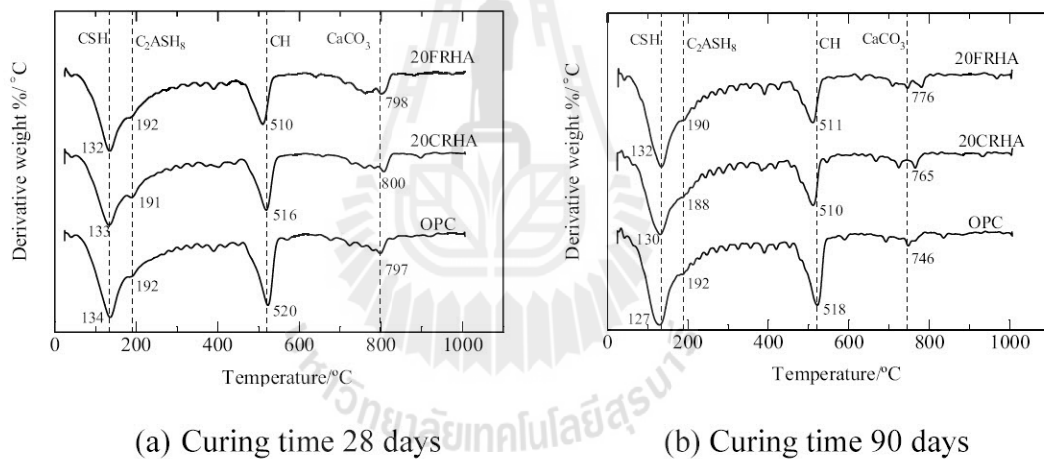


Figure 4.16 DTG curve results of OPC paste and 20RHA pastes

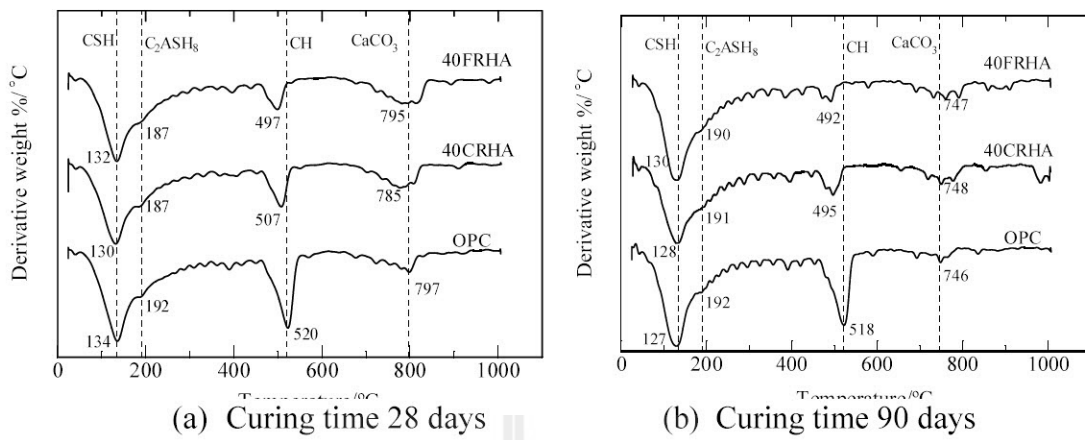


Figure 4.17 DTG curve results of OPC paste and 40RHA pastes

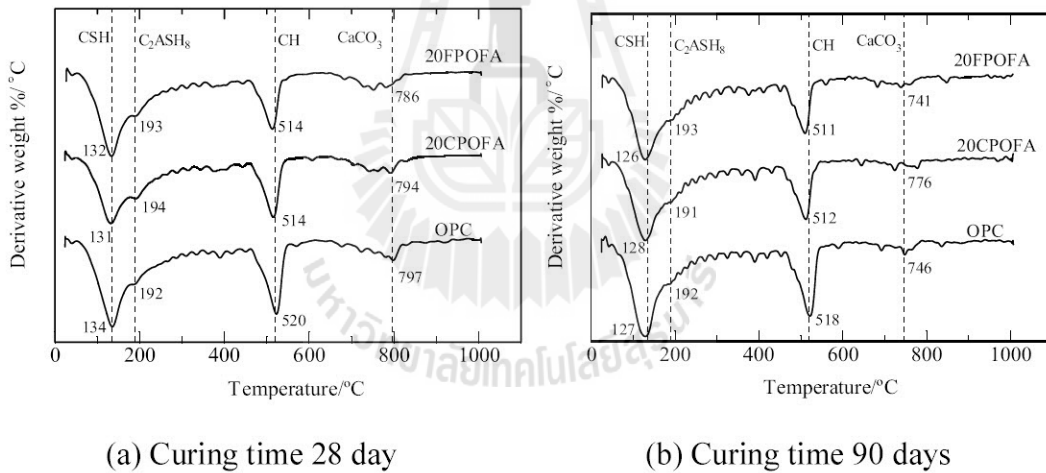


Figure 4.18 DTG curve results of OPC paste and 20POFA pastes

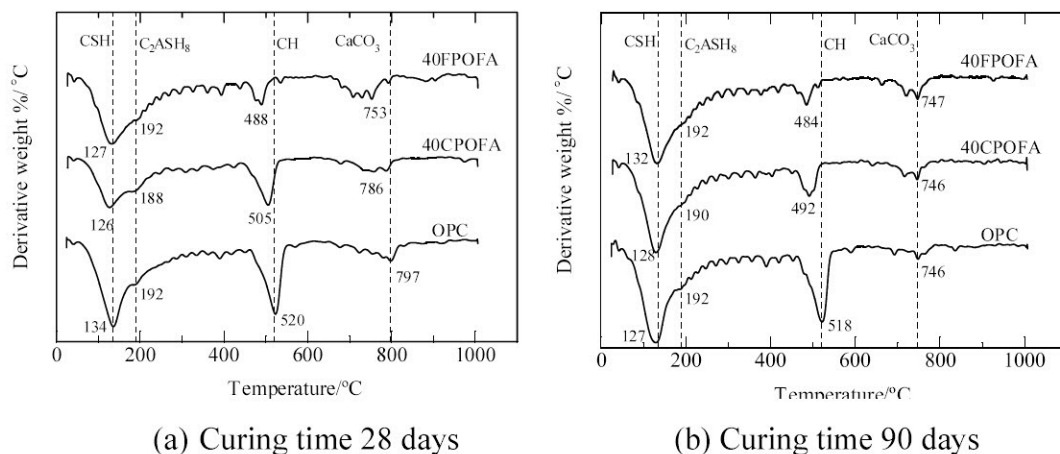


Figure 4.19 DTG curve results of OPC paste and 40POFA pastes

The derivative thermogravimetric (DTG) results of the OPC, RHA and POFA cement pastes are plotted in Figures 4.16, 4.17, 4.18 and 4.19. At 28 and 90 days, the DTG curves of all pastes showed similar phases, which are C-S-H, C₂ASH₈, Ca(OH)₂ and CaCO₃ detected at 126-134°C, 187-194°C, 484-520°C and 741-800°C, respectively. Similar findings have also been reported by other researchers (Chaipanich and Nochaiya, 2010; Nochaiya et al., 2010). The DTG curve peak for Ca(OH)₂ of the pastes containing rice husk ash and palm oil fuel ash decreased with increasing replacement of the rice husk ash and palm oil fuel ash and also decreased with curing time. The high fineness RHA and POFA were more effective for decreasing the peak intensity of Ca(OH)₂ than that with a large particle size because the high fineness RHA and POFA have a large surface area to provide the silica and alumina compounds for pozzolanic reaction. These compounds reacted and consumed Ca(OH)₂. The Ca(OH)₂ consumption was used as an indicator of the pozzolanic reaction. The reduction of Ca(OH)₂ in all RHA and POFA pastes became more subtle

with age. The fineness of the RHA and POFA had an effect on the pozzolanic reaction rate. The pastes containing high fineness RHA and POFA showed a higher pozzolanic reaction rate than the pastes containing coarse RHA and POFA. The reduction of Ca(OH)_2 led to an increased peak intensity for the C-S-H and C_2ASH_8 phases with increasing curing time, which resulted in an increase in the compressive strength.

4.5.2 Ca(OH)_2 content

The Ca(OH)_2 contents of RHA and POFA pastes at different ages are shown in Figures 4.20 and 4.21, respectively. The Ca(OH)_2 contents of the OPC paste at 7, 28, 60 and 90 days were 19.02%, 19.64%, 20.22% and 20.46%, respectively. The increase in the Ca(OH)_2 contents of the OPC paste was due to hydration of the cement. The Ca(OH)_2 contents of the pastes containing RHA and POFA decreased with the pozzolanic reaction of RHA and POFA. The Ca(OH)_2 contents of 20CRHA, 20FRHA, 20CPOFA and 20FPOFA were between 14.34%-15.57%, 13.33%-14.80%, 15.10%-15.82% and 13.93%-15.24% or reduced by approximately 8%, 10%, 5% and 9% of that of the 20CRHA, 20FRHA, 20CPOFA and 20FPOFA pastes at 7 days, respectively. The reduction of Ca(OH)_2 in the blended cement paste indicates its consumption by the pozzolanic reaction (Vedalakshmi et al., 2003). In addition, the pastes containing high fineness of RHA and POFA showed lower Ca(OH)_2 contents than that of the coarse fineness of RHA and POFA due to the high fineness of the particles and the silicon dioxide (SiO_2) contents in the RHA and POFA, which react with Ca(OH)_2 by the pozzolanic reaction. With a replacement ratio of 40% RHA and POFA, the Ca(OH)_2 contents of the 40CRHA, 40FRHA, 40CPOFA and 40FPOFA pastes were between 8.83%-12.12%, 6.43%-11.46%, 9.24%-12.18% and 7.19%-11.75% or reduced by approximately 27%, 44%, 24% and

39% as compared to the 40CRHA, 40FRHA, 40CPOFA and 40FPOFA pastes at 7 days, respectively. Moreover, the reduction of the Ca(OH)_2 contents of high replacement decreased more quickly than that of low replacement. These results suggest that the higher fineness rice husk ash and palm oil fuel ash, which has a higher surface area, produces a greater pozzolanic reaction. In addition, the Ca(OH)_2 contents of pastes containing RHA and POFA decrease with increasing RHA and POFA content. These results agree with Chindaprasirt et al., (2007).

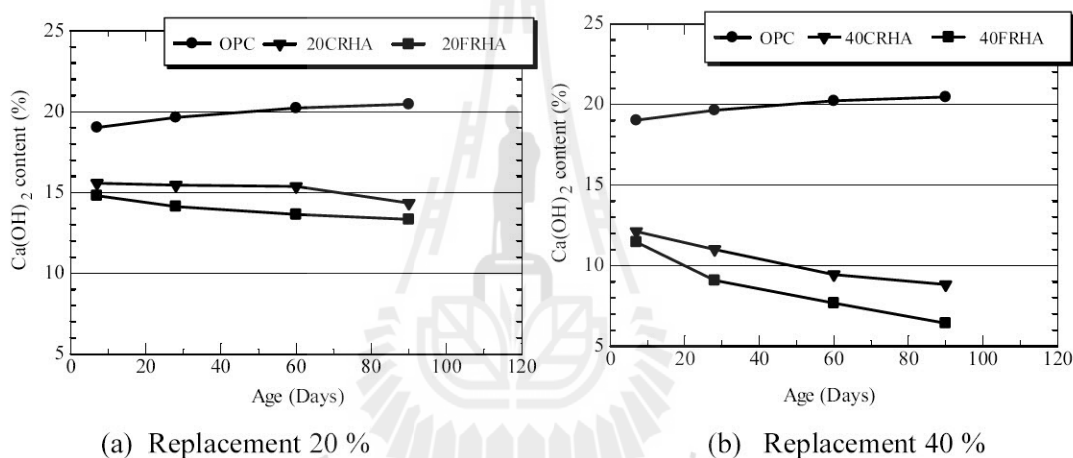


Figure 4.20 Ca(OH)_2 content of RHA paste

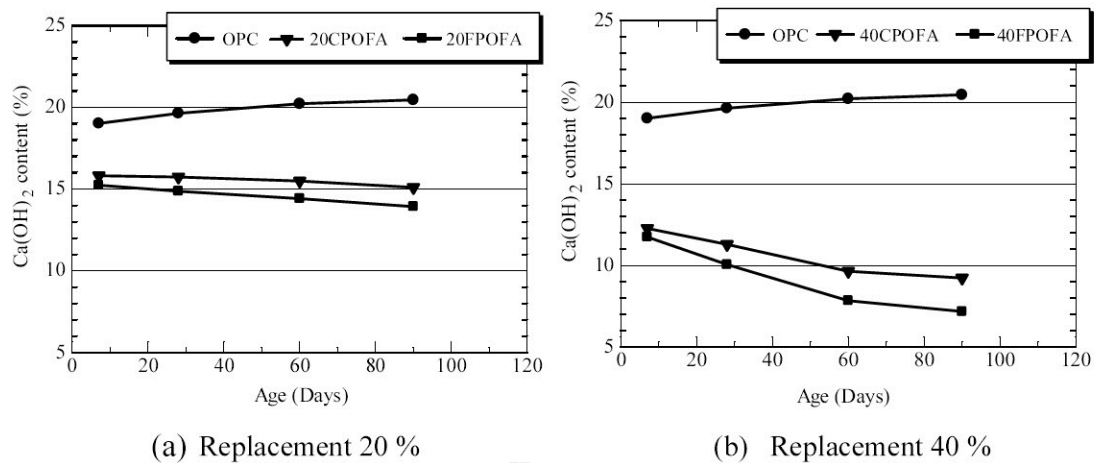


Figure 4.21 Ca(OH)₂ content of POFA paste

4.6 Effect of biomass ashes fineness on the pore size distribution of blended cement paste

4.6.1 Total porosity of the cement paste

The results for the total porosity of all pastes at different ages are presented in Table 4.5. The total porosities of the OPC paste at 7, 28, 60 and 90 days were 22.8%, 20.1%, 17.4% and 16.6%, respectively. The total porosities of the 20CRHA and 40CRHA pastes were 24.8%, 21.6%, 18.2%, 16.8% and 27.7%, 24.9%, 19.4%, 17.3% at 7, 28, 60 and 90 days, respectively, while the total porosities of the 20CPOFA and 40CPOFA pastes were 26.3%, 21.7%, 18.4%, 17.4% and 30.2%, 27.5%, 19.3%, 18.5% at 7, 28, 60 and 90 days, respectively, which were higher than that of the OPC paste. The results indicate that the total porosity of the pastes containing RHA and POFA with particle sizes that were the same as the cement was higher than that of the OPC cement paste. For the paste containing FRHA and FPOFA at 7 days, the total porosity of the paste containing 20% RHA and POFA were lower

than that of the OPC paste at all ages. In addition, the total porosity of the 40FPOFA paste at 60 days was 17.3%, which is slightly less than 17.4%, because the high fineness palm oil fuel ash had a faster pozzolanic reaction. The small particles showed a good filler effect in reducing the voids of the cement paste (Isaia et al., 2003). These results suggest that the addition of fine particles of rice husk ash and palm oil fuel ash makes the blended cement paste denser (Chindaprasirt et al., 2007).

Table 4.5 Total porosity of OPC paste and pastes containing RHA and POFA

Symbol	Total porosity (%)			
	7 days	28 days	60 days	90 days
OPC	22.8	20.1	17.4	16.6
20CRHA	24.8	21.6	18.2	16.8
20CPOFA	26.3	21.7	18.4	17.4
40CRHA	27.7	24.9	19.4	17.3
40CPOFA	30.2	27.5	19.3	18.5
20FRHA	21.9	19.1	15.8	13.2
20FPOFA	20.5	17.0	15.5	11.4
40FRHA	24.5	21.6	18.5	16.3
40FPOFA	23.8	19.7	17.3	15.6

4.6.2 Effect of rice husk ash and palm oil fuel ash fineness on the pore size distribution of the pastes

The cumulative pore volumes of pastes containing 20% RHA and POFA are shown in Figures 4.22 and 4.23, respectively. As shown in Figures 4.22 and 4.23, at 28 and 90 days, the cumulative pore volume of the 20FRHA and 20FPOFA paste were lower than that CRHA and CPOFA. The high fineness of FRHA and FPOFA had a fast pozzolanic reaction and a greater filler effect in the voids, thus reducing the porosity and increasing the density of the paste. For pastes containing 40% RHA and POFA, as shown in Figures 4.24 and 4.25, the cumulative pore volumes of the 40CRHA, 40FRHA, 40CPOFA and 40FPOFA pastes at 28 days were higher than that of the OPC cement paste. However, at 90 days, the cumulative pore volume of the 40FRHA and 40FPOFA pastes were lower than that of the OPC paste due to the fact that the silicon dioxide (SiO_2) reacted with the calcium hydroxide Ca(OH)_2 and reduced the Ca(OH)_2 content by the pozzolanic reaction. Thus, the pore structure in the blended cement paste was refined; these results are in agreement with Li and Ding (2003).

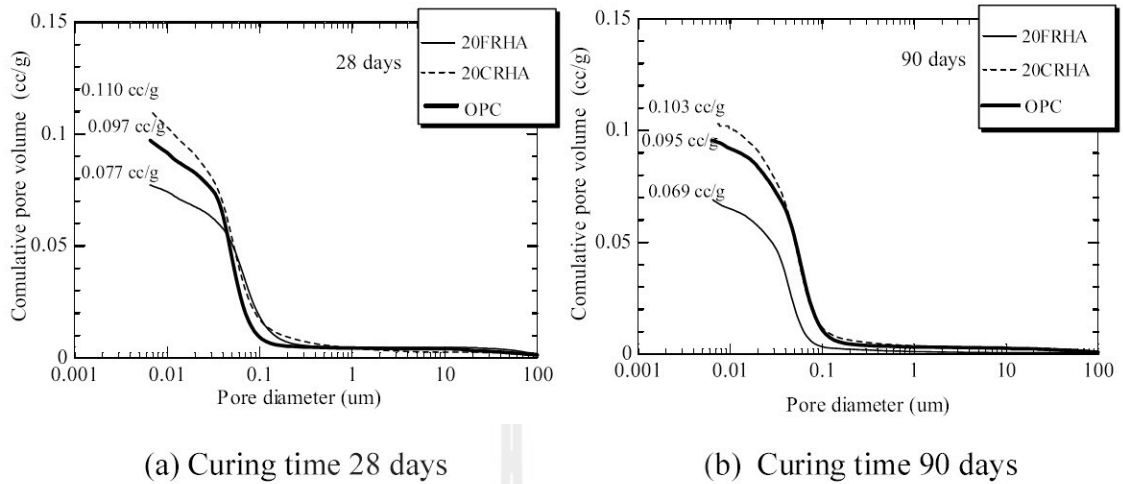


Figure 4.22 Relationships between the cumulative pore volume and pore diameter of 20RHA paste

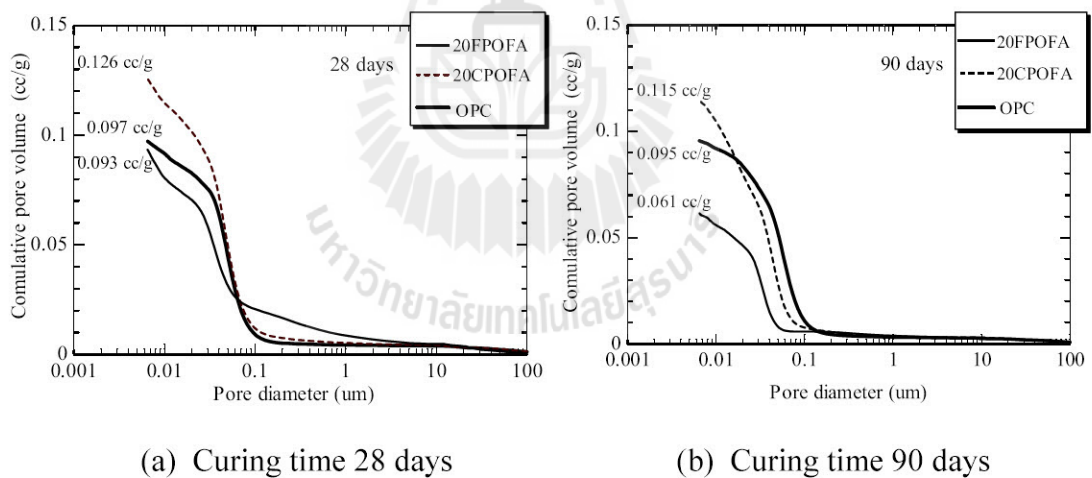


Figure 4.23 Relationships between the cumulative pore volume and pore diameter of 20POFA paste

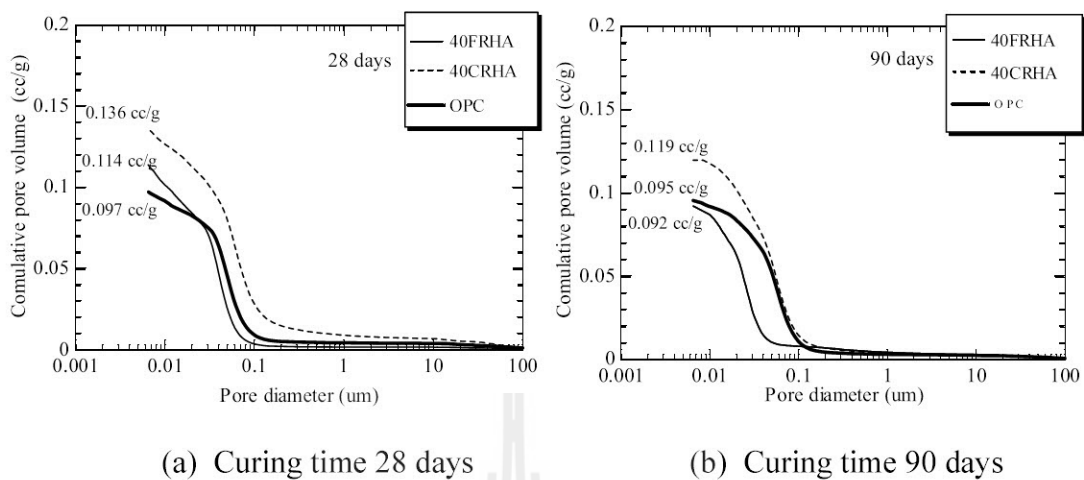


Figure 4.24 Relationships between the cumulative pore volume and pore diameter of 40RHA paste

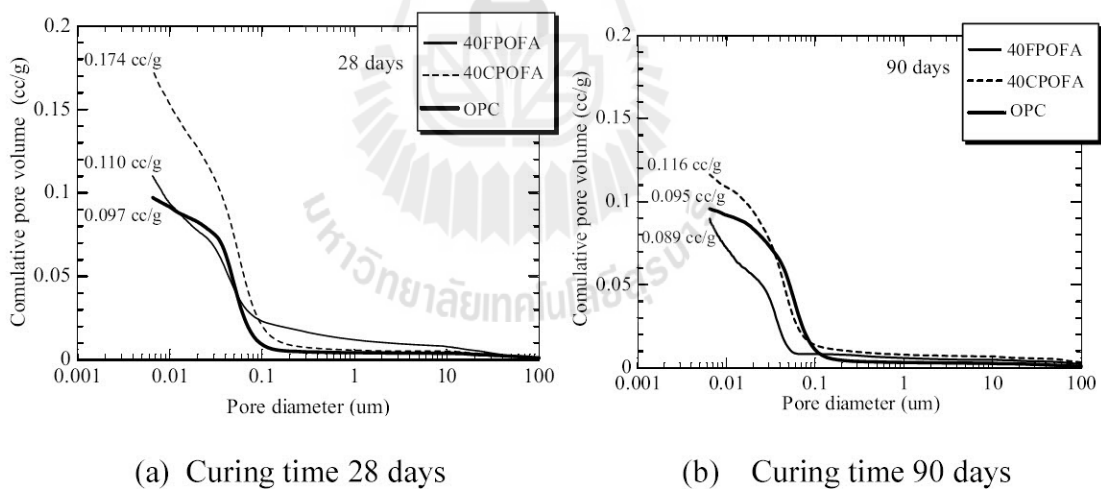


Figure 4.25 Relationships between the cumulative pore volume and pore diameter of 40POFA paste

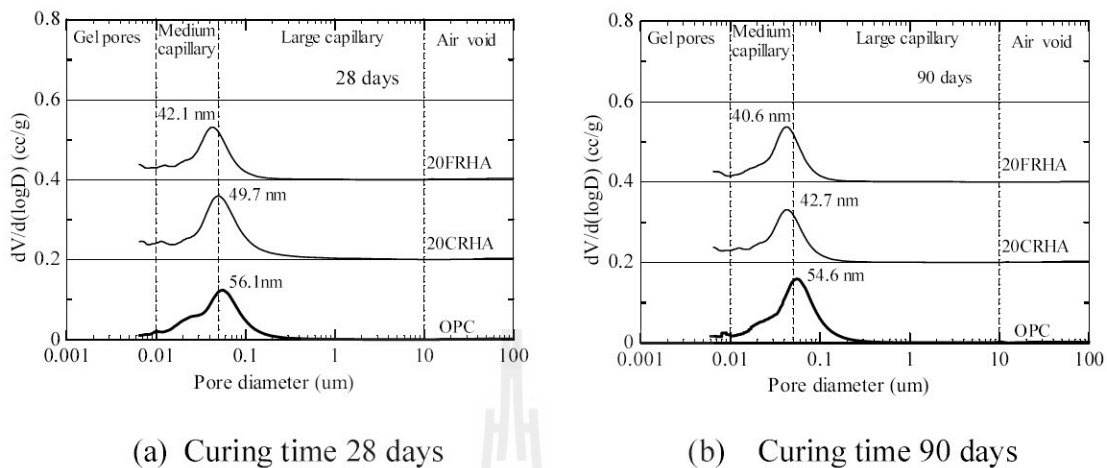


Figure 4.26 Relationships between the differential pore volume and pore diameter of 20RHA paste

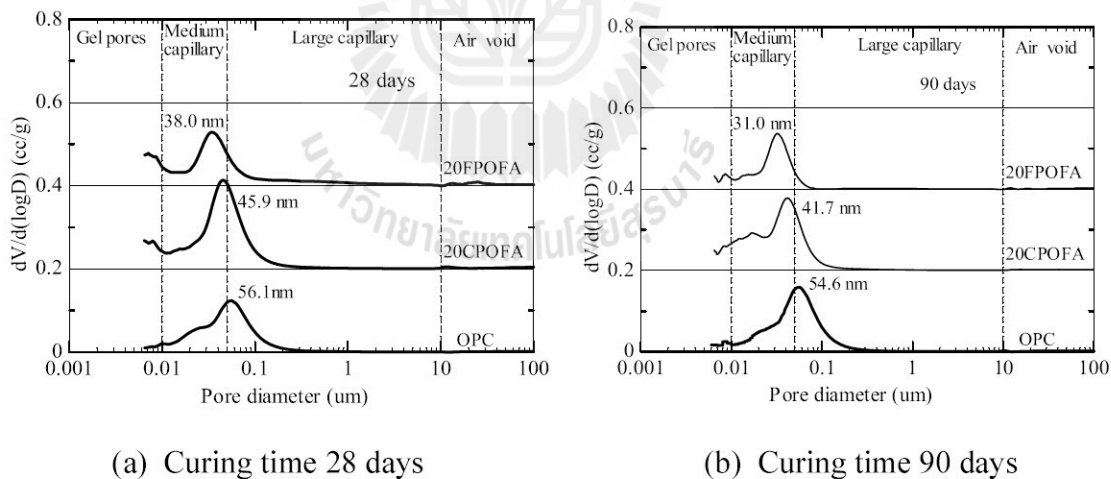


Figure 4.27 Relationships between the differential pore volume and pore diameter of 20POFA paste

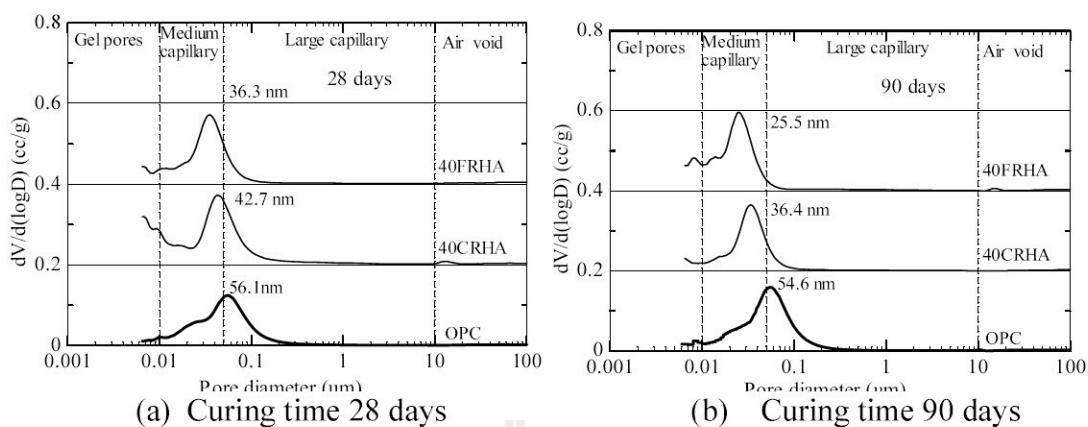


Figure 4.28 Relationships between the differential pore volume and pore diameter of 40RHA paste

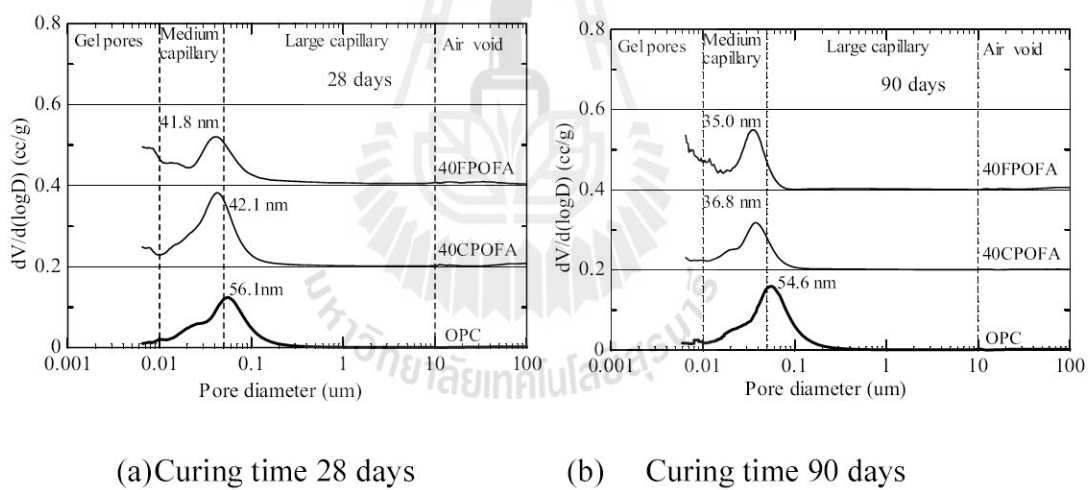


Figure 4.29 Relationships between the differential pore volume and pore diameter of 40POFA paste

The critical pore size is defined as the inflection point on the cumulative pore volume and pore diameter plot or as the maximum of $dv/d(\log D)$. The critical pore size is the most frequent continuous pores (Halamicikova et al., 1995; Pipilikaki and Beazi-Katsioti, 2009). For pastes containing 20% RHA and POFA at 28 days, as shown in Figures 4.26 and 4.27, the critical pores sizes of the 20CRHA, 20FRHA, 20CPOFA and 20FPOFA pastes were 49.7 nm, 42.1 nm, 45.9 nm and 38.0 nm, respectively, which were distributed as medium capillary pores. These values were lower than that of the OPC paste (56.1 nm), which was specified to contain large capillary pores. At 90 days, the critical pore sizes of the OPC, 20CRHA, 20FRHA, 20CPOFA and 20FPOFA pastes were 54.6 nm, 42.7 nm, 40.6 nm, 41.7 nm and 31.0 nm, respectively, due to the reaction of the rice husk ash or palm oil fuel ash with $\text{Ca}(\text{OH})_2$. Consequently, the pore structure was transformed from coarser pores to finer pores (Li and Ding, 2003). These results suggest that the paste containing RHA and POFA had a lower critical pore size than the OPC cement paste.

For pastes at 40% RHA and POFA, the relationships between the differential pore volume and pore diameter at 28 and 90 days are shown in Figures 4.28 and 4.29. The critical pore sizes of the 40CRHA, 40FRHA, 40CPOFA and 40FPOFA pastes at 28 and 90 days were 42.7 nm, 36.3 nm, 42.1 nm, 41.8 nm and 36.4 nm, 25.5 nm, respectively, which correspond to medium capillary pores. These values are smaller than that of the OPC cement paste. These results indicate that the pastes with RHA and POFA contained critical pore sizes smaller than the OPC paste.

The results suggest that the total porosity of the paste containing RHA and POFA with the same particle size as cement was higher than that of the OPC cement paste, but the paste containing RHA and POFA with smaller particle size of cement

had a lower total porosity than the OPC paste. In addition, the total porosity increased with an increase in the RHA and POFA replacement. Furthermore, the critical pore size of the pastes with RHA and POFA were smaller than that of the OPC cement paste due to the filler effect, pozzolanic reaction, dispersion effect and precipitation effect (Chindaprasirt et al., 2005; Poon et al., 1997). The pore size structure of the pastes changed from coarser pores to finer pores (Poon et al., 2001). Moreover, some researchers (Ye et al., 2006) have reported that the critical pore radius is the most important factor for permeability, and Halamickova et al., (1995) found that the critical pore size affects water permeability and chloride ion diffusion.

4.6.3 Effect of rice husk ash and palm oil fuel ash fineness on the average pore diameter of the cement paste

The results for the average pore diameter of pastes are shown in Figure 4.30. The average pore diameters of OPC paste at 7, 28, 60 and 90 days were 53.4 nm, 45.3 nm, 30.1 nm and 28.1 nm, respectively. For pastes containing CRHA and CPOFA, the average pore diameters of the 20CRHA, 40CRHA, 20CPOFA and 40CPOFA pastes were lower than that of the OPC paste at all ages, while the total porosity was higher than that of the OPC paste. For pastes containing FRHA and FPOFA, the average pore diameters of the 20FRHA, 40FRHA, 20POFA and 40FPOFA pastes were lower than that of the OPC paste, and the total porosity of the 20FRHA and 20FPOFA paste were lower than that of the OPC paste at all ages due to pore refinement and the reduction of calcium hydroxide in the paste (Poon et al., 2001). These results indicate that the average pore diameter decreases with the use of RHA or POFA and with an increase in the replacement level, which again confirms that RHA and POFA with high fineness is more effective in reducing the average pore

diameter as a result of the better dispersion, packing and pozzolanic reaction of the finer RHA and POFA particles. Similar results have been reported by other researchers (Chindapasirt et al., 2005; Frías and Cabrera, 2000).

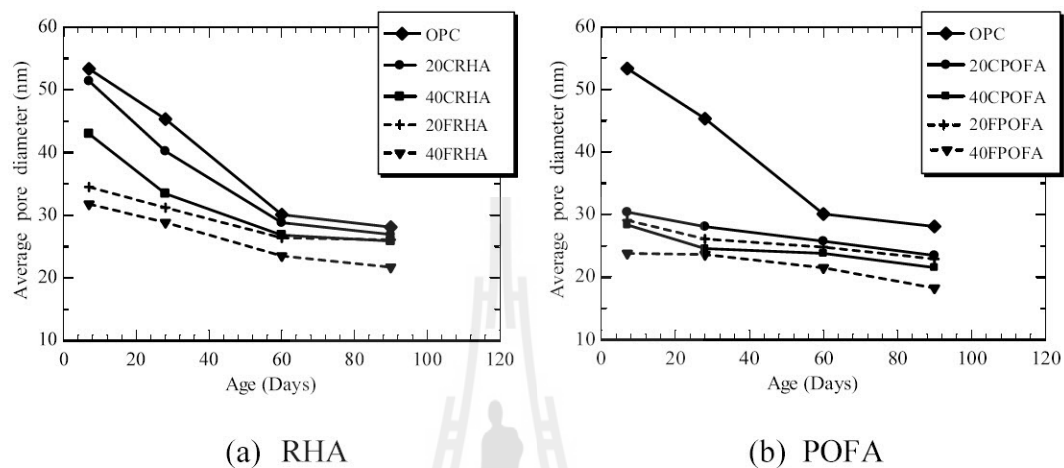


Figure 4.30 Relationship between average pore diameter and age

4.6.4 Relationships between the compressive strength and total porosity of the pastes

Relationships between the compressive strength and total porosity of the pastes containing RHA and POFA are shown in Figures 4.31 and 4.32, respectively. The figures are divided into four regions. Region I shows pastes that have both a compressive strength and total porosity higher than those of the OPC paste. Region II presents the pastes of lower compressive strength but higher total porosity in comparison to the OPC paste. Region III contains pastes that have both lower compressive strength and lower total porosity than the OPC paste. Pastes in region VI are the best pastes, which have a lower total porosity and a higher compressive strength than the OPC paste. At 28 days, the 20CRHA, 40CRHA,

40FRHA, 20CPOFA and 40CPOFA pastes were located in region II, while the 20FRHA and 20FPOFA paste were located in region IV and was designated as the best paste because its higher fineness ash can lead to greater filler effects, thus reducing the total porosity. Thus, the pastes containing POFA with high fineness increased the pozzolanic reaction rate and refined the pore structure of the paste.

At 90 days, the pastes containing RHA and POFA with the same particle size as cement were located in regions I and II. The 20FRHA and 20FPOFA pastes had a total porosity lower than that of the OPC paste, and the compressive strength was higher than that of the OPC paste, making it the best paste. However, the 40FRHA and 40FPOFA pastes had both a lower compressive strength and a lower total porosity than the OPC paste, which suggests that the high fineness RHA and POFA had a greater pozzolanic reaction and that the small particles of FRHA and FPOFA more efficiently filled the voids of the paste. Therefore, the 20FRHA and 20FPOFA pastes were more homogeneous and had a lower total porosity than the OPC paste.

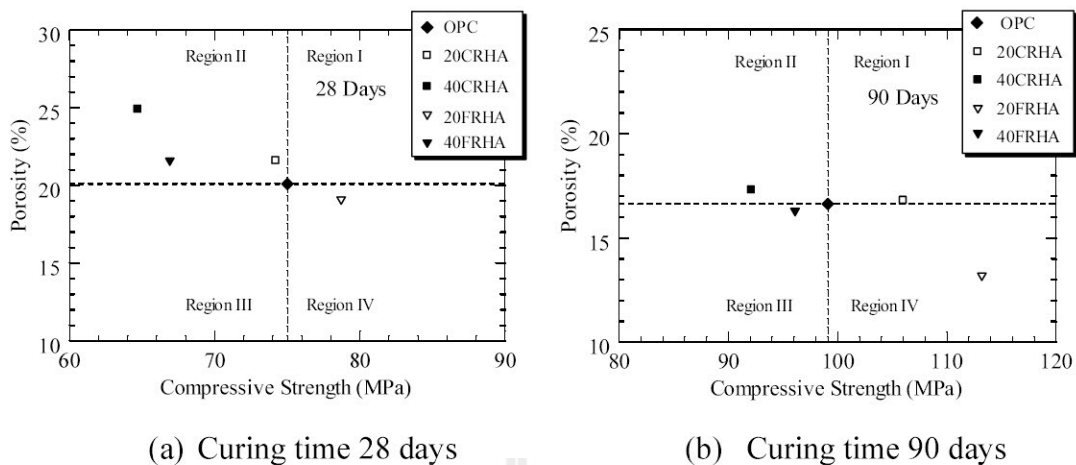


Figure 4.31 Relationships between compressive strength and total porosity of RHA paste

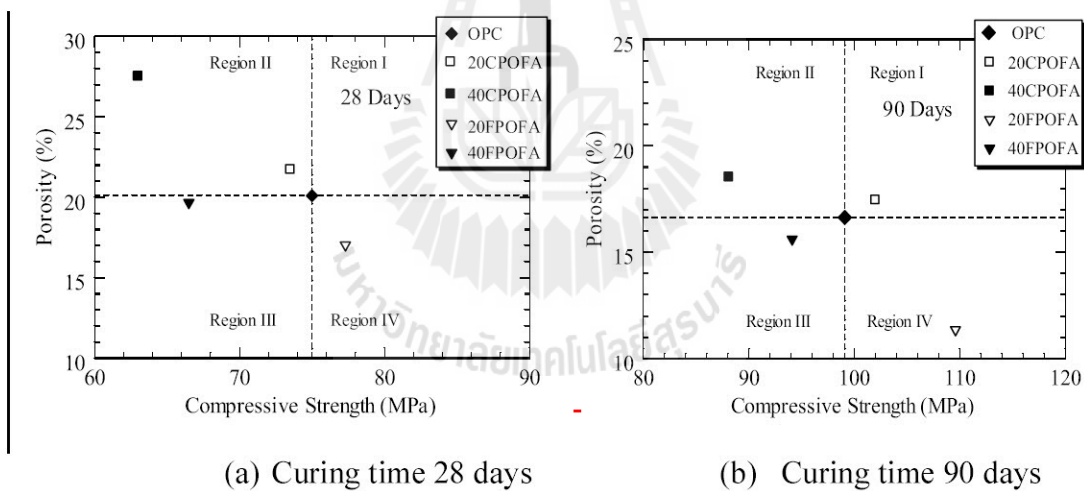


Figure 4.32 Relationships between compressive strength and total porosity of POFA paste

4.7 Role of filler effect and pozzolanic reaction of biomass ashes on hydrated phase of blended cement paste

4.7.1 Influence of ground river sand on hydrated phase

Figure 4.33 shows the TGA curves of OPC and RS pastes. The mass loss transitions occurred in three steps. The first step was the mass loss from dehydration of ettringite, C-S-H, C_2ASH_8 and C_4AH_{13} at 30-450 °C (Bai et al. 2003). The second step was the mass loss of $Ca(OH)_2$ occurred at 450-580 °C (El-Jazairi and Illston 1977), and the third at 580-1000°C represented the mass loss of calcium carbonate ($CaCO_3$) (El-Jazairi and Illston 1977). The results showed that the mass loss at 30-450°C of RS pastes increased with fineness and decreased with the replacement level. It was likely that the addition of fine RS whose particles were finer than those of Portland cement caused segmentation of large pores and increased nucleation sites for precipitation of hydration products in cement paste similar to the addition of fine fly ash (Mehta 1987). The result also showed that this mass loss increased with curing time as a result of the increase in hydration reaction which caused an increase in compressive strength (Kroehong et al. 2011).

Figure 4.34 shows the $Ca(OH)_2$ content of OPC and RS pastes. The $Ca(OH)_2$ content of all pastes increased with curing time as a result of hydration of cement. In addition, the $Ca(OH)_2$ content of RS pastes was lower than that of OPC paste especially at high replacement level due to the reduced reaction from the reduced OPC content and the non-reactive RS. The $Ca(OH)_2$ content of FRS pastes was lower than those of pastes with the CRS due to the higher nucleation effect of fine particles (Askarinejad et al. 2012; el-Bouny 1994; Metha 2007).

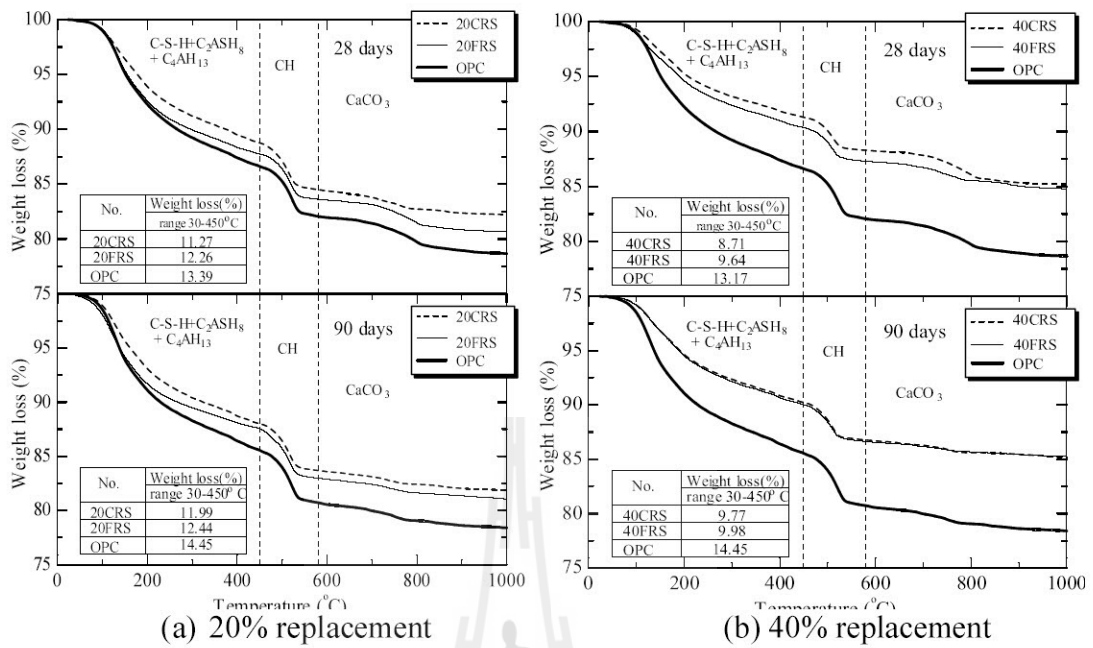


Figure 4.33 TGA curves results of OPC and RS pastes

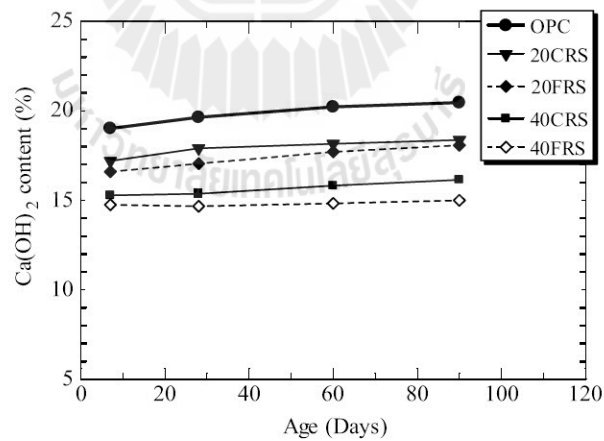


Figure 4.34 $\text{Ca}(\text{OH})_2$ content of OPC and RS pastes

4.7.2 Influence of pozzolanic reaction on hydrated phase

The results of Ca(OH)_2 contents of pastes at 7, 28, 60 and 90 days are shown in Table 4.6. Figures 4.35 and 4.36 showed the reductions of Ca(OH)_2 content of RHA and POFA pastes which were determined from the difference in Ca(OH)_2 content between RS pastes and RHA or POFA pastes with the same particle size, replacement level and age. The results showed that the Ca(OH)_2 content of RS pastes was higher than those of RHA and POFA pastes because the SiO_2 in RS was non-reactive. For the coarse pozzolans, the Ca(OH)_2 content of 20CRHA, 20CPOFA, 40CRHA and 40CPOFA pastes were reduced from the ages of 28 to 90 days from 15.57 to 14.34%, 15.82 to 15.10%, 12.12 to 8.83% and 12.28 to 9.24% or approximately 22%, 18%, 45% and 43% compared with RS pastes, respectively. The reductions of Ca(OH)_2 content in the RHA and POFA pastes indicated its consumption by the pozzolanic reaction. In addition, the reduction of Ca(OH)_2 content for high replacement level was higher than that of low replacement level. For fine pozzolans, the Ca(OH)_2 contents of 20FRHA, 20FPOFA, 40FRHA and 40FPOFA pastes were also reduced from the ages of 28 to 90 days from 14.80 to 13.33%, 15.24 to 13.93%, 11.46 to 6.43% and 11.75 to 7.19% or approximately 26%, 23%, 57% and 52% compared with RS pastes, respectively. The results confirmed that the Ca(OH)_2 contents of RHA and POFA pastes decreased with the increased of curing time, fineness and replacement level (Barbhuiya et al. 2009; Chindaprasirt et al. 2007; Poon et al. 2001).

Table 4.6 Ca(OH)₂ content of pastes

Symbol	Ca(OH) ₂ (%)			
	7 days	28 days	60 days	90 days
20CRS	17.20	17.91	18.16	18.37
20CRHA	15.57	15.45	15.37	14.34
20CPOFA	15.82	15.74	15.44	15.10
40CRS	15.28	15.37	15.82	16.15
40CRHA	12.12	11.01	9.45	8.83
40CPOFA	12.28	11.30	9.65	9.24
20FRS	16.60	17.05	17.71	18.08
20FRHA	14.80	14.13	13.64	13.33
20FPOFA	15.24	14.87	14.42	13.93
40FRS	14.75	14.67	14.83	15.00
40FRHA	11.46	9.09	7.68	6.43
40FPOFA	11.75	10.06	7.85	7.19



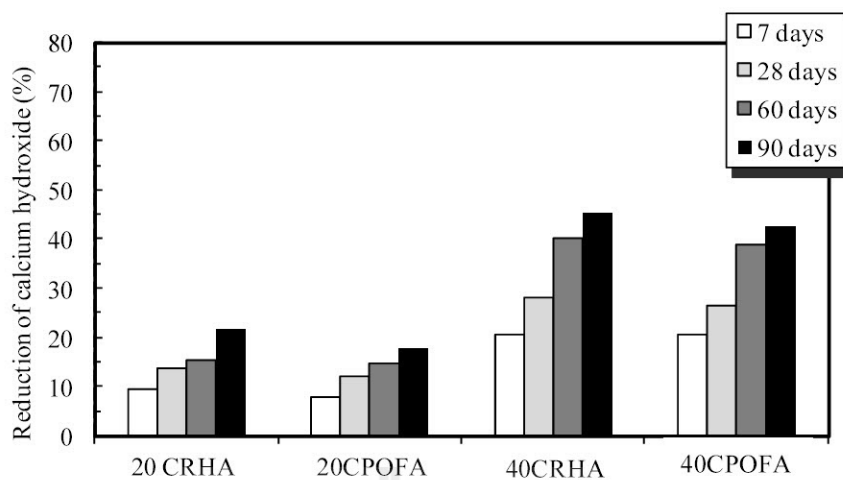


Figure 4.35 Reduction of $\text{Ca}(\text{OH})_2$ content of CRHA and CPOFA pastes

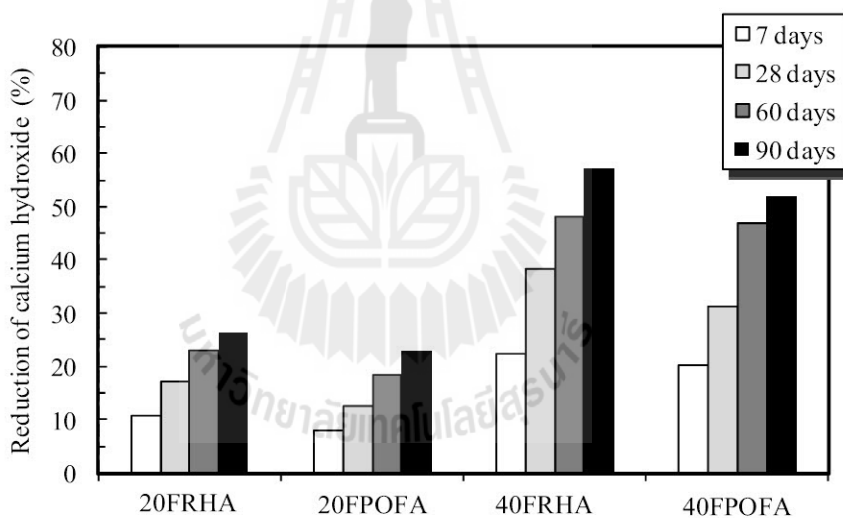


Figure 4.36 Reduction of $\text{Ca}(\text{OH})_2$ content of FRHA and FPOFA pastes

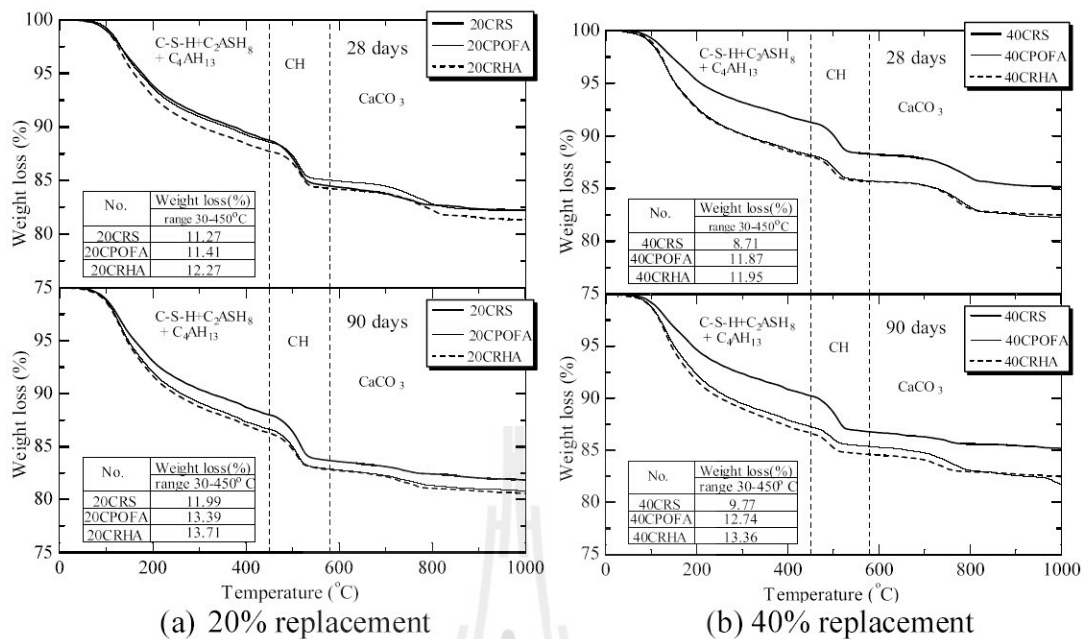


Figure 4.37 TGA curves results of CRS, CRHA and CPOFA pastes

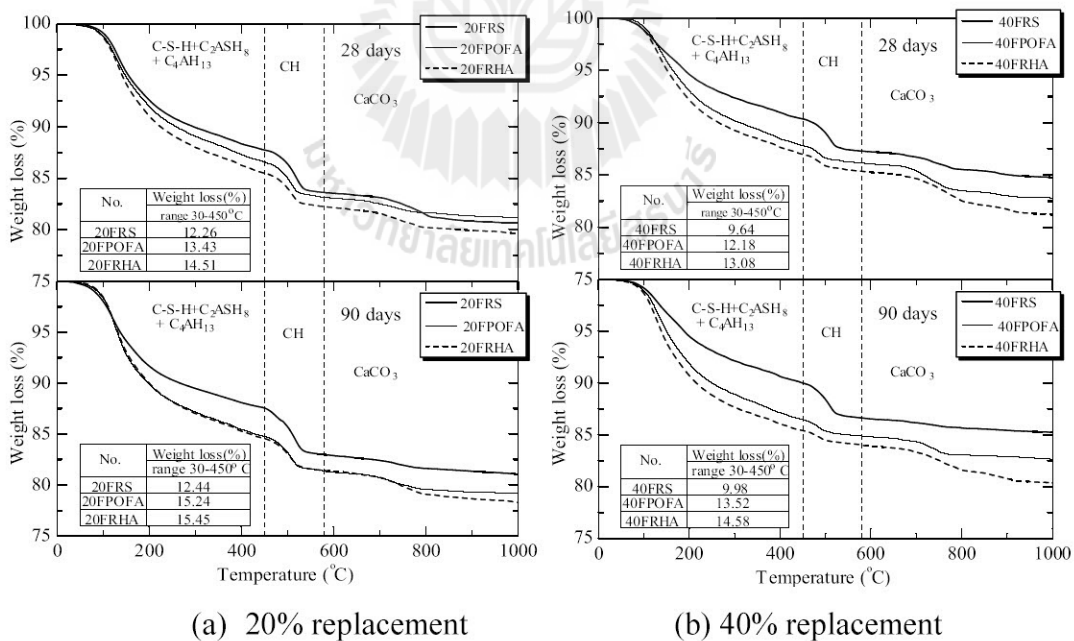


Figure 4.38 TGA curves results of OPC, FRHA and FPOFA pastes

The thermogravimetric analysis (TGA) results for RS, RHA and POFA pastes are shown in Figures 4.37 and 4.38. The first mass losses (at 30°C-450°C) of RHA and POFA pastes were higher than those of RS pastes. For example, the mass losses of 20CRHA, 20CPOFA, 40CRHA and 40CPOFA pastes at 28 days were 12.27%, 11.41%, 11.95% and 11.87%, respectively, while those of 20CRS and 40CRS pastes at 28 days were lower at 11.27% and 8.71%, respectively. At 90 days, they increased to 13.71%, 13.39%, 13.36 % and 12.74% while those of 20CRS and 40CRS pastes were still lower at 11.99% and 9.77%, respectively. The first mass losses of CRHA and CPOFA pastes were higher than those of RS pastes especially at high replacement level, due to the pozzolanic reaction of RHA and POFA compared with no pozzolanic reaction of RS. For pastes with fine ashes, the first mass loss of FRHA and FPOFA pastes were similar to those of CRHA and CPOFA pastes, but the first mass losses for the FRHA and FRHA pastes were higher than those of the CRHA and CRHA pastes because FRHA and FPOFA had large surface areas, which produced increased C-S-H, C_2ASH_8 and C_4AH_{13} . These results also indicated that the first mass loss (at 30°C-450°C) increased with curing time, particle fineness and cement replacement rate.

4.7.3 Relationships between mass losses of C-S-H+C₂ASH₈+C₄AH₁₃ and compressive strength

Figure 4.39 shows the relationships between mass losses of C-S-H+C₂ASH₈+C₄AH₁₃ and compressive strengths of FRHA and FPOFA pastes at 90 days. The mass losses of C-S-H+C₂ASH₈+C₄AH₁₃ were divided into three portions viz. cement hydration, filler effect and pozzolanic reaction. The use of 20% RHA and POFA increased the mass losses of C-S-H+C₂ASH₈+C₄AH₁₃ and increased the compressive strength compared with those of OPC paste at 90 days due to the filler effect and pozzolanic reaction of both RHA and POFA. However, the mass losses of C-S-H+C₂ASH₈+C₄AH₁₃ of 40% RHA and POFA were slightly lower than that of OPC paste. The mass losses of C-S-H+C₂ASH₈+C₄AH₁₃ due to the pozzolanic reaction increased with increasing replacement of RHA and POFA but the losses from cement hydration were reduced. In addition, the weight losses of C-S-H+C₂ASH₈+C₄AH₁₃ due to the pozzolanic reaction were higher than those due to the filler effect. At this range of displacement level of 0-40%, the cement hydration was the major contributor to strength development of the blended cement followed by the pozzolanic reaction and the filler effect also contributed but to a much lesser extent.

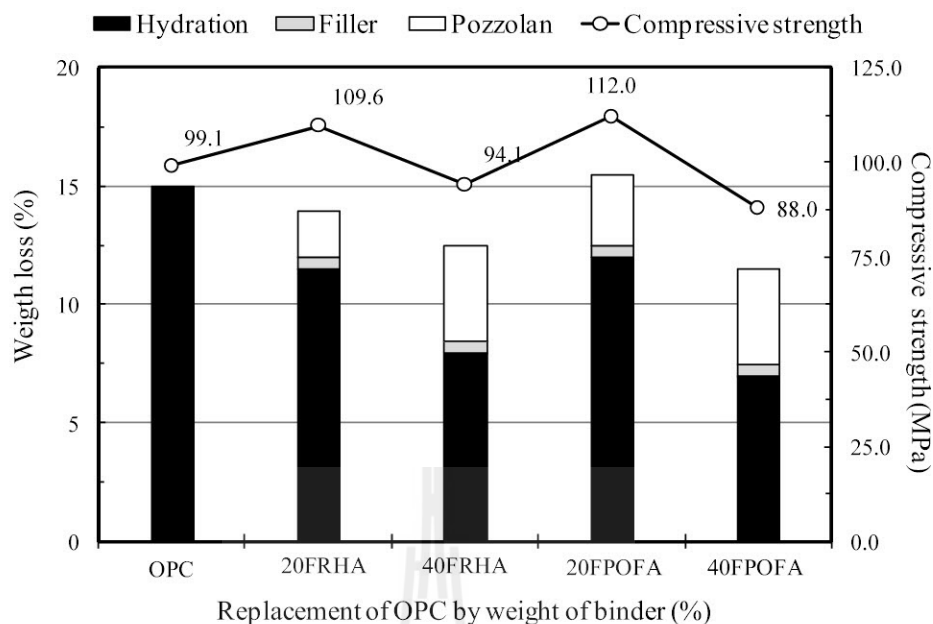


Figure 4.39 Mass losses of C-S-H+C₂ASH₈+C₄AH₁₃ and compressive strength of pastes at 90 days

4.8 Role of filler effect and pozzolanic reaction of biomass ashes on pore size distribution of blended cement paste

4.8.1 Influence of filler effect on total porosity

The results of total porosity of OPC and RS pastes are shown in Figure 4.40. The total porosities of pastes reduced with curing as expected. For example, the total porosities of OPC pastes were 22.8%, 20.1%, 17.4% and 16.6% at ages of 3, 7, 28 and 90 days. The results showed that total porosities of RS pastes are higher than that of OPC paste. In addition, the total porosities increased with the incorporation of RS and increased with the replacement level. For example, the total porosity of 20CRS pastes at 28 days was 24.0% while that of 40CRS paste was higher at 28.5% because of the reduction in cement content and the associated reduced C-S-H. The

differences between total porosities of fine RS and coarse RS pastes at the same replacement level and age was filler effect (ΔF_p). The total porosity of paste containing fine RS was lower than that of paste containing coarse RS because the small particle size led to good dispersion and filler effect and reduced the voids (Goldman and Bentur 1993; Isaia et al. 2003; Tangpagasit et al. 2005). The results indicate the total porosity of the paste due to the filler effect increased with an increase in the replacement of inert material.

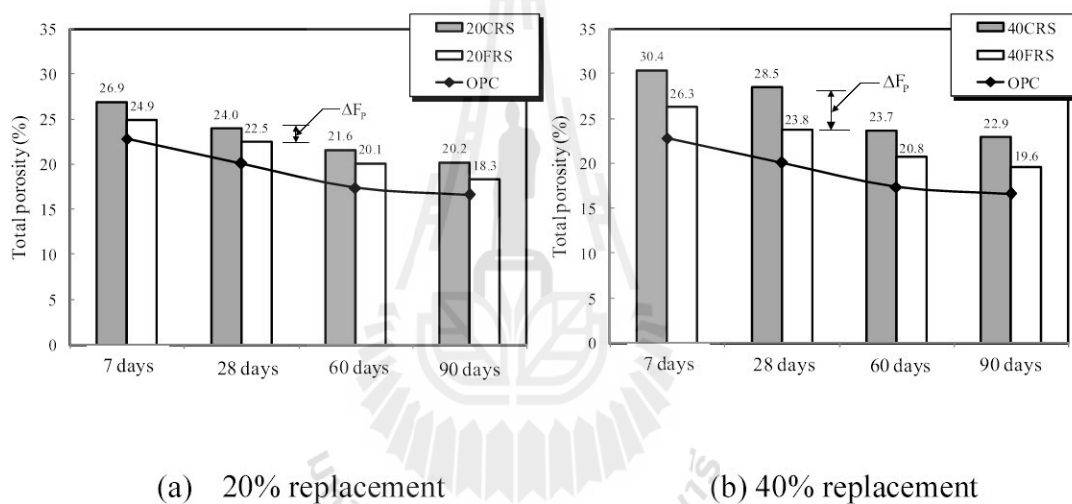


Figure 4.40 Total porosity of OPC and RS pastes

4.8.2 Influence of pozzolanic reaction on total porosity

The results of total porosity of pastes are shown in Figures 4.41, 4.42, 4.43 and 4.44. For pastes with CRHA and CPOFA with the same particle as the cement as shown in Figures 4.41 and 4.42, the total porosities of CRHA and CPOFA pastes were higher than those of OPC paste at all ages but lower than those of RS pastes at the same replacement and same curing time. However, at 90 days, the total porosities of 20CRHA, 20CPOFA, 40CRHA pastes were 16.8%, 17.3%, 17.4% which is slightly more than 16.6% of OPC paste because of the pozzolanic reaction of RHA and POFA. The results are in agreement with Li and Ding (2003). For the case of pastes with a small particle as shown in Figures 4.43 and 4.44, the total porosities of 20% FRHA and 20FPOFA pastes were lower than those of OPC pastes and RS pastes at all ages. In addition, total porosities of 40FRHA and 40FPOFA pastes at 90 days were lower than that OPC paste, because the high fineness RHA and POFA had a faster pozzolanic reaction. The differences between total porosities of RS pastes and RHA or POFA pastes at the same replacement level and age were pozzolanic reaction (ΔP_p). The small particles showed a good filler effect in reducing the voids of the cement paste. This again confirmed that the pozzolanic reaction of fine ashes was higher than that of the coarse ashes with also increased filler effect of the fine ashes. The results confirm that partial replacement of OPC with fine RHA and POFA at rate of 20% by weight of binder had lower total porosity than that of OPC paste at all age.

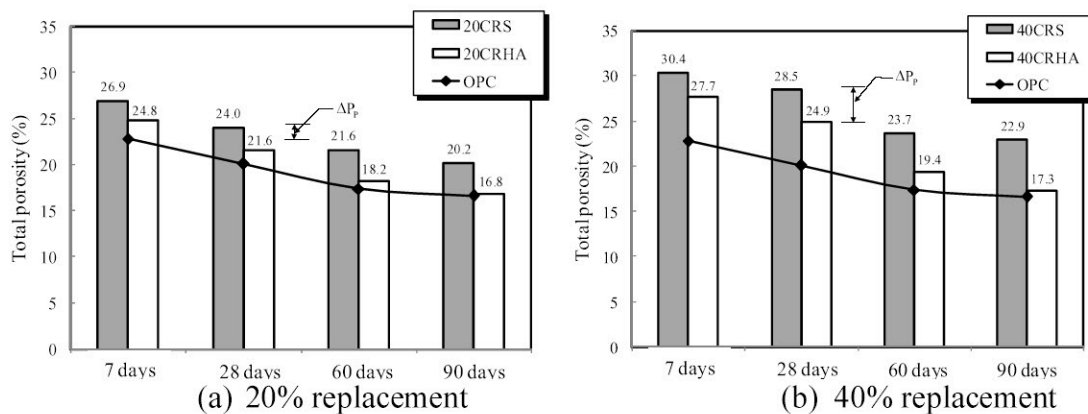


Figure 4.41 Total porosity of OPC, CRS and CRHA pastes

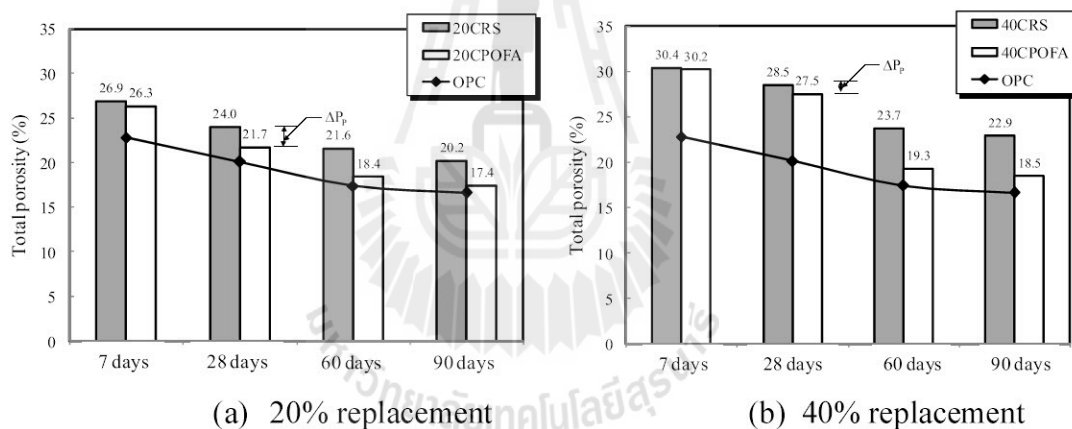


Figure 4.42 Total porosity of the OPC, CRS and CPOFA pastes

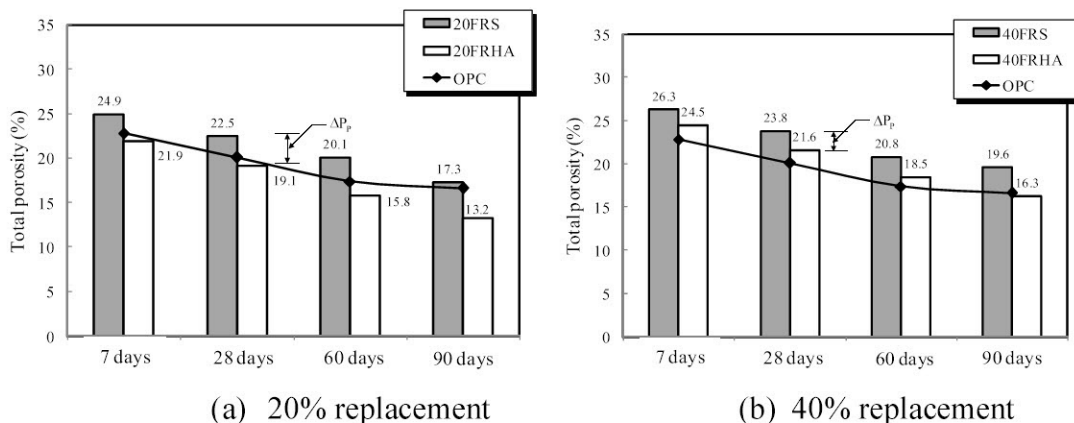


Figure 4.43 Total porosity of the OPC, FRS and FRHA pastes

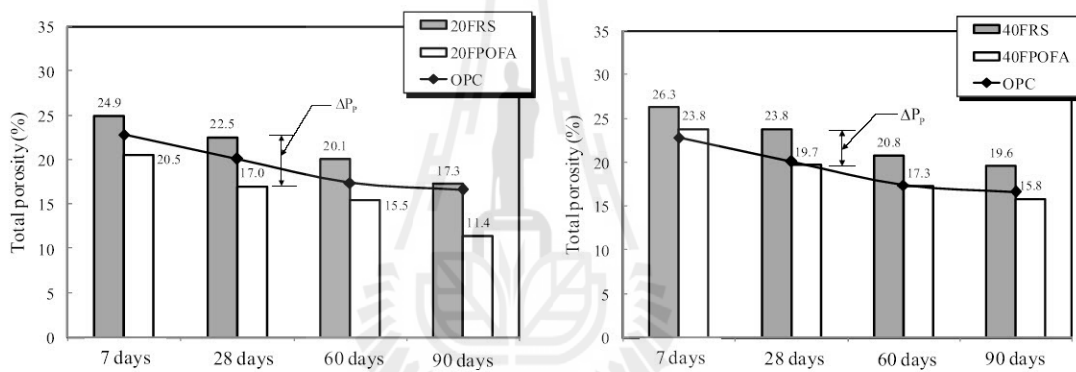


Figure 4.44 Total porosity of the OPC, FRS and FPOFA pastes

4.8.3 The effect of the pozzolanic reaction on the pore size distribution

The average pore diameters of all pastes are shown in Figure 4.45. The average pore diameters of the OPC paste at 7, 28, 60 and 90 days were 53.4 nm, 45.3 nm, 30.1 nm and 28.1 nm, respectively. For pastes with CRHA and CPOFA with the same particle sizes as the cement, the 20% and 40% CRHA or CPOFA pastes had average pore diameters lower than those of OPC paste at all ages, while the total porosity was higher than that of the OPC paste. For pastes containing high fineness RHA and POFA, the average pore diameters of the 20% and 40% of FRHA or FPOFA pastes were lower than that of the OPC paste and the total porosity of 20FRHA and 20FPOFA paste was lower than that of the OPC paste at all ages. The results suggest that the average pore diameter decreases with the use of RHA and POFA and with an increase in the replacement level. In addition, the fine particles of RHA and POFA are more effective in reducing the average pore diameter due to dispersion, the filler effect and the increased pozzolanic reactions (Chindaprasirt et al. 2005; Frías and Cabrera 2000).

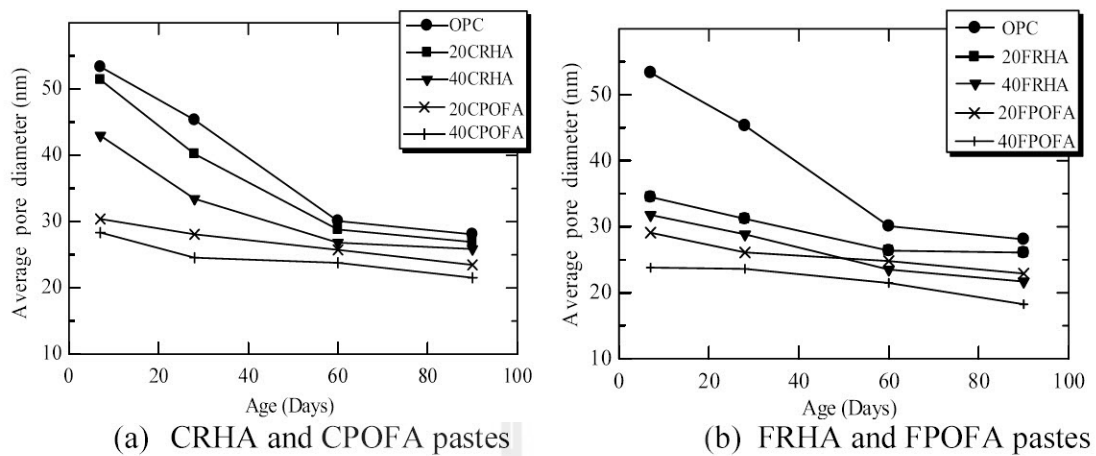


Figure 4.45 Average pore diameters with curing time.

Part II

4.9 Chloride penetration profile

4.9.1 Effect of cement type on the chloride penetration profile

Figure 4.46 shows the chloride penetration profile of Portland cement type I and V cement pastes at 90 days after immersion in 3% NaCl solution. The results showed that the OPC paste had lower chloride penetration than the SRPC paste. Since OPC paste had a higher content of C_3A than SRPC paste, and C_3A plays the most significant role in the chloride binding capacity. Similar results have been reported by other researchers (Arya et al., 1990; Zibara, 2001). In addition, the porosity of OPC paste is lower than that of SRPC paste because the reaction of SRPC with water is slower than that of OPC (Sumranwanich and Tangtermsirikul, 2004b). These results confirmed that OPC paste has a lower porosity than the SRPC paste, and the results agree with previous research findings (Page et al., 1981; Rasheeduzzafar et al., 1990)

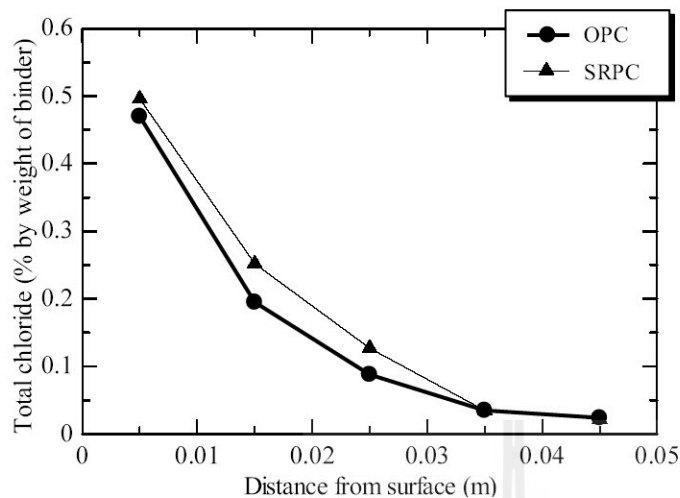
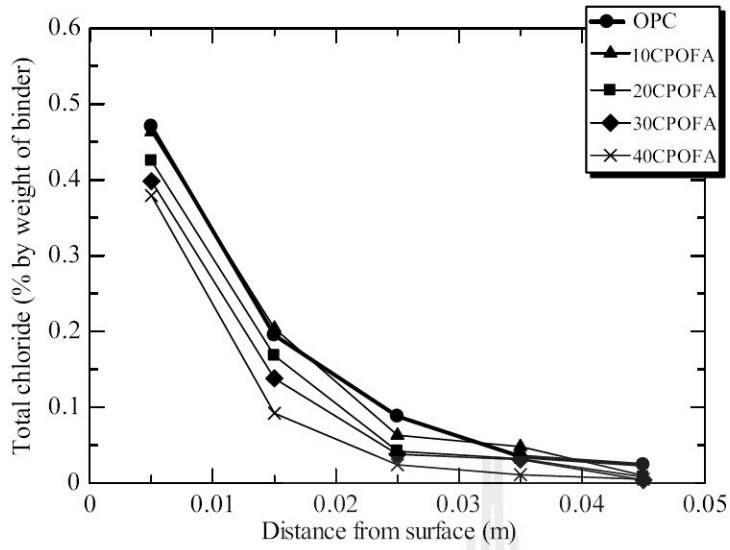


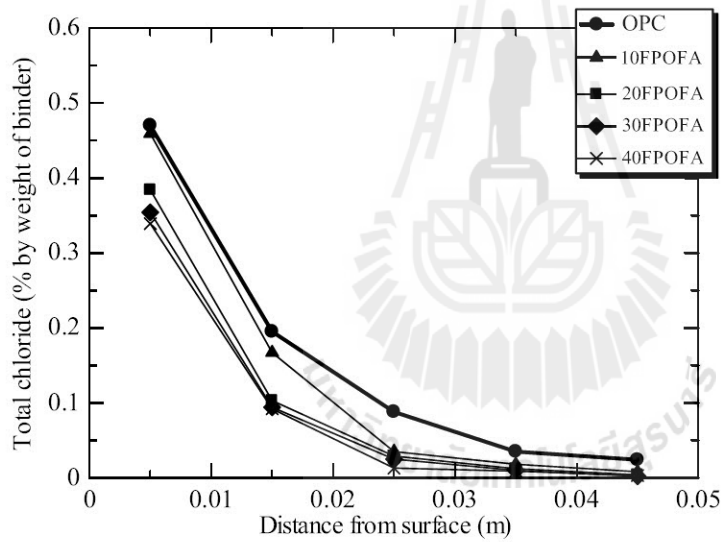
Figure 4.46 Chloride penetration profile of Portland cement type I (OPC) and V (SRPC) cement paste at 90 days immersion in 3% NaCl solution

4.9.2 Effect of palm oil fuel ash on the chloride penetration profile

Figure 4.47 shows the chloride penetration profile of Portland cement type I and V cement pastes at 90 days immersion in 3% NaCl solution. The results showed that both CPOFA and FPOFA pastes had lower chloride contents than the OPC paste. In addition, the chloride content decreased with increasing replacement with POFA. This finding is due to physical adsorption on the surface of the hydration or pozzolanic reaction product, such as C-S-H, C-A-H, ettringite and monosulfate (Luo et al., 2003; Sumranwanich and Tangtermsirikul, 2004a). The effect of POFA fineness shows that the chloride penetration of FPOFA paste was lower than that of CPOFA paste. This is due to the paste with high fineness POFA having a lower total porosity than the coarse POFA. These results agree with Chindaprasirt et al. (2005). The results suggest that the use of POFA to partially replace type I Portland cement could improve the resistance to chloride penetration.



(a) Coarse palm oil fuel ash (CPOFA)



(b) Fine palm oil fuel ash (FPOFA)

Figure 4.47 Chloride penetration profile of OPC paste and POFA pastes at 90 days immersion in 3% NaCl solution

4.10 Chloride diffusion coefficient (D_c)

4.10.1 Effect of cement type on the chloride diffusion coefficient

The chloride diffusion coefficient (D_c) was evaluated based on the general solution of Fick's second law of diffusion as given in Equation (3.10). The determination of D_c can be evaluated by fitting the Fick's second law on chloride penetration profile of the specimen from experimental. Figure 4.48 shows the fitting curve of the general solution of Fick's second law of cement type on the chloride diffusion coefficient of Portland cement type I and V cement paste at 90 days immersion in 3% NaCl solution. After the chloride concentration at paste surface (C_o) was obtained, the regression analysis yielded the chloride diffusion coefficient (D_c) at 90 days immersion in 3% NaCl solution. For the same procedure, the values of D_c and C_o could be evaluated in the other paste mixtures. The chloride diffusion coefficients of OPC and SRPC pastes were 15.9×10^{-12} and 19.4×10^{-12} m²/s, respectively. The results show that the chloride diffusion coefficient of OPC paste was lower than that of the SRPC paste. This finding is due to the SRPC having a lower content of C_3A than the OPC paste, resulting in lower chloride binding capacity. These results indicate that OPC paste has a lower chloride diffusion coefficient than SRPC paste.

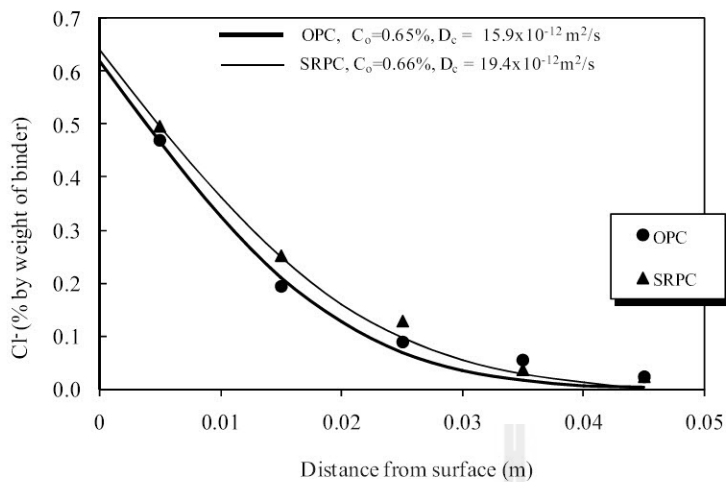


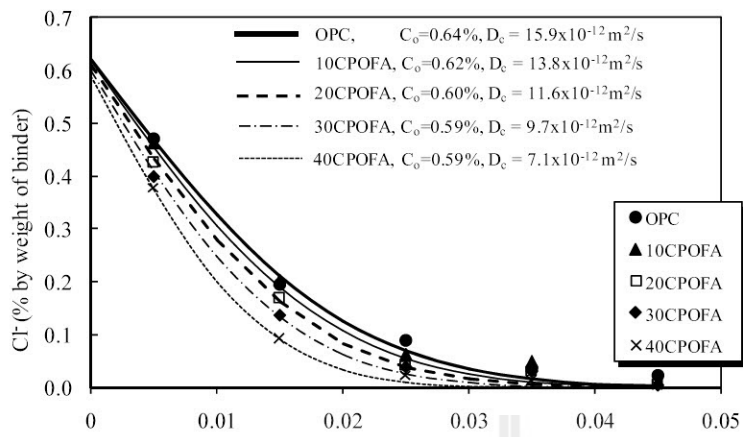
Figure 4.48 Chloride diffusion coefficient of Portland cement type I (OPC) and V (SRPC) cement paste at 90 days immersion in 3% NaCl solution

4.10.2 Effect of palm oil fuel ash on the chloride diffusion coefficient

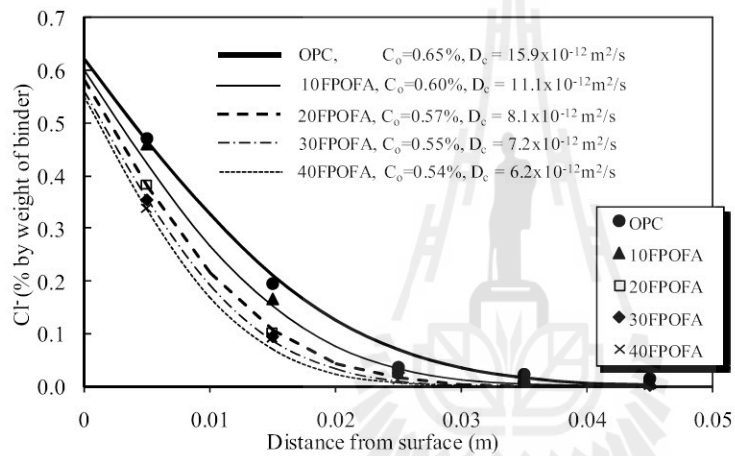
The effects of palm oil fuel ash on the chloride diffusion coefficients of blended cement pastes are shown in Figure 4.49. For coarse fineness palm oil fuel ash, the chloride diffusion coefficients of 10CPOFA, 20CPOFA, 30CPOFA and 40CPOFA pastes were 13.8×10^{-12} , 11.6×10^{-12} , 9.7×10^{-12} and 7.1×10^{-12} m²/s, respectively, while that of OPC paste was 15.9×10^{-12} m²/s. For the pastes with a small particle size, the chloride diffusion coefficients of the 10FPOFA, 20FPOFA, 30FPOFA and 40FPOFA pastes were 11.1×10^{-12} , 8.1×10^{-12} , 7.2×10^{-12} and 6.2×10^{-12} m²/s. The results showed that the use of POFA to replace Portland cement Type I had a lower chloride diffusion coefficient than the OPC paste. In addition, the chloride diffusion coefficients decreased with increasing fineness and an increase in the replacement rate of ash. This relationship is due to the pozzolanic reaction in palm oil fuel ash pastes. Thus, the pore structure in the blended cement pastes was refined. The small particles fill the voids of the paste (Gopalan, 1993; Isaia et al., 2003; Mehta

and Aietcin, 1990; Montgomery et al., 1981). Figure 4.50 shows the effect of palm oil fuel ash fineness on the chloride diffusion coefficient of blended cement paste at 90 days immersion in 3% NaCl solution. The results confirm that the chloride diffusion coefficients of blended cement paste containing POFA decreased with an increase in POFA replacement and POFA fineness. These results suggest that the use of palm oil fuel ash to replace Portland cement type I can provide a lower chloride diffusion coefficient than OPC paste. In addition, increasing the POFA fineness and the POFA replacement of cement resulted in a decrease of the chloride diffusion coefficient. This result agrees with Chalee and Jaturapitakkul (2009).





(a) Coarse palm oil fuel ash (CPOFA)



(b) Fine palm oil fuel ash (FPOFA)

Figure 4.49 Chloride diffusion coefficients of OPC paste and POFA pastes

at 90 days immersion in 3% NaCl solution

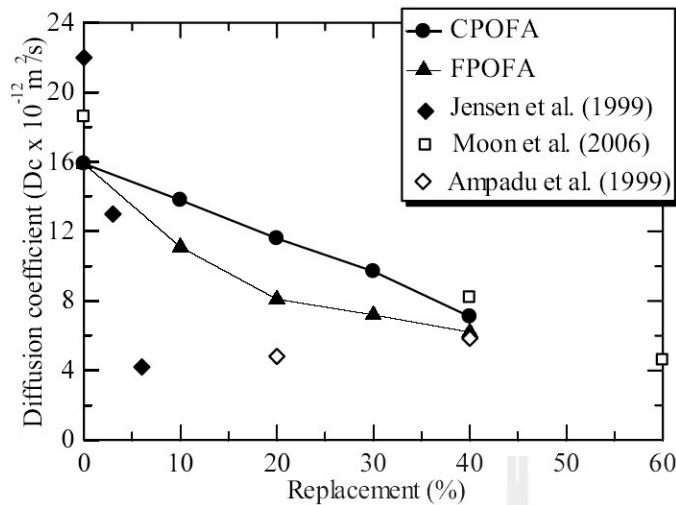


Figure 4.50 Effect of POFA on the chloride diffusion coefficients of blended cement paste at 90 days immersion in 3% NaCl solution

The chloride diffusion coefficients of blended cement paste containing 3% and 6% of silica fume from Jensen et al. (1999) are plotted in Figure 4.50 and compared with the trended line of POFA paste. The data from Jensen et al. (1999) are lower than that of the POFA paste. When the data of Moon et al. (2006) and Ampadu et al. (1999) are also plotted, the chloride diffusion coefficients of blended cement paste containing fly ash from Ampadu et al. (1999) are slightly lower than that of the POFA paste, while the chloride diffusion coefficients of concrete containing ground granulated blast furnace slag from Moon et al. (2006) are near the trend line of the POFA paste. The results confirm that the use of pozzolanic materials to replace Portland cement type I can provide a lower chloride diffusion coefficient than OPC paste.

4.11 Microstructure of blended cement paste chloride penetration

4.11.1 X-ray diffraction analysis

Figure 4.51 shows the X-ray diffraction patterns of pastes at 90 days immersion in 3% NaCl solution. The peak intensity at 2-theta of Friedel's salt and Ca(OH)_2 were 11.2° and 18.0° , respectively. Generally, chloride binding in concrete depends on chemically bound chloride and physically bound chloride.

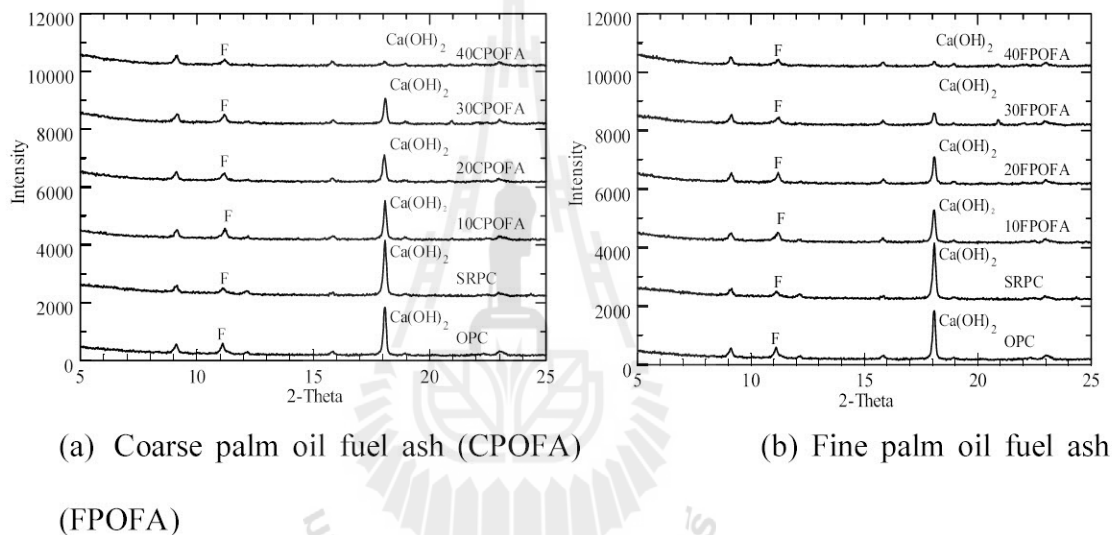


Figure 4.51 X-ray diffraction patterns of pastes at 90 days immersion in 3% NaCl solution F = Friedel's salt

Chemically bound chloride is a reaction between chloride and tricalcium aluminate (C_3A) to form calcium chloroaluminate $3CaO \cdot Al_2O_3 \cdot CaCl_2 \cdot 10H_2O$, which is called Friedel's salt. The results showed that POFA paste had a lower peak intensity of Friedel's salt than the OPC paste. Increased of the POFA to replace type I Portland cement resulted in low C_3A , leading to a low peak intensity of Friedel's salt from chemically bound chloride. In addition, POFA had a low Al_2O_3 content of 0.9%. Previous research had reported that the amount of chloride binding increases with the alumina content of the pozzolan material (Thomas et al., 2012).

For physically bound chloride, the results showed that the peak intensity of $Ca(OH)_2$ decreases with increasing fineness of the POFA and POFA replacement of cement, resulting in the increase of C-S-H, C-A-S-H and C-A-H. Thus, chloride can be physically adsorbed by surface hydration and the pozzolanic reaction. These results are similar to previous research (Luo et al., 2003; Sumranwanich and Tangtermsirikul, 2004a). These results indicate that the increased use of palm oil fuel ash as a replacement for cement resulted in an increase in physically bound chloride.

4.11.2 Relationships between the chloride diffusion coefficient and critical pore diameters of blended cement pastes

Figure 4.52 shows the relationship between the chloride diffusion coefficient and the critical pore diameters of blended cement pastes. It can be seen that the critical pore diameter increases proportionally with the chloride diffusion coefficient. Previous research had reported that the relationship between the chloride diffusion coefficient and critical pore diameters is linearly correlated and increases with an increase in the critical pore diameter (Halamickova et al., 1995; Yang et al., 2006). The equation to predict the chloride diffusion coefficient of blended cement paste is proposed as:

$$D_c = (0.525d_c - 13.74) \times 10^{-12} \quad (4.8)$$

where D_c is the chloride diffusion coefficient ($10^{-12} \text{ m}^2 \text{ s}^{-1}$) and d_c is the critical pore diameter (nm). The correlation value of 0.83 indicates a strong linear relationship between the chloride diffusion coefficient and critical pore diameter.

When the data of Halamickova et al. (1995) and Yang et al. (2006) are plotted in Figure 4.52, the data from Halamickova et al. (1995) are higher than the trend line because this study has lower W/B than the data from Halamickova et al. (1995). The chloride diffusion coefficient and critical pore diameters of concrete the data from Yang et al. (2006) are lower than the trend line.

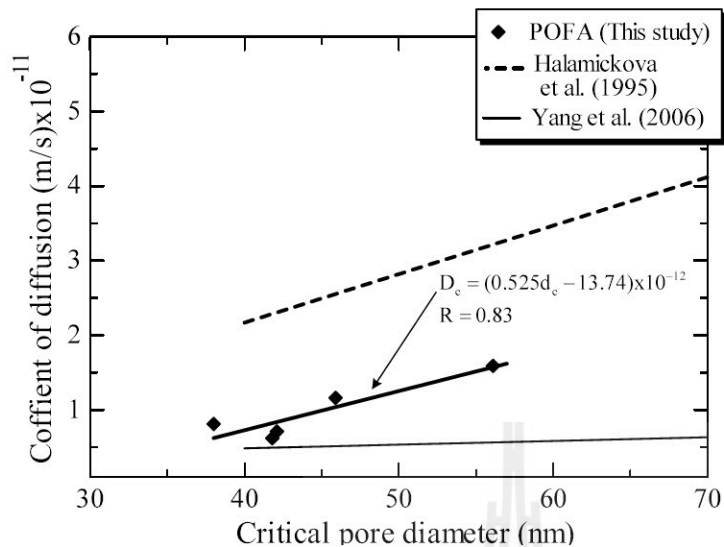


Figure 4.52 Relationship between the chloride diffusion coefficient and critical pore diameters of blended cement paste

4.12 Concentration profile of free chloride

4.12.1 Experimental results

Figure 4.53 shows the concentration profile of free chloride of OPC paste and SRPC paste at 90 days immersion in 3% NaCl solution. These results show that the free chloride concentration of the OPC paste was lower than that of the SRPC paste. This is because the SRPC has a lower C_3A content than the OPC paste. In addition, the SRPC paste had a higher chloride diffusion coefficient than the OPC paste. From Figure 4.54, it can be observed that for POFA pastes, the concentration profile of free chloride decreased with an increase in depth from the top surface. Furthermore, the concentration profile of free chloride decreased with an increase in the replacement and fineness of POFA. These results indicate that the use of palm oil fuel ash to replace OPC can provide a desirable concentration profile of free chloride.

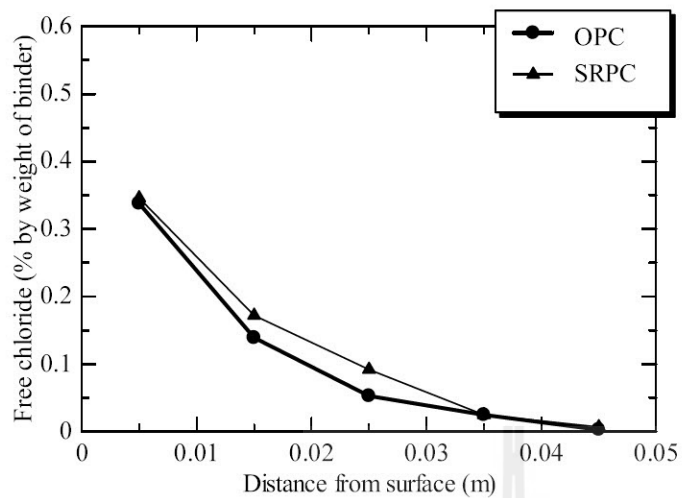
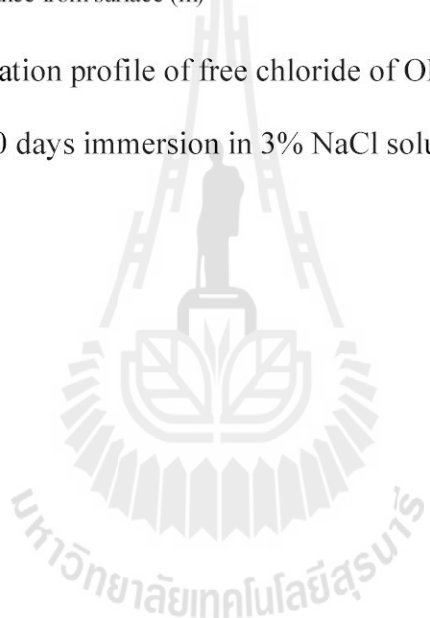
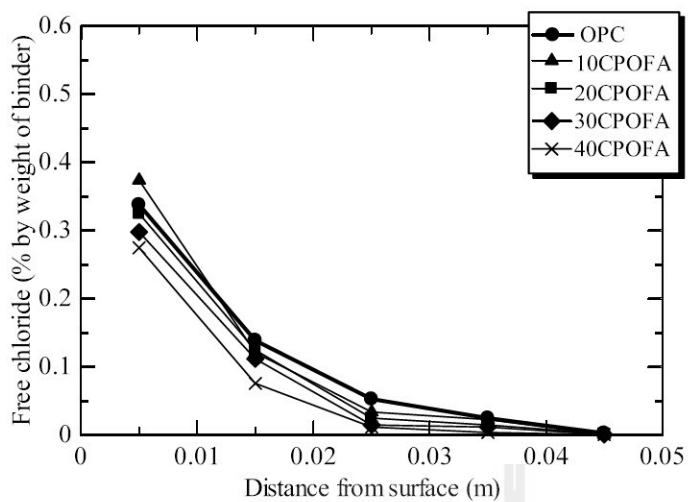
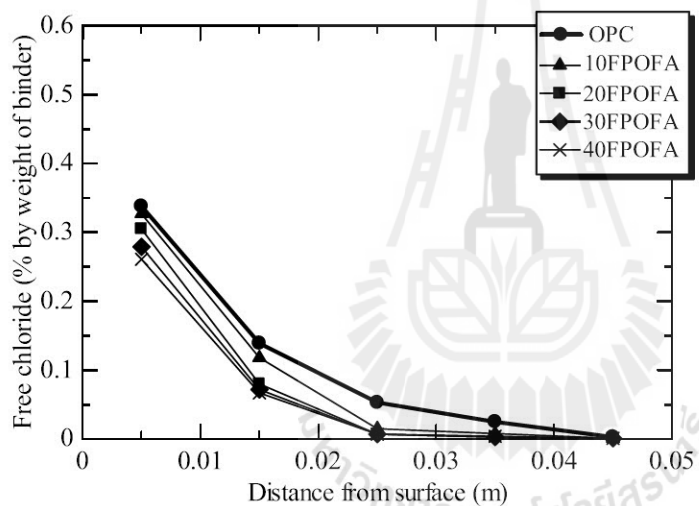


Figure 4.53 Concentration profile of free chloride of OPC paste and SRPC paste at 90 days immersion in 3% NaCl solution





(a) Coarse palm oil fuel ash (CPOFA)



(b) Fine palm oil fuel ash (FPOFA)

Figure 4.54 Concentration profile of free chloride of OPC paste and POFA paste

at 90 days immersion in 3% NaCl solution

4.12.2 Numerical results

The concentration profile of free chloride was determined using the commercial finite element program ABAQUS. Figure 4.55 shows the finite element model. The radial x-y plane of a half paste sample is 0.05 units in radius and 0.06 units in height. The paste sample is divided into 80 elements and 99 nodes by a 4-node linear axisymmetric heat transfer quadrilateral. The top boundary is exposed to 3% NaCl solution or 0.4 g chloride/g binder, while the other boundaries are assumed to be insulated. The material parameters and input data for the blended cement pastes are shown in Table 4.7. The chloride diffusion coefficients and chloride concentrations were determined from laboratory experimental results. The initial conditions at the top surface of the blended cement paste were proposed by Sergi et al. (1992).

Figure 4.56 shows the numerical results of OPC and SRPC pastes at 90 days immersion in 3% NaCl solution. The results showed that free chloride is highest near the top of the paste and decreased with increasing depth through the paste. The free chloride of the OPC paste was lower than that of the SRPC paste. Figures 4.57 and 4.58 show the numerical results of the POFA pastes at 90 days immersion in 3% NaCl solution. It was found that the free chloride decreased with increasing fineness and replacement rate of POFA. The fine particles of POFA reduced the total porosity and average pore size (Chindaprasirt et al., 2005). Chloride ions were also blocked from penetration into the pores of the paste by adsorption on the surface by hydration and the pozzolanic reaction. These results suggest that increasing the POFA replacement of cement and fineness resulted in a decrease of free chloride.

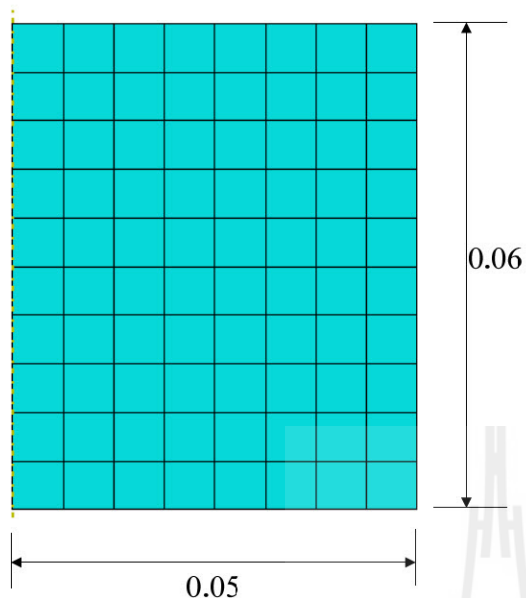


Figure 4.55 Finite element models for chloride penetration of paste specimen

Table 4.7 Material parameters and input data for blended cement pastes

Symbol	Chloride diffusion coefficient (m^2/s)	Chloride binding capacity	Initial condition at top surface of blended cement
OPC	15.9×10^{-12}	0.697	0.4
SRPC	19.4×10^{-12}	0.655	0.4
10CPOFA	13.8×10^{-12}	0.697	0.4
20CPOFA	11.6×10^{-12}	0.715	0.4
30CPOFA	9.7×10^{-12}	0.725	0.4
40CPOFA	7.1×10^{-12}	0.726	0.4
10FPOFA	11.1×10^{-12}	0.730	0.4
20FPOFA	8.1×10^{-12}	0.732	0.4
30FPOFA	7.2×10^{-12}	0.763	0.4
40FPOFA	6.2×10^{-12}	0.773	0.4

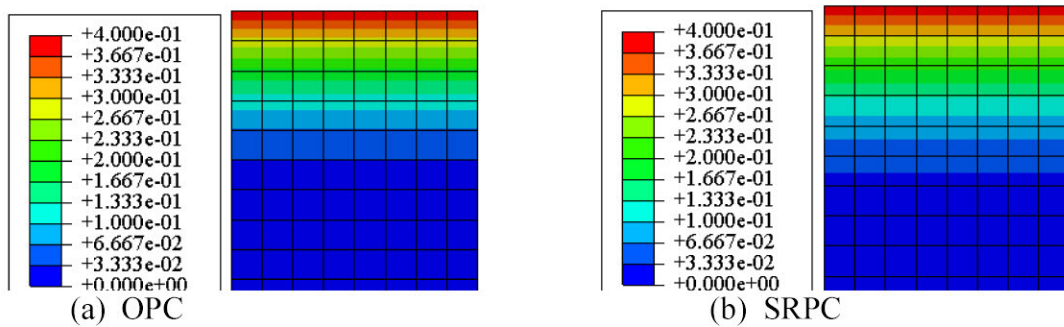


Figure 4.56 Numerical results of OPC and SRPC pastes at 90 days

immersion in 3% NaCl solution

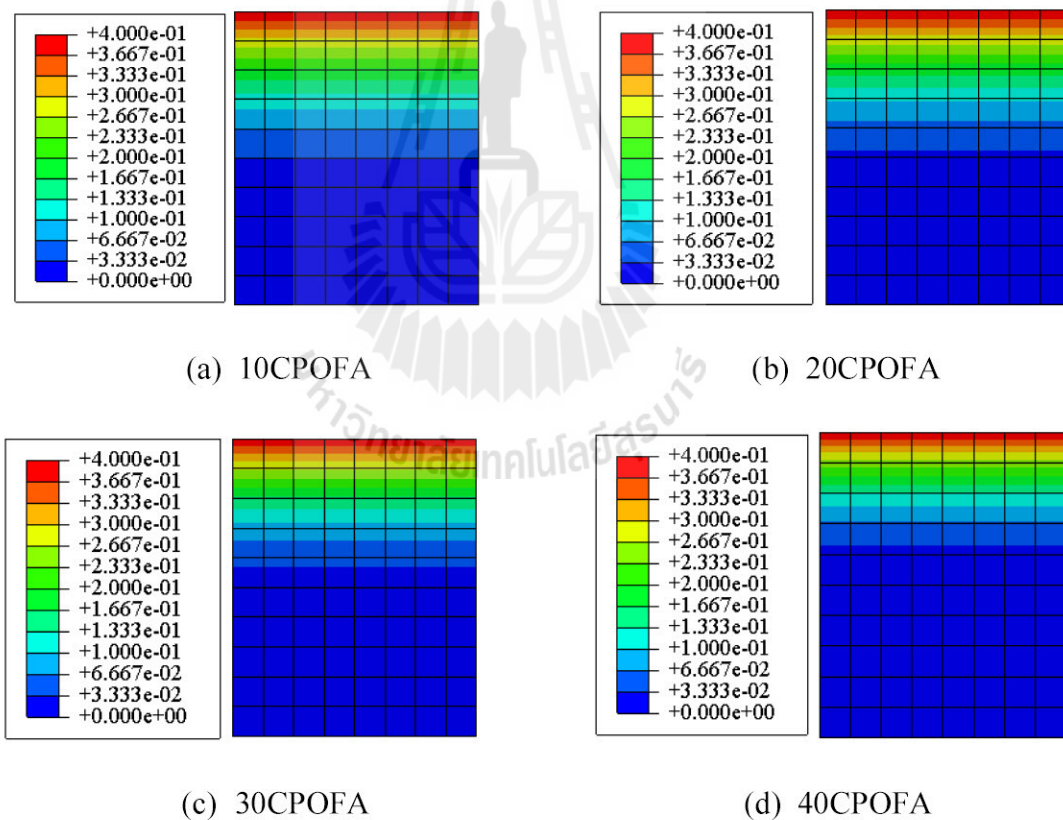


Figure 4.57 Numerical results of CPOFA pastes at 90 days immersion

in 3% NaCl solution

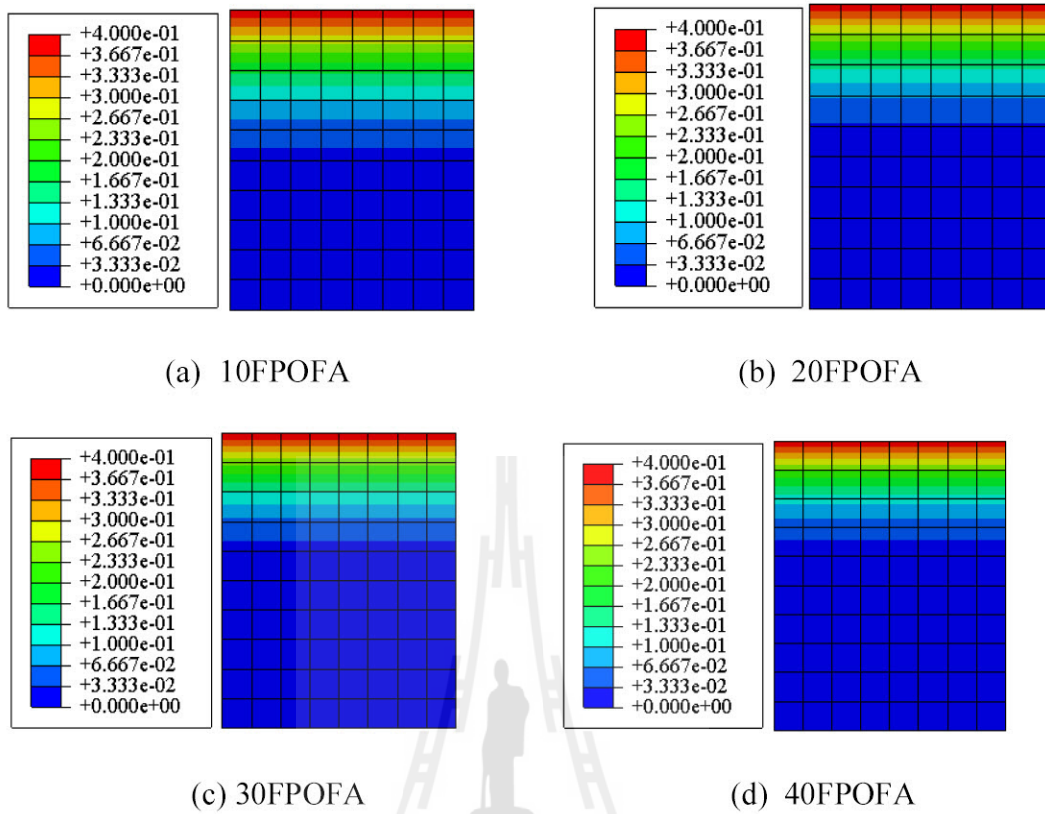


Figure 4.58 Numerical results of FPOFA pastes at 90 days immersion
in 3% NaCl solution

มหาวิทยาลัยเทคโนโลยีสุรนารี

4.12.3 Experimental and numerical results

Comparisons of numerical results are shown in Figures 4.59, 4.60 and 4.61. In this study, the paste is exposed to 3% NaCl solution and 100% relative humidity on the top surface and inside specimen. The results show that the free chloride agrees with numerical experimental and numerical results at any depth and at any time. Thus, chloride ion penetration can be estimated accurately by experimental testing of adapted paste as well as numerical analysis. Although the finite element program precisely estimated the free chloride concentration at any depth and at any time, this does not mean that the finite element program can be used in the chloride ion penetration analysis of all cases. Because parameters in actual site have different such ash effect of moisture, non-saturated, temperature, abrasion-erosion damage and so on. It is difficult to develop finite element program applicable to all cases.

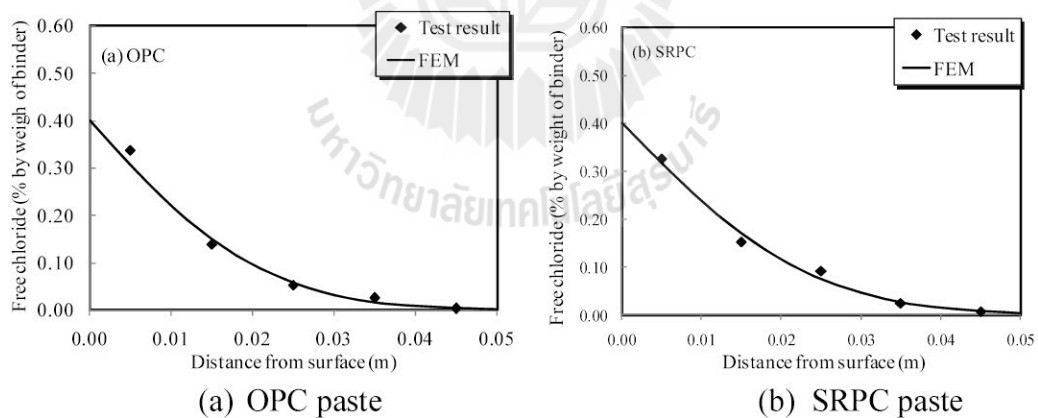


Figure 4.59 Comparison of numerical results of OPC and SRPC pastes at 90 days

immersion in 3% NaCl solution

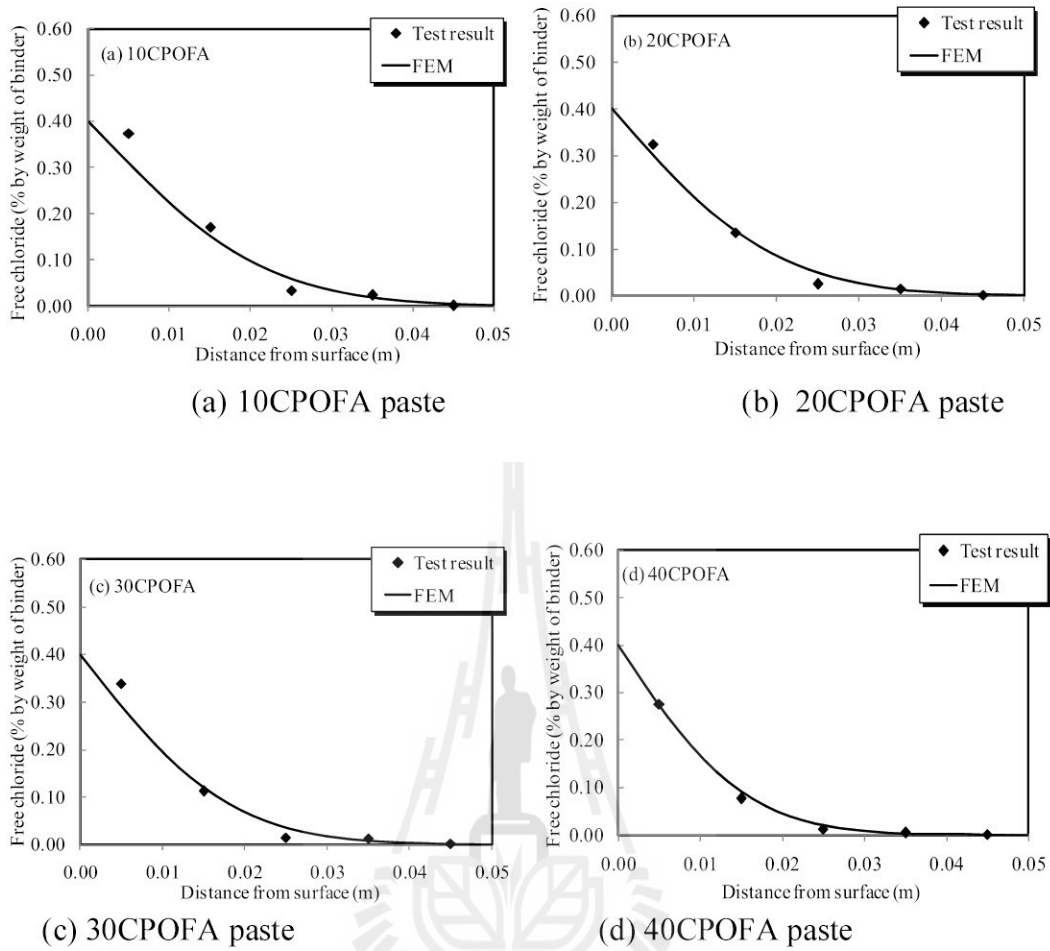


Figure 4.60 Comparison of numerical results of CPOFA pastes at 90 days immersion in 3% NaCl solution

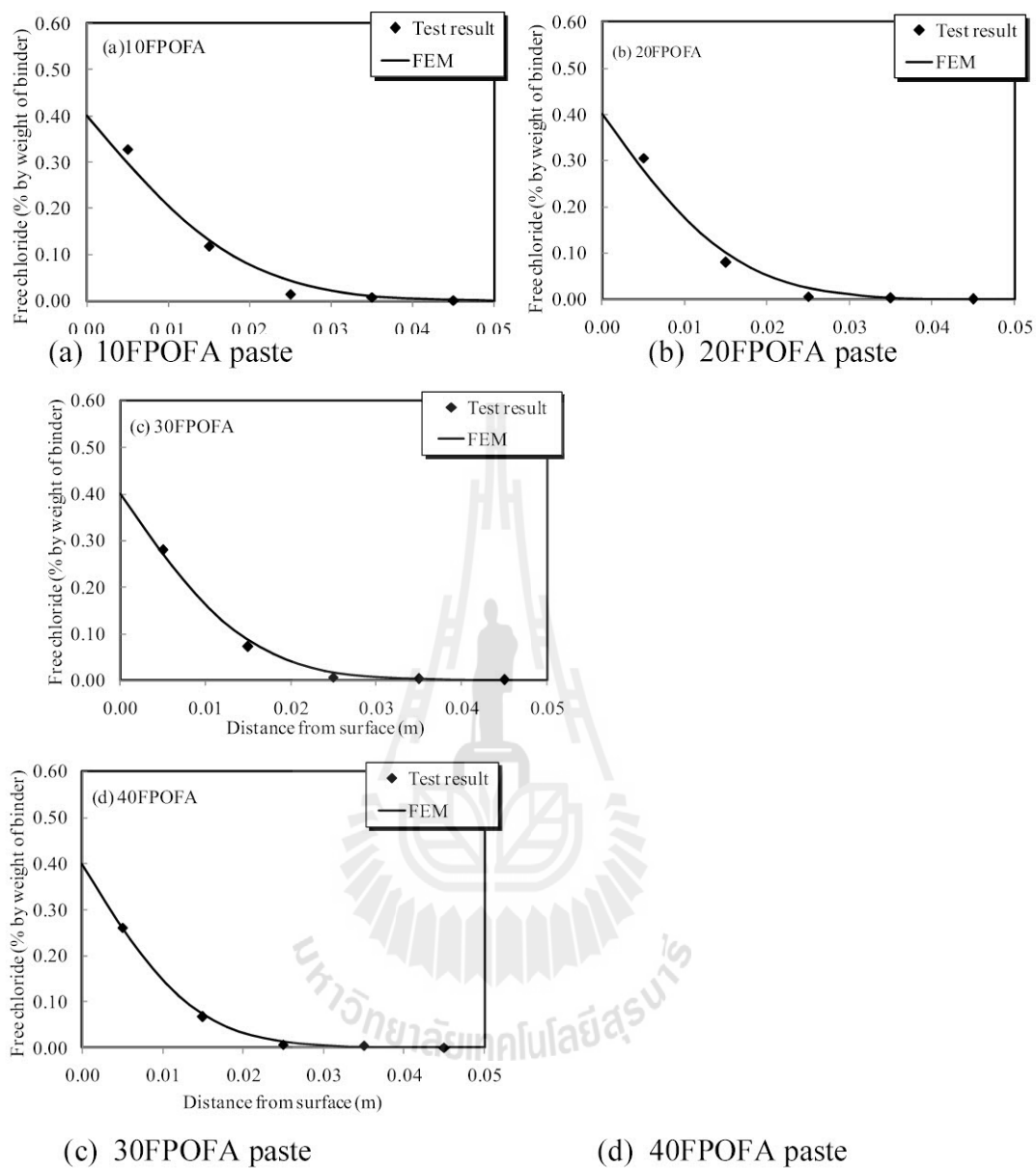


Figure 4.61 Comparison of numerical results of FPOFA pastes at 90 days immersion in 3% NaCl solution

4.13 References

- Aly, M., Hashmi, M. S. J., Olabi, A. G., Messeiry, M., Abadir, E. F., and Hussain, A. I. (2012). Effect of colloidal nano-silica on the mechanical and physical behaviour of waste-glass cement mortar. **Materials and Design**. 33(0): 127-135.
- Ampadu, K. O., Torii, K., and Kawamura, M. (1999). Beneficial effect of fly ash on chloride diffusivity of hardened cement paste. **Cement and Concrete Research**. 29(4): 585-590.
- Arya, C., Buenfeld, N. R., and Newman, J. B. (1990). Factors influencing chloride-binding in concrete. **Cement and Concrete Research**. 20(2): 291-300.
- ASTM C618. (2001). Standard specification for coal fly ash and raw or calcined natural pozzolan for use as a mineral admixture in concrete. **Annual book of ASTM standards**: vol. 04.02.
- Awal, A. S. M. A., and Hussin, M. W. (1997). The effectiveness of palm oil fuel ash in preventing expansion due to alkali-silica reaction. **Cement and Concrete Composites**. 19(4): 367-372.
- Bai, J., Chaipanich, A., Kinuthia, J. M., O'Farrell, M., Sabir, B. B., Wild, S., and Lewis, M. H. (2003). Compressive strength and hydration of wastepaper sludge ash-ground granulated blastfurnace slag blended pastes. **Cement and Concrete Research**. 33(8): 1189-1202.
- Bui, D. D., Hu, J., and Stroeven, P. (2005). Particle size effect on the strength of rice husk ash blended gap-graded Portland cement concrete. **Cement and Concrete Composites**. 27(3): 357-366.

- Chaipanich, A., and Nochaiya, T. (2010). Thermal analysis and microstructure of Portland cement-fly ash-silica fume pastes. **Journal of Thermal Analysis and Calorimetry**. 99(2): 487-493.
- Chalee, W., and Jaturapitakkul, C. (2009). Effects of W/B ratios and fly ash finenesses on chloride diffusion coefficient of concrete in marine environment. **Materials and Structures**. 42(4): 505-514.
- Chindapasirt, P., Jaturapitakkul, C., and Sinsiri, T. (2005). Effect of fly ash fineness on compressive strength and pore size of blended cement paste. **Cement and Concrete Composites**. 27(4): 425-428.
- Chindapasirt, P., Jaturapitakkul, C., and Sinsiri, T. (2007). Effect of fly ash fineness on microstructure of blended cement paste. **Construction and Building Materials**. 21(7): 1534-1541.
- Chindapasirt, P., Rukzon, S., and Sirivivatnanon, V. (2008). Resistance to chloride penetration of blended Portland cement mortar containing palm oil fuel ash, rice husk ash and fly ash. **Construction and Building Materials**. 22(5): 932-938.
- Cordeiro, G. C., Toledo Filho, R. D., Tavares, L. M., Fairbairn, E. d. M. R., and Hempel, S. (2011). Influence of particle size and specific surface area on the pozzolanic activity of residual rice husk ash. **Cement and Concrete Composites**. 33(5): 529-534.
- Cordeiro, G. C., Toledo Filho, R. D., Tavares, L. M., and Fairbairn, E. M. R. (2008). Pozzolanic activity and filler effect of sugar cane bagasse ash in Portland cement and lime mortars. **Cement and Concrete Composites**. 30(5): 410-418.

- Cyr, M., Lawrence, P., and Ringot, E. (2006). Efficiency of mineral admixtures in mortars: Quantification of the physical and chemical effects of fine admixtures in relation with compressive strength. **Cement and Concrete Research**. 36(2): 264-277.
- El-Jazairi, B., and Illston, J. M. (1977). A simultaneous semi-isothermal method of thermogravimetry and derivative thermogravimetry, and its application to cement pastes. **Cement and Concrete Research**. 7(3): 247-257.
- Frías, M., and Cabrera, J. (2000). Pore size distribution and degree of hydration of metakaolin-cement pastes. **Cement and Concrete Research**. 30(4): 561-569.
- Ganesan, K., Rajagopal, K., and Thangavel, K. (2008). Rice husk ash blended cement: Assessment of optimal level of replacement for strength and permeability properties of concrete. **Construction and Building Materials**. 22(8): 1675-1683.
- Gopalan, M. K. (1993). Nucleation and pozzolanic factors in strength development of class F fly ash concrete. **ACI Materials Journal**. 90(2): 117-121.
- Halamickova, P., Detwiler, R. J., Bentz, D. P., and Garboczi, E. J. (1995). Water permeability and chloride ion diffusion in portland cement mortars: Relationship to sand content and critical pore diameter. **Cement and Concrete Research**, 25(4): 790-802.
- Isaia, G. C., Gastaldini, A. L. G., and Moraes, R. (2003). Physical and pozzolanic action of mineral additions on the mechanical strength of high-performance concrete. **Cement and Concrete Composites**. 25(1): 69-76.

- Jensen, O. M., Hansen, P. F., Coats, A. M., and Glasser, F. P. (1999). Chloride ingress in cement paste and mortar. **Cement and Concrete Research**. 29(9): 1497-1504.
- Jaturapitakkul, C., Tangpagasit, J., Songmue, S., and Kiattikomol, K. (2011a). Filler effect and pozzolanic reaction of ground palm oil fuel ash. **Construction and Building Materials**. 25(11): 4287-4293.
- Jaturapitakkul, C., Tangpagasit, J., Songmue, S., and Kiattikomol, K. (2011b). Filler effect of fine particle sand on the compressive strength of mortar. **International Journal of Minerals, Metallurgy, and Materials**. 18(2): 240-246.
- Kroehong, W., Sinsiri, T., Jaturapitakkul, C., and Chindapasirt, P. (2011). Effect of palm oil fuel ash fineness on the microstructure of blended cement paste. **Construction and Building Materials**. 25(11): 4095-4104.
- Lee, C.-L., Huang, R., Lin, W.-T., and Weng, T.-L. (2012). Establishment of the durability indices for cement-based composite containing supplementary cementitious materials. **Materials and Design**. 37(0): 28-39.
- Li, Z., and Ding, Z. (2003). Property improvement of Portland cement by incorporating with metakaolin and slag. **Cement and Concrete Research**. 33(4): 579-584.
- Luo, R., Cai, Y., Wang, C., and Huang, X. (2003). Study of chloride binding and diffusion in GGBS concrete. **Cement and Concrete Research**. 33(1): 1-7.
- Megat Johari, M. A., Brooks, J. J., Kabir, S., and Rivard, P. (2011). Influence of supplementary cementitious materials on engineering properties of high strength concrete. **Construction and Building Materials**. 25(5): 2639-2648.

- Mehta, P. K. (1987). Proceedings of Int. **Workshop on Condensed Silica Fume in Concrete**.1.
- Mehta, P. K., and Aietcin, P.-C. C. (1990). Principles underlying production of high-performance concrete. **Cement, Concrete and Aggregates**. 12(2): 70-78.
- Montgomery, D. G., Hughes, D. C., and Williams, R. I. T. (1981). "Fly ash in concrete - a microstructure study. **Cement and Concrete Research**. 11(4): 591-603.
- Moon, H. Y., Kim, H. S., and Choi, D. S. (2006). Relationship between average pore diameter and chloride diffusivity in various concretes. **Construction and Building Materials**. 20(9): 725-732.
- Nochaiya, T., Wongkeo, W., Pimraksa, K., and Chaipanich, A. (2010). Microstructural, physical, and thermal analyses of Portland cement-fly ash-calcium hydroxide blended pastes. **Journal of Thermal Analysis and Calorimetry**. 100(1): 101-108.
- Page, C. L., Short, N. R., and El Tarras, A. (1981). Diffusion of chloride ions in hardened cement pastes. **Cement and Concrete Research**. 11(3): 395-406.
- Pipilikaki, P., and Beazi-Katsioti, M. (2009). The assessment of porosity and pore size distribution of limestone Portland cement pastes. **Construction and Building Materials**. 23(5): 1966-1970.
- Poon, C. S., Lam, L., Kou, S. C., Wong, Y. L., and Wong, R. (2001). Rate of pozzolanic reaction of metakaolin in high-performance cement pastes. **Cement and Concrete Research**. 31(9): 1301-1306.

- Poon, C. S., Wong, Y. L., and Lam, L. (1997). The influence of different curing conditions on the pore structure and related properties of fly-ash cement pastes and mortars. **Construction and Building Materials**. 11(7-8): 383-393.
- Rashad, A. M., Zeedan, S. R., and Hassan, H. A. (2012). A preliminary study of autoclaved alkali-activated slag blended with quartz powder. **Construction and Building Materials**. 33(0): 70-77.
- Rasheeduzzafar, Al-Saadoun, S. S., Al-Gahtani, A. S., and Dakhil, F. H. (1990). Effect of tricalcium aluminate content of cement on corrosion of reinforcing steel in concrete. **Cement and Concrete Research**. 20(5): 723-738.
- Rukzon, S., and Chindaprasirt, P. (2012). Utilization of bagasse ash in high-strength concrete. **Materials and Design**. 34(0): 45-50.
- Sergi, G., Yu, S. W., and Page, C. L. (1992). Diffusion of chloride and hydroxyl ions in cementitious materials exposed to a saline environment. **Magazine of Concrete Research**. 44(158): 63-69.
- Sumranwanich, T., and Tangtermsirikul, S. (2004a). A model for predicting time-dependent chloride binding capacity of cement-fly ash cementitious system. **Materials and Structures**. 37(6): 387-396.
- Sumranwanich, T., and Tangtermsirikul, S. (2004b). Time-dependent chloride binding capacity of various types of cement pastes. **ScienceAsia**. 30: 127-134.
- Tangchirapat, W., and Jaturapitakkul, C. (2010). Strength, drying shrinkage, and water permeability of concrete incorporating ground palm oil fuel ash. **Cement and Concrete Composites**. 32(10): 767-774.

- Tangpagasit, J., Cheerarot, R., Jaturapitakkul, C., and Kiattikomol, K. (2005). Packing effect and pozzolanic reaction of fly ash in mortar. **Cement and Concrete Research**. 35(6): 1145-1151.
- Thomas, M. D. A., Hooton, R. D., Scott, A., and Zibara, H. (2012). The effect of supplementary cementitious materials on chloride binding in hardened cement paste. **Cement and Concrete Research**. 42(1): 1-7.
- Vedalakshmi, R., Sundara Raj, A., Srinivasan, S., and Ganesh Babu, K. (2003). Quantification of hydrated cement products of blended cements in low and medium strength concrete using TG and DTA technique. **Thermochimica Acta**. 407(1-2): 49-60.
- Yang, C. C., Cho, S. W., and Wang, L. C. (2006). The relationship between pore structure and chloride diffusivity from ponding test in cement-based materials. **Materials Chemistry and Physics**. 100(2-3): 203-210.
- Ye, G., Lura, P., and van Breugel, K. (2006). Modelling of water permeability in cementitious materials. **Materials and Structures**. 39(9): 877-885.
- Zibara, H. (2001). Binding of external chlorides by cement paste. **PhD Thesis**, University of Toronto (Canada), 320.

CHAPTER V

CONCLUSIONS AND RECOMMENDATIONS

5.1 Conclusions

5.1.1 PART I Effect of biomass ashes fineness on compressive strength and microstructure of blended cement paste

5.1.1.1 The amorphous content of RHA and POFA was approximately 67–70%. Blended cement paste with high fineness RHA or POFA had a higher compressive strength than that with coarse ashes. In addition, the use of RHA or POFA with particle sizes smaller than those of OPC to replace Portland cement Type I at the rate of 10-30% by weight of binder resulted in good compressive strength from filler effect and pozzolanic reaction.

5.1.1.2 The percentage compressive strength of the pastes due to the hydration reaction decreased with decreasing cement content. The percentage compressive strength of pastes due to the filler effect increased with increasing inert matter material replacement. The percentage compressive strength of paste due to the pozzolanic reaction increased with increasing fineness of pozzolans, cement replacement and age of paste.

5.1.1.3 The Ca(OH)_2 contents of blended cement pastes containing RHA or POFA were lower than those of the OPC paste and decreased with increasing in the replacement and fineness of the ashes. Moreover, the reduction of Ca(OH)_2 affected the increased peak intensity of the C-S-H, C_2ASH_8 and C_4AH_{13} phases with increasing curing time, which resulted in an increase in the compressive strength.

5.1.1.4 The reduction of the $\text{Ca}(\text{OH})_2$ content in the RHA or POFA pastes were due to the pozzolanic reaction and caused the pore size structure of the paste to change from coarser pores to finer pores. Thus, the critical pore size and average pore diameter of the paste containing RHA and POFA were lower than those of the OPC paste.

5.1.1.5 The mass loss (at 30°C - 450°C) of RS pastes increased with fineness and decrease with the replacement level. In addition, it was likely that the addition of fine RS whose particles were finer than those of Portland cement caused segmentation of large pores and increased nucleation sites for precipitation of hydration products in cement paste as resulted in an increase compressive strength was due to the filler effect. In contrast, the $\text{Ca}(\text{OH})_2$ content in the fine RS pastes was lower than that of the coarse RS pastes.

5.1.1.6 The differences between mass loss (at 30°C - 450°C) of RS and RHA or POFA pastes at same fineness, curing time and replacement rate were due to the pozzolanic reaction which increased with particle fineness and cement replacement rate. In addition, the weight losses (at 30°C - 450°C) due to the pozzolanic reaction were higher than those due to the filler effect.

5.1.2 PART II Chloride penetration into blended cement paste

5.1.2.1 The OPC paste had a lower chloride penetration than the SRPC paste. The use of palm oil fuel ash results in a lower chloride diffusion coefficient and concentration profile of free chloride than the OPC paste. In addition, the chloride diffusion coefficient is linearly correlated and increases with an increase in the critical pore diameter.

5.1.2.2 The increase of fineness and replacement of cement with palm oil fuel ash resulted in the decrease of free chloride and the chloride diffusion coefficient.

5.1.2.3 The use of palm oil fuel ash to replace Portland cement type I had a lower peak intensity of Friedel's salt in paste than that of the OPC paste. In addition, the peak intensity of Friedel's salt in paste decreased with increasing replacement of POFA. However, increasing the replacement of cement by palm oil fuel ash resulted in an increasing physically bound chloride.

5.1.2.4 It is found that the numerical results obtained using the finite element method agrees with experimental results. Thus, the finite element solution can produce an accurate analysis of the concentration profile of free chloride in pastes at any depth and at any time.

5.2 Recommendations for future work

5.2.1 The study should attempted to find microstructure of paste, mortar and concrete under deterioration conditions such as sulfate attack, acid attack, carbonation, sea water attack etc.

5.2.2 In this study, the particle size of ground rice husk ash and palm oil fuel ash was in the micro scale. Next study, it is suggested to use particle at nano scale.





APPENDIX A
COMPRESSIVE STRENGTH OF OPC, RS, RHA AND
POFA PASTES

Table A.1 Compressive strength of OPC and 10CRS pastes

Mix	Age (day)	Sample	Cross section		Ultimate Load (Kg)	Compressive Strength (MPa)	Average Compressive Strength (MPa)
			Width (cm)	Height (cm)			
OPC	7	1	5.10	5.10	13,501	52.91	53.0
		2	5.05	5.10	13,323	52.73	
		3	5.10	5.00	14,011	56.01	
		4	5.05	5.10	12,703	50.28	
		5	5.10	5.10	15,737	61.68	
	28	1	5.00	5.10	18,893	75.53	75.0
		2	5.15	5.10	18,249	70.83	
		3	5.10	5.15	20,285	78.73	
		4	5.05	5.05	18,649	74.54	
		5	5.10	5.10	19,207	75.27	
	60	1	5.00	5.10	21,886	87.49	84.6
		2	5.15	5.10	21,673	84.11	
		3	5.10	5.15	19,904	77.25	
		4	5.05	5.10	24,984	98.89	
		5	5.10	5.10	22,893	89.72	
	90	1	5.00	5.10	28,271	113.01	99.1
		2	5.05	5.10	25,739	101.87	
		3	5.10	5.15	23,304	90.44	
		4	5.00	5.05	25,459	102.78	
		5	5.15	5.10	26,113	101.35	
10CRS	7	1	5.10	5.10	12443	48.77	48.3
		2	5.05	5.10	11,630	46.03	
		3	5.00	5.15	14,858	58.82	
		4	5.15	5.05	12,139	47.58	
		5	5.15	5.10	13,135	50.98	
	28	1	5.10	5.05	18,187	71.98	68.2
		2	5.10	5.15	16,794	65.18	
		3	5.00	5.10	20,439	81.71	
		4	5.15	5.10	17,320	67.22	
		5	5.00	5.05	16,937	68.38	
	60	1	5.10	5.10	20,052	78.59	77.2
		2	5.10	5.10	19,585	76.76	
		3	5.00	5.10	20,236	80.89	
		4	5.10	5.15	19,253	74.72	
		5	5.10	5.10	19,165	75.11	
	90	1	5.15	5.10	20,101	78.01	90.1
		2	5.10	5.10	23,510	92.14	
		3	5.10	5.05	22,106	87.49	
		4	5.05	5.10	21,883	86.61	
		5	5.15	5.05	25,054	98.20	

= Data are not applicable

Table A.2 Compressive strength of 20CRS and 30CRS pastes

Mix	Age (day)	Sample	Cross section		Ultimate Load (Kg)	Compressive Strength (MPa)	Average Compressive Strength (MPa)
			Width (cm)	Height (cm)			
20CRS	7	1	5.15	5.10	9,958	38.65	42.9
		2	5.00	5.10	11,456	45.80	
		3	5.10	5.15	11,652	45.22	
		4	5.10	5.05	10,876	43.05	
		5	5.10	5.10	10,659	41.77	
	28	1	5.05	5.10	14,823	58.67	60.8
		2	5.05	5.10	18,430	72.94	
		3	5.10	5.10	15,629	61.25	
		4	5.10	5.10	15,154	59.39	
		5	5.10	5.15	16,502	64.05	
	60	1	5.10	5.15	17,485	67.86	67.9
		2	5.10	5.15	17,503	67.93	
		3	5.05	5.10	20,139	79.71	
		4	5.10	5.15	18,243	70.80	
		5	5.15	5.10	16,793	65.18	
	90	1	5.15	5.05	18,847	73.87	78.6
		2	5.05	5.10	19,306	76.41	
		3	5.05	5.10	21,044	83.29	
		4	5.10	5.10	23,759	93.11	
		5	5.05	5.05	20,234	80.88	
30CRS	7	1	5.10	5.10	8,863	34.74	36.9
		2	5.05	5.05	11,045	44.15	
		3	5.10	5.10	9,542	37.40	
		4	5.10	5.10	8,953	35.09	
		5	5.00	5.10	10,128	40.49	
	28	1	5.15	5.05	12,743	49.95	53.1
		2	5.10	5.10	13,398	52.51	
		3	5.10	5.05	14,743	58.35	
		4	5.00	5.05	13,324	53.79	
		5	5.10	5.05	14,178	56.12	
	60	1	5.10	5.10	14,163	55.51	60.8
		2	5.10	5.10	15,639	61.29	
		3	5.00	5.10	14,954	59.78	
		4	5.10	5.15	16,340	63.42	
		5	5.15	5.10	16,453	63.86	
	90	1	5.15	5.10	20,367	79.05	70.2
		2	5.05	5.00	17,702	71.46	
		3	5.10	5.10	19,129	74.97	
		4	5.00	5.05	18,004	72.68	
		5	5.10	5.10	16,734	65.58	


 = Data are not applicable

Table A.3 Compressive strength of 40CRS and 10FRS pastes

Mix	Age (day)	Sample	Cross section		Ultimate Load (Kg)	Compressive Strength (MPa)	Average Compressive Strength (MPa)
			Width (cm)	Height (cm)			
40CRS	7	1	5.10	5.10	9,459	37.07	31.5
		2	5.05	5.05	8,301	33.18	
		3	5.00	5.15	7,930	31.39	
		4	5.10	5.05	8,073	31.95	
		5	5.15	5.10	7,608	29.53	
	28	1	5.10	5.05	12,483	49.41	45.6
		2	5.10	5.15	11,183	43.40	
		3	5.00	5.10	12,119	48.45	
		4	5.15	5.10	10,596	41.12	
		5	5.00	5.05	13,574	54.80	
	60	1	5.10	5.10	12,530	49.11	51.5
		2	5.05	5.05	15,634	62.49	
		3	5.05	5.10	14,020	55.49	
		4	5.10	5.05	13,343	52.81	
		5	5.10	5.05	12,305	48.70	
	90	1	5.15	5.10	14,398	55.88	59.6
		2	5.10	5.10	15,230	59.69	
		3	5.05	5.10	17,854	70.67	
		4	5.05	5.15	16,130	63.22	
		5	5.10	5.10	15,201	59.57	
10FRS	7	1	5.10	5.10	11,930	46.76	49.9
		2	5.05	5.10	13,050	51.65	
		3	5.15	5.05	12,397	48.59	
		4	5.00	5.15	13,794	55.61	
		5	5.10	5.10	12,203	47.83	
	28	1	5.00	5.10	16,940	67.72	69.9
		2	5.10	5.00	20,294	81.13	
		3	5.10	5.00	16,605	66.38	
		4	5.15	5.05	19,080	74.78	
		5	5.00	5.10	17,694	70.73	
	60	1	5.10	5.15	18,955	73.57	79.1
		2	5.10	5.10	19,749	77.40	
		3	5.10	5.10	20,285	79.50	
		4	5.05	5.00	23,485	94.81	
		5	5.15	5.05	21,902	85.85	
	90	1	5.10	5.10	25,140	98.53	92.8
		2	5.10	5.10	24,038	94.21	
		3	5.05	5.15	23,183	90.87	
		4	5.05	5.100	22,649	89.64	
		5	5.1	5.15	23,407	90.84	

■ = Data are not applicable

Table A.4 Compressive strength of 20FRS and 30FRS pastes

Mix	Age (day)	Sample	Cross section		Ultimate Load (Kg)	Compressive Strength (MPa)	Average Compressive Strength (MPa)
			Width (cm)	Height (cm)			
20FRS	7	1	5.15	5.10	10,843	42.50	45.0
		2	5.00	5.05	11,194	43.44	
		3	5.10	5.10	14,379	58.05	
		4	5.10	5.10	12,363	49.42	
		5	5.10	5.05	11,425	44.78	
	28	1	5.10	5.05	14,929	57.94	63.4
		2	5.05	5.05	16,222	65.49	
		3	5.05	5.10	17,210	67.45	
		4	5.10	5.15	18,604	72.91	
		5	5.10	5.10	15,820	62.61	
	60	1	5.10	5.10	16,934	67.02	70.8
		2	5.10	5.10	17,448	69.74	
		3	5.05	5.05	18,335	72.57	
		4	5.05	5.10	19,058	73.97	
		5	5.00	5.10	21,658	84.88	
	90	1	5.15	5.10	19,380	75.95	82.1
		2	5.00	5.05	20,497	80.33	
		3	5.10	5.10	21,048	84.13	
		4	5.10	5.10	22,384	88.59	
		5	5.10	5.05	20,409	81.59	
30FRS	7	1	5.00	5.10	9,707	38.80	39.1
		2	5.00	5.05	12,283	49.59	
		3	5.10	5.10	10,593	41.52	
		4	5.00	5.15	9,747	38.59	
		5	5.10	5.10	9,610	37.66	
	28	1	5.10	5.05	13,740	54.38	56.5
		2	5.10	5.05	14,353	56.81	
		3	5.15	5.00	15,594	61.73	
		4	5.00	5.05	17,824	71.96	
		5	5.05	5.10	13,403	53.05	
	60	1	5.10	5.10	19,338	75.79	64.1
		2	5.10	5.15	16,154	62.70	
		3	5.10	5.10	17,208	67.44	
		4	5.05	5.00	15,430	62.29	
		5	5.15	5.05	16,318	63.96	
	90	1	5.15	5.10	21,408	83.09	74.5
		2	5.05	5.10	17,805	70.47	
		3	5.05	5.05	20,194	80.72	
		4	5.00	5.10	18,068	72.23	
		5	5.00	5.15	16,390	64.88	

= Data are not applicable

Table A.5 Compressive strength of 40FRS and 10CRHA pastes

Mix	Age (day)	Sample	Cross section		Ultimate Load (Kg)	Compressive Strength (MPa)	Average Compressive Strength (MPa)
			Width (cm)	Height (cm)			
40FRS	7	1	5.05	5.15	8,643	33.88	34.2
		2	5.10	5.10	9,120	35.74	
		3	5.10	5.05	8,006	31.69	
		4	5.10	5.10	8,203	32.15	
		5	5.00	5.10	9,226	37.60	
	28	1	5.00	5.10	12,493	49.94	49.2
		2	5.10	5.10	15,190	59.53	
		3	5.10	5.15	12,448	48.31	
		4	5.10	5.05	11,430	45.24	
		5	5.10	5.05	13,507	53.46	
	60	1	5.10	5.05	13,490	53.39	55.4
		2	5.10	5.10	10,394	40.74	
		3	5.05	5.10	13,484	53.37	
		4	5.00	5.10	15,180	60.68	
		5	5.05	5.10	13,643	54.00	
	90	1	5.05	5.10	14,909	59.01	63.9
		2	5.05	5.05	16,165	64.61	
		3	5.05	5.10	17,443	69.04	
		4	5.10	5.00	15,769	63.04	
		5	5.10	5.15	12,482	48.44	
10CRHA	7	1	5.00	5.10	14,246	56.95	52.4
		2	5.10	5.10	12,379	48.52	
		3	5.05	5.10	13,135	51.99	
		4	5.10	5.05	13,490	53.39	
		5	5.15	5.00	12,938	51.22	
	28	1	5.10	5.05	19,149	75.79	76.5
		2	5.10	5.15	20,030	77.74	
		3	5.05	5.05	23,539	94.09	
		4	5.10	5.10	18,129	71.05	
		5	5.00	5.05	20,129	81.26	
	60	1	5.10	5.10	20,984	82.24	88.5
		2	5.10	5.05	22,393	88.63	
		3	5.10	5.05	23,185	91.76	
		4	5.10	5.15	24,417	94.76	
		5	5.10	5.05	21,503	85.11	
	90	1	5.10	5.05	27,193	107.63	107.6
		2	5.10	5.00	25,564	102.19	
		3	5.05	5.00	28,635	115.60	
		4	5.10	5.05	23,468	92.88	
		5	5.10	5.10	26,792	105.00	

= Data are not applicable

Table A.6 Compressive strength of 20CRHA and 30CRHA pastes

Mix	Age (day)	Sample	Cross section		Ultimate Load (Kg)	Compressive Strength (MPa)	Average Compressive Strength (MPa)
			Width (cm)	Height (cm)			
20CRHA	7	1	5.10	5.10	12,451	48.80	49.8
		2	5.10	5.00	10,128	40.49	
		3	5.05	5.05	11,917	47.63	
		4	5.00	5.05	13,484	54.44	
		5	5.00	5.15	12,164	48.15	
	28	1	5.10	5.10	15,474	60.64	74.2
		2	5.05	5.10	17,602	69.67	
		3	5.05	5.10	18,075	71.54	
		4	5.10	5.05	20,240	80.11	
		5	5.00	5.00	18,483	75.36	
	60	1	5.10	5.10	20,971	82.19	88.3
		2	5.10	5.10	21,963	86.08	
		3	5.05	5.05	24,104	96.35	
		4	5.10	5.10	22,870	89.63	
		5	5.10	5.05	22,064	87.33	
	90	1	5.10	5.10	20,214	79.22	106.0
		2	5.10	5.05	26,683	105.61	
		3	5.10	5.05	25,359	100.37	
		4	5.10	5.05	27,107	107.29	
		5	5.05	5.10	28,026	110.93	
30CRHA	7	1	5.05	5.00	10,973	44.30	46.5
		2	5.00	5.05	12,410	50.10	
		3	5.10	5.10	11,326	44.39	
		4	5.10	5.15	11,302	43.86	
		5	5.10	5.00	12,517	50.04	
	28	1	5.10	5.10	20,184	79.10	70.5
		2	5.05	5.10	17,060	67.52	
		3	5.10	5.05	19,103	75.61	
		4	5.10	5.05	18,030	71.36	
		5	5.10	5.05	17,068	67.55	
	60	1	5.10	5.10	21,874	85.73	83.7
		2	5.10	5.10	22,864	89.61	
		3	5.15	5.10	18,643	72.36	
		4	5.10	5.05	20,578	81.45	
		5	5.05	5.10	19,753	78.18	
	90	1	5.10	5.10	25,820	101.19	100.0
		2	5.10	5.10	24,341	95.40	
		3	5.10	5.05	24,628	97.48	
		4	5.05	5.05	21,964	87.79	
		5	5.00	5.00	26,010	106.06	

■ = Data are not applicable

Table A.7 Compressive strength of 40CRHA and 10FRHA pastes

Mix	Age (day)	Sample	Cross section		Ultimate Load (Kg)	Compressive Strength (MPa)	Average Compressive Strength (MPa)
			Width (cm)	Height (cm)			
40CRHA	7	1	5.00	5.10	10,513	42.03	42.4
		2	5.10	5.15	11,238	43.62	
		3	5.10	5.10	10,473	41.05	
		4	5.10	5.10	10,938	42.87	
		5	5.00	5.00	8,086	32.97	
	28	1	5.05	5.10	15,289	60.51	64.7
		2	5.10	5.05	17,011	67.33	
		3	5.05	5.05	16,243	64.93	
		4	5.05	5.10	15,624	61.84	
		5	5.05	5.05	17,240	68.91	
	60	1	5.05	5.10	19,162	75.84	77.4
		2	5.10	5.10	20,213	79.22	
		3	5.10	5.15	19,253	74.72	
		4	5.10	5.10	21,140	82.85	
		5	5.10	5.05	18,843	74.58	
	90	1	5.10	5.10	24,012	94.11	92.1
		2	5.10	5.10	22,533	88.31	
		3	5.05	5.05	23,340	93.29	
		4	5.15	5.15	20,193	77.61	
		5	5.15	5.15	24,138	92.77	
10FRHA	7	1	5.10	5.10	11,382	44.61	55.9
		2	5.10	5.15	15,121	58.69	
		3	5.05	5.10	13,821	54.70	
		4	5.05	5.05	14,002	55.97	
		5	5.05	5.10	13,744	54.40	
	28	1	5.10	5.10	21,073	82.59	81.7
		2	5.10	5.15	20,363	79.03	
		3	5.05	5.10	21,160	83.75	
		4	5.10	5.10	19,411	76.07	
		5	5.10	5.05	22,036	87.22	
	60	1	5.10	5.10	20,374	79.85	94.7
		2	5.10	5.05	24,392	96.54	
		3	5.00	5.10	23,742	94.91	
		4	5.15	5.10	25,041	97.19	
		5	5.10	5.05	22,780	90.16	
	90	1	5.05	5.10	25,672	101.61	116.2
		2	5.15	5.10	28,329	109.95	
		3	5.10	5.05	30,124	119.23	
		4	5.10	5.10	29,120	114.13	
		5	5.05	5.10	30,727	121.62	

= Data are not applicable

Table A.8 Compressive strength of 20FRHA and 30FRHA pastes

Mix	Age (day)	Sample	Cross section		Ultimate Load (Kg)	Compressive Strength (MPa)	Average Compressive Strength (MPa)
			Width (cm)	Height (cm)			
20FRHA	7	1	5.05	5.00	13,430	54.22	52.9
		2	5.10	5.10	12,517	49.06	
		3	5.10	5.10	10,349	40.56	
		4	5.05	5.10	13,120	51.93	
		5	5.10	5.05	14,262	56.45	
	28	1	5.10	5.05	20,029	79.27	78.7
		2	5.05	5.10	19,529	77.29	
		3	5.05	5.10	18,929	74.92	
		4	5.10	5.00	21,294	85.12	
		5	5.05	5.10	19,390	76.74	
	60	1	5.10	5.10	18,905	74.09	93.1
		2	5.10	5.10	22,591	88.54	
		3	5.00	5.05	22,390	90.39	
		4	5.10	5.05	23,578	93.32	
		5	5.00	5.10	25,093	100.31	
	90	1	5.10	5.05	26,555	105.10	113.2
		2	5.05	5.05	28,148	112.51	
		3	5.05	5.10	30,470	120.60	
		4	5.10	5.10	29,228	114.55	
		5	5.00	5.10	24,604	98.36	
30FRHA	7	1	5.10	5.05	12,558	49.70	50.3
		2	5.05	5.05	11,913	47.62	
		3	5.00	5.05	12,029	48.56	
		4	5.05	5.15	13,293	52.10	
		5	5.10	5.15	13,835	53.69	
	28	1	5.10	5.15	19,123	74.22	74.9
		2	5.10	5.05	18,415	72.89	
		3	5.10	5.10	19,239	75.40	
		4	5.15	5.10	20,810	80.77	
		5	5.10	5.10	18,230	71.45	
	60	1	5.10	5.10	22,683	88.90	89.6
		2	5.00	5.10	23,032	92.07	
		3	5.00	5.05	22,860	92.29	
		4	5.05	5.05	19,329	77.26	
		5	5.05	5.10	22,038	87.23	
	90	1	5.15	5.10	28,118	109.13	107.9
		2	5.10	5.10	27,029	105.93	
		3	5.05	5.05	26,919	107.60	
		4	5.10	5.10	26,612	104.30	
		5	5.10	5.15	29,043	112.72	

■ = Data are not applicable

Table A.9 Compressive strength of 40FRHA and 10CPOFA pastes

Mix	Age (day)	Sample	Cross section		Ultimate Load (Kg)	Compressive Strength (MPa)	Average Compressive Strength (MPa)
			Width (cm)	Height (cm)			
40FRHA	7	1	5.05	5.10	10,894	43.12	44.5
		2	5.05	5.15	13,270	52.01	
		3	5.10	5.15	10,948	42.49	
		4	5.10	5.10	11,274	44.18	
		5	5.10	5.05	12,143	48.06	
	28	1	5.10	5.10	16,929	66.35	66.9
		2	5.10	5.05	15,994	63.30	
		3	5.15	5.10	16,705	64.83	
		4	5.05	5.10	17,282	68.40	
		5	5.00	5.05	17,732	71.59	
	60	1	5.00	5.00	17,430	69.00	79.5
		2	5.05	5.00	19,273	77.81	
		3	5.05	5.00	20,143	81.32	
		4	5.00	5.05	18,874	76.20	
		5	5.05	5.05	21,132	84.47	
	90	1	5.10	5.00	23,228	92.85	96.1
		2	5.10	5.05	23,838	94.35	
		3	5.00	5.10	24,373	97.43	
		4	5.05	5.05	23,410	93.57	
		5	5.00	5.10	25,634	102.47	
10CPOFA	7	1	5.10	5.05	14,102	55.81	51.3
		2	5.10	5.05	13,118	51.92	
		3	5.05	5.05	12,563	50.22	
		4	5.05	5.10	10,127	40.08	
		5	5.10	5.10	12,039	47.18	
	28	1	5.05	5.15	19,447	76.22	74.8
		2	5.10	5.15	18,903	73.36	
		3	5.10	5.10	17,984	70.48	
		4	5.15	5.10	20,670	80.22	
		5	5.15	5.10	18,994	73.72	
	60	1	5.15	5.10	22,532	87.45	86.3
		2	5.10	5.05	18,547	73.41	
		3	5.15	5.10	21,473	83.34	
		4	5.10	5.05	23,189	91.78	
		5	5.05	5.10	20,854	82.54	
	90	1	5.05	5.10	26,254	103.91	104.5
		2	5.10	5.05	26,164	103.56	
		3	5.10	5.15	25,579	99.27	
		4	5.10	5.10	27,187	106.55	
		5	5.10	5.15	28,180	109.37	

= Data are not applicable

Table A.10 Compressive strength of 20CPOFA and 30CPOFA pastes

Mix	Age (day)	Sample	Cross section		Ultimate Load (Kg)	Compressive Strength (MPa)	Average Compressive Strength (MPa)
			Width (cm)	Height (cm)			
20CPOFA	7	1	5.10	5.10	11,868	46.51	48.3
		2	5.00	5.10	12,686	50.71	
		3	5.10	5.05	12,136	48.03	
		4	5.00	5.00	11,943	48.70	
		5	5.10	5.10	15,094	59.16	
	28	1	5.10	5.10	19,026	74.57	72.0
		2	5.10	5.10	17,337	67.95	
		3	5.10	5.05	18,173	71.93	
		4	5.10	5.10	19,303	75.65	
		5	5.05	5.05	17,540	70.11	
	60	1	5.10	5.05	20,858	82.55	84.6
		2	5.10	5.05	21,949	86.87	
		3	5.00	5.10	20,743	82.92	
		4	5.05	5.00	22,784	91.98	
		5	5.10	5.10	21,332	83.60	
	90	1	5.10	5.10	27,032	105.94	102.0
		2	5.10	5.10	25,538	100.09	
		3	5.05	5.05	26,030	104.05	
		4	5.05	5.05	29,663	118.57	
		5	5.10	5.00	24,514	98.00	
30CPOFA	7	1	5.10	5.00	13,453	53.78	44.5
		2	5.05	5.05	11,079	44.28	
		3	5.10	5.00	10,763	43.03	
		4	5.00	5.05	10,853	43.81	
		5	5.10	5.00	11,754	46.99	
	28	1	5.10	5.10	16,594	65.03	66.7
		2	5.00	5.00	17,043	69.49	
		3	5.05	5.00	16,539	66.77	
		4	5.10	5.05	16,307	64.54	
		5	5.05	5.10	17,093	67.65	
	60	1	5.10	5.10	21,002	82.31	78.6
		2	5.10	5.10	19,174	75.15	
		3	5.05	5.10	20,284	80.28	
		4	5.05	5.05	17,520	70.03	
		5	5.10	5.00	19,184	76.69	
	90	1	5.10	5.15	26,439	102.61	97.1
		2	5.10	5.05	24,184	95.72	
		3	5.10	5.10	25,163	98.62	
		4	5.05	5.10	24,280	96.10	
		5	5.10	5.15	23,808	92.40	

☐ = Data are not applicable

Table A.11 Compressive strength of 40CPOFA and 10FPOFA pastes

Mix	Age (day)	Sample	Cross section		Ultimate Load (Kg)	Compressive Strength (MPa)	Average Compressive Strength (MPa)
			Width (cm)	Height (cm)			
40CPOFA	7	1	5.05	5.00	9,936	40.11	41.0
		2	5.10	5.01	10,553	42.10	
		3	5.05	5.00	10,394	41.96	
		4	5.10	5.01	10,497	41.88	
		5	5.10	5.10	9,939	38.95	
	28	1	5.10	5.10	13,940	54.63	61.5
		2	5.10	5.00	14,986	59.91	
		3	5.10	5.05	14,812	58.63	
		4	5.05	5.05	15,683	62.69	
		5	5.05	5.10	16,398	64.90	
	60	1	5.10	5.10	19,439	76.18	72.8
		2	5.00	5.10	17,239	68.91	
		3	5.05	5.10	21,546	85.28	
		4	5.10	5.10	17,439	68.35	
		5	5.10	5.05	19,694	77.95	
	90	1	5.10	5.10	21,505	84.28	88.1
		2	5.10	5.10	23,098	90.52	
		3	5.10	5.05	22,195	87.85	
		4	5.05	5.05	24,196	96.71	
		5	5.15	5.10	20,895	81.10	
10FPOFA	7	1	5.05	5.10	14209	56.24	53.7
		2	5.10	5.10	11263	44.14	
		3	5.10	5.00	13165	52.63	
		4	5.05	5.10	12909	51.09	
		5	5.05	5.10	13804	54.64	
	28	1	5.10	5.15	19,857	77.07	79.3
		2	5.00	5.10	21,540	86.11	
		3	5.10	5.00	18,873	75.45	
		4	5.05	5.05	19,553	78.16	
		5	5.05	5.10	20,280	80.27	
	60	1	5.10	5.15	23,260	90.27	93.3
		2	5.10	5.10	23,690	92.84	
		3	5.10	5.10	20,289	79.52	
		4	5.05	5.00	24,108	97.33	
		5	5.00	5.10	23,189	92.70	
	90	1	5.10	5.10	30,028	117.68	111.3
		2	5.10	5.10	28,103	110.14	
		3	5.05	5.10	27,194	107.63	
		4	5.10	5.05	28,390	112.37	
		5	5.10	5.05	27,426	108.55	

☐ = Data are not applicable

Table A.12 Compressive strength of 20FPOFA and 30FPOFA pastes

Mix	Age (day)	Sample	Cross section		Ultimate Load (Kg)	Compressive Strength (MPa)	Average Compressive Strength (MPa)
			Width (cm)	Height (cm)			
20FPOFA	7	1	5.10	5.10	14,004	54.88	51.9
		2	5.10	5.10	13,184	51.67	
		3	5.00	5.05	12,733	51.40	
		4	5.05	5.00	16,548	66.81	
		5	5.15	5.10	12,807	49.71	
	28	1	5.10	5.10	21,076	82.60	77.3
		2	5.15	5.05	18,182	71.26	
		3	5.10	5.05	19,263	76.24	
		4	5.10	5.10	20,184	79.10	
		5	5.10	5.10	16,596	65.04	
	60	1	5.10	5.05	24,389	96.53	92.2
		2	5.10	5.15	26,530	102.97	
		3	5.10	5.10	24,143	94.62	
		4	5.10	5.15	23,120	89.73	
		5	5.10	5.15	22,687	88.05	
	90	1	5.05	5.10	29,259	115.81	109.6
		2	5.10	5.00	27,650	110.53	
		3	5.05	5.10	28,460	112.64	
		4	5.10	5.05	26,045	103.08	
		5	5.05	5.10	26,793	106.05	
30FPOFA	7	1	5.10	5.15	12,185	47.29	48.3
		2	5.05	5.10	11,139	50.82	
		3	5.10	5.10	13,297	52.11	
		4	5.05	5.05	13,120	52.44	
		5	5.15	5.10	11,650	45.21	
	28	1	5.10	5.00	19,082	76.28	72.8
		2	5.10	5.05	18,287	72.38	
		3	5.10	5.05	23,630	93.53	
		4	5.15	5.10	17,608	68.34	
		5	5.05	5.10	18,794	74.39	
	60	1	5.10	5.15	23,220	90.12	86.3
		2	5.00	5.10	21,185	84.69	
		3	5.10	5.05	22,353	88.47	
		4	5.05	5.10	20,476	81.04	
		5	5.05	5.10	22,032	87.20	
	90	1	5.05	5.00	27,350	110.41	104.0
		2	5.10	5.10	26,587	104.20	
		3	5.10	5.05	25,310	100.18	
		4	5.10	5.05	22,940	90.80	
		5	5.15	5.10	26,107	101.32	

☐ = Data are not applicable

Table A.13 Compressive strength of 40FPOFA paste

Mix	Age (day)	Sample	Cross section		Ultimate Load (Kg)	Compressive Strength (MPa)	Average Compressive Strength (MPa)
			Width (cm)	Height (cm)			
40FPOFA	7	1	5.05	5.05	11,189	44.72	44.0
		2	5.05	5.10	9,485	37.54	
		3	5.10	5.10	11,276	44.19	
		4	5.10	5.05	10,295	40.75	
		5	5.05	5.10	11,743	46.48	
	28	1	5.10	5.10	17,583	68.91	66.5
		2	5.00	5.10	16,387	65.51	
		3	5.05	5.15	16,494	64.65	
		4	5.10	5.15	20,174	78.30	
		5	5.10	5.10	17,039	66.78	
	60	1	5.10	5.15	20,426	79.28	78.6
		2	5.05	5.10	21,043	83.29	
		3	5.10	5.10	19,678	77.12	
		4	5.10	5.00	17,390	69.52	
		5	5.10	5.15	19,235	74.65	
	90	1	5.10	5.10	24,564	96.27	94.1
		2	5.05	5.10	23,408	92.65	
		3	5.10	5.10	25,195	98.74	
		4	5.10	5.15	22,397	86.92	
		5	5.05	5.10	24,276	96.08	

= Data are not applicable



APPENDIX B
TOTAL CHLORIDE OF OPC, SRPC AND
POFA PASTES

Table B.1 Total chloride of OPC, SRPC and POFA pastes

Mix	Distance from pastes surface (m)	Total chloride (% by weight of binder)
OPC	0.005	0.470
	0.015	0.195
	0.025	0.088
	0.035	0.035
	0.045	0.024
SRPC	0.005	0.496
	0.015	0.252
	0.025	0.127
	0.035	0.035
	0.045	0.022
10CPOFA	0.005	0.463
	0.015	0.204
	0.025	0.063
	0.035	0.048
	0.045	0.010
20CPOFA	0.005	0.425
	0.015	0.168
	0.025	0.042
	0.035	0.032
	0.045	0.008
30CPOFA	0.005	0.398
	0.015	0.138
	0.025	0.038
	0.035	0.031
	0.045	0.004
40CPOFA	0.005	0.379
	0.015	0.092
	0.025	0.024
	0.035	0.011
	0.045	0.005

Table B.2 Total chloride of OPC, SRPC and POFA pastes

Mix	Distance from blended surface (m)	Total chloride (% by weight of binder)
10FPOFA	0.005	0.459
	0.015	0.167
	0.025	0.035
	0.035	0.018
	0.045	0.008
20FPOFA	0.005	0.384
	0.015	0.103
	0.025	0.029
	0.035	0.012
	0.045	0.004
30FPOFA	0.005	0.354
	0.015	0.094
	0.025	0.025
	0.035	0.010
	0.045	0.002
40FPOFA	0.005	0.339
	0.015	0.092
	0.025	0.013
	0.035	0.009
	0.045	0.003



APPENDIX C
FREE CHLORIDE OF OPC, SRPC AND
POFA PASTES

Table C.1 Free chloride of OPC, SRPC and POFA pastes

Mix	Distance from blended surface (m)	Total chloride (% by weight of binder)
OPC	0.005	0.348
	0.015	0.139
	0.025	0.053
	0.035	0.015
	0.045	0.003
SRPC	0.005	0.346
	0.015	0.172
	0.025	0.092
	0.035	0.025
	0.045	0.007
10CPOFA	0.005	0.374
	0.015	0.121
	0.025	0.034
	0.035	0.023
	0.045	0.001
20CPOFA	0.005	0.325
	0.015	0.125
	0.025	0.025
	0.035	0.015
	0.045	0.002
30CPOFA	0.005	0.298
	0.015	0.112
	0.025	0.015
	0.035	0.012
	0.045	0.001
40CPOFA	0.005	0.275
	0.015	0.076
	0.025	0.012
	0.035	0.004
	0.045	0.001

Table C.2 Free chloride of OPC, SRPC and POFA pastes

Mix	Distance from blended surface (m)	Total chloride (% by weight of binder)
10FPOFA	0.005	0.328
	0.015	0.118
	0.025	0.015
	0.035	0.008
	0.045	0.001
20FPOFA	0.005	0.305
	0.015	0.080
	0.025	0.007
	0.035	0.003
	0.045	0.001
30FPOFA	0.005	0.279
	0.015	0.072
	0.025	0.007
	0.035	0.003
	0.045	0.001
40FPOFA	0.005	0.261
	0.015	0.067
	0.025	0.007
	0.035	0.004
	0.045	0.001

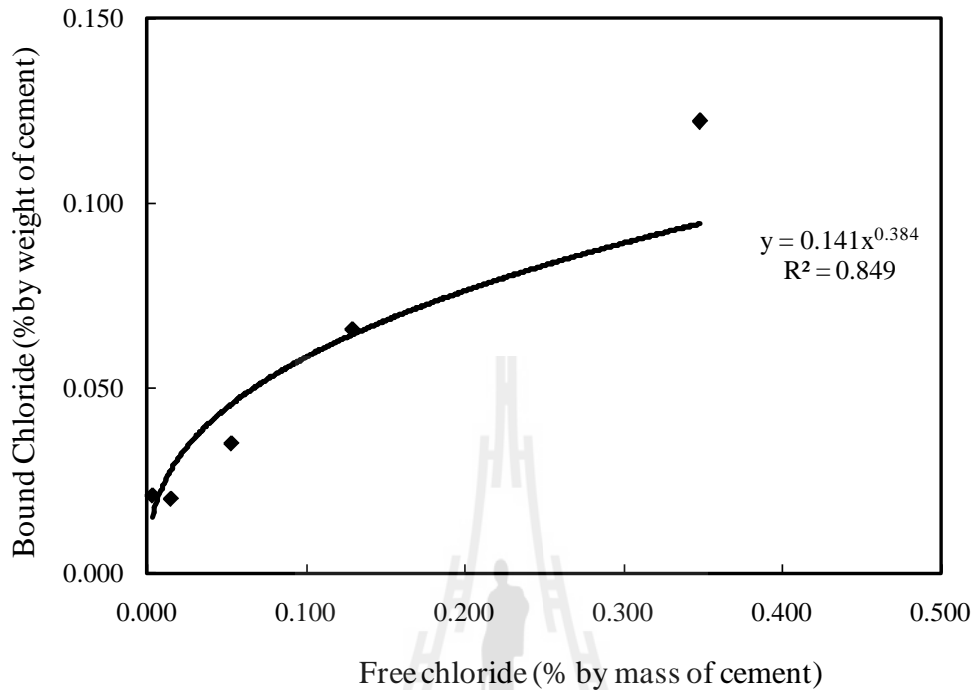


APPENDIX D

CHLORIDE BINDING CAPACITY OF OPC, SRPC AND

POFA PASTES

Example Chloride binding capacity of OPC paste



$$C_T = C_f + C_b \quad (1)$$

$$\frac{\partial C_f}{\partial C_T} = \alpha \quad (2)$$

Freundlich isotherm:

$$C_b = \alpha C_f^\beta \quad (3)$$

From experimental OPC paste

$$Y = 0.141x^{0.384} \quad (4)$$

$$\alpha = 0.141 \quad (5)$$

$$\beta = 0.384 \quad (6)$$

$$C_T = C_f + \alpha C_f^\beta \quad (7)$$

$$C_T = C_f(1 + \alpha^\beta) \quad (8)$$

$$\frac{C_f}{C_T} = \frac{1}{(1 + \alpha^\beta)} \quad (9)$$

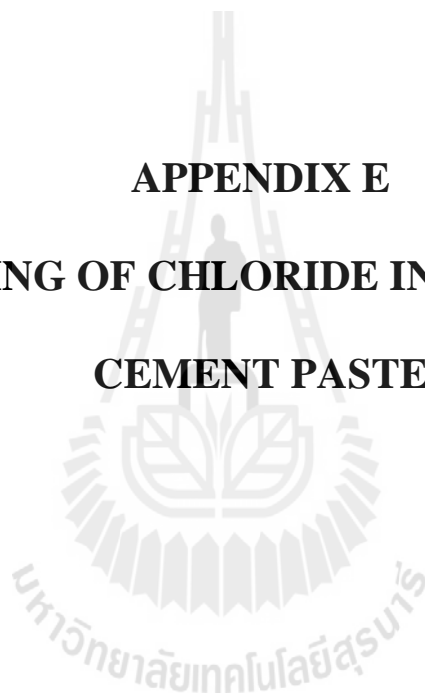
$$\frac{C_f}{C_T} = \frac{1}{(1 + 0.141^{0.384})} \quad (10)$$

$$\frac{\partial C_f}{\partial C_T} = \alpha = 0.697$$

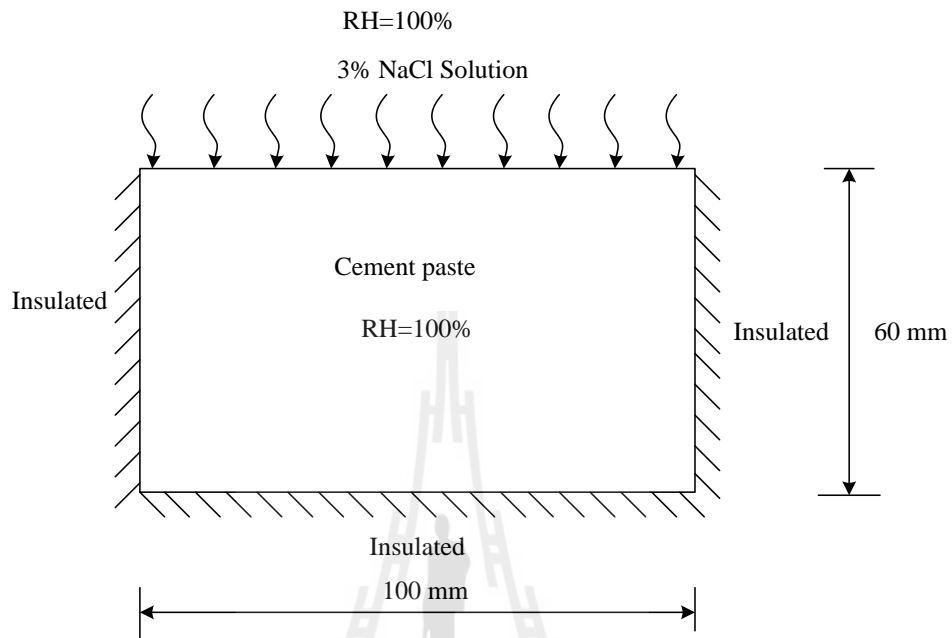
Table D.1 Chloride binding capacity of OPC, SRPC and POFA pastes

Mix	Chloride binding capacity
OPC	0.697
SRPC	0.655
10CPOFA	0.691
20CPOFA	0.733
30CPOFA	0.732
40CPOFA	0.749
10FPOFA	0.709
20FPOFA	0.731
30FPOFA	0.748
40FPOFA	0.762

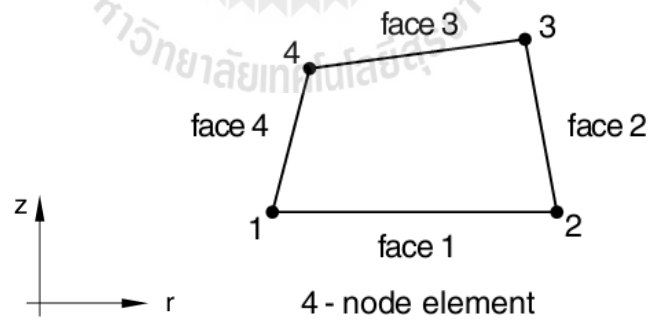
APPENDIX E
MODELING OF CHLORIDE INGRESS INTO
CEMENT PASTE



E.1 Finite element analysis



Element types : DCA X4 4-node linear axisymmetric heat transfer quadrilateral



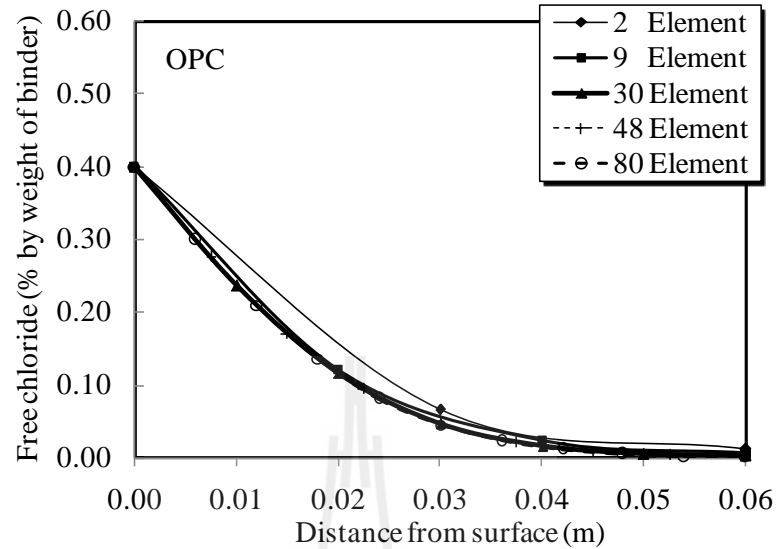
Element 4 node

Degree of freedom : 8

Conventions

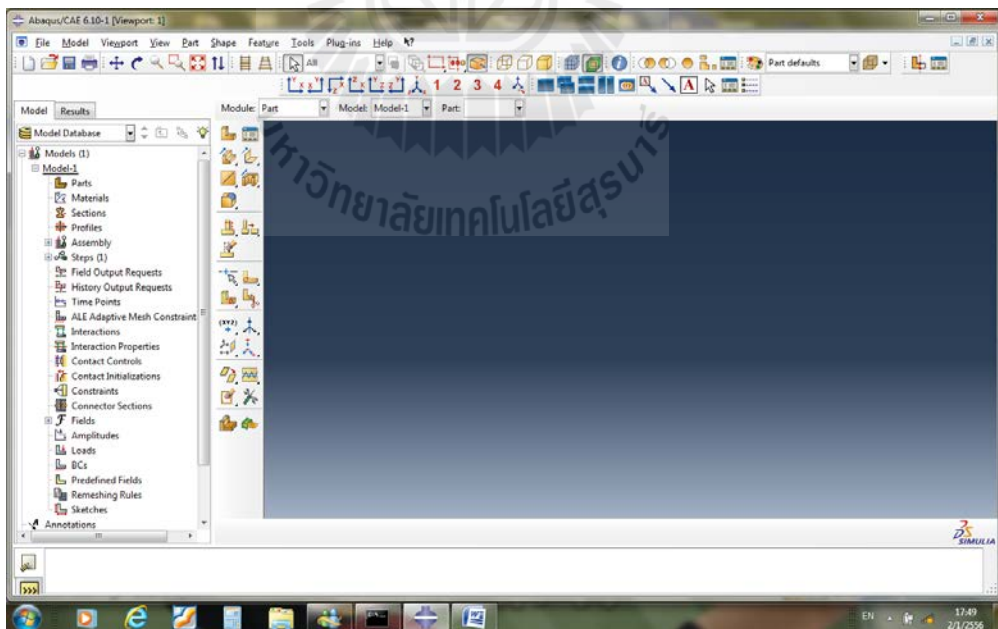
1. Coordinate 1 is r , coordinate 2 is z , At $\theta=0$ the r -direction corresponds to the global x -direction and the z -direction corresponds to the global y -direction. This is important when data must be given in global directions. Coordinate 1 must be greater than or equal to zero.
2. Degree of freedom 1 is u_r , degree of freedom 2 is u_z , Generalized axisymmetric elements with twist have an additional degree of freedom, 5, corresponding to the twist angle ϕ (in radians).
3. Abaqus does not automatically apply any boundary conditions to nodes located along the symmetry axis. You must apply radial or symmetry boundary conditions on these nodes if desired.
4. In certain situations in Abaqus/Standard it may become necessary to apply radial boundary conditions on node that are located on the symmetry axis to obtain convergence in nonlinear problems. Therefore, the application of radial boundary conditions on node on the symmetry axis is recommended for nonlinear problems.
5. Point load and moments, concentrated (nodal) fluxes, electrical currents, and seepage should be given as the value integrated around the circumference (that is, the total value on the ring).

E.2 Comparison of results for different numbers of elements

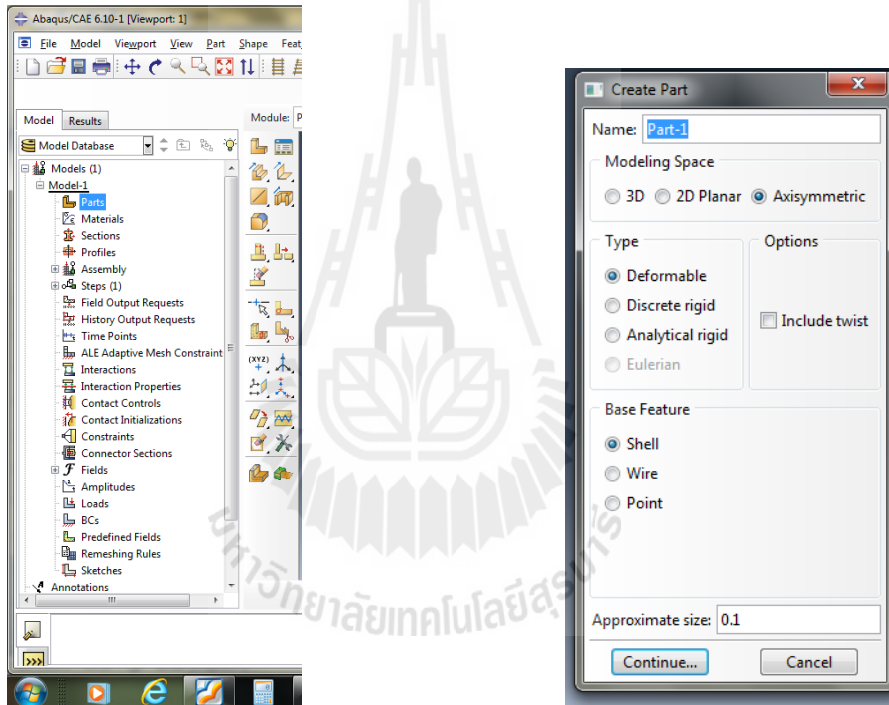


E. 3 Abaqus /CAE Chloride penetration ingress into blended cement paste

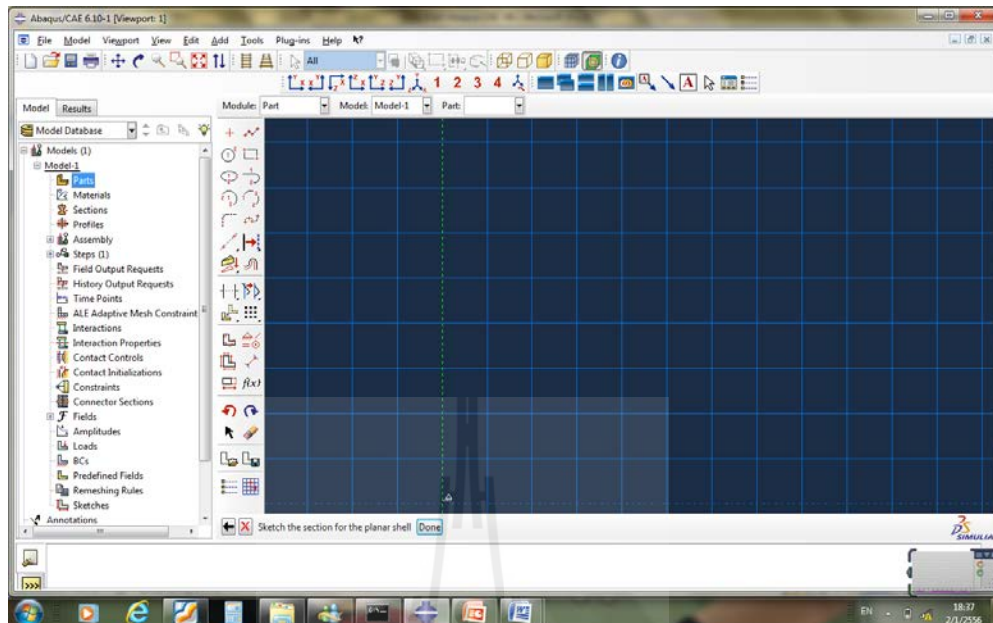
1. Start Abaqus CAE V6.10-1 and choose to create a new model database



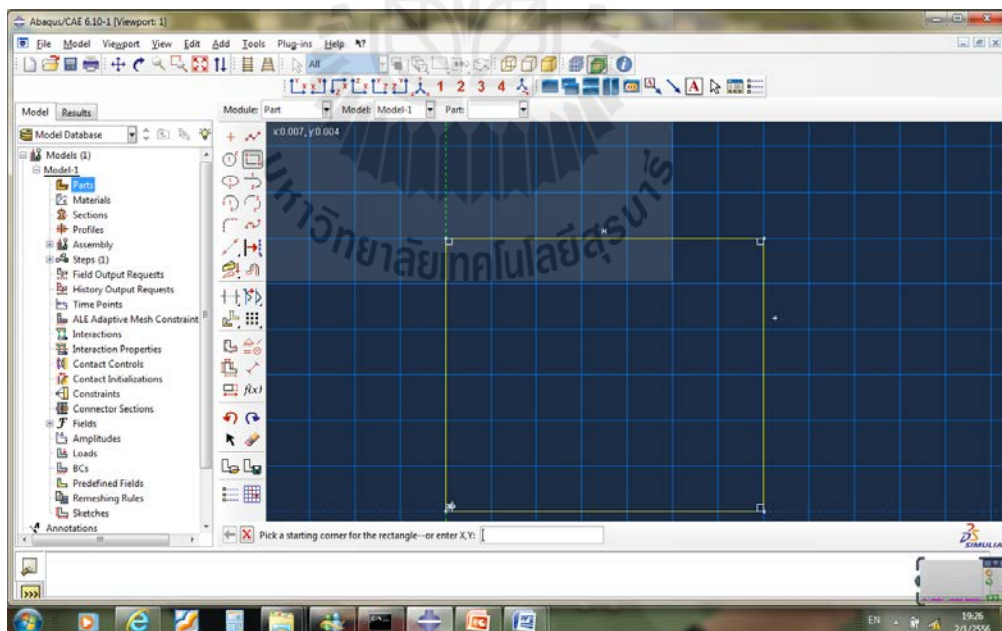
2. In the model tree double click on the “Part” node (or right or right click on “parts” and select Create)
 - a. Select “ Axisymmetric”
 - b. Select “ Deformable”
 - c. Select “ Shell”
 - d. Select “ Approximate size = 0.05”
 - e. Click “ Continue”



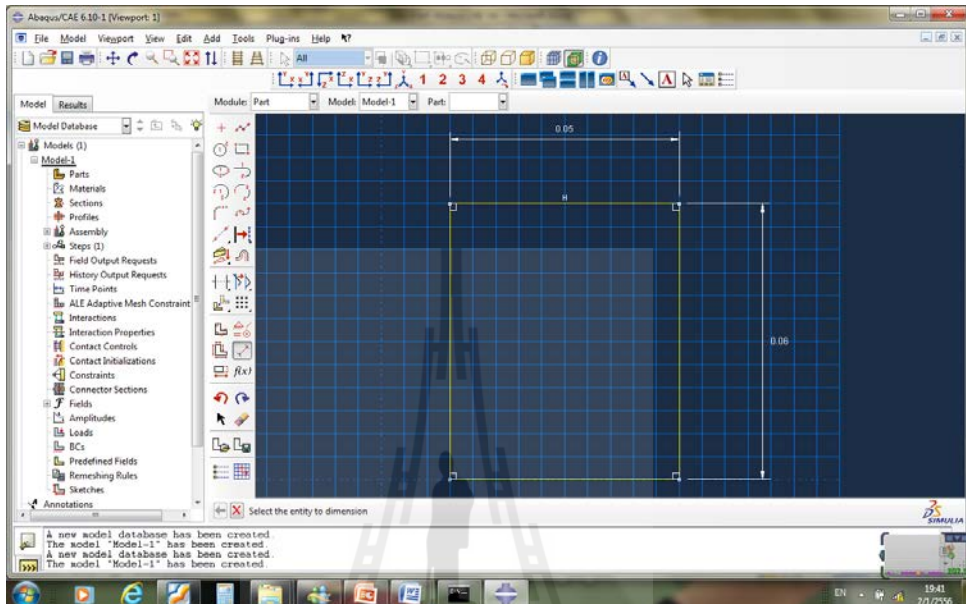
3. Create the geometry shown below



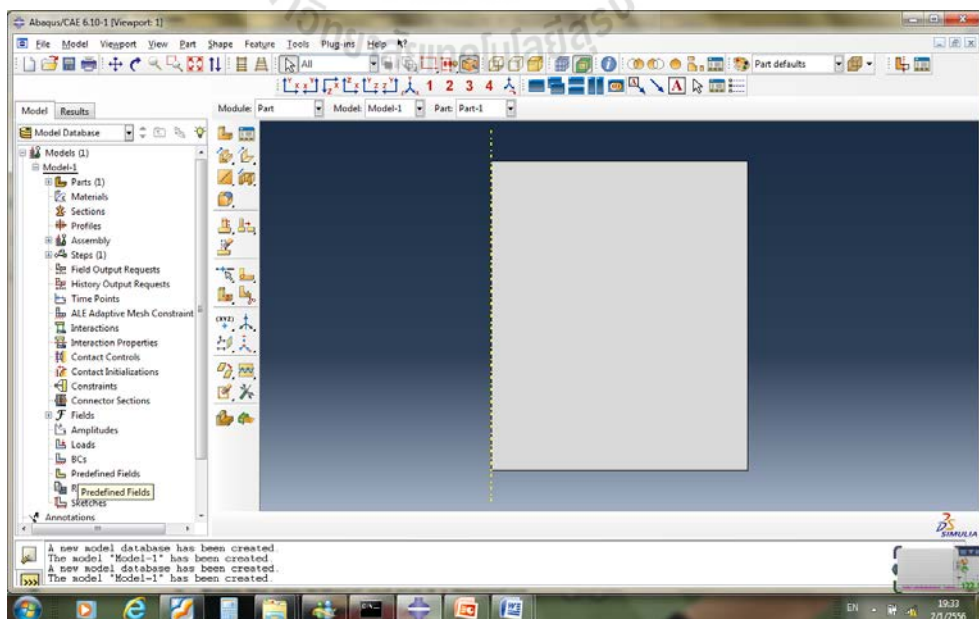
4. Click on the create line reaction
 - a. Pick a starting corner for the rectangle



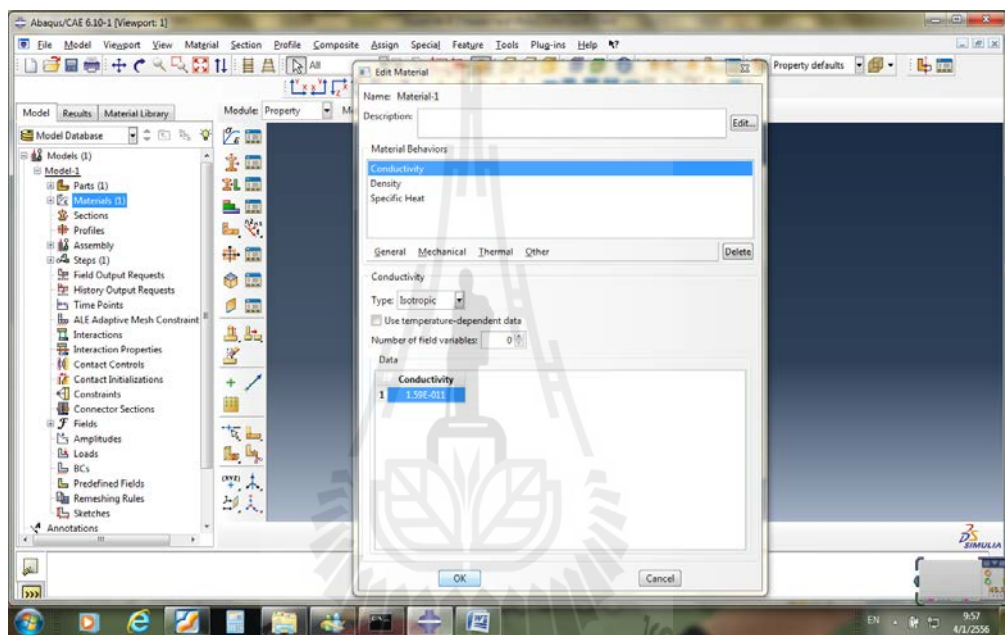
5. Click add dimension
 - a. New dimension = 0.06
 - b. New dimension = 0.05



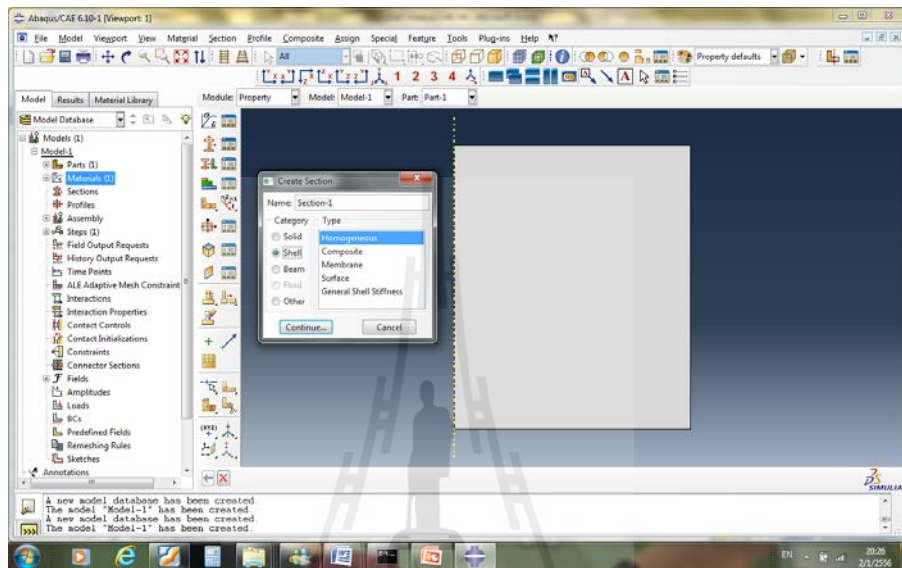
- c. Click select the entity to dimension
- d. Sketch the section for the planar shell "Done"



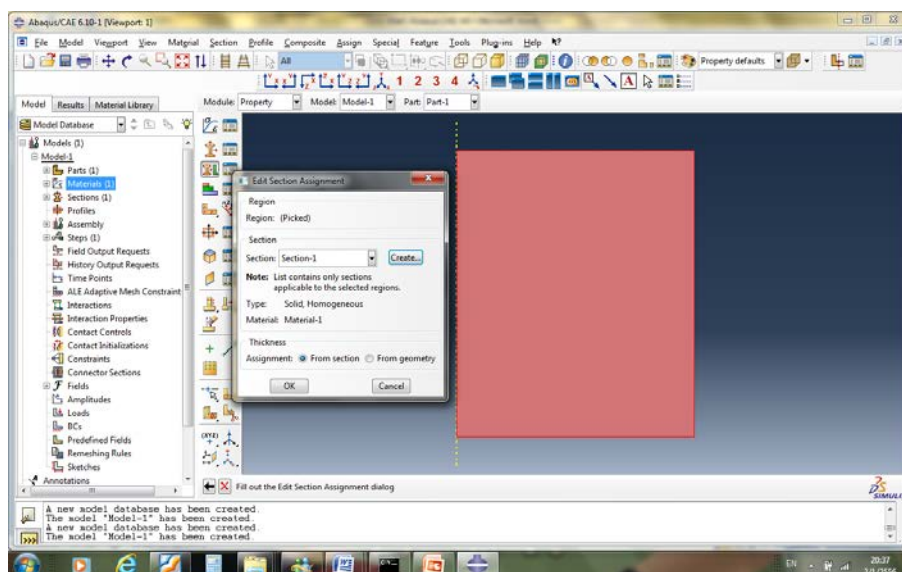
6. Double click on the “Materials” node in the model tree
 - a. Click on the “General” tab → Density=1
 - b. Click on the “Thermal” tab → Conductivity = 15.9×10^{-12}
 - c. Click on the “Thermal” tab → Specific heat=0.697
 - d. Click “OK”



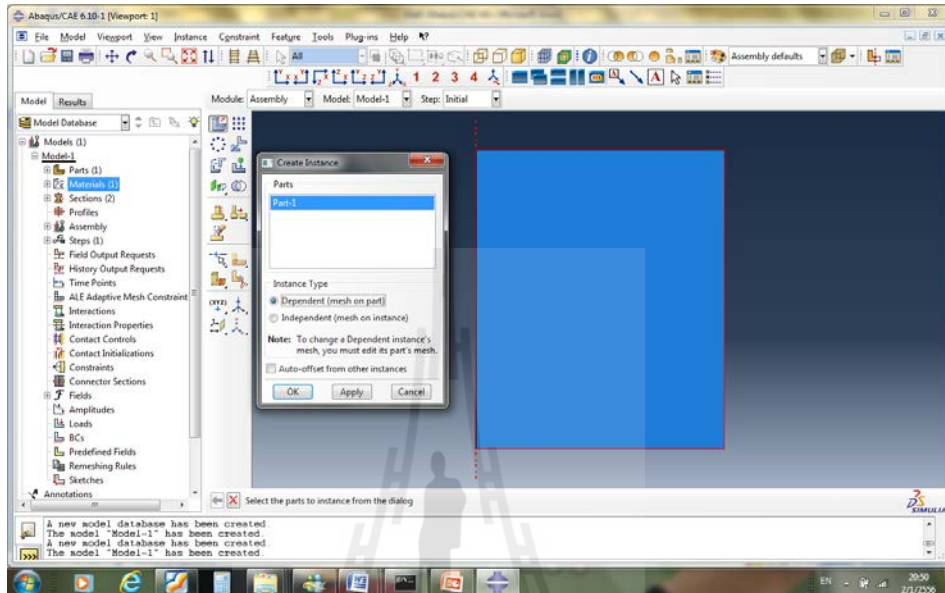
7. Double click on the “Sections” node in the model tree
 - a. Select “Solid” for the category and “Homogeneous” for the type
 - b. Click “Continue...”
 - c. Click “OK”



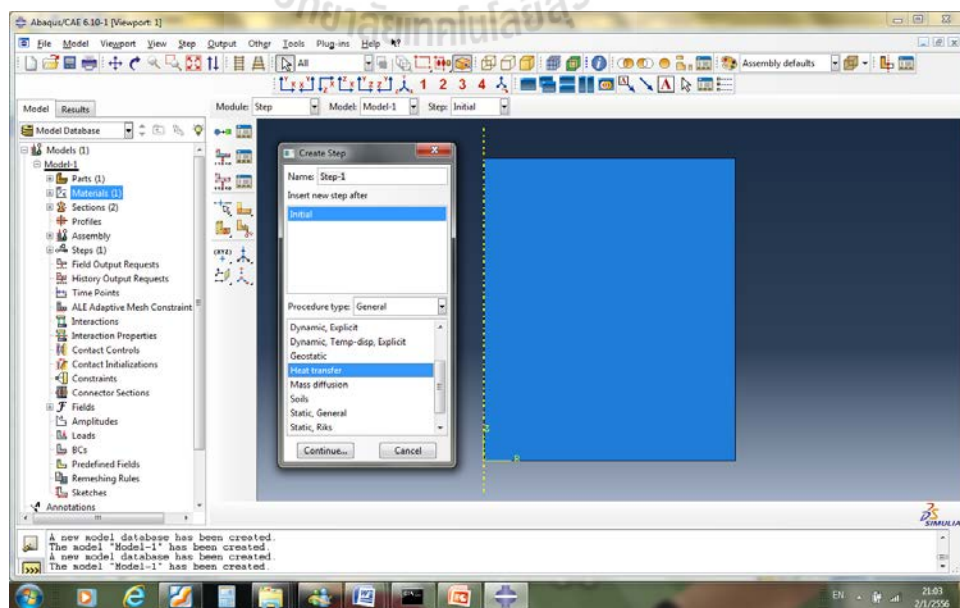
- d. Click “ Assign section”
- e. Click on the geometry
- f. Click “ Done “



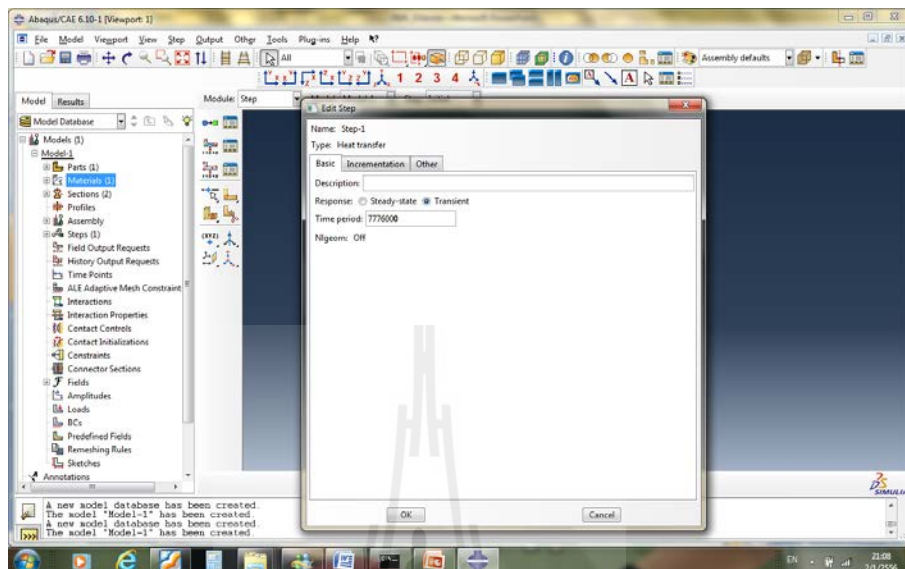
8. Click on the “Instances part”
 - a. Select “Dependent” for the instance type
 - b. Click “OK”



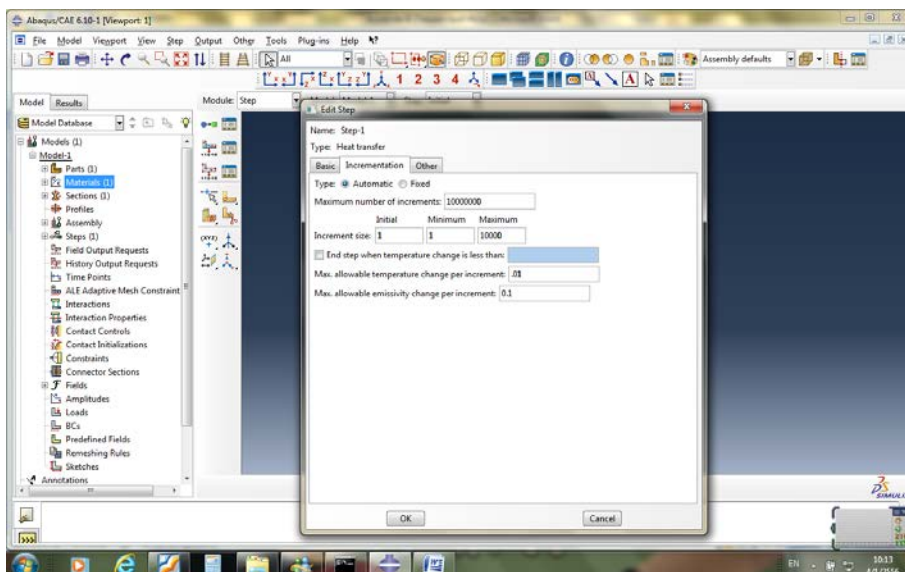
9. Click on the “Steps”
 - a. Click on the “Heat transfer”
 - b. Click “Continue...”



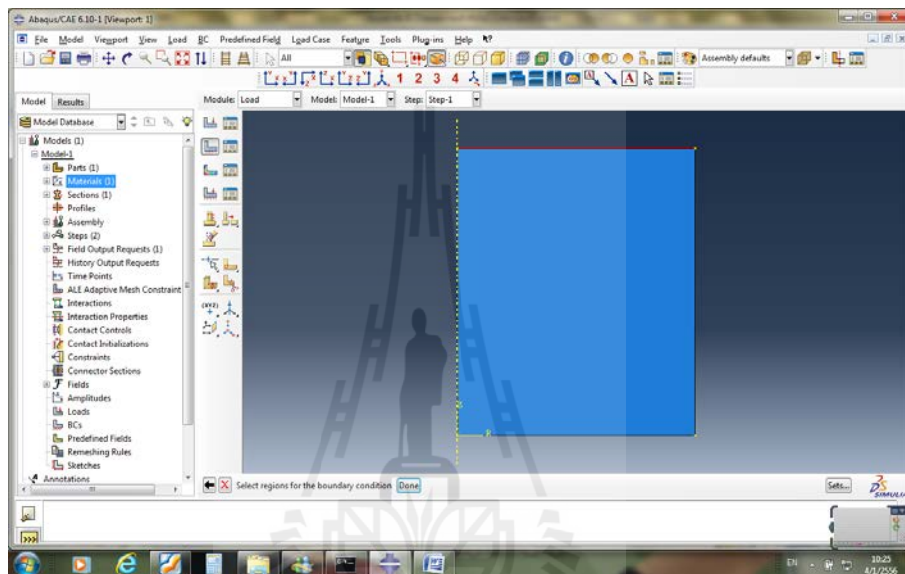
- c. Set the response to “Transient”
- d. Click on the “Basic” tab → Time period=7776000



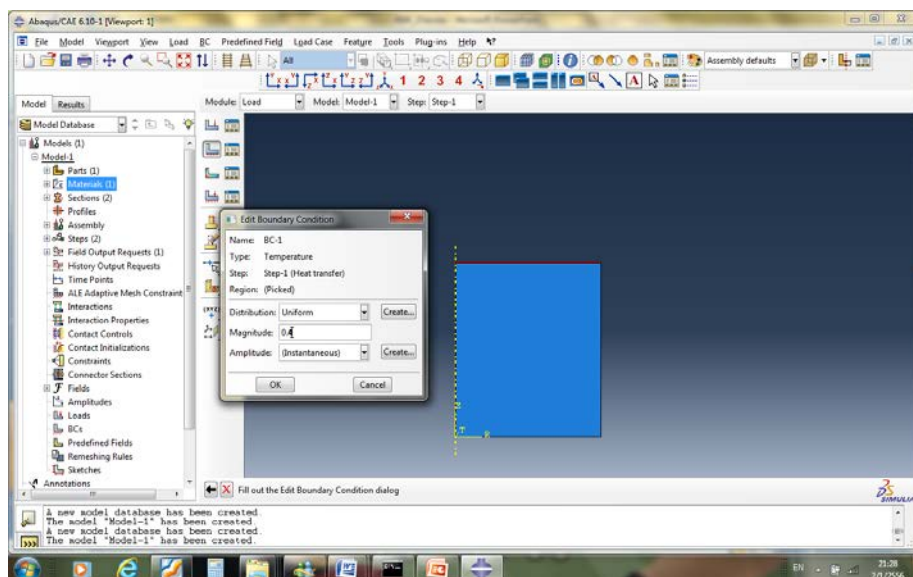
- e. Click on the “Incrementation” tab
- Maximum number of increments=10000000
 - Increment size/ initial =1/minimum=1/maximum=1000
 - Max. allowable temperature change per increment =0.01
 - Max. allowable emissivity change per increment =0.1



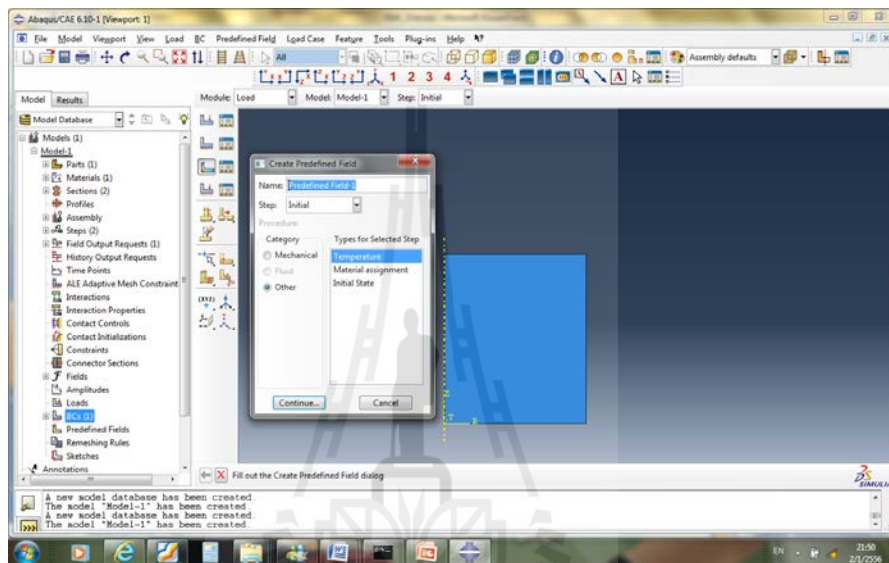
10. Click on the “Load”
 - a. Select on the “Temperature”
 - b. Click “Continue”
 - c. Pick top geometry
 - d. Click “Done”



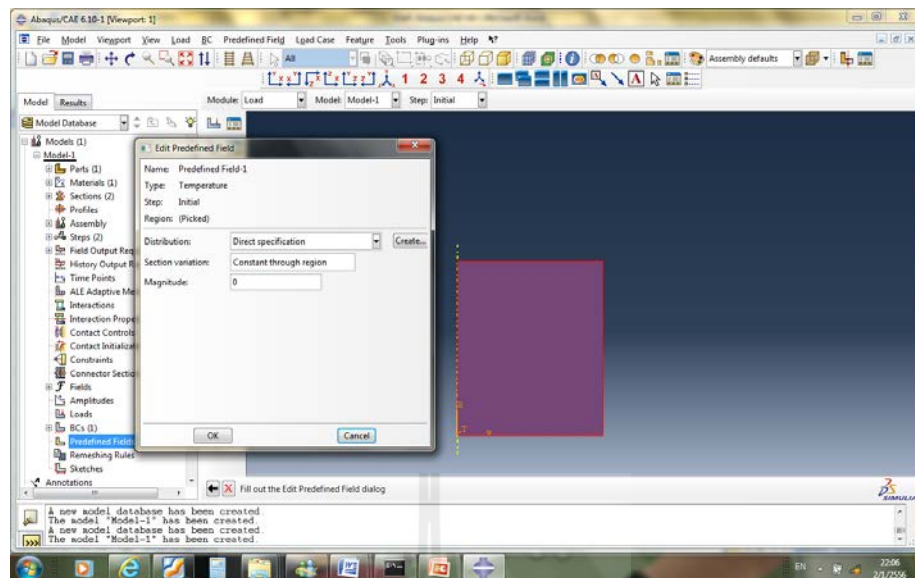
- e. Set the magnitude 0.4
- f. Click “Ok”



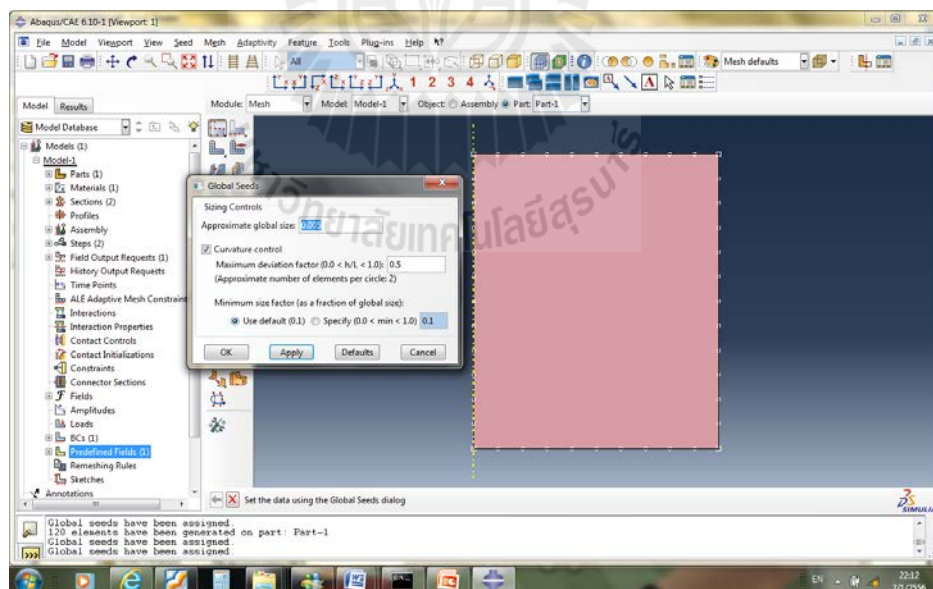
11. Click on the “Create predefined field”
 - a. Select step “Initial”
 - b. Select category “Other”
 - c. Type for select step “Temperature”
 - d. Click “Continue”



- e. Pick on the geometry
- f. Click “Done”
- g. Select magnitude =0
- h. Click “OK”

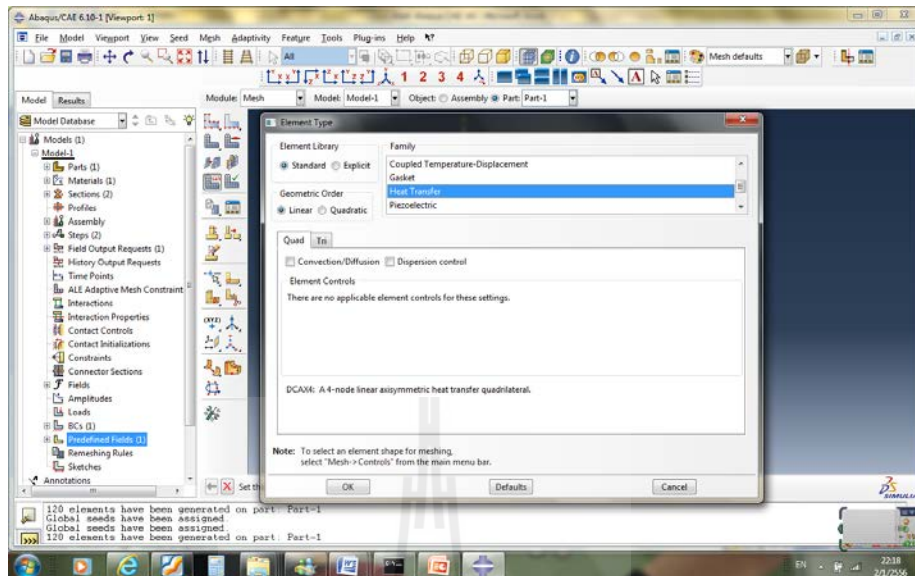


12. In the toolbox area click on the “Mesh”
 - a. Click on the “Seed part”
 - b. Set the approximate global size to 0.05
 - c. Click “OK”



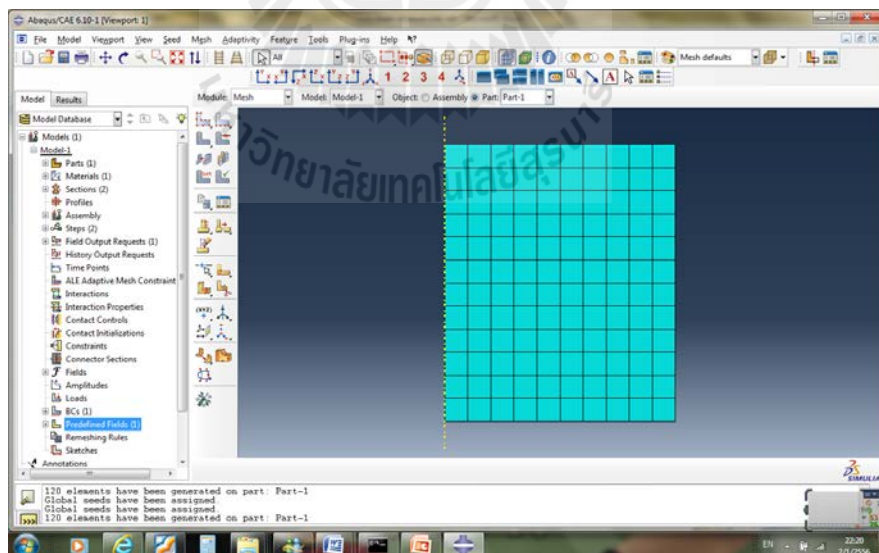
13. Click on the “Assign element type”
 - a. Select family “Heat transfer”
 - b. Select geometric order “Linear”

c. Click “OK”

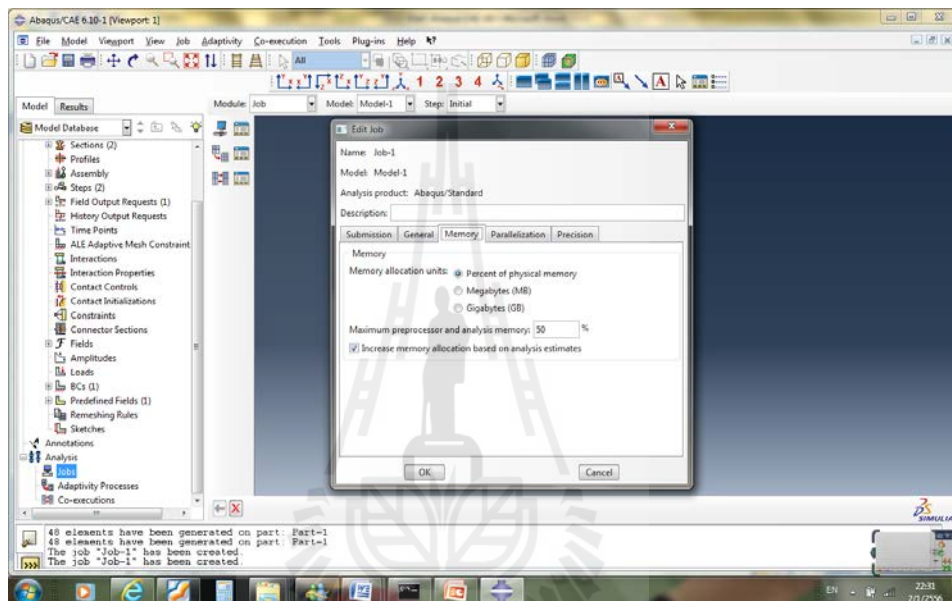


14. Click on the “ Mesh part “

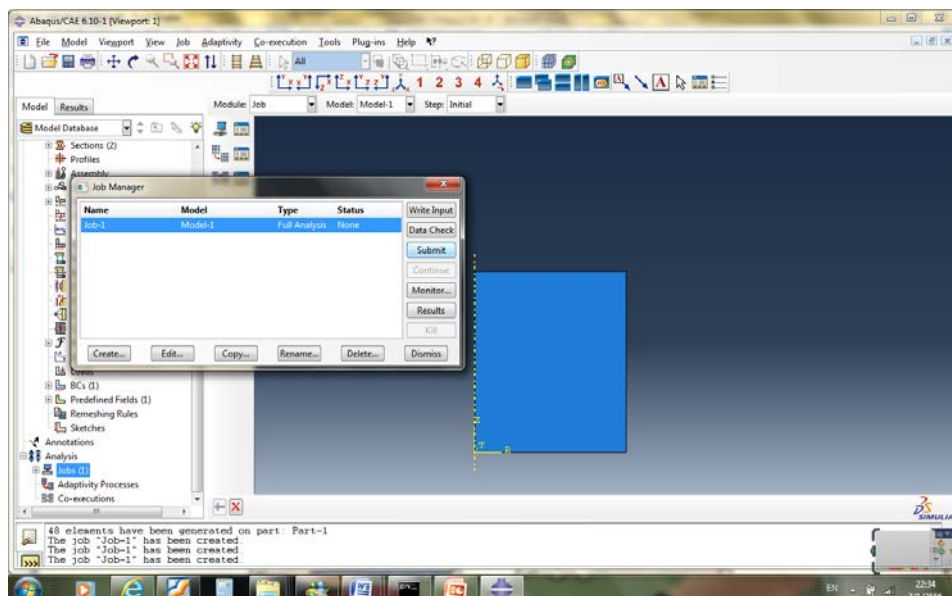
a. Click “ (Ok) ”



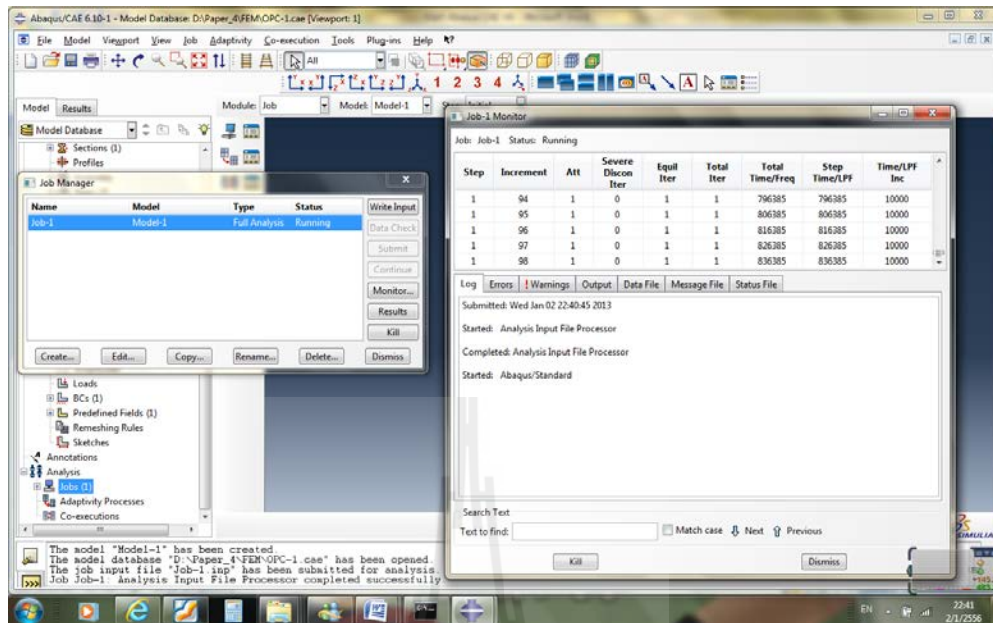
15. In the toolbox area click on the “Job”
 - a. Click on the “ Create job ”
 - b. Click “Continue...”
 - c. Give the job a description and accept all default parameters
 - d. Click “OK”



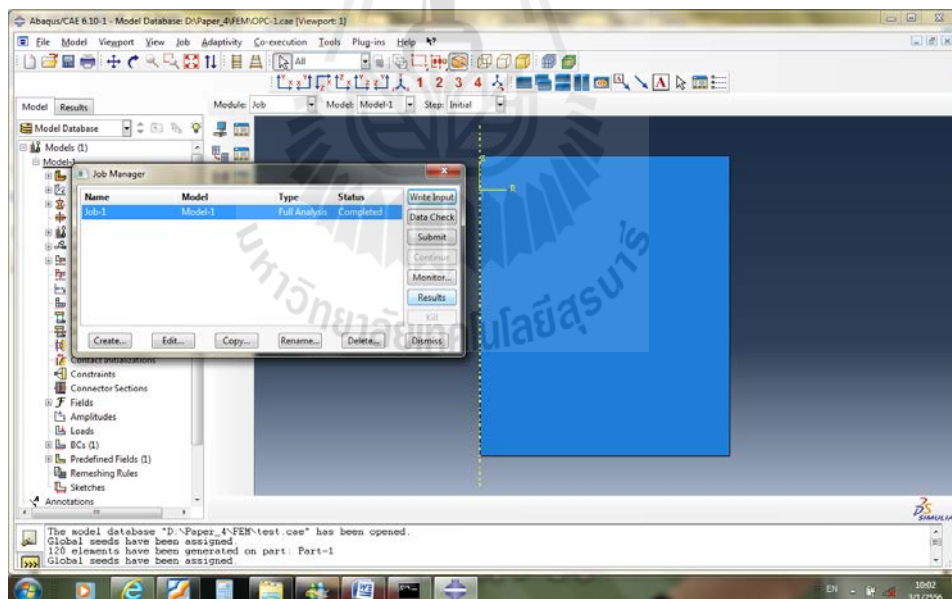
16. Click on the “ Job manager “
 - a. Select “Submit”



b. Select “Monitor”



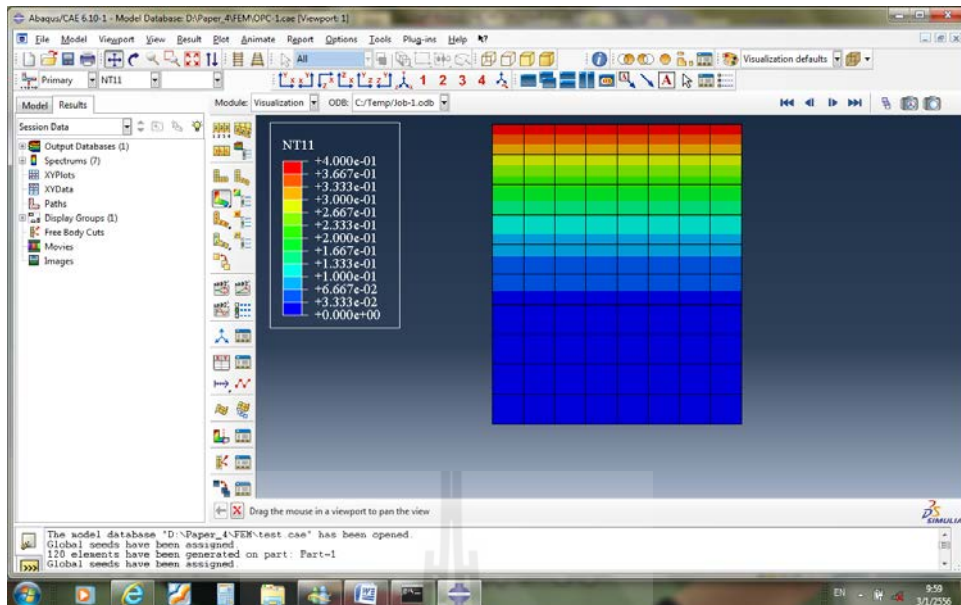
17. The submitted and successfully completed job and select “Results”



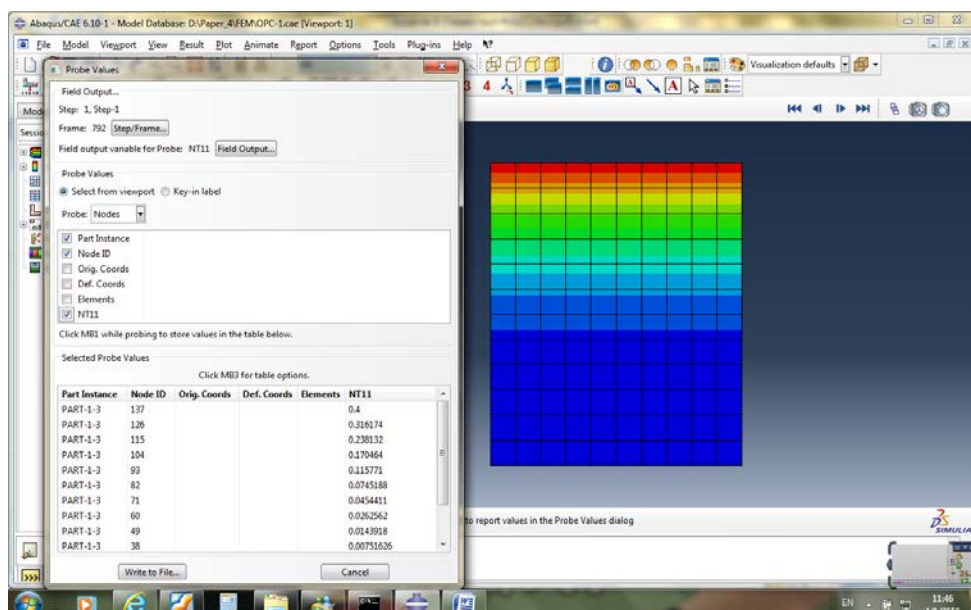
18. The menu bar click on the “Results Field Output”

a. Select “NT11 Nodal free chloride at nodes”

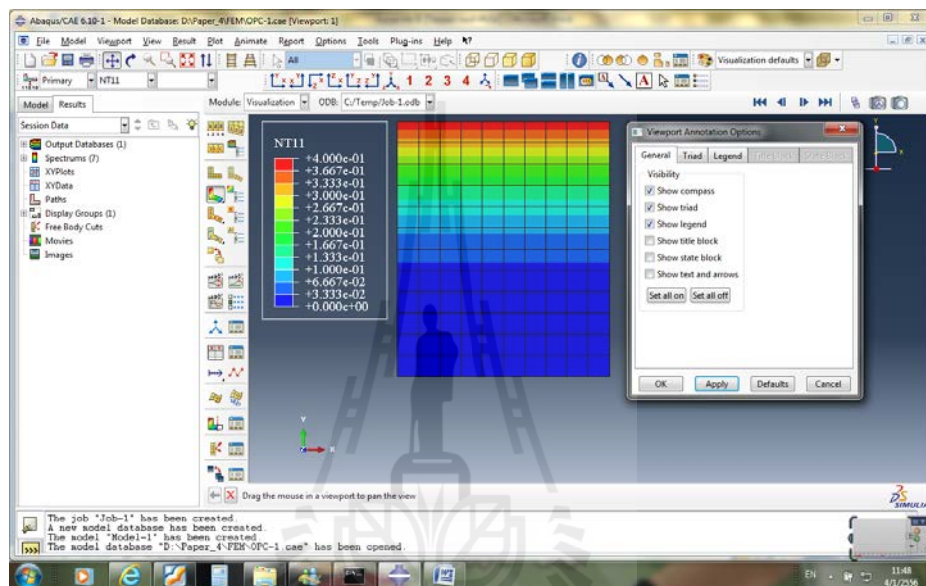
b. Click “OK”



19. To determine the free chloride values, from the menu bar click Tools → Query
 - a. Click on the “ Node ”
 - b. Click on the “ Probe values ”
 - c. Click on the “ Probe nodes ”
 - d. Check the boxes labeled “ Node ID ” and “NT11”
 - e. In the viewport mouse over the node of interest
 - f. When done click “ Cancel ”



20. In the menu bar click on Viewport → Viewport Annotations Options
 - a. Uncheck the “Show compass option”
 - b. The locations of viewport items can be specified on the corresponding tab in the Viewport Annotations Options
 - c. Click “OK”





APPENDIX F

LIST OF PUBLICATION

LIST OF PUBLICATION

INTERNATIONAL JOURNAL

Kroehong, W., Sinsiri, T., Jaturapitakkul, C., and Chindapasirt, P. (2011). **Effect of palm oil fuel ash fineness on the microstructure of blended cement paste.** Construction and Building Materials. 25(11): 4095-4104.

Sinsiri, T., Kroehong, W., Jaturapitakkul, C., and Chindapasirt, P. (2012). **Assessing the effect of biomass ashes with different finenesses on the compressive strength of blended cement paste.** Materials and Design. 42(0): 424-433.

INTERNATIONAL CONFERENCE

Kroehong, W., Sinsiri, T., and Jaturapitakkul, C. (2011a). **Effect of palm oil fuel ash fineness on packing effect and pozzolanic reaction of blended cement paste.** The Twelfth East Asia-Pacific Conference on Structural Engineering & Construction. Hong Kong SAR, China: 185-186.

NATIONAL JOURNAL

Kroehong, W., Sinsiri, T., Jaturapitakkul, C., and Chindapasirt, P. (2012). **A study microstructure of blended cement paste containing palm oil fuel ash.** KMUTT Research & Development Journal. 35(2): 187-200.

Suphawithayacharoenkun, P., Kroehong, W., and Sinsiri, T. (2012). **Influence of amorphous silica in perlite on compressive strength and pozzolanic reaction of blended cement paste.** KKU ENGINEERING JOURNAL 39(3): 257-266

NATIONAL CONFERENCE

Kroehong, W., Sinsiri, T., and Jaturapitakkul, C. (2009). **Effect of micro silica synthesis from rice husk ash properties of blended cement paste.**

Proceedings of the Annual concrete conference ACC5. October: 144-149.

Kroehong, W., Chuenta, P., Sinsiri, T., and Jaturapitakkul, C. (2009). **Pozzolanic reaction of rice husk ash and palm oil fuel ash on microstructure of blended cement paste.** Proceedings of the Annual concrete conference

ACC5. October: 136-143.

Limprayoonsawad, P., Kroehong, W., and Sinsiri, T. (2010). **Effect rice husk ash and bagasse ash fineness on microstructure of blended cement paste.**

Proceedings of the Annual concrete conference ACC6. October: 139-146.

Suphawithayacharoenkul, P., Kroehong, W., and Sinsiri, T. (2010). **Influence of amorphous silica in diatomite on compressive strength and pozzolanic reaction blended cement paste.** Proceedings of the Annual concrete

conference ACC6. October: 125-131.



Review

Effect of palm oil fuel ash fineness on the microstructure of blended cement paste

Wunchock Kroehong^a, Theerawat Sinsiri^{a,*}, Chai Jaturapitakkul^b, Prinya Chindaprasit^c^a School of Civil Engineering, Institute of Engineering, Suranaree University of Technology, Nakom Ratchasima 30000, Thailand^b Department of Civil Engineering, Faculty of Engineering, King Mongkut's University of Technology Thonburi, Bangkok 10140, Thailand^c Sustainable Infrastructure Research and Development Center, Department of Civil Engineering, Faculty of Engineering, Khon Kaen University, Khon Kaen 40002, Thailand

ARTICLE INFO

Article history:

Received 12 January 2011
 Received in revised form 2 March 2011
 Accepted 22 April 2011
 Available online 25 May 2011

Keywords:

Palm oil fuel ash
 Amorphous
 Compressive strength
 Thermogravimetric
 Porosity

ABSTRACT

This paper presents the effect of palm oil fuel ash fineness on the microstructure of blended cement paste. Palm oil fuel ash (POFA) was ground to two different finenesses. Coarse and high fineness palm oil fuel ash, with median particle sizes of 15.6 and 2.1 μm , respectively, were used to replace ordinary Portland cement (OPC) at 0%, 20% and 40% by binder weight. A water to binder (W/B) ratio of 0.35 was used for all blended cement pastes. The amorphous ground palm oil fuel ash was characterized by the Rietveld method. The compressive strength, thermogravimetric analysis and pore size distribution of the blended cement pastes were investigated. The test results indicate that the ground palm oil fuel ash was an amorphous silica material. The compressive strengths of the blended cement pastes containing coarse POFA were as high as that of OPC cement paste. Blended cement paste with high fineness POFA had a higher compressive strength than that with coarse POFA. The blended cement pastes containing 20% of POFA with high fineness had the lowest total porosity. The $\text{Ca}(\text{OH})_2$ contents of blended cement paste containing POFA decreased with increasing replacement of POFA and were lower than those of the OPC cement paste. In addition, the POFA fineness had an effect on the reduction rate of $\text{Ca}(\text{OH})_2$. Furthermore, the critical pore size and average pore size of blended cement paste containing POFA were lower than those of the OPC cement paste. The incorporation of high fineness POFA decreased the critical pore size and the average pore size of blended cement paste as compared to that with coarse POFA.

© 2011 Elsevier Ltd. All rights reserved.

Contents

1. Introduction	4096
2. Experimental details	4096
2.1. Materials	4096
2.2. Mix proportion and curing	4096
2.3. Compressive strength	4096
2.4. X-ray diffraction (XRD)	4097
2.5. Thermal analysis	4097
2.6. Determination of the porosity of the pastes	4097
3. Results and discussion	4097
3.1. Properties of OPC and POFA	4097
3.2. Compressive strength	4098
3.3. Thermogravimetric analysis	4099
3.3.1. Hydrated phase of cement pastes containing palm oil fuel ash	4099
3.3.2. $\text{Ca}(\text{OH})_2$ content	4099
3.4. Pore size distribution of the cement paste	4100
3.4.1. Total porosity of the cement paste	4100
3.4.2. Effect of palm oil fuel ash fineness on the pore size distribution of the pastes	4100
3.4.3. Effect of palm oil fuel ash fineness on the average pore diameter of the cement paste	4101
3.5. Relationships between the compressive strength and total porosity of the pastes	4102

* Corresponding author. Tel: +66 4422 4420; fax: +66 4422 4607.
 E-mail address: sinsiri@g.sut.ac.th (T. Sinsiri).

4. Conclusions	4103
Acknowledgments	4103
References	4103

1. Introduction

The Portland cement clinker process results in the emission of CO₂. Every ton of Portland cement produces around 850 kg of CO₂ emitted to the atmosphere, thus causing greenhouse effects [1]. Therefore, it is necessary to reduce the production of Portland cement clinker. To solve this problem, the partial replacement of ordinary Portland cement with pozzolanic materials has been proposed. Pozzolanic materials, such as fly ash, rice husk ash, palm oil fuel ash and baggage ash, are used as mineral admixtures to reduce the cement content in the mixtures. These materials have been reported to increase the durability of paste, mortar and concrete [2–4].

Palm oil fuel ash (POFA) is a by-product from biomass thermal power plants where oil palm residues are burned to generate electricity. More than approximately 100,000 tons of palm oil fuel ash are produced every year in Thailand [5]. Palm oil fuel ash is rarely utilized, and it may add to future environmental problems. Many researchers have studied the use of POFA as a partial replacement of cement in concrete. The main chemical constituent of palm oil fuel ash is silicon dioxide [4,6]. Tangchirapat et al. [4] found that ground palm oil fuel ash is a good pozzolanic material and can be used to replace Portland cement up to 30% by binder weight. Sata et al. [7] also showed that POFA with high fineness has an excellent pozzolanic reaction and can be used as a supplementary material to produce high strength concrete. In addition, the utilization of POFA can improve concrete strength and water permeability [5]. Furthermore, the partial replacement of OPC with POFA assists in the sulfate resistance [8] and chloride resistance of concrete [2].

Silicon dioxide (SiO₂) and aluminum trioxide (Al₂O₃) contents in pozzolanic material react with calcium hydroxide (Ca(OH)₂) to produce CSH, C₂ASH₈ and C₄AH₁₃. Most researchers have studied Ca(OH)₂ in cement paste containing pozzolanic material by thermogravimetry (TG). The Ca(OH)₂ content is reduced with increasing replacement of pozzolanic material and fineness [9]. Barbhuiya et al. [10] found that the reduction of the Ca(OH)₂ content indicates consumption in the pozzolanic reaction. In addition, the use of pozzolanic material to partially replace cement reduces the Ca(OH)₂ content in concrete, which could improve the sulfate resistance of the concrete. Furthermore, Chaipanich and Nochiya [11] used differential thermal analysis (DTG) to determine the hydration products involved and explained the increase in the compressive strength of paste. They showed that blended cement paste containing fly ash and silica fume reduces the amount of Ca(OH)₂ content while the mass loss of ettringite, C–S–H and C₂ASH₈ increases when the curing time is increased.

The porosity and pore structure are very important for permeability and durability. The pore system in cement-based materials consists of two types of pores [9,12]: (a) gel pores with a diameter less than 10 nm that affect shrinkage and fatigue and (b) capillary pores that are divided into large capillary pores with diameters between 50 and 10,000 nm, which affect the compressive strength and permeability, and medium capillary pores with diameters between 10 and 50 nm, which influence the compressive strength, permeability and shrinkage. Khatib and Wild [13] studied cement pastes containing metakaolin at 5%, 10% and 15% and found that the pore size of a cement paste depends on refinement of the pore

structure. In addition, Chindraprasirt et al. [14] used fly ash to replace Portland cement and showed that the cement paste containing fly ash had a smaller average pore diameter than that of control cement paste. In addition, Halamickova et al. [15] studied water permeability and chloride ion diffusion in Portland cement mortar and showed that they are influenced by the critical pore size.

Many researchers have already reported on the influence of palm oil fuel on the physical properties of mortar and concrete, including compressive strength, sulfate resistance and chloride resistance. However, the pore size distribution and microstructure of blended cement pastes containing palm oil fuel ash with different finenesses have not been well established. An understanding of the influence of the fineness of palm oil fuel ash on the pore size distribution and microstructure of cement paste could lead to an increase in the use of palm oil fuel ash in concrete and could be productive for the environment by reducing the volume of waste disposed of in landfills. Thus, the objective of this research was to study the effect of palm oil fuel ash fineness on the microstructure of blended cement paste. The chemical properties and amorphous structure of ground palm oil fuel ash were determined. The effects of ground palm oil fuel ash with two different finenesses on the compressive strength, calcium hydroxide and pore size distribution of blended cement pastes were investigated.

2. Experimental details

2.1. Materials

Type I Portland cement was used in this study. Palm oil fuel ash (POFA) from a thermal power plant in Thailand was used as a pozzolan. The POFA was sieved through a No. 16 sieve to remove large particles and incompletely combusted materials [16,17]. The POFA was ground to two different sizes. The first fineness was ground to have the same as that of OPC with grinding machine. The second fineness was ground by attrition mill for 60 min at 1000 rpm using 2 mm diameter steel ball [18,19]. The abbreviations G1 and G2 were used to identify the ground POFA as having the same particle size cement and the smaller particle size, respectively.

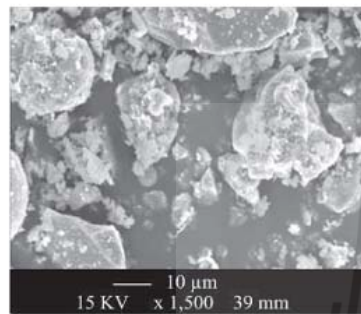
SEM photos of POFA with different finenesses are shown in Fig. 1. G1POFA and G2POFA consist of irregular and crushed shaped particles. A similar observation has also been reported by other researchers [4]. The physical properties of OPC and POFA are given in Table 1. The specific gravity of OPC was 3.14, and those of G1POFA and G2POFA were 2.36 and 2.48, respectively. The Blaine fineness values of OPC, G1POFA and G2POFA were 3600, 6700 and 14,900 cm²/g, respectively. The specific gravity and specific surface area of POFA increased with increasing grinding time [8,20,21]. The median particle sizes of OPC, G1POFA and G2POFA were 14.6, 15.6 and 2.2 μm, respectively. Fig. 2 shows a comparison of the particle size distributions of type I Portland cement and POFA. The two group of POFA particle size are similar to the particle size of the cement and smaller, respectively.

2.2. Mix proportion and curing

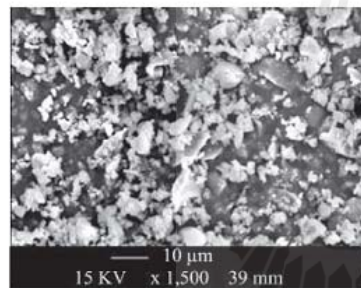
Type I Portland cement was partially replaced by POFA (G1POFA or G2POFA) at the rate of 0%, 20%, and 40% by binder weight. The water to binder (W/B) ratio was constant at 0.35 for all mixtures. The cast specimens were covered with plastic to prevent water loss. After casting for 24 h, the specimens were removed from the mold. Thereafter, they were cured in saturated lime water at a temperature of 23 ± 2 °C. The mix proportions of cement paste and blended pastes containing POFA are given in Table 2.

2.3. Compressive strength

Cube specimens of 50 × 50 × 50 mm were used for compressive strength tests of the pastes. The strengths were determined at 7, 28, 60 and 90 days according to ASTM C 109 [22]. The compressive strength of the pastes at each age was the average value of five samples.



(a)



(b)

Fig. 1. Scanning electron microscopy of palm oil fuel ash (a) ground palm oil fuel ash (G1POFA), (b) ground palm oil fuel ash (G2POFA).

Table 1
Physical properties of OPC and POFA.

Sample	Specific gravity	Median particle size, d_{50} (μm)	Blaine fineness (cm^2/g)
OPC	3.14	14.6	3600
G1POFA	2.36	15.6	6700
G2POFA	2.48	2.1	14,900

2.4. X-ray diffraction (XRD)

The XRD scans were performed for 2θ between 10° and 65° , with an increment of $0.02^\circ/\text{step}$ and a scan speed of $0.5^\circ/\text{step}$. The amorphous structure in the palm oil fuel ash was determined by quantitative XRD analysis using Bruker's TOPAS software.

2.5. Thermal analysis

Thermal analysis is a widely used method for determining hydration products such as ettringite, calcium silicate hydrate (C-S-H), calcium aluminum silicate hydrate (C_2ASH_4), calcium aluminate hydrate (C_4AH_{13}), calcium hydroxide ($\text{Ca}(\text{OH})_2$) and calcium carbonate (CaCO_3) [23]. Thermogravimetric analysis was carried out using Netzsch STA 409 C/CD equipment. The sample was heated from room temperature to 1000°C at a heating rate of $10^\circ\text{C}/\text{min}$ under a nitrogen atmosphere. The thermogravimetric (TG) signal was used to calculate the weight loss during heating and to estimate the content of $\text{Ca}(\text{OH})_2$ and carbonated phases. The $\text{Ca}(\text{OH})_2$ content was calculated from the weight loss between 450 and 580°C [24]. Furthermore, the derivative thermogravimetric (DTG) data of the weight loss can be used to further determine each phase [25].

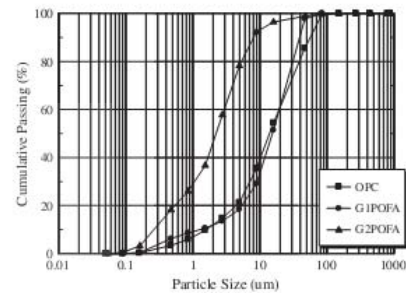


Fig. 2. Particle size distribution of OPC and POFA.

Table 2
Mix proportions of cement paste and pastes containing POFA.

Mix No.	Symbol	OPC	G1POFA	G2POFA	W/B
1	OPC	100	–	–	0.35
2	20G1POFA	80	20	–	0.35
3	40G1POFA	60	40	–	0.35
4	20G2POFA	80	–	20	0.35
5	40G2POFA	60	–	40	0.35

2.6. Determination of the porosity of the pastes

The measurement of the distribution of pore diameters in the hardened cement pastes, determined by mercury intrusion porosimetry (MIP), was conducted at a pressure capacity of 228 MPa. After curing, the samples were obtained by carefully breaking the cube specimens with a chisel. The representative samples of 3–6 mm pieces weighing between 1 and 1.5 g were taken from the middle of the specimen. To stop the hydration reaction, the samples were submerged directly into liquid nitrogen for 5 min and were then evacuated at a pressure of 0.5 Pa at -40°C for 48 h. This method has been used previously to stop the hydration reaction of cement paste [26,27]. The pressure is determined by the Washburn equation [28]. A constant contact angle of 140° and a constant surface tension of mercury of 480 dyne/cm were used for the pore size calculation.

3. Results and discussion

3.1. Properties of OPC and POFA

The chemical composition of the POFA is given in Table 3. The main chemical component of the POFA was silicon dioxide (SiO_2), which accounted for 54.0% and 55.7% for G1POFA and G2POFA, respectively. The losses on ignition (LOI) for G1POFA and G2POFA were 3.7% and 4.7%, respectively. The sums of SiO_2 , Al_2O_3 and Fe_2O_3 for G1POFA and G2POFA were 56.9% and 58.6%, respectively. Awal and Hussin [29] reported that POFA might be grouped between Class C and Class F pozzolan as specified by ASTM C 618 [30] and the sum of SiO_2 , Al_2O_3 and Fe_2O_3 content of palm oil fuel ash used in their study was 59.7%, which was close to the finding in this research. However, the LOI was 18.0%, which is much higher than that in this study. The burning efficiency and the material source are the major causes of differences in the chemical composition of palm oil fuel ash [7,31].

The X-ray diffraction (XRD) patterns of G1POFA and G2POFA are shown in Fig. 3. It was found that the major phase was α -quartz (SiO_2), and the minor phase was cristobalite (SiO_2). A similar result was reported by Chandara et al. [16]. Quantitative XRD analysis based on the Rietveld method was carried out using Bruker's TOPAS. The percentages of amorphous G1POFA and G2POFA were 70.2% and 67.2% (by mass), respectively. Moreover, the proportions

Table 3
Chemical composition of OPC and POFA.

Chemical composition (%)	OPC	G1POFA	G2POFA
Silicon dioxide (SiO ₂)	20.8	54.0	55.7
Aluminum trioxide (Al ₂ O ₃)	4.7	0.9	0.9
Iron oxide (Fe ₂ O ₃)	3.4	2.0	2.0
Calcium oxide (CaO)	65.3	12.9	12.5
Magnesium oxide (MgO)	–	4.9	5.1
Sodium oxide (Na ₂ O)	0.1	1.0	1.0
Potassium oxide (K ₂ O)	0.4	13.5	11.9
Sulfur trioxide (SO ₃)	2.7	4.0	2.9
Loss on ignition (LOI)	0.9	3.7	4.7
SiO ₂ + Al ₂ O ₃ + Fe ₂ O ₃	–	56.9	58.6

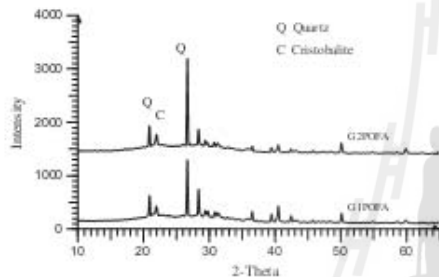


Fig. 3. X-ray diffraction patterns of G1POFA and G2POFA.

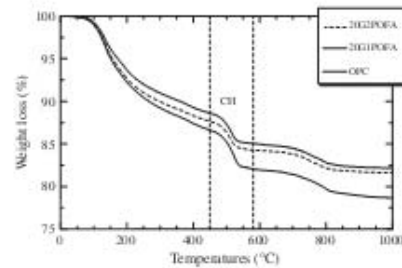
of quartz and cristobalite were 65% and 35% and 73% and 27% (by mass) for G1POFA and G2POFA, respectively. These results suggest that the amorphous content of the palm oil fuel ash was approximately 67–70%.

3.2. Compressive strength

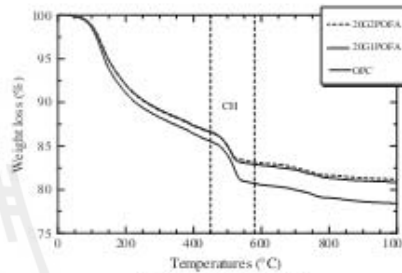
The compressive strength and normalized strength of pastes containing POFA compared to OPC paste (cement paste) are shown in Table 4. At 7 days, the compressive strength of the pastes containing palm oil fuel ash was less than that of OPC paste. For the paste containing POFA with the same particle size as cement at 28 days, the compressive strengths of the 20G1POFA and 40G1POFA pastes were 72.0 and 61.5 MPa or about 96% and 82% of that of the OPC paste, respectively. They increased to 102.0 and 88.1 MPa or about 103% and 89% of that of the OPC paste, respectively, at 90 days. The compressive strength of the 20G1POFA paste at 90 days was slightly higher than that of the OPC paste, and that of 40G1POFA was lower than that of the OPC paste. For pastes with the small particle size, the compressive strengths of 20G2POFA and 40G2POFA at 28 and 90 days were 77.3, 66.5 and 109.6, 94.1 MPa or about 103%, 89% and 111%, 95% of that of the OPC paste, respectively.

Table 4
Compressive strength of OPC paste and pastes containing ground palm oil fuel ash.

Mix no.	Symbol	Compressive strength (MPa)				Normalized compressive strength (%)			
		7 days	28 days	60 days	90 days	7 days	28 days	60 days	90 days
1	OPC	53.0	75.0	84.6	99.1	100	100	100	100
2	20G1POFA	48.3	72.0	84.6	102.0	91	96	100	103
3	40G1POFA	41.0	61.5	72.8	88.1	77	82	86	89
4	20G2POFA	51.9	77.3	92.2	109.6	98	103	109	111
5	40G2POFA	44.0	66.5	78.6	94.1	83	89	93	95



(a) Curing time 28 days



(b) Curing time 90 days

Fig. 4. TGA curve results of OPC paste and 20POFA pastes.

The compressive strength of the blended cement paste increased with curing time but decreased with an increase in the replacement of POFA. When the POFA was ground to a reasonably high fineness, the rate of compressive strength gain of the blended cement paste was significantly improved due to the hydration reaction, nucleation effect, packing effect and pozzolanic reaction. The hydration reaction occurs due to the chemical constituents in cement and water, while the pozzolanic reaction occurs due to the reaction of Ca(OH)₂ with SiO₂ and Al₂O₃ from palm oil fuel ash, which produces an increase in calcium silicate hydrate, C-S-H. The pozzolanic reaction of high fineness POFA is faster than that of coarse POFA [8,31]. The packing effect is exhibited as the small particles fill the voids of the paste, allowing for denser packing within the material particles and the matrix phase [32,33]. The nucleation effect, arising when the smaller particles are dispersed in the blended cement paste, accelerates the reactions and forms a smaller cementing paste product [34,35]. Thus, the paste containing POFA with high fineness was more homogeneous and denser, which improved the compressive strength of the paste. These

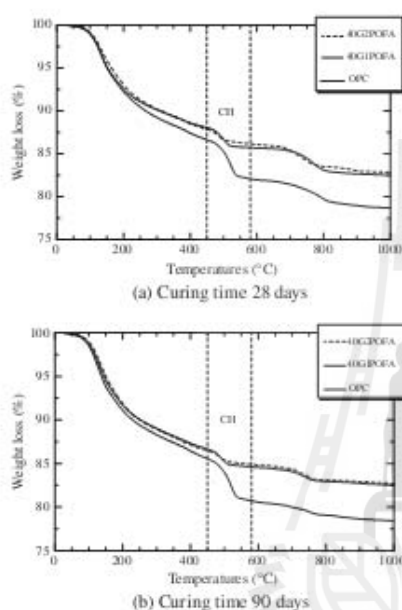


Fig. 5. TGA curve results of OPC paste and 40POFA pastes.

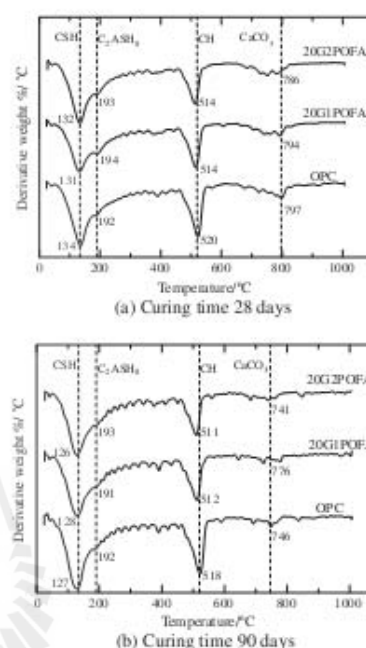


Fig. 6. DTG curve results of OPC paste and 20POFA pastes.

results are similar to those of Chindaprasit et al. [9,14]. From these results, it can be concluded that POFA with high fineness can be used as a good pozzolan in cement-based materials and can be used to replace Portland cement up to 20%. In addition, the compressive strength of 20G1POFA at which G1POFA has the same particle size as cement is 96% and 103% of that of OPC paste at 28 and 90 days, respectively.

3.3. Thermogravimetric analysis

3.3.1. Hydrated phase of cement pastes containing palm oil fuel ash

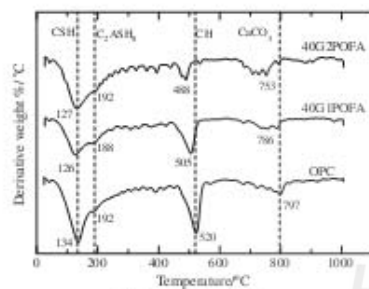
Thermogravimetric analysis (TGA) results of the OPC paste and pastes containing POFA are given in Figs. 4 and 5, respectively. Three step mass loss transitions were found. The first step shows the mass loss of dehydration such as ettringite, C-S-H and C₂ASH₄, which occurred at 105–450 °C [23]. The second step mass loss of Ca(OH)₂ was detected between 450 and 580 °C [24], and the third step at 580 and 1000 °C showed the mass loss of calcium carbonate (CaCO₃) [24].

The derivative thermogravimetric (DTG) results of the OPC paste and 20POFA cement paste are plotted in Figs. 6 and 7, respectively. At 28 and 90 days, the DTG curves of all pastes showed similar phases, which are C-S-H, C₂ASH₄, Ca(OH)₂ and CaCO₃ detected at 126–134 °C, 188–194 °C, 488–520 °C and 741–797 °C, respectively. Similar findings have also been reported by other researchers [11,36]. The DTG curve peak for Ca(OH)₂ of the pastes containing palm oil fuel ash decreased with increasing replacement of the palm oil fuel ash and also decreased with curing time. The high fineness palm oil fuel ash was more effective for decreasing the peak intensity of Ca(OH)₂ than that with a large particle

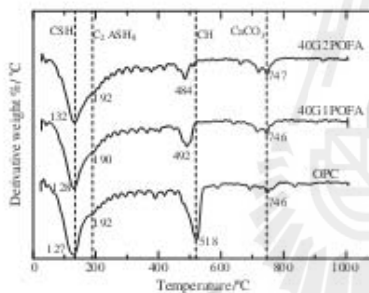
size because the high fineness palm oil fuel ash has a large surface area to provide the silica and alumina compounds for pozzolanic reaction. These compounds reacted and consumed Ca(OH)₂. The Ca(OH)₂ consumption was used as an indicator of the pozzolanic reaction. The reduction of Ca(OH)₂ in all palm oil fuel ash pastes became more subtle with age. The fineness of the palm oil fuel ash had an effect on the pozzolanic reaction rate. The paste containing high fineness palm oil fuel ash showed a higher pozzolanic reaction rate than the paste containing coarse palm oil fuel ash. The reduction of Ca(OH)₂ led to an increased peak intensity for the C-S-H and C₂ASH₄ phases with increasing curing time, which resulted in an increase in the compressive strength.

3.3.2. Ca(OH)₂ content

The Ca(OH)₂ contents of the pastes at different ages are shown in Fig. 8. The Ca(OH)₂ contents of the OPC paste at 7, 28, 60 and 90 days were 19.02%, 19.64%, 20.22% and 20.46%, respectively. The increase in the Ca(OH)₂ contents of the OPC paste was due to hydration of the cement. The Ca(OH)₂ contents of the pastes containing POFA decreased with the pozzolanic reaction of POFA. The Ca(OH)₂ contents of 20G1POFA and 20G2POFA were between 15.10–15.82% and 13.93–15.24% or reduced by approximately 5% and 9% of that of the 20G1POFA and 20G2POFA pastes at 7 days, respectively. The reduction of Ca(OH)₂ in the blended cement paste indicates its consumption by the pozzolanic reaction [37]. In addition, the pastes containing G2POFA showed lower Ca(OH)₂ contents than that of the G1POFA due to the high fineness of the particles and the silicon dioxide (SiO₂) contents in the POFA, which

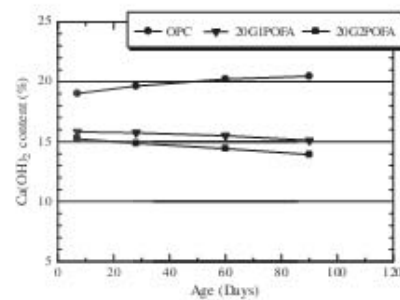


(a) Curing time 28 days

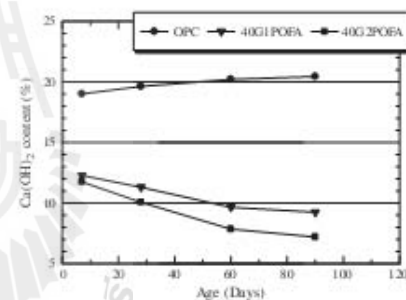


(b) Curing time 90 days

Fig. 7. DTG curve results of OPC paste and 40POFA pastes.



(a) Replacement 20 %



(b) Replacement 40 %

Fig. 8. $\text{Ca}(\text{OH})_2$ content.

react with $\text{Ca}(\text{OH})_2$ by the pozzolanic reaction. With a replacement ratio of 40% POFA, the $\text{Ca}(\text{OH})_2$ contents of the 40G1POFA and 40G2POFA pastes were between 9.24–12.18% and 7.19–11.75% or reduced by approximately 24% and 39% as compared to the 40G1POFA and 40G2POFA pastes at 7 days, respectively. Moreover, the reduction of the $\text{Ca}(\text{OH})_2$ contents of high replacement decreased more quickly than that of low replacement. These results suggest that the higher fineness palm oil fuel ash, which has a higher surface area, produces a greater pozzolanic reaction. In addition, the $\text{Ca}(\text{OH})_2$ contents of pastes containing POFA decrease with increasing POFA content. These results agree with [9].

3.4. Pore size distribution of the cement paste

3.4.1. Total porosity of the cement paste

The results for the total porosity of all pastes at different ages are presented in Table 5. The total porosities of the OPC paste at 7, 28, 60 and 90 days were 22.8%, 20.1%, 17.4% and 16.6%, respectively, while the total porosities of the 20G1POFA and 40G1POFA pastes were 26.3%, 21.7%, 18.4%, 17.4% and 30.2%, 27.5%, 19.3%, 18.5% at 7, 28, 60 and 90 days, respectively, which were higher than that of the OPC paste. The results indicate that the total porosity of the pastes containing POFA with particle sizes that were the same as the cement was higher than that of the OPC cement paste. For the paste containing G2POFA at 7 days, the total porosity of the paste containing 20% palm oil fuel ash was lower than that of the OPC paste at all ages. In addition, the total porosity of the 40G2POFA paste at 60 days was 17.3%, which is slightly less than

Table 5

Total porosity of OPC paste and pastes containing ground palm oil fuel ash.

Mix no.	Symbol	Total porosity (%)			
		7 days	28 days	60 days	90 days
1	OPC	22.8	20.1	17.4	16.6
2	20G1POFA	26.3	21.7	18.4	17.4
3	40G1POFA	30.2	27.5	19.3	18.5
4	20G2POFA	20.5	17.0	15.5	11.4
5	40G2POFA	23.8	19.7	17.3	15.6

17.4%, because the high fineness palm oil fuel ash had a faster pozzolanic reaction. The small particles showed a good filler effect in reducing the voids of the cement paste [32]. These results suggest that the addition of fine particles of palm oil fuel ash makes the blended cement paste denser [9].

3.4.2. Effect of palm oil fuel ash fineness on the pore size distribution of the pastes

The cumulative pore volumes of pastes containing 20% and 40% POFA are shown in Figs. 9 and 10, respectively. As shown in Fig. 9, at 28 and 90 days, the cumulative pore volume of the 20G2POFA paste is the lowest. The high fineness of G2POFA had a fast pozzolanic reaction and a greater filler effect in the voids, thus reducing the porosity and increasing the density of the paste. For pastes containing 40% POFA, as shown in Fig. 10, the cumulative pore volumes of the 40G1POFA and 40G2POFA pastes at 28 days were higher than that of the OPC cement paste. However, at 90 days,

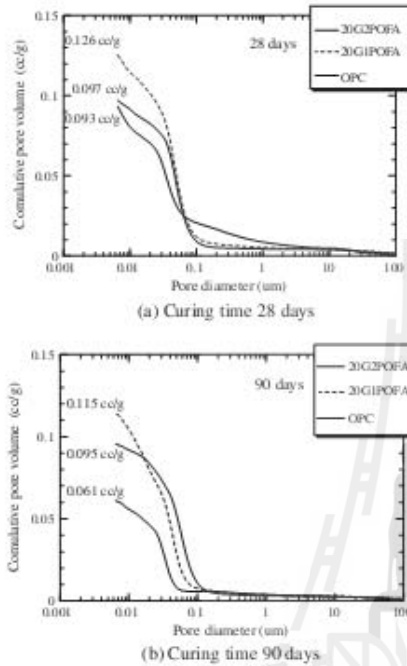


Fig. 9. Relationships between the cumulative pore volume and pore diameter of 20POFA paste.

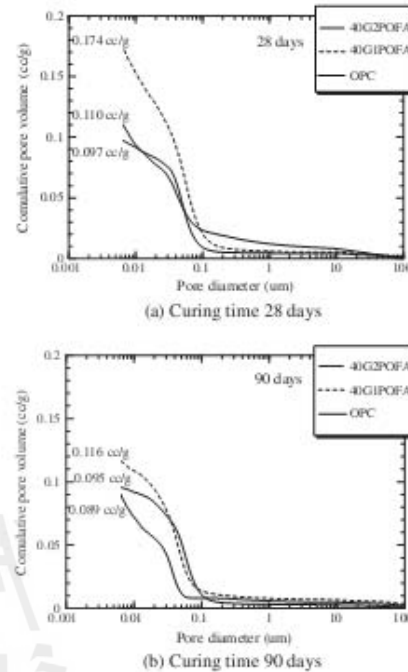


Fig. 10. Relationships between the cumulative pore volume and pore diameter of 40POFA paste.

the cumulative pore volume of the 40G2POFA paste was lower than that of the OPC paste due to the fact that the silicon dioxide (SiO_2) reacted with the calcium hydroxide Ca(OH)_2 and reduced the Ca(OH)_2 content by the pozzolanic reaction. Thus, the pore structure in the blended cement paste was refined; these results are in agreement with Li and Ding [38].

The critical pore size is defined as the inflection point on the cumulative pore volume and pore diameter plot or as the maximum of $dv/d(\log D)$. The critical pore size is the most frequent continuous pores [15,39]. For pastes containing 20% POFA at 28 days, as shown in Fig. 11, the critical pore sizes of the 20G1POFA and 20G2POFA pastes were 45.9 nm and 38.0 nm, respectively, which were distributed as medium capillary pores. These values were lower than that of the OPC paste (56.1 nm), which was specified to contain large capillary pores. At 90 days, the critical pore sizes of the OPC, 20G1POFA and 20G2POFA pastes were 54.6 nm, 41.7 nm and 31.0 nm, respectively, due to the reaction of the palm oil fuel ash with Ca(OH)_2 . Consequently, the pore structure was transformed from coarser pores to finer pores [38]. These results suggest that the paste containing POFA had a lower critical pore size than the OPC cement paste.

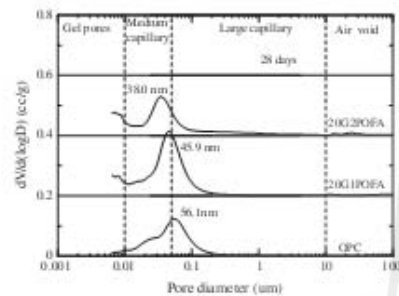
For pastes at 40% POFA, the relationships between the differential pore volume and pore diameter at 28 and 90 days are shown in Fig. 12. The critical pore sizes of the 40G1POFA and 40G2POFA pastes at 28 and 90 days were 42.1 nm, 41.8 nm and 36.8 nm, 35.0 nm, respectively, which correspond to medium capillary pores. These values are smaller than that of the OPC cement paste.

These results indicate that the paste with POFA contained critical pore sizes smaller than the OPC paste.

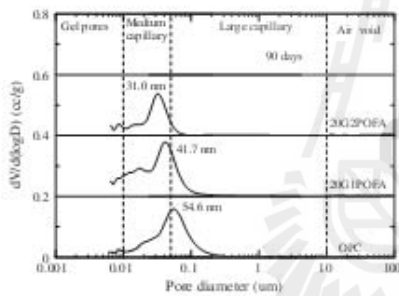
The results suggest that the total porosity of the paste containing POFA with the same particle size as cement was higher than that of the OPC cement paste, but the paste containing high fineness POFA had a lower total porosity than the OPC paste. In addition, the total porosity increased with an increase in the POFA replacement. Furthermore, the critical pore size of the paste with POFA was smaller than that of the OPC cement paste due to the filler effect, pozzolanic reaction, dispersion effect and precipitation effect [14,40]. The pore size structure of the pastes changed from coarser pores to finer pores [41]. Moreover, some researchers [42] have reported that the critical pore radius is the most important factor for permeability, and Halamicikova et al. [15] found that the critical pore size affects water permeability and chloride ion diffusion.

3.4.3. Effect of palm oil fuel ash fineness on the average pore diameter of the cement paste

The results for the average pore diameter of all pastes are shown in Fig. 13. The average pore diameters of OPC paste at 7, 28, 60 and 90 days were 53.4 nm, 45.3 nm, 30.1 nm and 28.1 nm, respectively. For pastes containing G1POFA, which has the same particle sizes as OPC, the average pore diameters of the 20G1POFA and 40G1POFA pastes were lower than that of the OPC paste at all ages, while the total porosity was higher than that of the OPC paste. For pastes containing high fineness POFA, the average pore



(a) Curing time 28 days



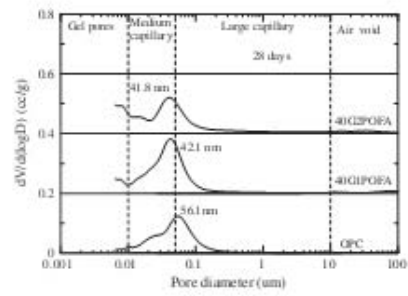
(b) Curing time 90 days

Fig. 11. Relationships between the differential pore volume and pore diameter of 20POFA paste.

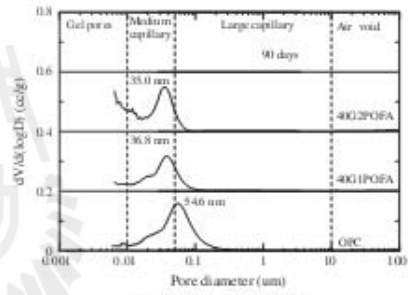
diameters of the 20G2POFA and 40G2POFA pastes were lower than that of the OPC paste, and the total porosity of the 20G2POFA paste was lower than that of the OPC paste at all ages due to pore refinement and the reduction of calcium hydroxide in the paste [41,43]. These results indicate that the average pore diameter decreases with the use of POFA and with an increase in the replacement level, which again confirms that POFA with high fineness is more effective in reducing the average pore diameter as a result of the better dispersion, packing and pozzolanic reaction of the finer POFA particles. Similar results have been reported by other researchers [14,44].

3.5. Relationships between the compressive strength and total porosity of the pastes

Relationships between the compressive strength and total porosity of the pastes are shown in Fig. 14. The figures are divided into four regions. Region I shows pastes that have both a compressive strength and total porosity higher than those of the OPC paste. Region II presents the pastes of lower compressive strength but higher total porosity in comparison to the OPC paste. Region III contains pastes that have both lower compressive strength and lower total porosity than the OPC paste. Pastes in region VI are the best pastes, which have a lower total porosity and a higher compressive strength than the OPC paste. At 28 days, the 20G1POFA, 40G1POFA and 40G2POFA pastes were located in region III, while the 20G2POFA paste was located in region VI and was designated as the best paste because its



(a) Curing time 28 days



(b) Curing time 90 days

Fig. 12. Relationships between the differential pore volume and pore diameter of 40POFA paste.

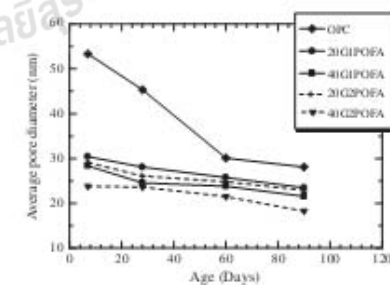


Fig. 13. Average pore diameter of curing days.

higher fineness ash can lead to greater filler effects, thus reducing the total porosity. Thus, the pastes containing POFA with high fineness increased the pozzolanic reaction rate and refined the pore structure of the paste.

At 90 days, the pastes containing POFA with the same particle size as cement were located in regions I and II. The 20G2POFA paste had a total porosity lower than that of the OPC paste, and the compressive strength was higher than that of the OPC paste, making it the best paste. However, the 40G2POFA paste had both

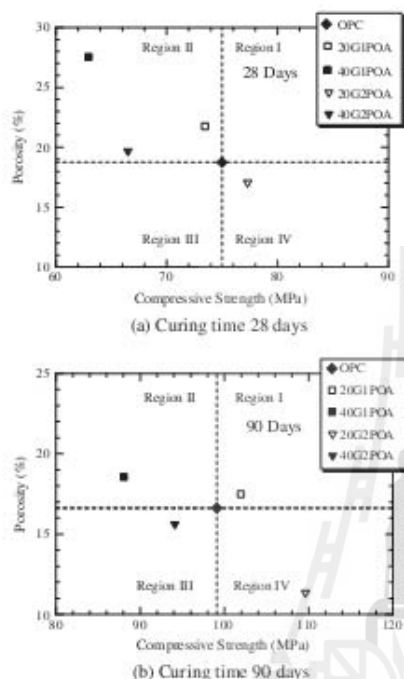


Fig. 14. Relationships between compressive strength and total porosity of paste.

a lower compressive strength and a lower total porosity than the OPC paste, which suggests that the high fineness POFA had a greater pozzolanic reaction and that the small particles of G2POFA more efficiently filled the voids of the paste. Therefore, the 20G2POFA paste was more homogeneous and had a lower total porosity than the OPC paste.

4. Conclusions

Based on the results of this study, the following conclusions can be drawn.

1. Fineness of palm oil fuel ash has the significant effect on the compressive strength of paste. Blended cement paste with high fineness palm oil fuel ash had a higher compressive strength than that with coarse palm oil fuel ash.
2. The paste containing palm oil fuel ash showed decreased $\text{Ca}(\text{OH})_2$ contents with increases in the replacement and fineness of the ash. Moreover, the reduction of $\text{Ca}(\text{OH})_2$ affected the increased peak intensity of the C-S-H and C_2ASH_4 phases with increasing curing time.
3. The reduction of the $\text{Ca}(\text{OH})_2$ content in the POFA paste was due to the pozzolanic reaction and caused the pore size structure of the paste to change from coarser pores to finer pores. Thus, the critical pore size and average pore diameter of the paste containing palm oil fuel ash were lower than those of the OPC paste.

4. The amorphous content of palm oil fuel ash was approximately 67–70%. The use of palm oil fuel ash with high fineness to replace type I Portland cement at a rate of 20% resulted in good compressive strength. In addition, the total porosity of the paste was lower than that of OPC paste.

Acknowledgments

The authors would like to acknowledge the financial support of the Commission on Higher Education of Thailand for a grant under the Strategic Scholarships for Frontier Research Network for the Joint Ph.D. Program, Thai Doctoral degree. Thanks are also extended to the Thailand Research Fund (TRF) for financial support under the TRF Senior Research Scholar, Grant No. RTA538002 and the TRF New Researcher Scholar, Grant No. MRG5280178.

References

- [1] Hendrik G, Os V, Padovani AC. Cement manufacture and the environment part II: environmental challenges and opportunities. *J Ind Ecol* 2003;7:93–126.
- [2] Chindaprasit P, Rukzon S, Sittivivatanon V. Resistance to chloride penetration of blended Portland cement mortar containing palm oil fuel ash, rice husk ash and fly ash. *Constr Build Mater* 2008;22(5):932–8.
- [3] Chusilp N, Jaturapitakul C, Kiatikomol K. Effects of LOI of ground bagasse ash on the compressive strength and sulfate resistance of mortars. *Constr Build Mater* 2009;23(12):3523–31.
- [4] Tangchirapat W, Saetang T, Jaturapitakul C, Kiatikomol K, Sirigunichgorn A. Use of waste ash from palm oil industry in concrete. *Waste Manage* 2007;27(1):81–8.
- [5] Chindaprasit P, Homwattiwong S, Jaturapitakul C. Strength and water permeability of concrete containing palm oil fuel ash and rice husk-bark ash. *Constr Build Mater* 2007;21(7):1492–9.
- [6] Chindaprasit P, Rukzon S, Sittivivatanon V. Effect of carbon dioxide on chloride penetration and chloride ion diffusion coefficient of blended Portland cement mortar. *Constr Build Mater* 2008;22(8):1701–7.
- [7] Sata V, Jaturapitakul C, Kiatikomol K. Utilization of palm oil fuel ash in high-strength concrete. *J Mater Civ Eng* 2004;16(6):623–8.
- [8] Tangchirapat W, Jaturapitakul C, Kiatikomol K. Compressive strength and expansion of blended cement mortar containing palm oil fuel ash. *J Mater Civ Eng* 2009;21(8):1426–31.
- [9] Chindaprasit P, Jaturapitakul C, Sinsiri T. Effect of fly ash fineness on microstructure of blended cement paste. *Constr Build Mater* 2007;21(7):1534–41.
- [10] Barbhuiya SA, Clugbo JK, Russell MI, Basheer PAM. Properties of fly ash concrete modified with hydrated lime and silica fume. *Constr Build Mater* 2009;23(10):3233–9.
- [11] Chaiprasit A, Nuchaiya T. Thermal analysis and microstructure of Portland cement-fly ash-silica fume pastes. *J Therm Anal Calorim* 2010;99(2):487–91.
- [12] Mindess S, Young JF. *Concrete*. Engle Cliffs: Prentice-Hall; 1981.
- [13] Kharib JM, Wild S. Pore size distribution of metakaolin paste. *Cem Concr Res* 1986;26(1):1545–51.
- [14] Chindaprasit P, Jaturapitakul C, Sinsiri T. Effect of fly ash fineness on compressive strength and pore size of blended cement paste. *Cem Concr Compos* 2005;27(4):425–8.
- [15] Halanickova P, Detwiler RJ, Benze DP, Garboczi EJ. Water permeability and chloride ion diffusion in Portland cement mortars: relationship to sand content and critical pore diameter. *Cem Concr Res* 1995;23(4):790–802.
- [16] Chandara C, Sakai E, Azizli KAM, Ahmad ZA, Hashim SFS. The effect of unburned carbon in palm oil fuel ash on fluidity of cement pastes containing superplasticizer. *Constr Build Mater* 2010;24(9):1590–3.
- [17] Jaturapitakul C, Kiatikomol K, Tangchirapat W, Saetang T. Evaluation of the sulfate resistance of concrete containing palm oil fuel ash. *Constr Build Mater* 2007;21(7):399–405.
- [18] Kumar S, Kumar R. Mechanical activation of fly ash: effect on reaction, structure and properties of resulting geopolymers. *Ceramics International* 2011;37(2):533–41.
- [19] Kumar S, Kumar R, Bandipadhyay A, Alex T, Ravi Kumar B, Das SK, et al. Mechanical activation of granulated blast furnace slag and its effect on the properties and structure of Portland slag cement. *Cem Concr Compos* 2008;30(8):679–85.
- [20] Rukzon S, Chindaprasit P, Mahachai R. Effect of grinding on chemical and physical properties of rice husk ash. *Int J Miner Metall Mater* 2009;16(2):242–7.
- [21] Bouzouba N, Zhang MH, Bilodeau A, Malhotra VM. The effect of grinding on the physical properties of fly ashes and a Portland cement clinker. *Cem Concr Res* 1997;27(12):1861–74.
- [22] ASTM C109. Standard test method for compressive strength of hydraulic cement mortars (using 2-in. or [50mm] cube specimens). Annual book of ASTM standards, vol. 04.01; 2001, p. 83–8.

- [23] Bai J, Chaipanich A, Kinsurua JM, O'Farrell M, Sabir BB, Wild S, et al. Compressive strength and hydration of wastepaper sludge ash-ground granulated blastfurnace slag blended pastes. *Cem Concr Res* 2003;33(8):1189–202.
- [24] El-Jazairi B, Illston JM. A simultaneous semi-isothermal method of thermogravimetry and derivative thermogravimetry, and its application to cement pastes. *Cem Concr Res* 1977;7(3):247–57.
- [25] Chaipanich A, Nochaiya T. Thermal analysis and microstructure of Portland cement-fly ash-silica fume pastes. *J Therm Anal Calorim* 2010;99:487–98.
- [26] Gallo C. Effect of drying on cement-based materials pore structure as identified by mercury intrusion porosimetry: a comparative study between oven-, vacuum-, and freeze-drying. *Cem Concr Res* 2001;31(10):1467–77.
- [27] Kosecny L, Naqvi SJ. The effect of different drying techniques on the pore size distribution of blended cement mortars. *Cem Concr Res* 1993;23(5):1223–8.
- [28] Washburn EW. Note on method of determining the distribution of pore size in porous materials. *Proc Natl Acad Sci USA* 1921;7:115–6.
- [29] Awal ASMA, Hussin MW. The effectiveness of palm oil fuel ash in preventing expansion due to alkali-silica reaction. *Cem Concr Compos* 1997;19(4):367–72.
- [30] ASTM C618. A standard specification for coal fly ash and raw or calcined natural pozzolan for use as a mineral admixture in concrete. *Annual book of ASTM standards*, vol. 04.02; 2008. p. 310–3.
- [31] Sara V, Jaturapitakul C, Ratanasathien C. Compressive strength and heat evolution of concretes containing palm oil fuel ash. *J Mater Civ Eng* 2010;22.
- [32] Icala GC, Castaldini ALG, Moraes R. Physical and pozzolanic action of mineral additions on the mechanical strength of high-performance concrete. *Cem Concr Compos* 2003;25(1):69–76.
- [33] Mehta PK, Aietcin P-CC. Principles underlying production of high-performance concrete. *Cem Concr Aggr* 1990;12(2):70–8.
- [34] Gopalan MK. Nucleation and pozzolanic factors in strength development of class F fly ash concrete. *ACI Mater J* 1993;90(2):117–21.
- [35] Montgomery DG, Hughes DC, Williams RT. Fly ash in concrete – a microstructure study. *Cem Concr Res* 1981;11(4):591–603.
- [36] Nochaiya T, Wongkeo W, Pimraksa K, Chaipanich A. Microstructural, physical, and thermal analyses of Portland cement-fly ash-calcium hydroxide blended pastes. *J Therm Anal Calorim* 2010;100(1):101–8.
- [37] Vedakrishni R, Sundara Raj A, Srinivasan S, Ganesh Babu K. Quantification of hydrated cement products of blended cements in low and medium strength concrete using TG and DTA technique. *Thermochim Acta* 2003;407(1–2):49–60.
- [38] Li Z, Ding Z. Property improvement of Portland cement by incorporating with metakaolin and slag. *Cem Concr Res* 2003;33(4):579–84.
- [39] Pipitkati P, Beazi-Katsioti M. The assessment of porosity and pore size distribution of limestone Portland cement pastes. *Constr Build Mater* 2009;23(5):1966–70.
- [40] Poon CS, Wong YL, Lam L. The influence of different curing conditions on the pore structure and related properties of fly-ash cement pastes and mortars. *Constr Build Mater* 1997;11(7–8):383–93.
- [41] Poon CS, Lam L, Kou SC, Wong YL, Wong R. Rate of pozzolanic reaction of metakaolin in high-performance cement pastes. *Cem Concr Res* 2001;31(9):1301–6.
- [42] Ye G, Lara P, van Breugel K. Modelling of water permeability in cementitious materials. *Mater Struct* 2006;39(9):877–85.
- [43] Chindaprasit P, Rulzon S. Strength, porosity and corrosion resistance of ternary blend Portland cement, rice husk ash and fly ash mortar. *Constr Build Mater* 2008;22(8):1601–6.
- [44] Frias M, Cabrera J. Pore size distribution and degree of hydration of metakaolin-cement pastes. *Cem Concr Res* 2000;30(4):561–9.



Contents lists available at SciVerse ScienceDirect

Materials and Design

journal homepage: www.elsevier.com/locate/matdes

Assessing the effect of biomass ashes with different finenesses on the compressive strength of blended cement paste

Theerawat Sinsiri^{a,*}, Wunchock Kroehong^a, Chai Jaturapitakkul^b, Prinya Chindaprasirt^c

^a School of Civil Engineering, Institute of Engineering, Suranaree University of Technology, Nakorn Ratchasima 30000, Thailand

^b Department of Civil Engineering, Faculty of Engineering, King Mongkut's University of Technology Thonburi, Bangkok 10140, Thailand

^c Sustainable Infrastructure Research and Development Center, Department of Civil Engineering, Faculty of Engineering, Khon Kaen University, Khon Kaen 40002, Thailand

ARTICLE INFO

Article history:

Received 28 March 2012

Accepted 16 June 2012

Available online 23 June 2012

Keywords:

Rice husk ash

Palm oil fuel ash

Amorphous

Hydration reaction

Filler effect

Pozzolanic reaction

ABSTRACT

This study assesses the effect of biomass ashes with different finenesses on the compressive strength of blended cement paste. rice husk ash (RHA), palm oil fuel ash (POFA) and river sand (RS) were ground to obtain two finenesses: one was the same size as the cement, and the other was smaller than the cement. Type I Portland cement was replaced by RHA, POFA and RS at 0%, 10%, 20%, 30% and 40% by weight of binder. A water to binder ratio (W/B) of 0.35 was used for all blended cement paste mixes. The percentages of amorphous materials and the compressive strength of the pastes due to the hydration reaction, filler effect and pozzolanic reaction were investigated. The results showed that ground rice husk ash and ground palm oil fuel ash were composed of amorphous silica material. The compressive strength of the pastes due to the hydration reaction decreased with decreasing cement content. The compressive strength of the pastes due to the filler effect increased with increasing cement replacement. The compressive strengths of the pastes due to the pozzolanic reaction were nonlinear and were fit with nonlinear isotherms that increased with increasing fineness of RHA and POFA, cement replacement rate and age of the paste. In addition, the model that was proposed to predict the percentage compressive strength of the blended cement pastes on the basis of the age of the paste and the percentage replacement with biomass ash was in good agreement with the experimental results. The optimum replacement level of rice husk ash and palm oil fuel ash in pastes was 30% by weight of binder; this replacement percentage resulted in good compressive strengths.

© 2012 Elsevier Ltd. All rights reserved.

1. Introduction

In the manufacture of cement, the clinker production process requires a great amount of energy and emits a large amount of carbon dioxide (CO₂) into the atmosphere. According to the Intergovernmental Panel on Climate Change (IPCC), the production of cement in 2005 accounted for approximately 7% of the CO₂ emissions worldwide [1]. Global cement production will increase by an average of 2.1% every year between 2005 and 2030, reaching a level that is 1.7 times greater than that in 2005 because of the growth of countries [2]. The increase in CO₂ emissions has led to the greenhouse effect and an increase in the earth's temperature. The environmental impact of cement production must be reduced by reducing the production of ordinary Portland cement. To reduce the environmental problems, pozzolanic materials, such as fly ash, silica fume and agro-waste ashes, are used as mineral admixtures to reduce the production of cement, thus reducing the emission of CO₂ and the use of energy. This solution has been reported to

be environmentally friendly. In addition, the incorporation of mineral admixtures in concrete can also improve the mechanical properties and durability of the concrete [3–5].

Rice husk ash (RHA) is a by-product of electricity generation biomass power plants. In Thailand, the annual production of RHA has been approximated at 1.6 million tons [6]. Several researchers have shown that the main chemical composition of rice husk is silicon dioxide (SiO₂), and the highest amount of amorphous silica was achieved when rice husk ash was burned between 500 and 700 °C [7,8]. Thus, RHA is a pozzolanic material and can be used as a supplementary cementitious material to replace Type I Portland cement by up to 30% [9,10]. Rukzon et al. [11] found that rice husk ash with high fineness can improve the compressive strength and produce a mortar with low porosity. For durability, the results showed that the use of RHA to partially replace Type I Portland cement improves the concrete water permeability [12], chloride penetration [10,13], and resistance to deterioration due to sulfate [3,4].

Palm oil fuel ash (POFA) is a by-product of palm oil factories, where palm shells, empty fruit bunches and palm fiber are burnt as fuel at temperatures of 800–900 °C. It has been estimated that more than 100,000 tons of palm oil fuel ash are produced in

* Corresponding author. Tel: +66 4422 4420; fax: +66 4422 4607.
E-mail address: sinsiri@sut.ac.th (T. Sinsiri).

Thailand every year [14]. Palm oil fuel ash is rarely utilized, and the amount produced is increasing annually. Previous researchers have found that POFA is a pozzolanic material, and ground POFA with high fineness can be used to replace Type I Portland cement at a rate of up to 30% by weight of binder. Chindaprasirt et al. [13] indicated that POFA improves the compressive strength and provides good resistance to chloride penetration. Tangchirapat and Jaturapitakkul [15] showed that POFA with high fineness can reduce the drying shrinkage and water permeability of concrete.

Cyr et al. [16] reported that the effect of mineral admixtures on the compressive strength involved three factors. First, the dilution effect is the strength proportional to the amount of cement in the mixture. Second, the physical effect is the strength that depends on the fineness and the amount of powder, which lead to the nucleation effect and filler effect. The nucleation effect accelerates the hydration production and leads to a more homogeneous paste. The filler effect is due to a suitable arrangement of small particles that fill the voids of the paste and increase its compressive strength. Third, the pozzolanic reaction occurs between $\text{Ca}(\text{OH})_2$ and the SiO_2 and Al_2O_3 from pozzolanic materials, which produces an increase in calcium silicate hydrate C–S–H [17–19]. However, many researchers have studied the pozzolanic reaction, using, for example, ASTM C618, strength activity index ASTM C311, X-ray diffraction (XRD), thermogravimetric analysis (TGA) and chemical titration. Moreover, Tangpagasit et al. [20] studied the use of river sand as an inert material to replace Type I Portland cement to evaluate the packing effect and pozzolanic reaction of fly ash in mortar. They found that river sand is an inert material and that the packing effect is not dependent on the age of the mortar but rather on the particle size while the pozzolanic reaction depends on the fineness and age of the mortar.

Previous studies have already reported the influence of the finenesses of RHA and POFA on the compressive strength and observed that ashes with a median particle size larger than OPC ($\sim 15 \mu\text{m}$) can be used to replace OPC at 10% [10] while smaller sizes than OPC can be used at 20% to 30% by weight of binder [15]. However, the separation of the influences of the hydration reaction, the filler effect and the pozzolanic reaction on compressive strength of blended cement pastes has not been well defined. If a by-product material from biomass plants can be used as a cement replacement in concrete, it will help reduce energy use by reducing the production of cement clinker and reducing the volume of waste disposed to landfills. Thus, the objective of this study is to quantify the effect of the hydration reaction, the filler effect and the pozzolanic reaction on compressive strength of paste. In addition, equation derived from results determine from experimental testing was derived to predict the compressive strength of a paste due to the hydration reaction, filler effect, and pozzolanic reaction. The chemical properties and percentages of amorphous materials were investigated. The effects of ground rice husk ash and ground palm oil fuel ash with two different finenesses, which influences the hydration reaction, filler effect, and pozzolanic reaction, on the compressive strength of blended cement pastes were determined.

2. Experimental details

2.1. Materials

The materials used in this study were Type I Ordinary Portland cement (OPC), rice husk ash (RHA), palm oil fuel ash (POFA), and river sand. RHA and POFA were collected from thermal power plants in Thailand, and the inert material used was ground river sand (RS). The original RHA and POFA had large particles with low pozzolanic properties [11,21]. Thus, the original RHA and POFA

were sieved through a sieve No. 16 to remove the large particles and any incompletely combusted material. The difference in compressive strength between the pozzolan paste and inert material paste can be determined as the compressive strength due to the pozzolanic reaction [20]. Then, the RHA, POFA and RS were ground to two different sizes. To eliminate the filler effect, RHA, POFA and RS were ground to have the same particle size as OPC for the first fineness of materials (CRHA, CPOFA and CRS). For the second fineness from the filler effect of materials (FRHA, FPOFA and FRS), the materials were ground to have particles that could act as fillers between the particles of cement by an attrition mill for 60 min at 1000 rpm using 2 mm diameter steel balls.

As shown in Fig. 1a, if the median particle size of a material is the same as that of OPC ($\sim 15 \mu\text{m}$), the filler should have the same particle size as OPC.

$$d = D = 15 \mu\text{m} \quad (1)$$

If the median particle size of the material is smaller than that of cement and acts as filler between the particles of cement, as shown in Fig. 1(b), the median size of the material can be calculated with Eq. (3) [22]:

$$d = \cos 30^\circ \frac{D/2}{D/2 + d/2} \quad (2)$$

$$d = 0.15D = 0.15(15) = 2.25 \mu\text{m} \quad (3)$$

The SEM photographs of the materials are shown in Fig. 2. It was found that the ground RHA and POFA consisted of irregular, crushed particles. A similar conclusion was also reported by other researchers [13]. The physical properties of the materials are presented in Table 1. The first group of materials (CRHA, CPOFA and CRS) had particle sizes equal to that of cement. The specific gravity of CRHA, CPOFA and CRS was 2.29, 2.36 and 2.59, respectively. The Blaine fineness values of CRHA, CPOFA and CRS were 7600, 6700 and 3900 cm^2/g , respectively. For the small particle group (FRHA, FPOFA and FRS), the specific gravity and Blaine fineness of FRHA, FPOFA and FRS were 2.31, 2.48, 2.61 and 18,000, 14,900 and 6300 cm^2/g , respectively. The particle size distributions of the materials are shown in Fig. 3. The median particle sizes of CRHA, CPOFA and CRS were close to the particle size of the cement, while those of FRHA, FPOFA and FRS were smaller than that of cement.

2.2. Mix proportion

Ground RHA, POFA and RS were used to partially replace Type I Portland cement at the rates of 0%, 10%, 20%, 30% and 40% by weight of binder. A water to binder (W/B) ratio of 0.35 was used for all mixtures and is shown in Table 2. To ensure homogeneity, the OPC, RHA, POFA and RS were first mixed together for 3 min in the mixer, and then the water was added. Afterwards, the mixture was mixed for another 2 min. After mixing, the cement pastes were immediately cast into cube specimens of $50 \times 50 \times 50 \text{ mm}$. The cast specimens were covered with plastic to prevent water loss. After casting for 24 h, the specimens were removed from the molds and cured in saturated lime water at a temperature of $23 \pm 2^\circ\text{C}$.

2.3. Compressive strength

The cube specimens of $50 \times 50 \times 50 \text{ mm}$ were prepared in accordance with ASTM C109 [23]. They were tested to determine the compressive strength at the ages of 7, 28, 60 and 90 days. Each compressive strength value reported is the average of five samples.

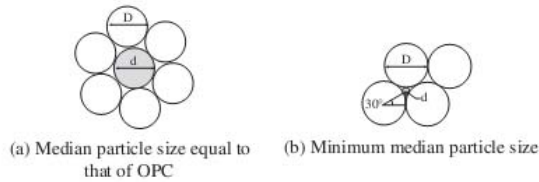


Fig. 1. Plan view illustration of the relationship between the particles of cement.

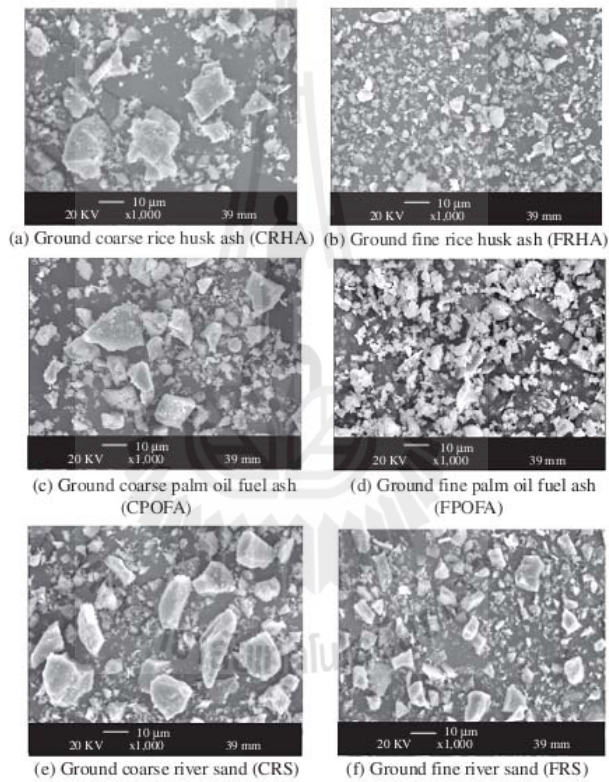


Fig. 2. Scanning electron micrographs of the materials.

Table 1
Physical properties of the materials.

Sample (cm ³ /g)	Specific gravity	Median particle size, d_{50} (μm)	Blaine fineness
OPC	3.14	14.6	3600
CRHA	2.29	14.8	7600
CPOFA	2.36	15.6	6700
CRS	2.59	15.9	3900
FRHA	2.31	1.9	18,100
FPOFA	2.48	2.1	14,900
FRS	2.61	2.2	6300

2.3.1. Evaluation of the percentage compressive strength of paste due to the hydration reaction

The percentage compressive strength of a paste due to the hydration reaction (P_H) is the ratio between the compressive strength of the paste containing inert material with the same particle size of cement and the compressive strength of the OPC paste. The percentage compressive strength of a paste due to the hydration reaction is calculated by the following equation:

$$P_H = \left(\frac{C_c}{C_{\text{opc}}} \right) \times 100 \quad (4)$$

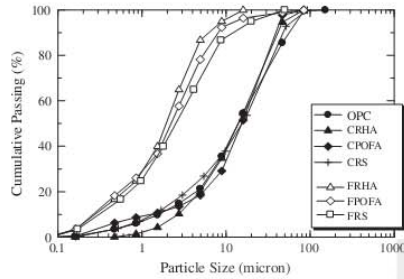


Fig. 3. Particle size distributions of the materials.

where P_H is the percentage compressive strength of the paste due to the hydration reaction (%), C_{ic} is the compressive strength of the paste containing inert material with the same particle size of cement (MPa) and C_{opc} is the compressive strength of OPC paste (MPa).

2.3.2. Evaluation of the percentage compressive strength of paste due to the filler effect

The percentage compressive strength of paste due to the filler effect (P_f) is the difference in the percentage compressive strength between the paste with inert material with high fineness and the paste with inert material with the same particle size as the cement. The percentage compressive strength of paste due to the filler effect is calculated by the following equation:

$$P_f = (P_{f(p,t)} - P_{s(p,t)}) \tag{5}$$

where P_f is the percentage compressive strength of the paste due to the filler effect (%), $P_{f(p,t)}$ is the percentage compressive strength of the paste containing inert material with high fineness compared with OPC paste (%) and $P_{s(p,t)}$ is the percentage compressive strength of the paste containing inert material with the same parti-

cle size as the cement compared with OPC paste (%). $P_{f(p,t)}$ and $P_{s(p,t)}$ have the same replacement (p) and the same age (t).

2.3.3. Evaluation of the percentage compressive strength due to the pozzolanic reaction

The percentage compressive strength of paste due to the pozzolanic reaction (P_{pz}) is the difference in the percentage compressive strength between the RHA or POFA paste and the inert material paste. The percentage compressive strengths of paste due to the pozzolanic reaction were calculated by the following equation:

$$P_{pz,t} = (P_{b(p,s,t)} - P_{i(p,s,t)}) \tag{6}$$

where $P_{pz,t}$ is the percentage compressive strength of the paste due to the pozzolanic reaction (%), $P_{b(p,s,t)}$ is the percentage compressive strength of the paste containing RHA or POA compared with OPC paste (%) and $P_{i(p,s,t)}$ is the percentage compressive strength of the paste containing inert material compared with OPC paste (%) $P_{b(p,s,t)}$ and $P_{i(p,s,t)}$ have the same replacement (p), fineness (s) and age (t).

3. Results and discussion

3.1. Chemical and mineralogical analysis

The chemical compositions of the materials are shown in Table 3. SiO_2 is the major chemical component of CRHA, FRHA, CPOFA and FPOFA and is 88.8%, 87.8%, 54.0% and 55.7%, respectively. LOI and SO_3 are within the limits of 10.0% and 4%, respectively. The total amounts of SiO_2 , Al_2O_3 and Fe_2O_3 in CRHA and FRHA were 91.1% and 89.2%, respectively, which are higher than the 70% for Class N pozzolan specified by ASTM C 618 [24]. However, the total amounts of SiO_2 , Al_2O_3 and Fe_2O_3 of CPOFA and FPOFA were 56.9% and 58.6%, respectively, both of which are less than 70%. A similar finding was also reported by other researchers [25]. They found that POFA had a total SiO_2 , Al_2O_3 and Fe_2O_3 content less than 70%. In the case of insoluble material (river sand (RS)), the main chemical component of CRS and FRS was also SiO_2 and was 92.0% and 91.2%, respectively. In addition, the X-ray diffraction patterns of the materials are shown in Fig. 4. The percentage of amorphous material was determined by the quantitative XRD analysis based

Table 2
Mixture proportions of the pastes.

Mix No	Symbol	OPC	CRS	CRHA	CPOFA	FRS	FRHA	FPOFA	W/B
1	OPC	100	-	-	-	-	-	-	0.35
2	10CRS	90	10	-	-	-	-	-	0.35
3	20CRS	80	20	-	-	-	-	-	0.35
4	30CRS	70	30	-	-	-	-	-	0.35
5	40CRS	60	40	-	-	-	-	-	0.35
6	10CRHA	90	-	10	-	-	-	-	0.35
7	20CRHA	80	-	20	-	-	-	-	0.35
8	30CRHA	70	-	30	-	-	-	-	0.35
9	40CRHA	60	-	40	-	-	-	-	0.35
10	10CPOFA	90	-	-	10	-	-	-	0.35
11	20CPOFA	80	-	-	20	-	-	-	0.35
12	30CPOFA	70	-	-	30	-	-	-	0.35
13	40CPOFA	60	-	-	40	-	-	-	0.35
14	10FRS	90	-	-	-	10	-	-	0.35
15	20FRS	80	-	-	-	20	-	-	0.35
16	30FRS	70	-	-	-	30	-	-	0.35
17	40FRS	60	-	-	-	40	-	-	0.35
18	10FRHA	90	-	-	-	-	10	-	0.35
19	20FRHA	80	-	-	-	-	20	-	0.35
20	30FRHA	70	-	-	-	-	30	-	0.35
21	40FRHA	60	-	-	-	-	40	-	0.35
22	10FPOFA	90	-	-	-	-	-	10	0.35
23	20FPOFA	80	-	-	-	-	-	20	0.35
24	30FPOFA	70	-	-	-	-	-	30	0.35
25	40FPOFA	60	-	-	-	-	-	40	0.35

Table 3
Chemical compositions of the materials.

Chemical composition (%)	OPC	CRHA	FRHA	CPOFA	FPOFA	CRS	FRS
Silicon dioxide (SiO ₂)	20.8	88.8	87.8	54.0	55.7	92.0	91.2
Aluminum oxide (Al ₂ O ₃)	4.7	0.6	0.5	0.9	0.9	1.6	1.8
Iron oxide (Fe ₂ O ₃)	3.4	1.7	0.9	2.0	2.0	0.6	0.2
Calcium oxide (CaO)	65.3	1.1	1.2	12.9	12.5	0.9	0.7
Magnesium oxide (MgO)	–	0.6	0.6	4.9	5.1	0.1	0.1
Sodium oxide (Na ₂ O)	0.1	0.2	0.2	1.0	1.0	0.1	0.1
Potassium oxide (K ₂ O)	0.4	2.0	2.2	13.5	11.9	2.2	2.3
Sulfur trioxide (SO ₃)	2.7	0.1	0.1	4.0	2.9	–	–
Loss on ignition (LOI)	0.9	3.6	5.2	3.7	4.7	2.1	1.8
SiO ₂ + Al ₂ O ₃ + Fe ₂ O ₃	–	91.1	89.2	56.9	58.6	94.2	93.2
<i>Quantitative XRD, Rietveld method</i>							
Amorphous (%)	–	70.1	69.6	70.2	67.2	–	–
Crystalline (%)	–	29.9	30.4	29.8	32.8	100.0	100.0
Quartz	–	59.3	56.2	65.0	73.0	100.0	100.0
Cristobalite	–	40.7	43.8	35.0	27.0	–	–

on the Rietveld method, which was calculated using Bruker's TOPAS. The amorphous contents of CRHA, FRHA, CPOFA and FPOFA were 70.1%, 69.6%, 70.2% and 67.2% (by mass), respectively. The percentages of crystalline CRS and FRS were 100% (by mass). The results confirm that river sand is an inert material, which is similar to the results of previous research [20].

3.2. Compressive strength

Table 4 shows the compressive strengths at 7, 28, 60 and 90 days for the OPC paste, which were 53.0, 75.0, 84.6 and 99.1 MPa, respectively. At 7 days, the compressive strengths of pastes containing 10–40% of CRHA with the same particle size as cement were lower than that of the OPC paste because of the low cement content, which resulted in a significant reduction in the normalized strength [15,26]. Additionally, the compressive strengths of the 10CRHA and 20CRHA pastes at 28 days were 76.5 and 74.2 MPa or about 102% and 98.9% of that of the OPC paste, respectively, while those of the 30CRHA and 40CRHA pastes at 28 and 90 days were 70.5, 64.7 and 100.0, 92.1 MPa or about 94%, 86.3% and 100.9%, 92.9% of that of the OPC paste, respectively. In the case of pastes containing FRHA (small particle size of RHA), the compressive strengths of the 10FRHA, 20FRHA and 30FRHA pastes were 55.9, 52.9 and 50.3 MPa or 105.5%, 99.8% and 94.9% of that of the OPC paste at 7 days but increased to 81.7, 78.7 and 74.9 MPa or 108.9%, 104.9% and 99.9% of that of the OPC paste at 28 days, respectively.

For the group mixed with ground palm oil fuel ash, the pastes containing 10–40% CPOFA had compressive strengths that were lower than that of OPC paste at 7 days. The 28 days compressive strengths were 74.8, 72.0, 66.7 and 61.5 MPa with a normalized strength of 99.7%, 96.0%, 88.9% and 82.0% for the 10CPOFA, 20CPOFA, 30CPOFA and 40CPOFA pastes, respectively. At 90 days, they increased to 104.5, 102.0, 97.1 and 88.1 MPa with a normalized strength of 105.4%, 102.9%, 98.0% and 88.9% of the OPC paste, respectively. For the pastes with a small particle size, the compressive strengths of the 10FPOFA and 20FPOFA pastes at 28 and 90 days were 79.3, 77.3 and 111.3, 109.6 MPa or about 105.7%, 103.1% and 112.3%, 110.6% of the strength of the OPC paste, respectively. However, at 30% and 40% FPOFA, the compressive strengths at 90 days were 104.0 and 94.1 MPa or about 104.9% and 95.0% of that of the OPC paste, respectively.

The compressive strength of blended cement paste increased with age but decreased with an increase in the replacement of ash. The increased compressive strength of blended cement paste can be explained by three factors: the hydration reaction, the filler effect and the pozzolanic reaction. The hydration reaction is the

strength proportionate to the amount of cement in the mix. The filler effect has two causes, the nucleation effect and packing effect, which depend significantly on the fineness of material. The nucleation effect arises when the small particles are dispersed in the blended cement paste and enhance the cement hydrate while the packing effect occurs when small particles fill the voids of the paste [16,18,27,28]. Therefore, the blended cement paste containing biomass ash with high fineness was more homogeneous and denser, which increased the compressive strength of the paste. Finally, the pozzolanic reaction occurs because of the SiO₂ and Al₂O₃ contained in the biomass ash, which react with Ca(OH)₂ and produce an additional calcium silicate hydrate (C–S–H).

Comparing the RHA and POFA blended cement pastes in terms of the same replacement and same fineness, the normalized strengths of RHA pastes were slightly higher than those of POFA pastes because RHA contains more SiO₂ than POFA. The results indicated that RHA was more reactive than POFA, and the results agree with [20]. In addition, the results suggest that the replacement of cement type I by RHA and POFA up to 30% by weight of binder does not impair the compressive strength of pastes. The results are nearly identical to the results obtained by other researchers [10,29], who reported that the optimum replacement level of Portland cement Type I by RHA or POFA is 30% by weight of binder.

3.3. Influence of cement content on the percentage compressive strength of paste

The percentage compressive strength of ground river sand paste with age (P_H) is shown in Fig. 5. For pastes containing CRS with the same particle size as that of cement, the percentage compressive strengths of CRS pastes at any age were almost constant. The same trend was also reported by [20,29]. In contrast, the relationship between the percentage compressive strengths of pastes due to the hydration reaction and the percentage replacement of CRS paste is shown in Fig. 6. The percentage compressive strengths decreased linearly with replacement of CRS. The results suggest that the percentage compressive strength of pastes containing inert material with the same particle size as cement does not depend on age but rather depends on the cement content.

The empirical equations can be expressed for the percentage compressive strength of paste due to the hydration reaction in terms of (R) as follows:

$$P_H = 100.4 - 0.996(R) \quad (7)$$

where P_H is percentage compressive strength due to the hydration reaction of paste (%) and R is the replacement of Portland cement by an inert material (%). The correlation value of 0.997 indicates a

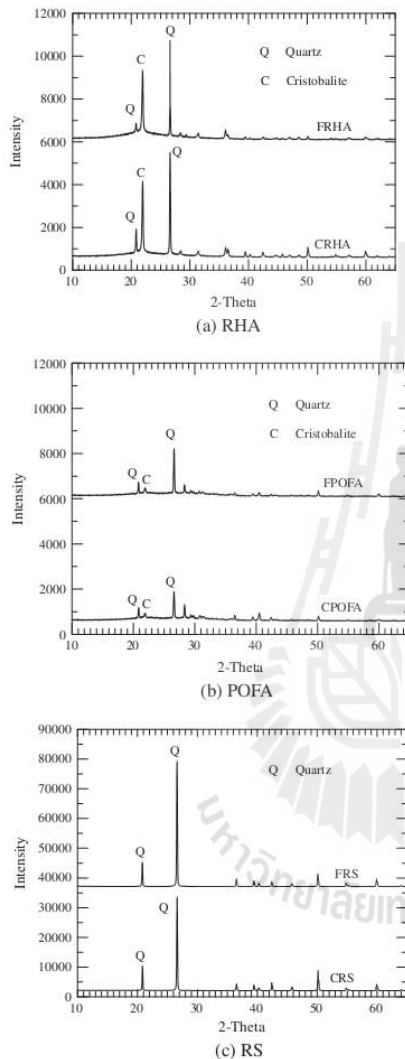


Fig. 4. X-ray diffraction patterns of the materials.

strong linear relationship between the percentage compressive strength and the percentage replacement of CRS.

3.4. Influence of the filler effect on the percentage compressive strength of paste

The relationship between the percentage compressive strength of ground river sand with different finenesses of paste and age are

shown in Fig. 5. The pastes with particles smaller than OPC had a higher percentage compressive strength than the pastes with large particle size and had an almost constant value [20,29]. Fig. 7 shows the percentage compressive strengths of ground river sand with different finenesses of paste and replacements with river sand. The percentage compressive strength of paste due to the filler effect tended to increase with the amount of cement replacement and was approximately 2.2–5.1% of the strength of the OPC paste because the small particles dispersed into the blended cement paste and accelerated the hydration reaction. In addition, the packing effect occurred as the small particles filled the voids of the paste [16,18,27,28]. Therefore, the paste was more homogeneous and denser, which resulted in the increased compressive strength of the paste. These results suggest that a particle size smaller than OPC has very important role in increasing the compressive strength because of the filler effect [30]. The results of the filler effect for pastes agrees closely with the result obtained by Jatrapitakkul et al. [31], who reported that the difference in the percentage compressive strengths between mortar containing the same particle sizes of inert material and small sizes of inert material was up to 5.8% of the strength of the mortar.

The empirical equation to predict the percentage of the compressive strength of the paste due to the filler effect in terms of replacement (R) is proposed as follows:

$$P_f = 1.542Ln(R) - 1.002 \quad (8)$$

where P_f is the percentage compressive strength of the paste due to the filler effect (%) and R is the replacement of Portland cement by inert material (%). It was found that P_f is represented by a logarithmic equation and has good correlation. The percentage compressive strength of the paste due to the filler effect of the blended cement paste increased with an increase in the replacement of inert material.

3.5. Influence of the pozzolanic reaction on the percentage compressive strength of pastes

Figs. 8 and 9 show the percentage compressive strength of paste due to the pozzolanic reaction of RHA and POFA, respectively. The pozzolanic reaction increased with age and with the replacement of RHA or POFA. In addition, the high fineness of RHA or POFA was more efficient for the pozzolanic reaction than the coarse fineness because the high fineness of the ash provided a large surface area to contribute silica and alumina compounds for the pozzolanic reaction [32,33]. These compounds reacted with $Ca(OH)_2$ from the hydrated cement and produced an increase in calcium silicate hydrate. In addition, the percentage compressive strength due to the pozzolanic reaction of higher replacement paste increased more than that of the lower replacement paste. The blended cement paste containing a high replacement of the ash showed a decrease of $Ca(OH)_2$ content compared with the low replacement paste [34]. In addition, the reduction of $Ca(OH)_2$ affected the increase of the calcium silicate hydrate from the pozzolanic reaction [35].

Comparing the percentage compressive strength of paste due to the pozzolanic reaction in Figs. 8 and 9, the RHA pastes had a higher percentage compressive strength of paste due to the pozzolanic reaction than the POFA pastes. The maximum percentage compressive strength due to the pozzolanic reaction of RHA and POFA pastes were 33.7% and 30.5% that of the OPC paste, respectively, because RHA has a higher SiO_2 content than POFA. The results confirmed that the percentage compressive strength of paste due to the pozzolanic reaction increased with age, fineness, and the replacement rate of the ash.

Figs. 8 and 9 show that the percentage compressive strength due to the pozzolanic reaction is explicitly nonlinear and is best fit with nonlinear isotherms, which are shown in the same figure.

Table 4
Compressive strengths of the pastes.

Symbol	Compressive strength (MPa)				Normalized compressive strength (%)			
	7 days	28 days	60 days	90 days	7 days	28 days	60 days	90 days
OPC	53.0	75.0	84.6	99.1	100.0	100.0	100.0	100.0
10CRHA	52.4	76.5	88.5	107.6	98.9	102.0	104.6	108.6
20CRHA	49.8	74.2	88.3	106.0	94.0	98.9	104.4	107.0
30CRHA	46.5	70.5	83.7	100.0	87.7	94.0	98.9	100.9
40CRHA	42.4	64.7	77.4	92.1	80.0	86.3	91.5	92.9
10FRHA	55.9	81.7	94.7	116.2	105.5	108.9	111.9	117.3
20FRHA	52.9	78.7	93.1	113.2	99.8	104.9	110.0	114.2
30FRHA	50.3	74.9	89.6	107.9	94.9	99.9	105.9	108.9
40FRHA	44.5	66.9	79.5	96.1	84.0	89.2	94.0	97.0
10CPOFA	51.3	74.8	86.3	104.5	96.8	99.7	101.6	105.4
20CPOFA	48.3	72.0	84.6	102.0	91.1	96.0	99.6	102.9
30CPOFA	44.5	66.7	78.6	97.1	84.0	88.9	92.9	98.0
40CPOFA	41.0	61.5	72.8	88.1	77.4	82.0	85.7	88.9
10FPOFA	53.7	79.3	93.3	111.3	101.3	105.7	109.9	112.3
20FPOFA	51.9	77.3	92.2	109.6	97.9	103.1	108.6	110.6
30FPOFA	48.3	72.8	86.3	104.0	91.1	96.9	101.6	104.9
40FPOFA	44.0	66.5	78.6	94.1	83.0	88.7	92.6	95.0
10CRS	48.3	68.2	77.2	90.1	91.1	90.9	91.3	90.9
20CRS	42.9	60.8	67.9	78.6	80.9	81.1	80.3	79.3
30CRS	36.9	53.1	60.8	70.2	69.6	70.8	71.9	70.8
40CRS	31.5	45.6	51.5	59.6	59.4	60.8	60.9	60.1
10FRS	49.9	69.9	79.1	92.8	94.2	93.2	93.5	93.6
20FRS	45.0	63.4	70.8	82.1	84.9	84.5	83.7	82.8
30FRS	39.1	56.5	64.1	74.5	73.8	75.3	75.8	75.2
40FRS	34.2	49.2	55.4	63.9	64.5	65.6	65.5	64.5

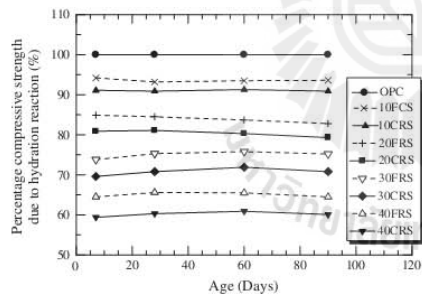


Fig. 5. Relationship between the percentage compressive strength of ground rice sand paste and age.

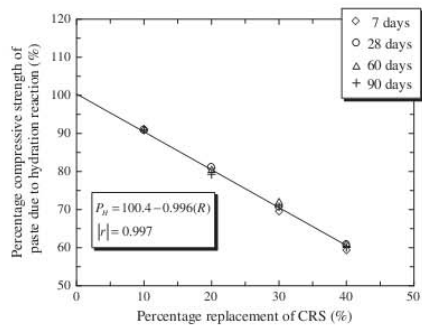


Fig. 6. Relationship between the percentage compressive strength of paste due to the hydration reaction and the percentage replacement of CRS.

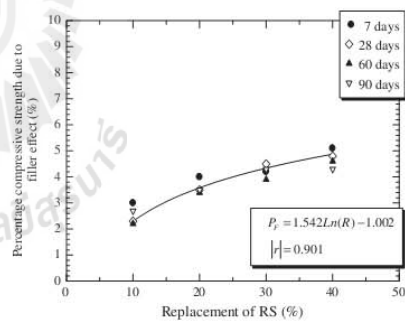


Fig. 7. Relationships between the percentage compressive strength of paste due to the filler effect and the replacement of RS.

Thus, the equation to predict the percentage compressive strength of paste due to the pozzolanic reaction is:

$$P_{PZ,t} = \alpha R^\beta \tag{9}$$

where $P_{PZ,t}$ is the percentage compressive strength of the paste due to the pozzolanic reaction at a specified age ($t = 7, 28, 60$ and 90 days) (%), R is the rice husk ash or palm oil fuel ash replacement (%) and α and β are the pozzolanic constants. The pozzolanic constants for the isotherm fitted from experimental results of the pastes are presented in Table 5.

3.6. Generating an empirical equation for the prediction of the percentage compressive strength of the blended cement paste

3.6.1. Role of the blended cement paste containing biomass ash on the percentage of compressive strength

The percentage compressive strength of the blended cement paste containing biomass ash with the same particle size as cement

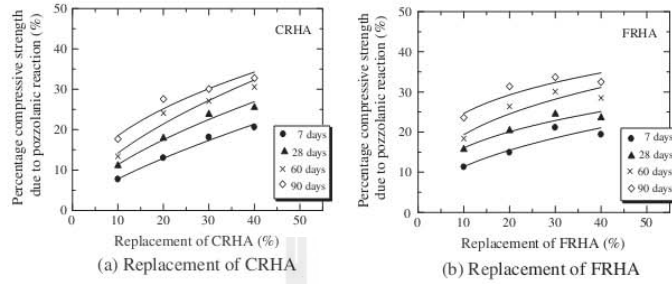


Fig. 8. Relationships between the percentage compressive strength due to the pozzolanic reaction of RHA pastes and age.

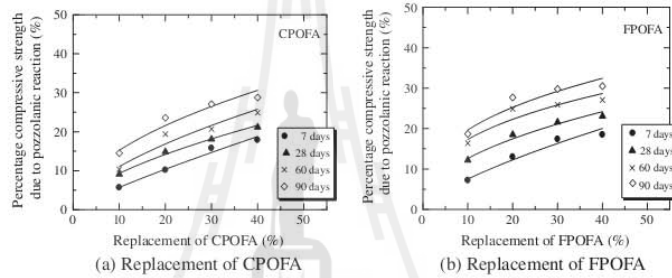


Fig. 9. Relationships between the percentage compressive strength due to the pozzolanic reaction of POFA paste and age.

Table 5
Best fit of the pozzolanic constants for the isotherms.

Binder Type	Days	Pozzolanic constants		Correlation
		α	β	
CRHA	7	1.479	0.723	0.993
	28	2.728	0.617	0.988
	60	3.593	0.595	0.948
	90	6.633	0.445	0.943
FRHA	7	4.098	0.444	0.895
	28	7.667	0.321	0.923
	60	8.817	0.341	0.865
	90	13.940	0.247	0.837
CPOFA	7	0.792	0.856	0.993
	28	2.273	0.611	0.991
	60	2.703	0.611	0.939
	90	4.798	0.502	0.949
FPOFA	7	1.462	0.709	0.972
	28	4.590	0.449	0.974
	60	7.513	0.363	0.884
	90	8.551	0.361	0.899

is related to the hydration reaction and pozzolanic reaction as follows:

$$P_{C,t} = P_H + P_{PZ,t} \tag{10}$$

Eq. (10) can be rewritten as follows:

$$P_{C,t} = 100.4 - 0.99(R) + \alpha R^\beta \tag{11}$$

where $P_{C,t}$ is the total percentage compressive strength of the paste at a specified age ($t = 7, 28, 60$ and 90 days) (%), P_H is the percentage

compressive strength of the paste due to the hydration reaction (%), $P_{PZ,t}$ is the percentage compressive strength of the paste due to the pozzolanic reaction at various curing times ($t = 7, 28, 60$ and 90 days) (%), R is the percentage replacement of RHA or POFA and α and β are the pozzolanic constants. The prediction using Eq. (11) and experimental results are shown in Fig. 10. This equation is useful to predict the percentage compressive strength of blended cement pastes containing RHA and POFA.

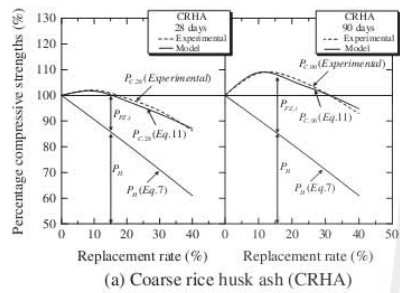
For the mixture of biomass ash with a particle size smaller than that of OPC, the percentage compressive strength of paste is due to the hydration reaction, filler effect and pozzolanic reaction as follows:

$$P_{C,t} = P_H + P_F + P_{PZ,t} \tag{12}$$

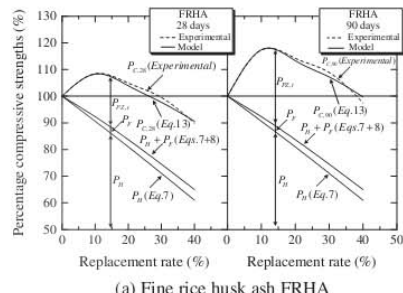
Eq. (12) can be rewritten as follows:

$$P_{C,t} = 99.398 - 0.996(R) + 1.542\ln(R) + \alpha R^\beta \tag{13}$$

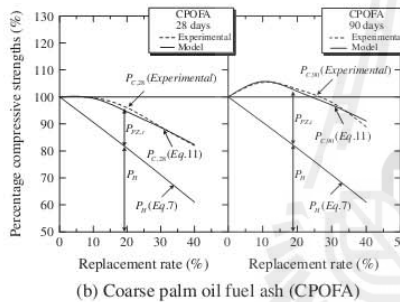
where $P_{C,t}$ is the total percentage compressive strength of the paste at a specified age ($t = 7, 28, 60$ and 90 days) (%), P_H is the percentage compressive strength of the paste due to the hydration reaction (%), P_F is the percentage compressive strength of the paste due to the filler effect (%), $P_{PZ,t}$ is the percentage compressive strength of the paste due to the pozzolanic reaction at a specified age ($t = 7, 28, 60$ and 90 days) (%), R is the percentage replacement of RHA or POFA, and α and β are the pozzolanic constants. The percentage compressive strength of the pastes according to this equation was compared with the actual test specimens, as shown in Fig. 11. The equation suggests that the percentage compressive strength of the paste due to the pozzolanic reaction is higher than that due to the filler effect. Moreover, it is also useful to predict the percentage



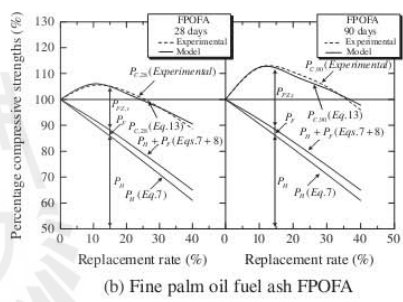
(a) Coarse rice husk ash (CRHA)



(a) Fine rice husk ash (FRHA)



(b) Coarse palm oil fuel ash (CPOFA)



(b) Fine palm oil fuel ash (FPOFA)

Fig. 10. Relationships between the percentage compressive strengths of blended cement pastes containing CRHA and CPOFA with the same particle size as that of OPC.

Fig. 11. Relationships between the percentage compressive strengths of the blended cement paste containing FRHA and FPOFA with particle sizes smaller than that of OPC.

compressive strength of pastes with the curing time and amounts of replacement of RHA and POFA.

3.6.2. Verification

The measured percentage compressive strengths of the pastes for $W/B = 0.35$, $R = 10\text{--}40\%$, and $d = 7, 28, 60$ and 90 days were compared with the predicted results according to Eqs. (11) and (13), which are shown in Fig. 12. The measured and predicted values are reasonably close. The error from prediction is satisfied with the mean absolute percent error, $(\sum | \frac{P_{pred} - P_{meas}}{P_{meas}} | \times 100\%)$, which is less than 2.4%.

4. Conclusions

The results of this study provide the following conclusions.

1. The percentage compressive strength of the pastes due to the hydration reaction decreased with decreasing cement content. In addition, the percentage compressive strength of the paste due to the hydration reaction showed a linear best-fit relationship.
2. Ground inert material with particle sizes smaller than that of OPC was a very important factor affecting the percentage compressive strength due to the filler effect. In addition, the percentage compressive strength of pastes due to the filler effect increased with increasing inert matter material replacement. The percentage compressive strength of pastes due to the filler effect can be predicted with a logarithmic best-fit relationship.

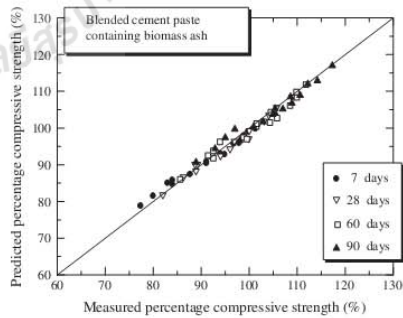


Fig. 12. Comparison between the predicted and experimental percentage compressive strength in blended cement pastes containing biomass ash.

3. The percentage compressive strength of paste due to the pozzolanic reaction increased with increasing fineness of RHA or POFA, cement replacement and age of paste. Moreover, it had a greater effect than the filler effect. The percentage compressive strength due to the pozzolanic reaction is explicitly nonlinear.
4. The use of RHA or POFA with particle sizes smaller than those of OPC to replace Portland cement Type I at the rate of 30% by weight of binder resulted in good compressive strength from filler effect and pozzolanic reaction. Moreover, the proposed

empirical model can be used to predict the percentage compressive strength of blended cement pastes in good agreement with the experimental results.

Acknowledgments

The authors would like to acknowledge the financial support of the Commission on Higher Education of Thailand for a grant under the Strategic Scholarships for Frontier Research Network for the Joint Ph.D. Program, Thai Doctoral degree. They also thank the Thailand Research Fund (TRF) for the financial support under the TRF Senior Research Scholar, Grant No. RTA5380002 and the TRF New Researcher Scholar, Grant No. MRG5280178.

References

- [1] Metz B, Davidson OR, Bosch PR, Dave R, Meyer LA. Climate change 2007. Contribution of working group III to the fourth assessment report of the intergovernmental panel on climate change. Cambridge, United Kingdom and New York, NY, USA: University Press; 2007.
- [2] Akashi O, Hanaoka T, Matsuoka Y, Kainuma M. A projection for global CO₂ emissions from the industrial sector through 2030 based on activity level and technology changes. *Energy* 2011;36(4):1855–67.
- [3] Chatveera B, Lertwattanaruk P. Durability of conventional concretes containing black rice husk ash. *J Environ Manage* 2011;92(1):59–6.
- [4] Chindaprasit P, Homwuttivong S, Sirivivatnanon V. Influence of fly ash fineness on strength, drying shrinkage and sulfate resistance of blended cement mortar. *Cem Concr Res* 2004;34(7):1087–92.
- [5] Rukzon S, Chindaprasit P. Utilization of bagasse ash in high-strength concrete. *Mater Des* 2012;34:45–50.
- [6] Wansom S, Janjaturaphan S, Sinthupinyo S. Characterizing pozzolanic activity of rice husk ash by impedance spectroscopy. *Cem Concr Res* 2010;40(12):1714–22.
- [7] de Senisale GR, Ribeiro AB, Gonçalves A. Effects of RHA on autogenous shrinkage of Portland cement pastes. *Cem Concr Compos* 2008;30(10):892–7.
- [8] Nair DG, Fraaij A, Klaassen AAK, Kentgens APM. A structural investigation relating to the pozzolanic activity of rice husk ashes. *Cem Concr Res* 2008;38(6):861–9.
- [9] Chatveera B, Lertwattanaruk P. Evaluation of sulfate resistance of cement mortars containing black rice husk ash. *J Environ Manage* 2009;90(3):1435–41.
- [10] Ganesan K, Rajagopal K, Thangavel K. Rice husk ash blended cement: assessment of optimal level of replacement for strength and permeability properties of concrete. *Constr Build Mater* 2008;22(8):1675–83.
- [11] Rukzon S, Chindaprasit P, Mahachai R. Effect of grinding on chemical and physical properties of rice husk ash. *Int J Miner Met Mater* 2009;16(2):242–7.
- [12] Givi AN, Rashid SA, Aziz FNA, Salleh MAM. Assessment of the effects of rice husk ash particle size on strength, water permeability and workability of binary blended concrete. *Constr Build Mater* 2010;24(11):2145–50.
- [13] Chindaprasit P, Rukzon S, Sirivivatnanon V. Resistance to chloride penetration of blended Portland cement mortar containing palm oil fuel ash, rice husk ash and fly ash. *Constr Build Mater* 2008;22(5):932–8.
- [14] Chindaprasit P, Homwuttivong S, Jaturapitakkul C. Strength and water permeability of concrete containing palm oil fuel ash and rice husk-bark ash. *Constr Build Mater* 2007;21(7):1492–9.
- [15] Tangchirapat W, Jaturapitakkul C. Strength, drying shrinkage, and water permeability of concrete incorporating ground palm oil fuel ash. *Cem Concr Compos* 2010;32(10):767–74.
- [16] Cyr M, Lawrence P, Ringot E. Efficiency of mineral admixtures in mortars: quantification of the physical and chemical effects of fine admixtures in relation with compressive strength. *Cem Concr Res* 2006;36(2):264–77.
- [17] Goldman A, Bentur A. The influence of microfillers on enhancement of concrete strength. *Cem Concr Res* 1993;23(4):962–72.
- [18] Gopalan MK. Nucleation and pozzolanic factors in strength development of class F fly ash concrete. *ACI Mater J* 1993;90(2):117–21.
- [19] Isala GC, Gastaldini ALG, Moraes R. Physical and pozzolanic action of mineral additions on the mechanical strength of high-performance concrete. *Cem Concr Compos* 2003;25(1):69–76.
- [20] Tangpagasit J, Cheerarat R, Jaturapitakkul C, Kiattikomol K. Packing effect and pozzolanic reaction of fly ash in mortar. *Cem Concr Res* 2005;35(6):1145–51.
- [21] Sata V, Jaturapitakkul C, Kiattikomol K. Utilization of palm oil fuel ash in high-strength concrete. *J ASCE Mater Civil Eng* 2004;16(6):623–8.
- [22] Lu N, Likos WJ. Unsaturated soil mechanics. New Jersey: John Wiley & Sons Inc.; 2004.
- [23] ASTM C109. Standard test method for compressive strength of hydraulic cement mortars (using 2-in. or [50 mm] cube specimens). Annual book of ASTM standards; 2001.
- [24] ASTM C618. Standard specification for coal fly ash and raw or calcined natural pozzolan for use as a mineral admixture in concrete. Annual book of ASTM standards; 2001.
- [25] Awal ASMA, Hussain MW. The effectiveness of palm oil fuel ash in preventing expansion due to alkali-silica reaction. *Cem Concr Compos* 1997;19(4):367–72.
- [26] Megat Johari MA, Brooks JJ, Kabir S, Rivard P. Influence of supplementary cementitious materials on engineering properties of high strength concrete. *Constr Build Mater* 2011;25(5):2639–48.
- [27] Montgomery DG, Hughes DC, Williams RIT. Fly ash in concrete – a microstructure study. *Cem Concr Res* 1981;11(4):591–03.
- [28] Lee C-L, Huang R, Lin W-T, Weng T-L. Establishment of the durability indices for cement-based composite containing supplementary cementitious materials. *Mater Des* 2012;37:28–39.
- [29] Jaturapitakkul C, Tangpagasit J, Songmue S, Kiattikomol K. Filler effect and pozzolanic reaction of ground palm oil fuel ash. *Constr Build Mater* 2011;25(11):4287–93.
- [30] Chindaprasit P, Jaturapitakkul C, Sinsiri T. Effect of fly ash fineness on compressive strength and pore size of blended cement paste. *Cem Concr Compos* 2005;27(4):425–8.
- [31] Jaturapitakkul C, Tangpagasit J, Songmue S, Kiattikomol K. Filler effect of fine particle sand on the compressive strength of mortar. *Int J Miner Metal Mater* 2011;18(2):240–6.
- [32] Cordeiro GC, Toledo Filho RD, Tavares LM, Fairbairn EMR. Pozzolanic activity and filler effect of sugar cane bagasse ash in Portland cement and lime mortars. *Cem Concr Compos* 2008;30(5):410–8.
- [33] Cordeiro GC, Toledo Filho RD, Tavares LM, Fairbairn GC, Hempel S. Influence of particle size and specific surface area on the pozzolanic activity of residual rice husk ash. *Cem Concr Compos* 2011;33(5):529–34.
- [34] Kroehong W, Sinsiri T, Jaturapitakkul C, Chindaprasit P. Effect of palm oil fuel ash fineness on the microstructure of blended cement paste. *Constr Build Mater* 2011;25(11):4095–04.
- [35] Aly M, Hashmi MSJ, Olabi AG, Messeiry M, Abadir EF, Hussain AI. Effect of colloidal nano-silica on the mechanical and physical behaviour of waste-glass cement mortar. *Mater Des* 2012;33:127–35.

BIOGRAPHY

Mr. Wunchock Kroehong was born on March 25, 1974 in Chumphon, Thailand. He received my bachelor's degree in Civil Engineering from Rajamangala University of Technology Thanyaburi in 1996. In 2000, He enrolled in the Master's degree program in the school of Civil Engineering at Mahanakorn University of Technology and obtained his degree in Civil Engineering in 2004. In 2008, He received a scholarship to pursue Ph.D. study in Civil Engineering at SUT from the Commission on Higher Education of Thailand from a grant under the Strategic Scholarships for Frontier Research Network for the Joint Ph.D. Program, Thai Doctoral degree. During my Ph.D. study, He published 2-international papers, 2-national journal papers and 1-international conference papers and 4-national conference papers. He is currently working as a full-time lecturer in Civil Engineering department at the Uthenthawai Campus, Rajamangala University of Technology Tawan-ok.